RHODES UNIVERSITY
Where leaders learn

Department of Geology

Genetic relationships between migmatites and the Swartoup Pluton in the Swartoup Hills (central Namaqua Belt)

A thesis submitted in fulfilment of the
requirement for the degree of

Master of Science in Geology

of

Rhodes University

by

Graeme A. Schmeldt

Supervised by

Professor Steffen H. Büttner

and co-supervised by

Professor Stephen A. Prevec

September 2021

Abstract

The central Namaqua Metamorphic Complex can be characterised by long-standing high-temperature (up to granulite/amphibolite facies) conditions between $\sim$ 1300 and 1100 Ma, inevitably resulting in widespread metamorphism and plutonism. Hosted within a NW–SE striking antiformal structure about 40 km east of Onseepkans, Northen Cape, South Africa, in the Swartoup Hills, lies the Swartoup Pluton.

The Swartoup Pluton was sampled and described in hand specimen and thin section. The study area was photographed, with all data presented in this study. The various rock types are readily discerned in the field due to their characteristic weathering colours and overall fabrics.

The Swartoup granodioritic body is hosted within metasediments of the Bysteek and Koenap Formations, of the Arribees Group. The package was later intruded by another later granitoid, the Polisiehoek Granite-gneiss.

The Bysteek Formation, a wall rock to the S-type Swartoup Pluton, reacted at the contact with the igneous body resulting in localised feldspathic granites and granodiorites with prominent, often euhedral, garnet, pryoxene and titanite.

The Swartoup Pluton is divided into two subgroups. The first is characterised by higher P_2O_5 contents, $\sim 0.3 - 0.4$ wt.%, shown with a narrower constraint on its Rb contents, $\sim 80 - 160$ ppm, than the second, with $\sim 0.14 - 0.4$ wt.% P_2O_5 and 20 – 310 ppm Rb. Meanwhile the Polisiehoek Granite-gneiss shows $\sim 50 - 420$ ppm Rb and $\sim 0.04 - 0.1$ wt% P_2O_5.

As a whole, the Swartoup Pluton is characterised by somewhat elevated CaO concentrations ($\sim 1.5 - 6.0$ wt.%), relative to calculated averages of granites (1.8 wt.% CaO, Le Maitre, 1976) and granodiorites (3.9 wt.% CaO, Le Maitre, 1976). Whilst most of the Swartoup specimens were classified as granodiorites, some orthopyroxene-bearing monzodiorite and orthopyroxene-bearing monzonite were locally found and sampled. However, much of the body appears to be granodioritic to granitic in composition.

The Polisiehoek Granite-gneiss is characterised by its orange-brown weathering colour in the field, sheared texture, lower P_2O_5 and higher total alkali content than the Swartoup Pluton.

The Polisiehoek Granite-gneiss is a highly fractionated S-type granite, as shown by plots of (a) (Na_2O + K_2O)/CaO and (b) FeO^T/MgO versus Zr + Nb + Ce + Y (Whalen et al., 1987; Zhang et al., 2019) and also of (c) (Al_2O_3 + CaO)/(FeO^T + Na_2O + K_2O) versus 100 × (MgO + FeO^T + TiO2)/SiO_2 (after Sylvester, 1989). Classification schemes identify the Polisiehoek Granite-gneiss as either a granite (TAS diagram, after Middlemost, 1994) or alkali granite (R_1R_2 diagram, after De la Roche et al., 1980).

Declaration

I hereby declare that this thesis has not been submitted, either in the same or different form, to this or any other university for a degree and that it represents my own work. I know the meaning of plagiarism and declare that all of the work in the thesis, save for that which is properly acknowledged, is my own.

Graeme A. Schmeldt

September 2021

Acknowledgements

My greatest thanks must be given to the Lord Jesus Christ, for He gave me the strength to write this thesis and complete my years of study. I must also thank my parents, Walter and Renée Schmeldt, for their love and support throughout my studies and indeed my entire life.

I would like to give thanks to my principal supervisor, Professor Steffen H. Büttner, for initiating and supervising this project. I also must greatly thank my co-supervisor, Professor Stephen Prevec, for his invaluable help and insight into the world of radiogenic isotopes in geology and his encouragement seeing this project to completion. Thanks must also be given for their patience with me whilst writing this project. I would also like to give my thanks to my examiners, whose contributions undoubtedly helped to improve this work.

Aiden van Huyssteen and Joshua-Luke Van Schalkwyk assisted with field work. I must thank them both for thieir efforts and a very enjoyable trip.

Thanks must also be given to Andrea King and the Technical staff of Rhodes University's Department of Geology for thin section preparation, to Stellenbosch University's Central Analytical Facilities for whole rock geochemical analyses, and to the Univeristy of Cape Town's Department of Geological Sciences for Rb/Sr and Sm/Nd isotope analyses. Gratitude must also be given to Rhodes University and it's Geology Department, for facilitating and providing funding for this project.

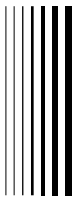

Contents

Contents **1**

1 Introduction **4**

1.1 Introduction 4

1.2 Geological Framework 5

1.2.1 Tectono-metamorphic history 6

1.2.2 Previous work on potential sources and geochemical relationships of granitoids in the central NMC 9

1.3 Aims the study 10

1.4 Geology of the Onseepkans area 11

1.4.1 Koenap Formation 11

1.4.2 Bysteek Formation 13

1.4.3 Swartoup Pluton 14

1.4.4 Polisiehoek Granite-gneiss 14

2 Methods and analytical procedures **16**

2.1 Methods 16

2.2 Thin section preparation 17

2.3 Whole-rock analysis 17

2.3.1 X-ray fluorescence 18

2.3.2 Laser Ablation Inductively Coupled Plasma Mass Spectrometry 22

2.3.3 Multi-collector Inductively Coupled Plasma Mass Spectrometry 23

2.4 U/Pb Zircon dating 23

3 Field relationships and petrography 25

3.1 Field overview and rock type distinctions 27

3.1.1 Koenap migmatite field observations 29

3.1.2 Bysteek Formation field observations 31

3.1.3 Swartoup Pluton field observations 32

3.1.4 Hybrid rock field observations 38

3.1.5 Polisiehoek Granite-gneiss field observations 40

3.1.6 Mafic dyke field observations 42

3.2 Sample Petrography 43

3.2.1 Koenap migmatite 44

3.2.2 Bysteek Formation 50

3.2.3 Swartoup granitoids 54

3.2.4 Hybrid rocks 65

3.2.5 Polisiehoek Granite-gneiss 71

3.2.6 Mafic dyke 78

3.3 Summary 79

4 Geochemistry 89

4.1 Rock classification schemes 90

4.1.1 Total-alkali versus silica diagram 90

4.1.2 R_1R_2 plutonic rock classification 96

4.1.3 Summary and interpretation of the TAS and R_1R_2 diagram classifications 98

4.2 Fe-number, MALI and ASI classification 101

4.3 I-, S- and A-type granitoid characteristics 108

4.3.1 P_2O_5 against Rb 108

4.3.2 Ce against Rb 110

4.3.3 Y against Rb 111

4.3.4 La against SiO_2 113

4.4 Further chemical variation diagrams 114

4.4.1 Major and minor element oxide plots 114

4.4.2 Plots against maficity 125

4.4.3 Chondrite normalised rare-earth diagrams 132

4.5 Isotope diagrams 135

4.5.1 Sm/Nd isotope diagram . . . 135
4.5.2 Rb/Sr isotope diagram . . . 137
4.5.3 Summary and interpretation . . . 139
4.6 U/Pb zircon ages . . . 142

5 Discussion **144**
5.1 Summary of characteristics . . . 144
5.1.1 Koenap migmatite . . . 144
5.1.2 Swartoup Pluton . . . 145
5.1.3 Polisiehoek Granite-gneiss . . . 146
5.2 Age and isotopic evidence for origin of Swartoup Pluton . . . 147
5.2.1 Zircon ages . . . 147
5.2.2 Isotopic relationships . . . 148
5.3 Genetic relationships . . . 151
5.3.1 Assessing protolith composition . . . 151
5.3.2 Did the Swartoup Pluton originate from melting of the the Koenap Formation? . . . 157
5.3.3 The hybrid rock . . . 158

6 Conclusion **161**
6.1 The Koenap Formation . . . 161
6.2 The Swartoup Pluton . . . 161
6.2.1 The hybrid rock . . . 162
6.3 The Polisiehoek Granite-gneiss . . . 162

A Appendix **164**
A.1 Chemical variation diagram descriptions . . . 164
A.1.1 Rock classification schemes . . . 165
A.2 A-type granitoid discrimination . . . 172
A.2.1 $(Na_2O + K_2O)/CaO$ and FeO^T/MgO versus Zr + Nb + Ce + Y . . . 172
A.2.2 $(Al_2O_3 + CaO)/(FeO^T + Na_2O + K_2O)$ versus $100 \times (MgO + FeO^T + TiO2)/SiO_2$ . . . 174
A.3 Trace element chemical variation diagrams . . . 176
A.4 U/Pb Zircon data . . . 180

References **183**

CHAPTER 1

Introduction

1.1 Introduction

The Namaqua–Natal Province (NNP) is a Mesoproterozoic tectono-metamorphic belt in southern Africa (Figure 1.1) which stretches from southern Namibia and Namaqualand in the west to Natal in the east (e.g., Thomas et al., 1994a,b; Cornell et al., 2006). The NNP comprises the igneous and metamorphic rocks which formed and acquired a pervasive structural fabric during the Namaqua Orogeny from *ca.* 1300 to 1000 Ma, the western part of which is known as the Namaqua Metamorphic Complex (NMC) (e.g., Thomas et al., 1994b; Cornell et al., 2006; Bial et al., 2015a,b). Granitoid plutons and metasedimentary sequences constitute the largest portion of NMC crust, however few geochemical studies have investigated the potential sources and genetic relationships of these granitoid plutons which have magmatic histories spanning over 200 m.y. (e.g., Bial et al., 2015a,b). This research presents a petrological (Chapter 3) and geochemical (Chapter 4) study of a granitoid, the Swartoup Pluton, from the Swartoup Hills in the central Kakamas Domain of the NMC and also surrounding rock-types with which it is spatially associated. Major and trace element composition data have been produced for the various lithologies (Sections 4.1–4.4) as well as Sm/Nd and Rb/Sr isotopic data (Section 4.5). Preliminary U/Pb zircon ages provided by Professor Dirk Frei (University of the Western Cape) are also presented in Section 4.6.

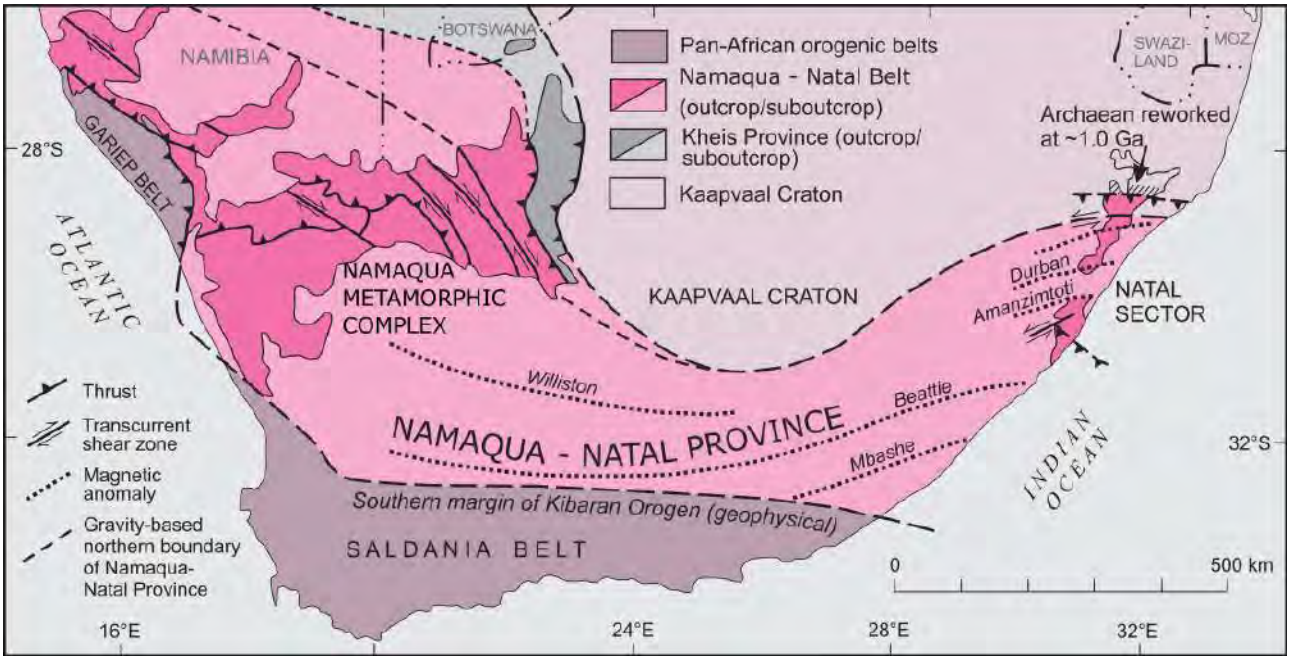

Figure 1.1: *Geological setting of the Namaqua—Natal Province (modified after Cornell et al., 2006). The Province stretches from southern Namibia and Namaqualand in the west, across central Africa (beneath Phanerozoic cover) and into Natal in the east (Thomas et al., 1994b). The Namaqua Metamorphic Complex is also referred to by some authors as the Namaqua Sector (of the Namaqua–Natal Province) (e.g., Cornell et al., 2006).*

1.2 Geological Framework

Traditionally, the NMC has been subdivided into numerous 'terranes' or 'domains', separated by major tectonic structures and distinguished lithostratigraphically, with much controversy (Hartnady et al., 1985; Thomas et al., 1994b; Colliston and Schoch, 1996; Cornell et al., 2006; Moen and Toogood, 2007; Miller and Becker, 2008). In light of new mapping in southern Namibia (Macey et al., 2015; Gresse et al., 2016), the term 'domain' is used by Thomas et al. (2016) to avoid genetic implications associated with the accretionary term 'terrane', as suggested by Thomas et al. (2016). Thomas et al. (1994b) subdivided the NMC into four different NW to SE domains. From west to east, these are the Bushmanland, Kakamas, Areachap, and Kaaien Domains (Figure 1.2a).

The study area is located in the central part of the NMC (Figure 1.2a), within the Kakamas Domain (e.g., Cornell et al., 2006; Moen and Toogood, 2007; Bial et al., 2015a,b). Samples were collected from the farm 'Oup 80', *ca.* 30 km east of Onseepkans, Northern Cape (Figure 1.2). The Kakamas Domain has also been called the Aus or Grünau 'terrane' (e.g. Colliston and Schoch, 1996) or the Gordonia Subprovince (Hartnady et al., 1985).

The tectonic boundaries of the Kakamas Domain are controversial within published literature (e.g., Colliston et al., 1989; Thomas et al., 1994b; Colliston and Schoch, 2006; Moen and

Toogood, 2007; Colliston et al., 2015). However, the Onseepkans Thrust (Figure 1.2b) in the west appears to be the least disputable boundary (Moen and Toogood, 2007; Bial et al., 2015b), along which granulite-facies rock of the Kakamas Domain were thrust over the Palaeoproterozoic Richtersveld Subprovince. The study area lies well within the Kakamas Domain as this thrust zone lies *ca.* 30 km west of the study area (Figure 1.2b). Northwest-trending stratigraphic units and structures characterise the Kakamas Domain, in contrast to the east-west trending Bushmanland Domain's structural grain to the south and south-east (Hartnady et al., 1985; Cornell et al., 2006).

The highly reworked Kakamas Domain comprises Palaeozoic basement rocks and Mesoproterozoic igneous and supracrustal sequences (e.g., Pettersson et al., 2009; Bial et al., 2015a). The majority of these rocks are metasedimentary gneisses with lesser quartzites, mafic granulites, calc-silicates and marbles, intruded by syn- to late-tectonic granitoids or granitoid-gneisses, deformed under low-pressure, granulite-facies conditions, between *ca.* 1.2 and 1.0 Ga (Hartnady et al., 1985; Thomas et al., 1994a; Bial et al., 2015a).

1.2.1 Tectono-metamorphic history

Recent studies have placed previous models of the tectono-metamorphic history of the Namaqua–Natal Province under review. Previous work suggests that the high-grade metamorphic rocks and granitoids of the Namaqua Orogeny resulted from terrane accretion, which was then accreted onto the southern margin of the Kaapvaal craton during prolonged phases of southwest- to northeast-directed convergence, resulting in closure of the Natal basin (Jacobs et al., 1993; Thomas et al., 1994a). Polyphase deformation resulted from formation of the NNP, along with high-grade metamorphism and granitoid intrusions (Hartnady et al., 1985; Thomas et al., 1994b). This has been interpreted as a complete Wilson Cycle model (Thomas et al., 1994b; Miller, 2012).

More recently, however, a continental back-arc geotectonic setting has been proposed for the region (Bial et al., 2015a,b, 2016), with supporting evidence from Diener (2014) and Macey et al. (2015). Peak metamorphic conditions vary within the belt, between amphibolite and upper granulite facies conditions, locally reaching ultra-high temperatures at low pressure (850–900°C at 4–6 kbar; Bial et al., 2015a; Fisher, 2016).

In contrast to earlier models, Bial et al. (2015a,b) propose a long standing heat source and thin crust produced the necessary conditions for large-scale granitoid formation as in the central NMC. The temperatures and pressures of peak metamorphism within the Kakamas Domain are

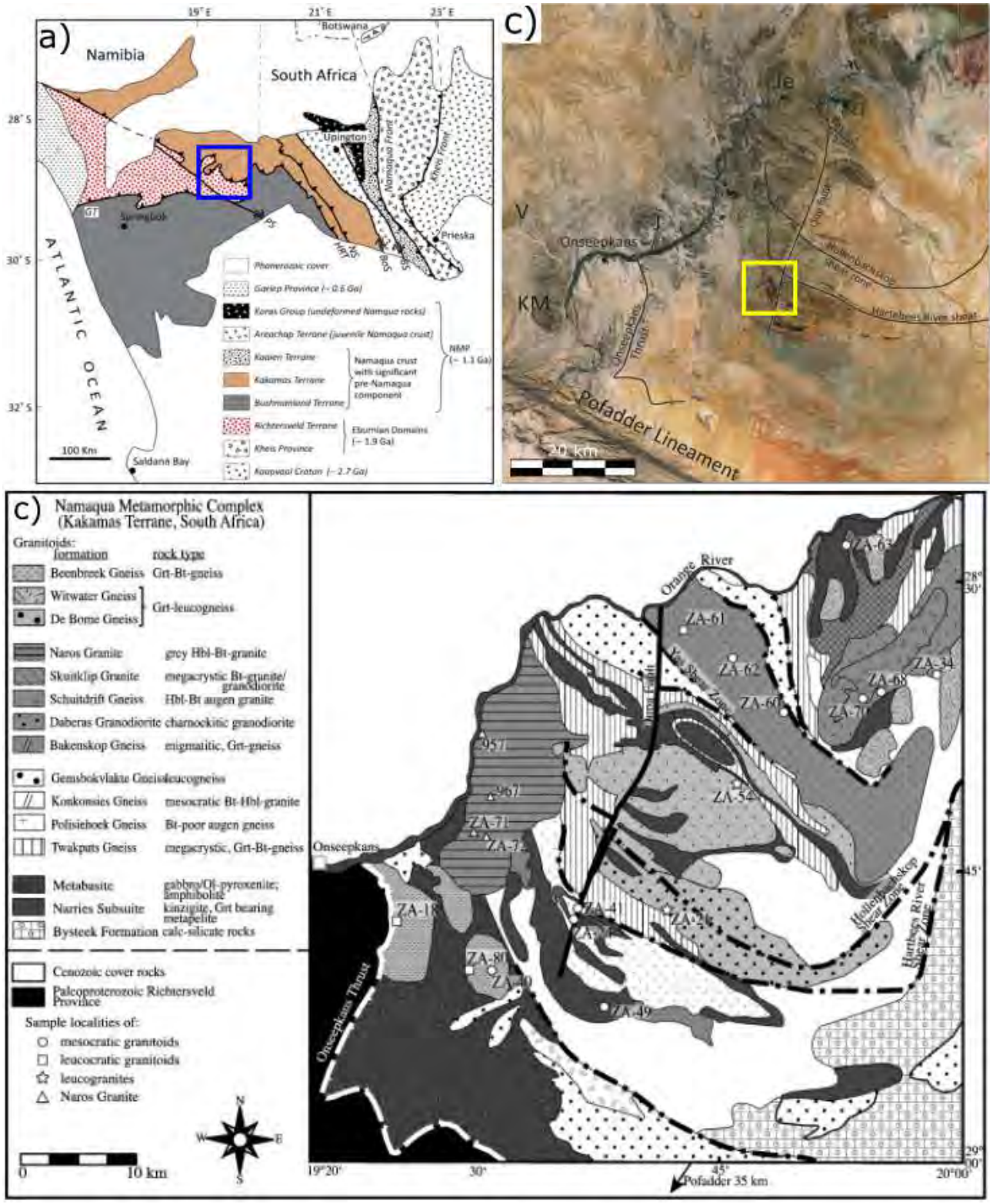

Figure 1.2: *(a) Simplified geological map of the Namaqua Metamorphic Complex (modified after Thomas et al., 1994b). Blue indicates the area shown in (b), in relation to the Namaqua Metamorphic Complex. (b) Satellite image of the sample locality, indicated in yellow, relative to Onseepkans and the Onseepkans Thrust (Image©2013 Google). (c) Simplified geological map showing the sampling locality (modified after Moen, 2001).*

well established within the literature. Stowe (1983), for example, reported upper amphibolite to granulite-facies conditions of 650–750°C at 5 kbar within a metapelite near the Hartebeest River shear zone (Figure 1.2). Further to the east, near Uppington and Kheimoes (Figure 1.2a),

Humphreys and van Bever Donker (1990) found lower amphibolite-facies conditions where staurolite-cordierite-andalusite schists equilibrated at around 550°C and a low pressure of *ca.* 2 kbar. Within the central Kakamas Domain, nearer the study area, Bial et al. (2015b) found a long-lasting high-temperature (> 650°C) history between *ca.* 1300 and 1100 Ma, locally reaching UHT-conditions, with slow cooling and heating episodes at near-constant mid-crustal pressures. Collision-related settings do not reach upper granulite-facies/UHT conditions at low crustal pressures (Collins, 2002). As such conditions are not compatible with crustal thickening and continent-continent collisional models, Bial et al. (2015b) proposed crustal evolution in a continental back-arc setting. Characteristic of such settings are up to 1000 km wide regions of thin, hot lithosphere behind active continental margins ((Hyndman et al., 2005). Low crustal pressures and upper granulite-facies metamorphism are also characteristic of such environments (Bial et al., 2015b), which can experience prolonged stable, extensional or contractional periods that last hundreds of millions of years (e.g. Ellis et al., 1998; Hyndman et al., 2005).

The palaeogeographic configuration of Rodinia between *ca.* 1200 and 1100 Ma, with a separation between the Kalahari Craton and Laurentia (Dalziel et al., 2000), is consistent with a continental back-arc model. Major collisions at that time, however, conflict with the configuration of Rodinia (Bial et al., 2015b). An active plate margin is probable in central Namibia, close to the younger Damara front (Miller and Becker, 2008), proposed to be active at 1260 to 1200 Ma (Cornell et al., 2015). This is consistent with the presence of a back-arc continental mobile belt in the NMC at the time of major crustal heat influx (Bial et al., 2015b).

Also, Diener (2014) found that peak metamorphic conditions of the western NMC, during the somewhat older O'okiepian Orogeny (*ca.* 1.17–1.13 Ga), require higher-than-average heat flows, such as those resulting from mafic underplating, or from burial and slow erosion of highly radiogenic crust, allowing for elevated crustal heat production followed by near isobaric cooling.

Previously, a Palaeoproterozoic model age of 2.27 Ga for the 1203 ± 11 Ma Polisiehoek Granite-gneiss was established regarding the magmatic history of the Kakamas Domain (Pettersson, 2008; Pettersson et al., 2009). Local or regional sediment deposition are documented within the early stages of the Namaquan Orogeny, whereby 1.3 to 1.57 Ga detrital zircons are reported from the Kenhardt Formation (Cornell and Pettersson, 2007). Metamorphism subsequently took place in these rocks between *ca.* 1190 and 1197 Ma (Cornell and Pettersson, 2007). Colliston et al. (2015) report similar ages of metamorphism and deformation (*ca.* 1195–1155 Ma) from studies of supracrustal rocks and syntectonic granitoids. Bial et al. (2015a) found that widespread A- and S-type plutonism took place within the Kakamas Domain around 1.2 Ga. Late-orogenic

intrusions followed, around 1.1 Ga, such as the Keimos Suite (Cornell and Pettersson, 2012) and the Naros Granite (Bial et al., 2015a).

1.2.2 Previous work on potential sources and geochemical relationships of granitoids in the central NMC

Bial et al. (2015a) presented geochemical assessments of granitoids from the Kakamas Domain in South Africa and the Grünau Domain (Colliston et al., 1989) in southern Namibia. These authors subdivided the granitoids into three main groups; (i) mesocratic granitoids, (ii) leucocratic granitoids (which have a coulour index, M' = 10–35) and (iii) leucogranites (M' = 0–10).

Bial et al. (2015a) found the mesocratic granitoids to be high-K, ferroan and granitic to tonalitic in composition with 54–75 wt.% SiO_2. These granitoids show enrichment in large-ion lithophile elements (LILEs) and rare-earth elements (REEs; Bial et al., 2015a), characteristic of A-type granitoids (e.g., King et al., 1997; Zhang et al., 2019). These mesocratic granitoids are proposed to have resulted from fractional crystallisation of a hot (900°C), mafic parental magma (Bial et al., 2015a).

The leucocratic granitoids and leucogranites were found to vary from granite- to quartz syenite-compositions with 68–76 wt.% SiO_2 (Bial et al., 2015a). These granitoids show relatively lower REEs, CaO, FeO^T, MgO, MnO and TiO_2. However, they show relatively higher Na_2O and K_2O contents. Bial et al. (2015a) suggested these rocks formed through water–rich fluid-infiltration and low-temperature (< 730°C), fluid-present partial melting of a felsic metasedimentary source.

Bial et al. (2015a) find both the mafic and leucocratic granitoid types were emplaced between *ca.* 1220 and 1180 Ma. During this period the crust reached its thermal peak, leading to formation and emplacement of the leucocratic granitoids and leucogranites Bial et al. (2015a). Following a protracted period of high crustal temperatures, a second heat pulse around 1100 Ma was enough to facilitate zircon growth in older plutons and also to produce a younger granite suite (Bial et al., 2015a). Only after a further 100 m.yr. did the crust cool down below amphibolite-facies conditions (Bial et al., 2015a).

1.3 Aims the study

This study presents a petrological (Sections 3.1.3, 3.2.3 and 5.1.2) and geochemical (Chapter 4) assessment of a granitoid, the Swartoup Pluton, and of its potential source rocks (Sections 5.3, 6.2 and 6.1), the migmatites of the Koenap Formation (Sections 3.1.1, 3.2.1, Chapter 4 and Section 5.1.1), with which it is spatially associated (Figures 1.2c and 1.3, Section 1.4). In addition, the petrological and geochemical characteristics of the neighbouring Polisiehoek Granite-gneiss is presented for comparison (Sections 3.1.5, 3.2.5 and 5.1.3), as well as three samples from the Bysteek Formation. Both Koenap Formation migmatite and the Swartoup Pluton are spatially associated with the Polisiehoek Granite-gneiss (Moen and Toogood, 2007). A proposed 'hybrid rock' is also petrologically and geochemically assessed (5.1.2, 5.3.3). This rock crops out in only small volumes and is proximally associated with both the Swartoup Pluton and calc-silcates of the Bysteek Formation (Section 3.1.4). This rock resulted from contamination of Swartoup melt with Bysteek material (Sections 5.3.3, 6.2.1). An unidentified mafic dyke is also presented (Sections 3.1.6, 3.2.6). The body was originally sampled as a potential contaminant of the Swartoup Pluton. However, the dyke shows cross-cutting relationships with both Polisiehoek Granite-gneiss and pegmatitic material, and so post-dates intrusion of the Swartoup Pluton. The mafic dyke data remain in the study as a proxy of potential mantle contaminants of the Pluton. The rock compositions are compared to published pelite and greywacke compositions (see Section 2.1).

The geochemical assessment of these rock-types was done using whole-rock major and trace-element analyses (Sections 2.3, 4.1–4.4) in addition to Rb/Sr and Sm/Nd isotopic data (Sections 2.3.3, 4.5). Some zircon U/Pb age data have also been acquired during the course of this study courtesy of Professor Dirk Frei (University of Cape Town) and are presented as well (Sections 2.4, 4.6).

Moen and Toogood (2007) proposed the 'Swartoup Enderbite' as a relative of the Polisiehoek Granite-gneiss. A compositional blend of a calcic host and intruding granite caused, according to Moen and Toogood, an enderbitic pluton referred to as the 'Swartoup Enderbite'. However, this study will demonstrate (i) there is very little enderbite in the locality and (ii) the Swartoup Pluton is comprised of mostly granitoids with granodioritic and granitic compositions (see Table 3.4, Section 3.1.3).

1.4 Geology of the Onseepkans area

The study area is located on the farm 'Oup 80', situated *ca.* 30 km east of Onseepkans, Northern Cape (Figure 1.2). Regional lithostratigraphic mapping was undertaken by Moen and Toogood, who produced a geological map published in 2007 by the Council for Geosciences (Sheet 2818 Onseepkans). This study adopts the nomenclature and description of lithological units as described in the map explanation to Sheet 2818 Onseepkans by Moen and Toogood (2007), published by the Council for Geosciences, Pretoria.

The main focus of this study are rocks of the Swartoup Pluton (referred to as the 'Swartoup Enderbite' by Moen and Toogood, 2007) and its surrounding rock types, chiefly migmatite of the Koenap Formation but also the Bysteek Formation and the Polisiehoek Granite-gneiss (referred to as the Polisiehoek Gneiss by Moen and Toogood, 2007). These two metasedimentary units, the Koenap and Bysteek Formations, are correlated with the Arribees Group (Moen and Toogood, 2007). In addition, small volumes of hybrid rock are spatially associated with granitoid of the Swartoup Pluton and Bysteek Formation rocks, with which it is always in contact. Figure 1.3 shows a cross-section produced by Moen and Toogood (2007) through the antiformal structure within the study area, highlighting the spatial relationship between the rock types. A single mafic dyke sample is also presented but remains unidentified. The Twakputs Granite-gneiss Moen and Toogood (2007) lies to the northeast of the study area (Figure 1.2c, 1.3).

Mapping of the region established a transitional relationship between marbles and calc-silicates of the Bysteek Formation and the predominantly metapelitic Koenap Formation (Moen, 2001; Moen and Toogood, 2007). The Arribees Group comprises a variable succession of compositions from quartzite and quartz-feldspar paragneiss through to calc-silicate rocks and pure dolomitic marble (Moen and Toogood, 2007). The pelitic part of the Group is referred to as the Koenap Formation and the more calcic parts the Bysteek Formation (Moen and Toogood, 2007).

1.4.1 Koenap Formation

Moen and Toogood (2007) describe the migmatites of the Koenap Formation as gneissic rocks containing quartz + alkali-feldspar + biotite + garnet ± cordierite ± sillimanite, to which they apply the term kinzigite. Kinzigite, as defined by Mehnert (1968), is high-grade metapelite which is quartz–K-feldspar–plagioclase-rich, with less abundant (almandine/pyrope) garnet. However, this study adopts term migmatite, reflecting the anatectic fabric of the Koenap Formation in the study area. Migmatites are composite silicate metamorphic rocks, pervasively heterogeneous and typically exhibiting two or more petrographically different parts, one of

which is the country rock, often melanocratic and metamorphic, and the other leucocratic, with igneous-looking parts (*c.f.* Mehnert, 1968; Wimmenauer and Bryhni, 2007).

The Koenap migmatites are dark-coloured rocks and often display an irregular, migmatitic layering (Moen and Toogood, 2007). The hard, almost isotropic rocks form prominent boulder-outcrops, often mantled by extensive black-coloured scree aprons (Moen and Toogood, 2007).

Quartz is commonly the most abundant mineral, but Moen and Toogood (2007) note microcline is locally dominant in areas. Garnet (almandine) forms up to 20 mm anhedral porphyroblasts, usually surrounded by leucocratic depletion haloes (depleted in iron and magnesium Moen and Toogood, 2007). On the farm Oup 80, Moen and Toogood (2007) describe Koenap migmatite within the western limb of the antiform locally hosting Bysteek Formation calc-silicate rocks, which grade into the migmatitic host. Though Moen and Toogood (2007) do not associate these calc-silicate rocks with marble layers, this study does find small marble layers locally present (e.g. Locality GS13, Section 3.1.4).

Detrital zircon geochronology carried out on one sample by Moen and Toogood (2007) revealed

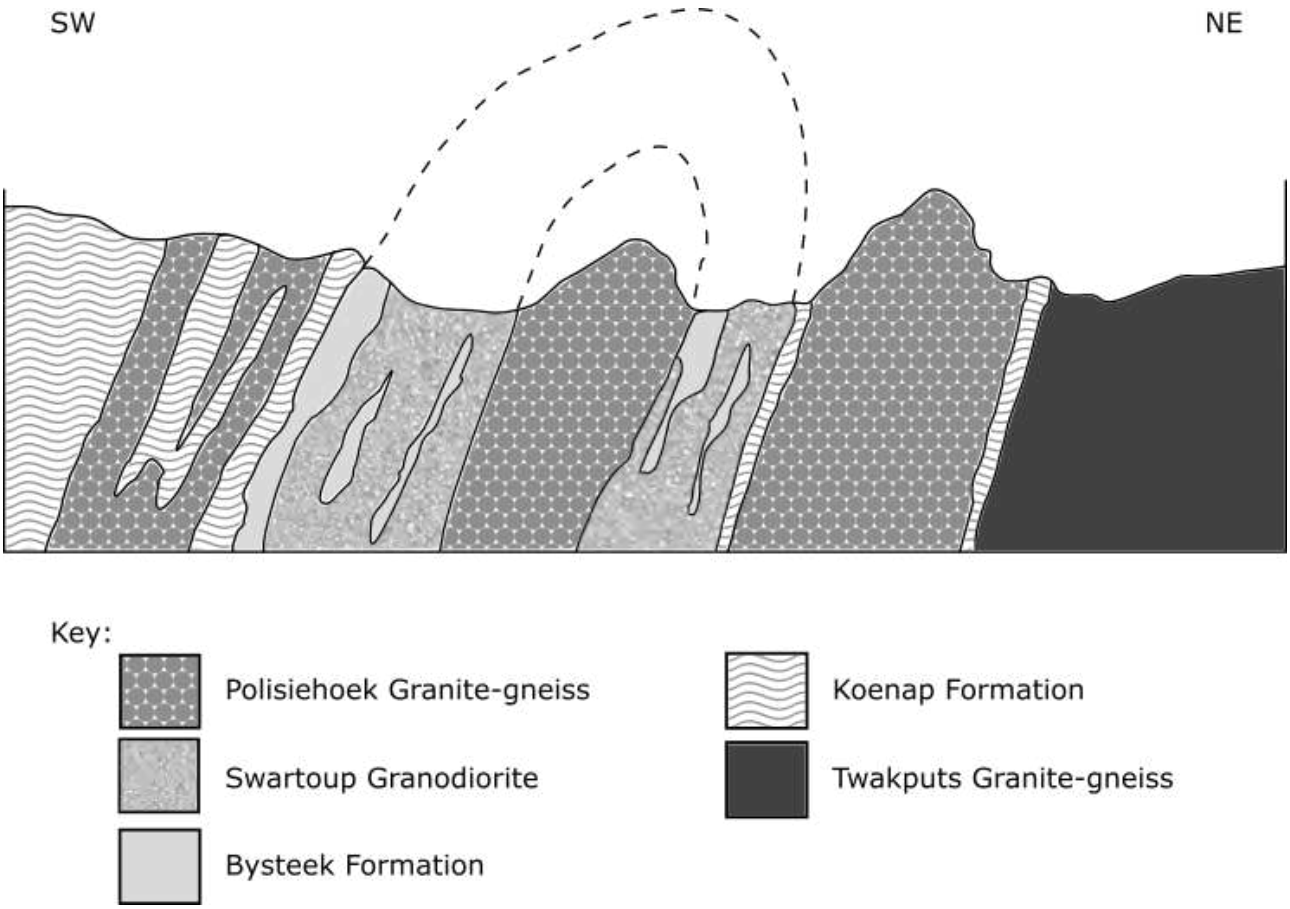

Figure 1.3: *Southwest to northeast cross-section of the antiformal structure on the farm Oup 80, situated ca. 30 km east of Onseepkans, Northern Cape, South Africa (modified after Moen and Toogood, 2007).*

the succession to be no older than *c.a.* 2.0 Ga, with components dated *c.a.* 1.85 Ga. The depositional age is constrained between 1.3 and 1.8 Ga, with no Archaean crust exposed during supracrustal deposition.

van Huyssteen (2017) found leucosome textures to reveal melt crystallised (i) *in situ*, (ii) in source and (iii) within accumulated leucocratic veins within migmatite of the Koenap Formation. However, nowhere in the study area could van Huyssteen find accumulations of leucocratic veins over a metre scale, or Koenap migmatite leucosome over 20–30%. This suggests the melt fraction within Koenap Formation migmatite was insufficient for granite formation (van Huyssteen, 2017). Accumulations of leucosome material over the rheologically critical melt percent (30–50%) are required for large scale mobility (e.g., Ashworth and Brown, 2012).

1.4.2 Bysteek Formation

Moen and Toogood (2007) describe the Bysteek Formation as light- to dark-grey coloured, layered, quartz-rich metasedimentary calc-silicate rocks. Grain sizes vary from fine- to very-fine–grained crystals of quartz, microcline, hornblende and titanite with variable amounts of calcic plagioclase, diopside and opaque minerals (Moen and Toogood, 2007). Accessory phases commonly include grossularite, epidote, scapolite, zoisite and calcite (Moen and Toogood, 2007).

Quartz and microcline independently vary form about 10 to 40 vol.%. However, some samples contain no feldspar and are comprised of scapolite, diopside and titanite with accessory calcite and quartz (Moen and Toogood, 2007). The Bysteek Formation rocks were not susceptible to incipient meting due to their somewhat high calcium contents (Moen and Toogood, 2007). As a result, they are not migmatitic despite the high metamorphic grade (granulite facies) of the region (Moen and Toogood, 2007).

Moen and Toogood (2007) found, interbedded within the Bysteek Formation, several stratigraphic horizons which contain white to blue-grey marble layers ∼2–20 m thick. These marbles contain relatively pure calcite/dolomite with small olivine, diopside or phlogopite porphyroblasts (Moen and Toogood, 2007) and appear laterally extensive, being traced over hundreds of metres, and up to 3 km, in some localities.

Moen and Toogood (2007) often associate the marbles with a silicic rock with a cavernous weathering structure, which the marble also often laterally grade into. This study refers to this specific rock-type as Bysteek mafic calc-silicate rock in field petrography, and is pictured in Figure 3.5a, Section 3.1.2. This Bysteek mafic calc-silicate rock comprises quartz, microcline

and/or anorthite, minor diopside, grossularite and carbonate (Moen and Toogood, 2007). The Bysteek mafic calc-silicate rock has a geochemical composition comparable to basalt (Moodley, 2012) though the rock is a metamorphosed calc-silicate and not a basalt. Within the study area on the farm Oup 80, Moen and Toogood (2007) describe marble layers with average thicknesses of 10–15 m and restricted to within the Swartoup Pluton (Figure 1.3).

1.4.3 Swartoup Pluton

Moen and Toogood (2007) describe the igneous body surrounding the Polisiehoek Granite gneiss 'core' of the antiform in Figure 1.3 as the 'Swartoup Enderbite'. However, this study will demonstrate that this 'Swartoup Enderbite' is in fact a granodiorite. As such, we propose the name of this granodioritic body be changed to the Swartoup Pluton.

The Swartoup Pluton occurs on the farm Oup 80, in an antiformal structure surrounded by Polisiehoek Granite-gneiss (Figure 1.3). Moen and Toogood (2007) associate the rock with Bysteek Formation calc-silicates, which are intermittently present over a 10 km strike. The antiformal closure is well defined and has a core consisting of Polisiehoek Granite-gneiss (Figures 1.2c, 1.3). Structurally upwards from the antiform 'core' is the Swartoup Pluton. It encloses laterally extensive layers of calc-silicates (Moen and Toogood, 2007).

Moen and Toogood (2007) propose the 'Swartoup Enderbite' developed as a compositional blend of calcic host (Bysteek Formation) and granitic intrusive (Polisiehoek Granite-gneiss). However, this study will demonstrate that there is very little enderbite in this region. What has been mapped as enderbite is largely a granodiorite that contains no orthopyroxene but shows a large modal proportion of alkali feldspar.

Furthermore, field evidence suggests the Polisiehoek Granite-gneiss is much younger, as it intrudes and cross-cuts the Swartoup Pluton body along sharp contacts. This suggests that the Swartoup Pluton was solid (or at least mostly crystalline) at the time of emplacement of the Polisiehoek magma (*pers. comm.* Büttner, 2016).

1.4.4 Polisiehoek Granite-gneiss

The Polisiehoek Granite-gneiss (referred to as the 'Polisiehoek Gneiss' by Moen and Toogood, 2007) is an orthogneiss that forms a rugged, mountainous terrain, with a conspicuous red-brown weathering colour, throughout most of its exposure (Moen and Toogood, 2007). The Polisiehoek Granite-gneiss intruded into the metapelitic facies of the Arribees Group(that is, the Koenap

Formation). These kinzigites form laterally extensive rafts within the Polisiehoek Granite-gneiss, forming high, black-weathering ridges (Figure 1.2c) (Moen and Toogood, 2007).

In most of the Polisiehoek Granite-gneiss' distribution, Moen and Toogood (2007) describe the Granite-gneiss as having a streaky to domained, augen-like texture while, in the low-strain areas, it is a medium-grained augen gneiss with composite, flattened augen. The low biotite content causes these augen to be only vaguely defined. Moen and Toogood (2007) note that kinzigite forms prominent rafts within the Polisiehoek Granite-gneiss, and these contacts are always sharp. Moen and Toogood noted clear intrusive relationships at several localities in the body. They propose that it was generated through a fractionation process, and emplaced under granulite-facies conditions. The magma then crystallised as a syntectonic body.

Moen and Toogood (2007) report Swartoup rock grading into Polisiehoek Granite-gneiss, which this study could not verify. However, mylonitic (van Huyssteen, 2017) contacts between Polisiehoek Granite-gneiss and the Swartoup Pluton were found in a recent Honours study (see van Huyssteen, 2017). This study also will show sharp intrusive contacts between these two units (Figure 3.14b, Section 3.1.5).

CHAPTER 2

Methods and analytical procedures

2.1 Methods

A total of forty-four representative rock samples were collected from the study area; ten from the Koenap Formation migmatites, three from the Bysteek Formation, sixteen from the Swartoup Pluton, nine from the Polisiehoek Granite-gneiss, five of a hybrid rock associated with the Bysteek Formation and the Swartoup Pluton, and one sample from the mafic Dyke (Chapter 3). Sampling localities are shown on Figure 3.1. Samples are labelled by their localities, with an appended alphanumeric letter dependant on their sampling sequence. For example, GS9A and GS9B are the first and second specimens collected, respectively, from locality GS9.

Table 2.1 shows all the sample numbers of specimens collected, as well as the analytical methods used on each specimen. Petrographic analysis was conducted with the intention of understanding the textural relationships, determining modal quantities of phases and for detailed description of specimens on both macroscopic and microscopic levels. Thin sections were prepared at the Rhodes University's Department of Geology. Mineral abbreviations follow the nomenclature outlined by Whitney and Evans (2010).

For the purposes of quantitative chemical evaluation of the rocks, multiple techniques were employed. These include X-ray Fluorescence (XRF) analysis and Laser Ablation Inductively Coupled Plasma Mass Spectrometry (LA-ICP-MS). These have also been used to classify the igneous rocks of the study (Section 4.1), using the TAS diagram classification schemes after Le Bas et al. (1986) and Middlemost (1994), and also the R_1R_2 classification scheme of De la Roche et al.

(1980). As per Frost and Frost (2008), orthopyroxene-bearing and orthopyrozene–clinopyroxene-bearing igneous rocks include the modifiers 'orthopyroxene-bearing' and 'pyroxene-bearing'. The geochemical compositions of the analysed samples are compared to published pelite and greywacke compositions (Tables 2.2–2.4) taken from, Shaw (1956),Gromet et al. (1984), Carmichael (1989), Condie (1993) and Absar and Sreenivas (2015). Pelites are considered the most likely protolith of the Koenap Formation (Moen and Toogood, 2007), but greywackes are considered more fertile protoliths of granitoids (Clemens, 2012).

The rare earth plots of Section 4.4.3 are normalised using CI carbonaceous chondrite of McDonough and Sun (1995).

Analyses of Rb/Sr and Sm/Nd isotopic systems was done on twenty-seven powdered whole-rock samples (Table 2.1); four from the Koenap Formation migmatites, one from the Bysteek Formation, eleven from the Swartoup Pluton, five from the Polisiehoek Granite-gneiss, five of the hybrid rock and one sample from the mafic Dyke (Section 4.5). These were done for further evaluation of potential genetic relationships between the spatially associated rock-types.

2.2 Thin section preparation

A total of forty-four rock samples were collected from the study area, shown in Figure 1.2c, from which fifty-six thin sections were prepared. From the Koenap Formation specimens, twelve thin sections were prepared; twenty-one from the Swartoup granitoid samples, and eleven from the Polisiehoek Granite-gneiss were also collected. Six thin sections were prepared from the three Bysteek Formation samples, along with five thin sections from the Hybrid Rocks, and one from the Mafic dyke sample. Thin section preparation was done in the Department of Geology, Rhodes University.

2.3 Whole-rock analysis

Clean whole-rock samples were coarsely crushed at the Department of Geology at Rhodes University using an Osborn-Massco Jaw Crusher, equipped with manganese steel teeth. The crushed samples were then milled to a fine powder using a Herzog Swing Mill. The silicon carbide swing mill vessel comprises 2 rings and 1 central puck, whose compositions are C - 0.90%, P - 0.30%, Mn - 2.00% and Si - 0.20%. The resulting fine powder was then sent to the Central Analytical Facility of Stellenbosch University for whole-rock analysis.

Table 2.1: *Sample numbers, rock formations, rock names and analytical methods used on the sample set. The igneous rocks are classified according to the TAS (Middlemost, 1994) and R_1R_2 (De la Roche et al., 1980) classification diagrams. Orthopyroxene- and orthopyrozene–clinopyroxene-bearing igneous rocks include the modifiers 'orthopyroxene-' and 'pyroxene-bearing', as per Frost and Frost (2008). Mineral abbreviations follow the nomenclature outlined by Whitney and Evans (2010).*

Sample	Formation	Rock name	Thin section	XRF	LA-ICP-MS	Rb/Sr	Sm/Nd
1137A	Koenap migmatite	Grt-Pl-Kfs-Crd-Qz gneiss	✓	✓	✓	✓	✓
1138A	Koenap migmatite	Crd-Kfs-Grt-Qz gneiss	✓	✓	✓	✓	✓
1141A	Koenap migmatite	Kfs-Crd-Grt-Qz granofels	✓	✓	✓	✗	✗
1141B	Koenap migmatite	Crd-Ms-Pl-Kfs-Grt-Qz gneiss	✓	✗	✗	✗	✗
1143A	Koenap migmatite	Bt-bearing Pl-Kfs-Crd-Grt-Qz gneiss	✓	✓	✓	✗	✗
1143B	Koenap migmatite	Crd-Pl-Kfs-Grt-Qz-Bt gneiss	✓	✓	✓	✓	✓
1147A	Koenap migmatite	Crd-Bt-Grt-Pl-Kfs-Qz gneiss	✓	✗	✗	✗	✗
1147B	Koenap migmatite	Grt-bearing Bt-Ms-Qz gneiss	✓	✓	✓	✓	✓
GS4C	Koenap migmatite	Crd-Pl-Bt-Kfs-Grt-Qz gneiss	✓	✓	✓	✗	✗
GS4D	Koenap migmatite	Crd-bearing Bt-Kfs-Pl-Grt-Qtz gneiss	✓	✓	✓	✗	✗
GS10A	Bysteek Formation	Calc-silicate	✓	✓	✓	✗	✗
GS15A	Bysteek Formation	Opq-Bt-Hbl-Pl-Kfs-Qz gneiss	✓	✗	✗	✗	✗
GS19A	Bysteek Formation	Marble	✓	✓	✓	✓	✓
1139A	Swartoup Pluton	Granodiorite	✓	✓	✓	✗	✗
1140A	Swartoup Pluton	Granodiorite	✓	✓	✓	✗	✗
1144A	Swartoup Pluton	Granodiorite	✓	✓	✓	✗	✗
1145A	Swartoup Pluton	Granodiorite	✓	✓	✓	✓	✓
1146A	Swartoup Pluton	Granodiorite	✓	✓	✓	✓	✓
1149A	Swartoup Pluton	Granite	✓	✓	✓	✓	✓
1151A	Swartoup Pluton	Orthopyroxene-bearing monzodiorite	✓	✓	✓	✓	✓
GS5A	Swartoup Pluton	Granite	✓	✓	✓	✓	✓
GS9A	Swartoup Pluton	Leucogranite	✓	✓	✓	✓	✓
GS9B	Swartoup Pluton	Granite	✓	✓	✓	✓	✓
GS10B	Swartoup Pluton	Orthopyroxene-bearing monzodiorite	✓	✓	✓	✓	✓
GS11A	Swartoup Pluton	Granite	✓	✗	✗	✗	✗
GS11C	Swartoup Pluton	Orthopyroxene-bearing monzodiorite	✓	✗	✗	✗	✗
GS15B	Swartoup Pluton	Orthopyroxene-bearing quartz monzonite	✓	✓	✓	✓	✓
GS15C	Swartoup Pluton	Granite	✓	✓	✓	✓	✓
GS16A	Swartoup Pluton	Quartzolite	✓	✓	✓	✓	✓
GS1A	Hybrid rock	Granodiorite	✓	✓	✓	✓	✓
GS7A	Hybrid rock	Granodiorite	✓	✓	✓	✓	✓
GS11D	Hybrid rock	Pyroxene-bearing granodiorite	✓	✓	✓	✓	✓
GS13A	Hybrid rock	Pyroxene-bearing granite	✓	✓	✓	✓	✓
GS13B	Hybrid rock	Pyroxene-bearing granite	✓	✓	✓	✓	✓
1136A	Polisiehoek Gg	Bt-Kfs-Pl-Qz gneiss	✓	✓	✓	✓	✓
1142A	Polisiehoek Gg	White granite	✓	✓	✓	✓	✓
1147C	Polisiehoek Gg	Bt-Kfs-Pl-Qz gneiss	✓	✓	✓	✗	✗
1148A	Polisiehoek Gg	Qz-Kfs gneiss	✓	✓	✓	✓	✓
1148B	Polisiehoek Gg	Qz-Kfs gneiss	✓	✓	✓	✗	✗
1152A	Polisiehoek Gg	Grt-Pl-Qz-Kfs granofels	✓	✓	✓	✓	✓
GS4B	Polisiehoek Gg		✓	✓	✓	✗	✗
GS4E	Polisiehoek Gg	Pl-Kfs-Qz gneiss	✓	✓	✓	✗	✗
GS11B	Polisiehoek Gg	Pl-Kfs-Qz gneiss	✓	✓	✓	✓	✓
GS12A	Mafic dyke	Pyroxenite	✓	✓	✓	✓	✓

Polisiehoek Gg = Polisiehoek Granite-gneiss

2.3.1 X-ray fluorescence

Major and minor element oxides of whole rocks were analysed at the Central Analytical Facility of the University of Stellenbosch. The following procedure was provided by Mareli Grobler, CAF, University of Stellenbosch.

Glass disks were prepared for XRF analysis using 7 g of high purity, trace- and Rare Earth

Table 2.2: *Major, minor and trace element compositions of average greywackes and cratonic shales from Condie (1993).*

	Greywackes				Cratonic shales			
	Archaean		Proterozoic		Archaean	Proterozoic	PAAS†	NASC‡
	Early	Late	Early	Middle				
wt%								
SiO_2	66.10	65.00	65.40	66.10	60.95	63.10	62.80	64.80
TiO_2	0.56	0.61	0.74	0.77	0.62	0.64	1.00	0.70
Al_2O_3	15.30	15.20	15.50	15.00	17.50	17.50	18.90	16.90
FeO^T *	5.50	5.90	6.10	5.80	7.53	5.65	6.50	5.67
MgO	3.50	3.30	2.20	2.10	3.88	2.20	2.20	2.86
CaO	2.50	2.60	2.50	2.60	0.64	0.71	1.30	3.63
Na_2O	2.90	3.10	3.00	2.80	0.68	1.06	1.20	1.14
K_2O	2.00	2.10	2.40	2.50	3.07	3.62	3.70	3.97
P_2O_5	0.12	0.14	0.15	0.14	0.10	0.12	0.16	0.13
ppm								
Ba	325	390	600	600	456	642	650	636
Ce	50.0	52.0	68.0	60.0	60.9	81.7	80.0	67.0
Co	28	30	25	20	31	18	23	26
Cr	318	175	139	80	507	115	110	125
Eu	1.10	1.10	1.20	0.93	1.12	1.32	1.10	1.20
Gd	3.69	3.69	4.45	4.34	4.55	5.60	4.70	5.20
Hf	3.6	4.0	4.0	4.2	4.5	5.2	5.0	6.3
La	25.0	26.0	32.0	28.0	30.7	38.0	38.0	31.0
Lu	0.25	0.25	0.29	0.38	0.39	0.48	0.43	0.46
Nb	12	11	10	10	11.3	16.8	19.0	13.0
Nd	21.0	22.0	29.0	26.0	27.7	37.5	32.0	27.4
Ni	190	75	68	45	221	52	55	58
Pb	17	20	15	10	13	27	20	20
Rb	65	70	80	80	111	165	160	125
Sc	14	15	15	17	21	17	16	15
Sm	3.90	3.90	5.60	4.90	4.85	6.68	5.60	5.60
Sr	220	265	290	240	61	108	200	142
Ta	0.90	0.70	0.76	0.80	0.84	1.4	1.2	1.1
Tb	0.58	0.58	0.66	0.66	0.71	0.90	0.77	0.85
Th	6.0	8.0	8.0	9.0	8.5	14.3	14.6	12.3
U	1.3	1.70	1.8	1.7	2.4	3.4	3.1	2.7
V	106	115	111	140	154	100	150	130
Y	24	25	25	27	28	35	33	27
Yb	1.40	1.40	1.80	2.20	2.43	2.86	2.80	3.10
Zr	154	160	156	148	151	196	210	200

* = total Fe as FeO
† = "post-Archaean Australian Shale"
‡ = "North American shale composite".

Table 2.3: *Major, minor and trace element compositions of average cratonic sandstones (Condie, 1993) and selected* ~ 1.6 Ga *greywackes (Absar and Sreenivas, 2015).*

	Cratonic sandstones (Condie, 1993)		Greywackes (Absar and Sreenivas, 2015)				
	Archaean	Proterozoic	N6†	S1†	S2†	S3†	Average‡
wt%							
SiO_2	91.53	92.15	67.88	66.35	59.47	67.50	66.78
TiO_2	0.40	0.17	0.58	0.62	1.01	0.66	0.61
Al_2O_3	4.28	3.87	14.24	17.12	14.09	11.70	16.08
FeO^T *	0.38	1.32	4.04	5.79	9.82	8.60	5.01
MnO			0.09	0.06	0.12	0.06	0.08
MgO	0.76	0.55	2.27	2.01	3.44	3.35	2.84
CaO	0.20	0.45	4.36	3.21	2.56	4.25	1.96
Na_2O	0.32	0.51	2.51	0.09	4.69	0.08	1.42
K_2O	0.96	0.88	3.34	3.92	3.39	2.62	4.41
P_2O_5	0.02	0.03	0.13	0.19	0.31	0.22	0.16
ppm							
Ba	161	190		1583	2935	942	
Ce	21.0	21.6		92.3	67.0	66.1	
Co	7	3		19.5	30.2	28.8	
Cr	102	24		57	130	129	
Cs				5.92	2.11	3.12	
Dy				5.31	4.33	4.23	
Er				3.21	2.72	2.12	
Eu	0.34	0.36		1.42	1.59	1.14	
Ga				13.9	19.7	12.7	
Gd	1.04	1.52		5.09	4.3	4.12	
Hf	2.7	2.5		4.45	3.38	4.57	
La	11.3	10.1		55.5	41.0	43.0	
Lu	0.09	0.13		0.43	0.39	0.39	
Nb	4	4		7.98	8.76	7.95	
Nd	9.0	9.0		39.0	30.7	29.2	
Ni	23	11		14.3	8.5	20.8	
Pb	19	20		17.5	26.5	29.0	
Pr				9.41	7.69	7.37	
Rb	32	30		133	72	116	
Sc	2	2		15.80	26.90	14.00	
Sm	1.35	1.75		6.99	5.46	4.85	
Sr	18	27		243	391	204	
Ta	0.31	0.24		0.78	0.66	0.89	
Tb	0.14	0.23					
Th	3.9	4.2		20.6	13.1	12.4	
U	1.1	1.20		2.17	2.37	2.51	
V	11	29		83	152	136	
Y	6	10		33.0	30.1	27.1	
Yb	0.52	0.84		2.95	2.31	2.55	
Zn				110.0	115.3	134.9	
Zr	87	89		115	113	117	

* = total Fe as FeO
† = selected analyses of Absar and Sreenivas (2015)
‡ = average of the analyses of Absar and Sreenivas (2015).

Table 2.4: *Major, minor and trace element data of representative or average pelites. The data is from Gromet et al. (1984), Shaw (1956) and Carmichael (1989).*

	Gromet et al. (1984)			Shaw (1956)					Carmichael (1989)
	1†	2†	3†	4‡,1	5‡,2	6‡,2	7‡,3	8‡,4	9*
wt%									
SiO_2	64.80	64.82	64.82	65.03	64.33	62.93	59.01	67.25	
TiO_2	0.78	0.79	0.80	0.80	1.06	0.99	1.00	0.97	
Al_2O_3	16.90	16.88	17.05	16.52	17.98	18.95	18.93	16.42	
Fe_2O_3				1.69	1.41	1.80	1.27	1.76	
FeO	5.70	5.59	5.70	4.36	4.80	4.34	6.03	4.29	
MnO	0.06	0.07	0.25	0.02	0.06	0.02	0.06	0.02	
MgO	2.85	2.86	2.83	2.45	1.19	1.32	3.08	1.05	
CaO	3.56	3.68	3.51	0.10	0.03	0.15	0.24	0.05	
Na_2O	1.15	1.12	1.13	0.16	0.54	0.68	0.77	0.79	
K_2O	3.99	3.87	3.97	4.26	3.49	3.44	4.42	2.81	
P_2O_5	0.11	0.17	0.15	0.09	0.11	0.12	0.14	0.07	
ppm									
Cr				86	93	160	150	93	
Rb	125								
Eu	2.0	1.24	1.28						
Zr	200			180	260	310	84	310	
Ta	1.12								
Y									30
Yb									3
Nb									20

† = "North American shale composite"
‡,1 = black-grey shale
‡,2 = black slate
‡,3 = grey shale
‡,4 = slate
* = average abundance of elements in shale.

Element-free flux (LiBO2 = 32.83%, Li2B4O7 = 66.67%, LiI = 0.50%) mixed with 0.7 g of the powder sample. Whole-rock major element compositions were determined by XRF spectrometry on a PANalytical AxiosWavelength Dispersive spectrometer at the Central of Analytical Facilities, Stellenbosch University, South Africa. The spectrometer is fitted with a Rh-tube and the following analysing crystals: LIF200, LIF220, PE 002, Ge 111 and PX1. The instrument is fitted with a gas-flow proportional counter and a scintillation detector. The gas-flow proportional counter uses a 90% Argon-10% methane gas mixture. Major elements were analysed on a fused glass disk using a 2.4kW Rhodium tube. Matrix effects in the samples were corrected for by applying theoretical alpha factors and measured line overlap factors to the raw intensities measured with the SuperQ PANalytical software. The concentration of the control standards that were used in the calibration procedures for major element analyses fit the range of concentration of the samples. Amongst these standards were NIM-G (Granite from the Council for Mineral Technology, South Africa) and BE-N (Basalt from the International Working Group).

2.3.2 Laser Ablation Inductively Coupled Plasma Mass Spectrometry

Contents of Sc, V, Cr, Co, Ni, Cu, Zn, Rb, Sr, Y, Zr, Nb, Mo, Cs, Ba, La, Ce, Pr, Nd, Sm, Eu, Gd, Tb, Dy, Ho, Er, Tm, Yb, Lu, Hf, Ta, Pb, Th, and U were determined using inductively coupled plasma mass spectrometry (ICP-MS) at the Central Analytical Facility of the University of Stellenbosch. The following was provided by Riana Rossouw, CAF, University of Stellenbosch.

Instrumental set-up A Resonetics 193 nm Excimer laser connected to an Agilent 7700 ICP-MS is used in the analysis of trace elements in bulk rock samples as well as on single mineral grains. Ablation is performed in He gas at a flow rate of 0.35 L/min, then mixed with argon (0.9 L/min) and nitrogen (0.004 L/min) just before introduction into the ICP plasma. For traces in fusions, 2 spots of 100 µm is ablated on each sample using a frequency of 10 Hz and 2 mJ energy.

Sample preparation Fusion disks prepared for XRF analysis by an automatic Claisse M4 Gas Fusion instrument and ultra-pure Claisse Flux, using a ratio of 1/10 sample/flux, were coarsely crushed and a chip of sample mounted along with up to 12 other samples in a 2.4 cm round resin disk. The mount was mapped, and then polished for analysis.

Quantification Trace elements are quantified using NIST612 for calibration and the %SiO2 from XRF measurement as internal standard, using standard–sample bracketing. Two replicate measurements are made on each sample. The calibration standard was run every 12 samples. A quality control standard is run in the beginning of the sequence as well as with the calibration standards throughout. BCR-2 or BHVO 2G, both basaltic glass certified reference standards produced by USGS (Dr Steve Wilson, Denver, CO 80225), is used for this purpose. A fusion control standard from certified basaltic reference material (BCR-2, also from USGS) is also analysed in the beginning of a sequence to verify the effective ablation of fused material. Data was processed using Glitter software, distributed by Access Macquarie Ltd., Macquarie University NSW 2009.

2.3.3 Multi-collector Inductively Coupled Plasma Mass Spectrometry

Rb/Sr and Sm/Nd isotopic ratios were determined for twenty-seven samples, in solution, using MC-ICP-MS at the University of Cape Town's Department of Geological Sciences, Rondebosch, South Africa. The analytical procedure was kindly provided by Petrus Le Roux, Department of Geological Sciences, University of Cape Town. Further descriptions of the isotopic analyses used may be found in Harris et al. (2015).

Analyses are performed using a Nu Instruments HR in the MC-ICP-MS facility, housed in the University of Cape Town's Department of Geological Sciences. Powdered samples are digested in concentrated HF:HNO_3 for 48 hours at 140°C in closed Teflon beakers. They are then dried and converted to nitrate. Following this the samples undergo concentrated HNO3 enamel digestion for 1 hour at 140°C in closed Teflon beakers. Separation of Sr for enamel samples is done following the procedure of Pin et al. (1994). Sequential Sr, Pb and Nd separation is done after Pin et al. (2014).

Strontium is analysed as 200 ppb 0.2% HNO3 solution, using NIST SRM987 as a reference standard. A normalising value of 0.710255 is used for $^{87}Sr/^{86}Sr$. Strontium isotope data is corrected for; (i) Rb interference using the measured ^{85}Rb signal and natural $^{85}Rb/^{87}Rb$ ratio, and (ii) instrumental mass fractionation using exponent laws and $^{86}Sr/^{88}Sr = 0.1194$.

Neodymium isotopes are analysed as 50 ppb 2% HNO3 solution, using a Nu Instruments DSN-100 desolvating nebuliser. JNDi-1 is used as reference standard, and 0.512115 is used as the $^{143}Nd/^{144}Nd$ normalising value (*c.f.* Tanaka et al., 2000). Data are corrected for; (i) Sm and Ce interference using the measured ^{147}Sm and ^{140}Ce signals, and natural Sm and Ce abundances, and (ii) instrumental mass fractionation using exponent laws and $^{146}Nd/^{144}Nd = 0.7219$.

2.4 U/Pb Zircon dating

U/Pb zicon age data were provided by Professor Dirk Frie (University of Cape Town, formerly University of Stellenbosch). The results are reported in Section 4.6. The analytical procedures used are as in Bial et al. (2015a), and are summarised here.

At the Central Analytical Facility of the University of Stellenbosch, zircon was dated from one sample from the Koenap Formation migmatite, one sample from the Swartoup Pluton and one sample from the Polisiehoek Granite-gneiss, using SF-LA-ICP-MS (Frei and Gerdes,

2009). The U-Pb data were acquired by laser ablation–single collector–magnetic sectorfield–inductively coupled plasma–mass spectrometry employing a Thermo Finnigan Element2 mass spectrometer coupled to a Resonetics Resolution S155 excimer laser ablation system. The age data were obtained by single spot analyses with a spot diameter of 30 µm and a crater depth of approximately $15 - 20$ µm. Zircon reference materials used were the 91500 (Wiedenbeck et al., 1995) and M127 (Nasdala et al., 2008; Mattinson, 2010). The calculation of concordia ages and plotting of concordia diagrams were performed using Isoplot (Ludwig, 2012).

CHAPTER 3

Field relationships and petrography

The study area is located on farm Oup 80, *ca.* 30 km east of Onseepkans, Northern Cape, South Africa (Figure 1.2). The antiformal structure (Figure 1.3) described by Moen and Toogood (2007) lies within the study area and is clearly visible in satellite imagery. Figure 3.1 shows a sample map superimposed onto a satellite image of the area. The Swartoup Pluton is readily distinguished from other rock types by its grey colour and its upper margin has been overlain by red dashes (Figure 3.1). The Polisiehoek Granite-gneiss bounds the Swartoup Pluton stratigraphically from above and below and is distinguished from other rock types by its red-brown weathering colour. The upper margins of the Polisiehoek Granite-gneiss layers have been traced with a green dashed line in Figure 3.1. West of the antiform are Koenap Formation migmatites and Bysteek Formation metabasites and calc-silicates, which form parts of the Arribees Group. The migmatites of the Koenap Formation are from here on referred to as Koenap migmatites. Large rafts of Koenap migmatite are exposed in the western limb of the antiform, commonly surrounded by Polisiehoek Granite-gneiss, but are also found within the Swartoup Pluton (Figures 3.1, 3.2b). Bysteek Formation calc-silicates and metabasite commonly are exposed within the Swartoup Pluton but are also found intercalated with Koenap migmatite outcropping in the western Polisiehoek Granite-gneiss limb of the antiform (Section 3.1). Marbles of the Bysteek Formation are exposed within the Swartoup Pluton and are visible on the sample map as white layers that curve with the pluton, reflecting the deformation of the units. Pegmatite outcrops are also highly visible in the sample map as white coloured bodies. They intruded throughout the sequence, but do not form layers curving

with the pluton like marble does. The pegmatites exposed as dykes within the Swartoup Pluton commonly mimic isogons near the hinge of the pluton.

Specific rocks from the Swartoup Pluton are referred to as Swartoup granitoids unless they have been geochemically analysed and classified, in which case the appropriate nomenclature is used. Igneous rocks are classified using the TAS diagram (Figure 4.1a; after Middlemost, 1994) and the R_1R_2 diagram (Figure 4.1b; after De la Roche et al., 1980). Calc-silicates of the Bysteek Formation are from here on referred to as Bysteek calc-silicates, and the Formation's mafic calc-silicate rock as Bysteek mafic calc-silicate. Mineral abbreviations used are after Whitney and Evans (2010). The abbreviation Afs is used to indicate alkali feldspar, whether potassic or sodic, where no analyses to determine the feldspar composition were carried out. When white mica is identified, the abbreviation Ms is used, though no analyses to confirm muscovite were performed.

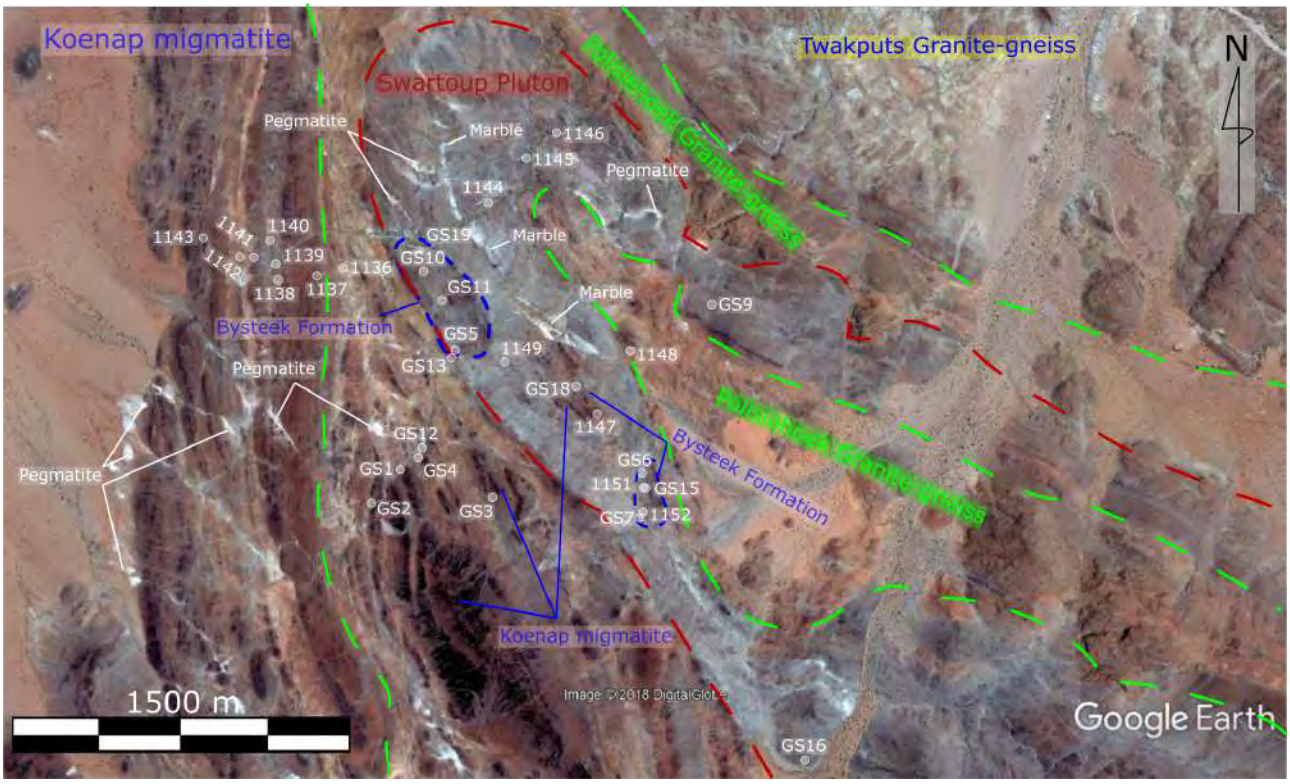

Figure 3.1: *The satellite image shows the spatial relationships of the rock-types of the study. Hosted in an antiformal structure are the Swartoup Pluton (bounded in red) and its Polisiehoek Granite-gneiss core (bounded in green). Stratigraphically upward from the Swartoup Pluton is another Polisiehoek Granite-gneiss layer. West of the antiform are migmatites of the Koenap Formation and calc-silicates of the Bysteek Formation. These metasediments are also exposed within the Swartoup Pluton itself. Rafts of Koenap migmatite outcrop within the Polisiehoek Granite-gneiss on the western limb of the antiform. Pegmatites intrude throughout the sequence (image ©2018 Google).*

Section 3.1 presents an overview of the study area, along with key features that differentiate the various rock types from one another. Macroscopic and microscopic petrographic descriptions

of the collected rock specimens are presented in Section 3.2. The various rock types of the study are presented chronologically. The metasedimentary Koenap and Bysteek Formations are the oldest rocks. The Swartoup Pluton post-dates (Section 4.6) Koenap migmatite and is believed to have intruded them (see Figure 3.9, Section 3.1.3). The hybrid rock is subsequently presented, and using field associations and geochemical evidence (Sections 3.1.4, 3.2.4, 3.3), this study will demonstrate this rock type developed after intrusion of the Swartoup Pluton. Geochemical considerations suggest the hybrid rock is genetically related to the Swartoup Pluton and the Bysteek calc-silicates (Section 5.1). The Polisiehoek Granite-gneiss is described and is believed to post-date intrusion of the Swartoup magma. This is supported by field evidence (Section 3.1.5) and U/Pb zircon data (Section 4.6). Lastly a mafic dyke is described, which was investigated as a possible contaminant of Swartoup magma.

3.1 Field overview and rock type distinctions

Figure 3.2 shows typical scenery encountered in the study area. The Koenap migmatites have a black 'desert varnish' weathering colour, which aides in their distinction (Figure 3.2d). Jointing and subsequent erosion also leave them more rounded than other rock types, especially the calc-silicate and mafic calc-silicate rocks of the Bysteek Formation, which are more angular (Figure 3.2a,b,d). Weathering of the Polisiehoek Granite-gneiss leaves them with a characteristic red-brown colour, readily distinguishing them from the Koenap migmatites (Figure 3.2c,d).

Between ridges of weathered rock, the ground is usually covered by scree. Commonly this scree comes from the metasediments that form ridges, but within the Swartoup Pluton smaller ridges and boulders of granitoid are commonplace as well. Domes of Swartoup granitoid are also commonplace within the Pluton. At locality GS18, ridges of Bysteek calc-silicate (Figure 3.2a) and Koenap migmatite (Figure 3.2b) crop out in the western limb of the Swartoup Pluton. The photographs also show the typical scree covering both the ground and the Swartoup Pluton.

The granitoids of the Swartoup Pluton are readily distinguished in the field by their typical grey colour and biotite modes which are higher than the other rock types in the study area (except for the Bysteek Formation, which is generally darker coloured and is not igneous). Large feldspar phenocrysts, larger than those in other rock types, are also indicative of the Swartoup Pluton rocks (Figure 3.7a,b,c), though not a characteristic shared by all of them (Section 3.2.3). Localities of typical Swartoup granite are shown in Figures 3.7a and 3.7b.

The hybrid rock of this study is easily distinguished in the field by its felsic nature (see Section 3.1.4). The rocks are commonly pale-cream or off-white coloured and rich in plagioclase

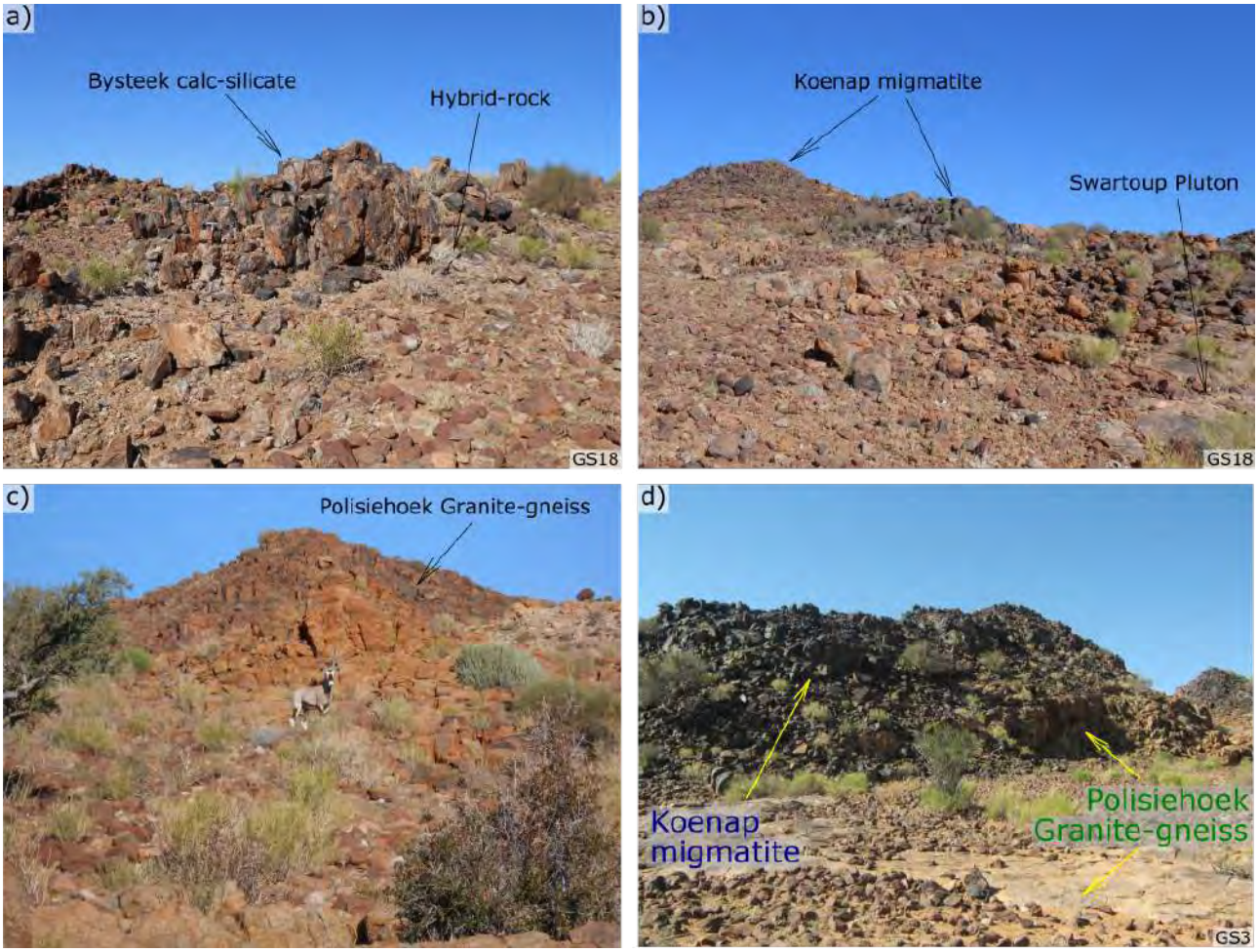

Figure 3.2: *The field photographs show scenery typical of the study area. Locality GS18 is situated within the western limb of the Swartoup Pluton, surrounded by exposed ridges of weathered Bysteek calc-silicate (a) and Koenap migmatite (b). Between these ridges the ground is covered by Swartoup granitoids and scree sourced from both the granitoids and the metasediments. At the contact between the calc-silicate ridge in (a) and the Swartoup Pluton is a thin layer (< 0.5 m) of hybrid rock. (c) The Polisiehoek Granite-gneiss has a characteristic red-brown weathering colour (gemsbok for scale). (d) Black, desert varnish weathered Koenap migmatite contacting red-brown coloured Polisiehoek Granite-gneiss.*

and K-feldspar. They have characteristically high modes of subhedral to euhedral mafic minerals (typically garnet and pyroxene) (Figure 3.26). One exception to this is a grey-coloured, quartz-biotite-rich granodiorite (sample GS1A). This sample, along with all other hybrid rocks, is in contact with Bysteek Formation rocks. Swartoup granitoids are always proximal to these localities, commonly within 10 m.

The Polisiehoek Granite-gneiss is distinguished in the field by its red-brown weathering colour. If the rocks are fresher, they commonly are orange coloured. The Polisiehoek Granite-gneiss characteristically have very low biotite modes relative to other rocks found in the study area. The Polisiehoek rocks typically vary from pencil gneisses (high strain rocks, containing elongated, rod-shaped feldspar lenses) to granofelses (low strain rocks, almost isotropic). Pegmatitic veins also crop out in the study area which, because of their orange colour and cross-cutting relationships,

are assumed to be part of the Polisiehoek Granite-gneiss. One sample of leucogranite associated with the Polisiehoek Granite-gneiss was collected for this study. This rock (sample 1142A, Figure 3.28b) is distinct from leucogranite associated with the Swartoup Pluton by its field associations in its sampling locality.

A mafic dyke striking north-northwest–south-southeast is identified at locality GS12. The pyroxenite is easily distinguished in the field by its dark, black colour and high pyroxene mode (see Figures 3.15 and 3.30). A specimen from the dyke was collected (sample GS12A) to investigate the mafic material as a potential contaminant of the Swartoup Pluton, elaborated on in Section 3.1.6.

3.1.1 Koenap migmatite field observations

Figure 3.3 shows a map of the study localities related to the Koenap Formation. Samples were retrieved from localities 1137, 1138, 1141, 1143, 1147 and GS4. Koenap migmatite sample petrography is presented in Section 3.2.1. Figure 3.4 shows a field photograph of typical stromatic migmatites (locality GS2) of the Koenap Formation in the study area. The Koenap migmatites vary in their leucosome to melanosome ratios, and in the degree to which the melanosome and leucosome have segregated (see Section 3.2.1). However, they all share characteristically high garnet modes in both the leucosome and melanosome (Figure 3.4). Figure 3.4b also shows a mobilised vein of leucosome which cuts the stromatic layering at an acute angle (see van Huyssteen, 2017). Few contacts between the Koenap migmatites and the Polisiehoek Granite-gneiss could be investigated in the study area. The Koenap migmatites form prominent ridges outcropping from the Polisiehoek Granite-gneiss. The Polisiehoek is more susceptible to erosion than the hard Koenap migmatites and forms valleys. The contacts between the two rock types are then sheltered by the migmatites and buried under scree and boulders (for example, see Figure 3.2d).

At locality GS4 a contact was found, however. A raft of Koenap migmatite shares a lit-par-lit intrusive contact with the Polisiehoek Granite-gneiss. This contact is elaborated on in Section 3.1.5, after the Polisiehoek Granite-gneiss has been described. The Koenap migmatite at locality GS4 are compositionally layered. Large layers of leucosome (up to ∼20 cm) are well-segregated from melanosome (5 cm to $>$ 1 m), with sharp, curved contacts between them. The leucosome comprises quartz + plagioclase + K-feldspar + garnet, while the melanosome supports small amounts of leucosome in its quartz-biotite-garnet matrix (Section 3.2.1).

Locality GS18 exposes a contact between Koenap migmatites and the Swartoup Pluton. The

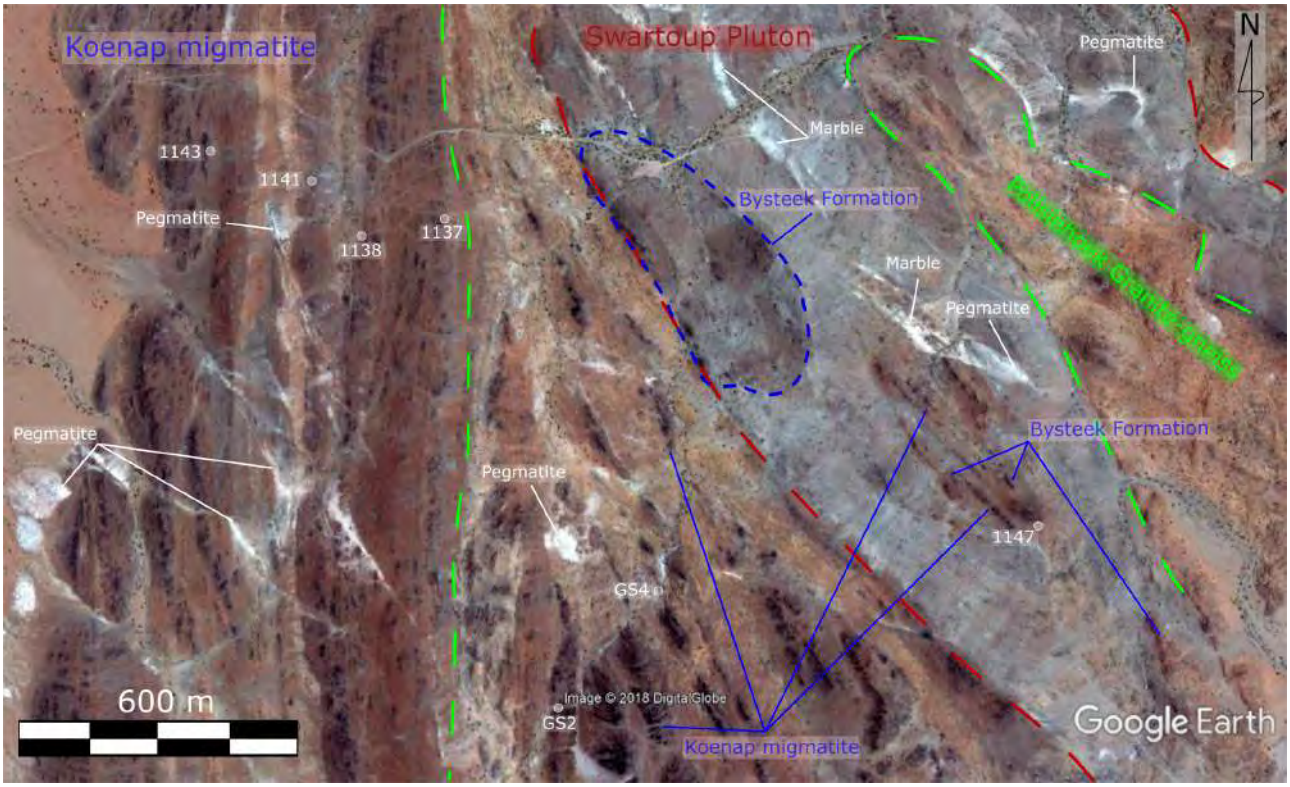

Figure 3.3: *The satellite image shows the investigated localities of the Koenap Formation. Notice the prominent black-weathered rafts of Koenap migmatites outcropping in both the Polisiehoek Granite-gneiss and the Swartoup Pluton (image ©2018 Google).*

contact between the two rock types is sharp, linear and mylonitic. The grain size of the granitoid decreases as the accommodated strain increases towards the migmatite. This strain partitioning suggests syn-shearing of the Swartoup Pluton during its emplacement. However, the Koenap migmatite does not appear to have accomodated any strain during Swartoup Pluton emplacement (see Figure 3.9, Section 3.1.3), so the migmatites were likely already solidified at the time of pluton intrusion.

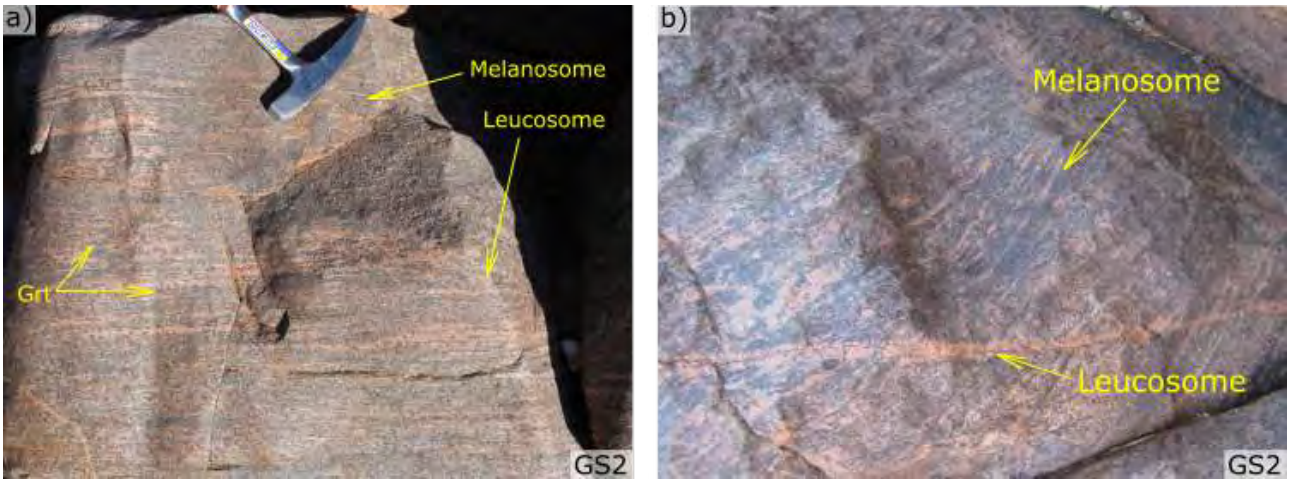

Figure 3.4: *Stromatic migmatites typical of the Koenap Formation in the study area. (a) Notice the garnet porphyroblasts prominent in the leucosome. (b) Mobilised vein of leucosome within stromatic Koenap migmatite, cross-cutting the layering (photograph courtesy of A. van Huyssteen).*

3.1.2 Bysteek Formation field observations

Samples of the Bysteek Formation were retrieved from three localities in this study. These are representative of mylonitic Bysteek mafic calc-silicate (sample GS15A), calc-silicate (sample GS10A) and marble (sample GS19A) of the Bysteek Formation. The sampling localities are shown on the sample map in Section 3.1.4, as there are relatively few Bysteek Formation specimens in the samples set and the hybrid rocks are proximally associated with the Bysteek Formation. Sample petrography of the Bysteek Formation specimens is presented in Section 3.2.2.

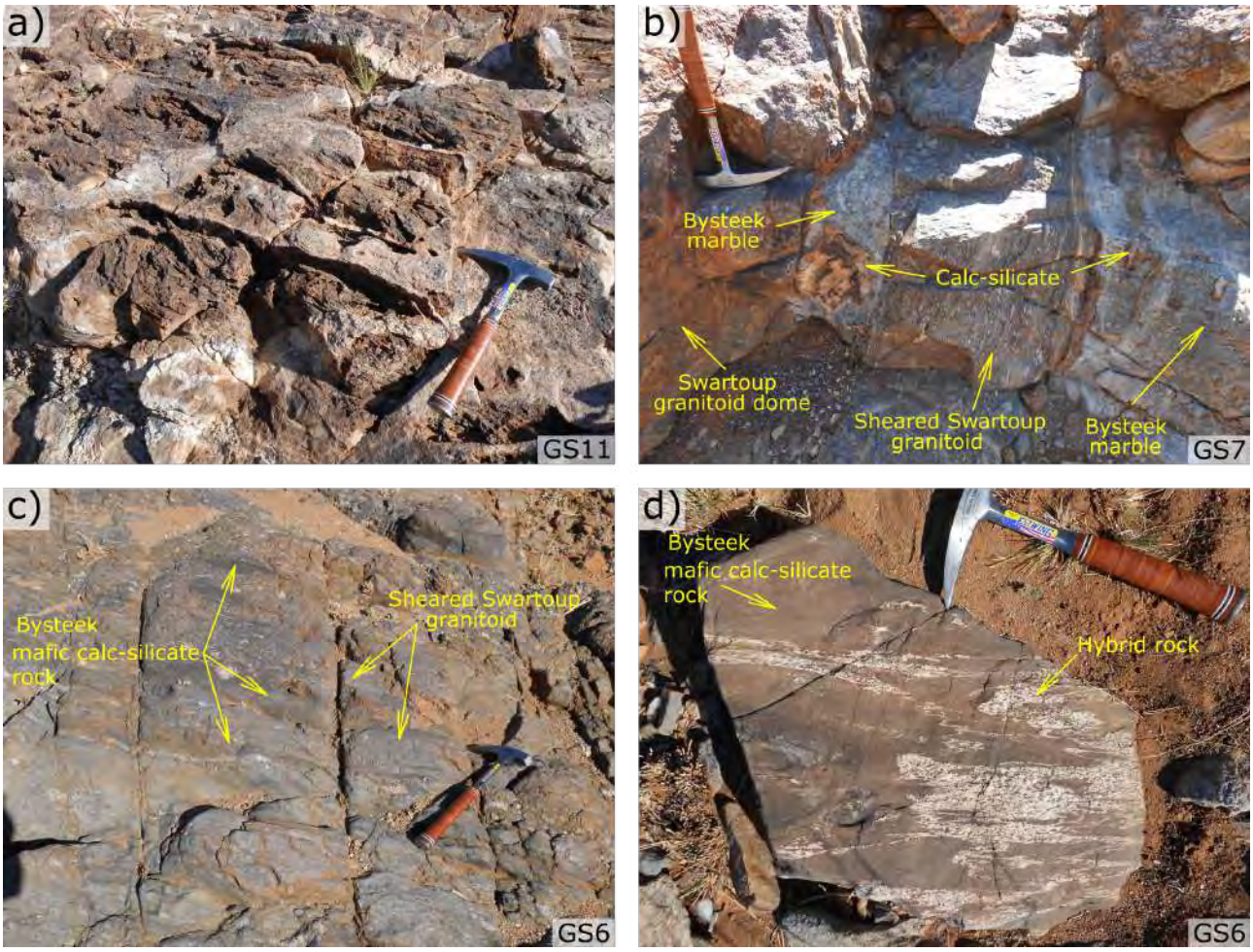

Figure 3.5: *(a) Weathering of Bysteek calc-silicate produces a characteristic structure which helps identify outcrops of Bysteek rock in the field. (b) A dome Swartoup granitoid shares a sharp, linear contact with a blue-grey coloured Bysteek marble. Near the contact lies a sheared dyke of Swartoup granitoid. The surrounding marble hosts fragments of calc-silicate and (out of view) hybrid rock. (c) Lit-par-lit intrusion of Swartoup granitoid into Bysteek mafic calc-silicate. (d) Veins of hybrid rock are folded within a block of Bysteek mafic calc-silicate.*

Figure 3.5a shows weathering structures typical of Bysteek calc-silicate commonly encountered in the study area. Figure 3.5b shows a contact between blue-grey coloured Bysteek marble and a Swartoup granitoid dome, with another sheared dyke of Swartoup granitoid intruding the marble. The contacts between Bysteek marble and Swartoup material are sharp and linear.

The Bysteek marble hosts cm- to dm-sized clasts of folded calc-silicate (Figure 3.5b) and hybrid rock (not pictured).

Bysteek metabasite is intruded lit-par-lit by Swartoup granitoid about 20 m north of locality GS6 (Figure 3.5c). The 5–20 cm wide darker coloured, almost isotropic metabasite layers share sharp, gently curved contacts with the lighter coloured (relative to Bysteek metabasite), feldspathic layers of Swartoup granitoid (10–20 cm wide). At locality GS6, a metabasite boulder (Figure 3.5d) hosts folded veins of hybrid rock. Locality GS6 is at the mouth of a north-northeast—south-southwest directed valley. A ridge of Bysteek Formation forms the western valley side, while the eastern side comprises a ridge of Koenap migmatite. Within this valley are localities 1151 and GS15 (see Section 3.1.3).

About 20 m north of locality GS15, a mylonite from the Bysteek Formation was collected (sample GS15A, Section 3.2.2). The LS-tectonite specimen hosts a 1 cm wide leucocratic vein. This vein appears to be an off-shoot from a nearby 40 cm wide vein of hybrid rock. This vein intrudes the Bysteek outcrop sub-perpendicular to the layering of the Bysteek rocks. Bysteek metabasite layers curve into this dyke of hybrid rock toward the outcrop from which sample GS15A was collected.

At locality GS10 Bysteek calc-silicate outcrops on the eastern slope of a ridge of Bysteek metabasite. The calc-silicate has a grey colour when fresh and contacts a thin (up to 30 cm in places) layer of hybrid rock to the east (Figure 3.12b). Between the grey calc-silicate and the hybrid rock, a layer of orange-coloured calc-silicate pinches and swells (up to 5 cm thick, see Section 3.2.2). A specimen of this calc-silicate and the hybrid rock was collected, though only the calc-silicate portion was crushed and analysed (sample GS10A). Further to the east of this outcrop lies a dyke of Swartoup monzodiorite, from which a specimen was collected (sample GS10B, see Section 3.1.3). The hybrid rock is presented in detail in Section 3.1.4. The Bysteek marble specimen collected for analysis (sample GS19A, Figure 3.18d) was sampled from a white marble layer near the stratigraphic centre of the Swartoup Pluton (locality GS19). This marble layer follows the curvature of the Swartoup Pluton partway around the antiform, which helps distinguish it from pegmatite in satellite imagery.

3.1.3 Swartoup Pluton field observations

Figure 3.6 shows a sample map of all the collected Swartoup granitoid specimens of this study. Samples 1139A and 1140A were collected to the east of the Swartoup Pluton, from a dyke intruded into Koenap migmatite. Samples 1144A, 1145A and 1146A were collected nearer the

hinge of the antiform. These 5 samples together form a group geochemically distinct from the rest of the analysed Swartoup granitoid specimens. These 5 specimens are all granodiorites by the R_1R_2 classification scheme (De la Roche et al., 1980) and together are referred to as Swartoup group 1 from Chapter 4 onwards. The remaining analysed specimens vary geochemically and are referred to as Swartoup group 2 (samples 1149A, 1151A, GS5A, GS9A, GS9B, GS10B, GS15B, GS15C, and GS16A). Swartoup group 2 are geochemically distinct from Swartoup group 1 and each other, in many cases (see Chapters 4, 5 and 6). Petrography of Swartoup granitoid specimens are presented in Section 3.2.3.

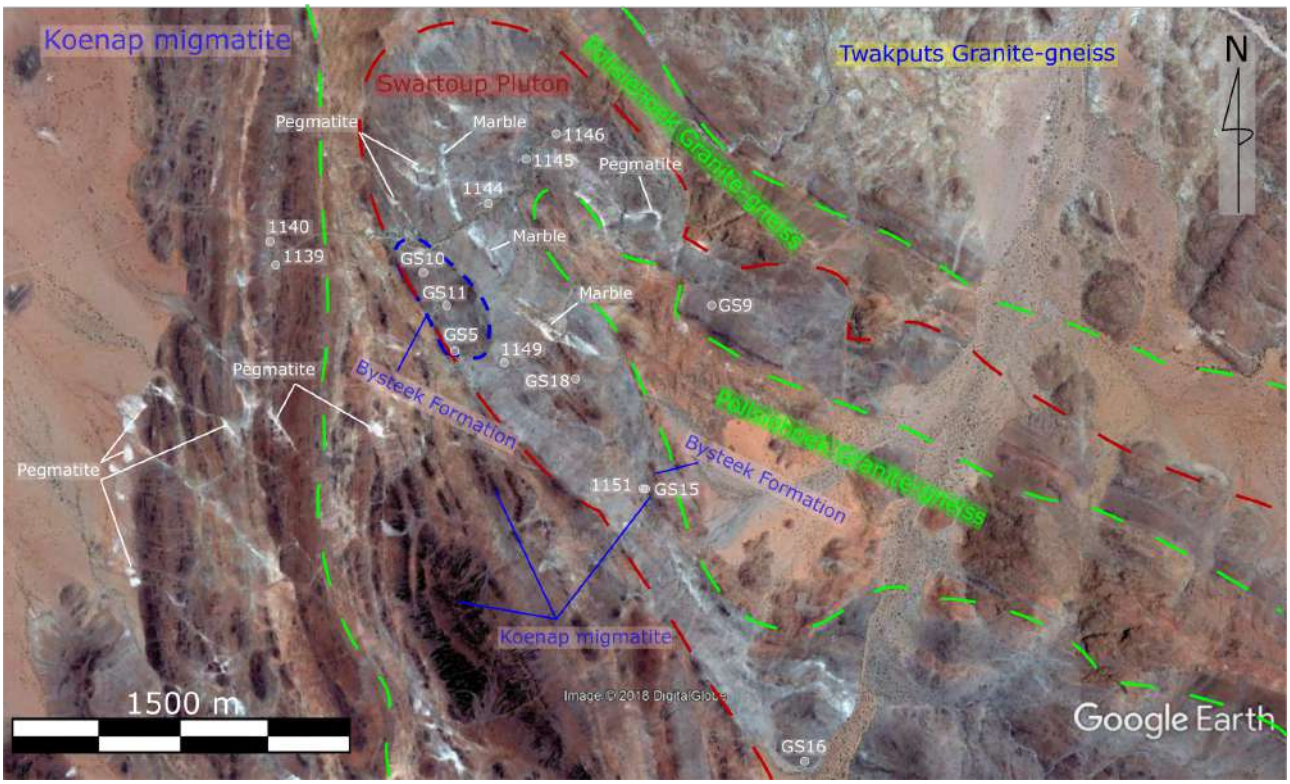

Figure 3.6: *The satellite image shows investigated localities of the Swartoup Pluton. Notice the proximal relationship of garnet-bearing granitoids (1140A, GS15C, GS16A) to Koenap migmatite outcrops, and of pyroxene-bearing rocks (1151A, GS15B, GS10B) to Bysteek Formation. The specimens comprising the geochemically distinct group Swartoup 1 were collected in the north of the study area. Samples 1139A and 1140A were sampled from a dyke to the west of the Pluton, surrounded by Koenap Formation. Samples 1144A, 1145A and 1146A were collected nearer the hinge of the antiform (image ©2018 Google).*

Figures 3.7a and 3.7b show two Swartoup granites. These two rocks were determined to be the dominant, typical varieties of the Swartoup Pluton during field work. Swartoup granites such as in Figure 3.7a (sample GS5A) have a medium-grey colour, and higher biotite modes than the granite in Figure 3.7b, which has a grey-green colour, caused by grey—green-coloured K-feldspar. Discrimination of the different granitoids was impaired in the field due to intense weathering (Figure 3.7b,c). Sampling was conducted with a focus on collecting fresh material for geochemical evaluation. Therefore, the relative proportions of different granitoids, such

as granite, granodiorite and orthopyroxene-bearing monzodiorite, in the sample set are not reflective of the proportions of these within the Swartoup Pluton.

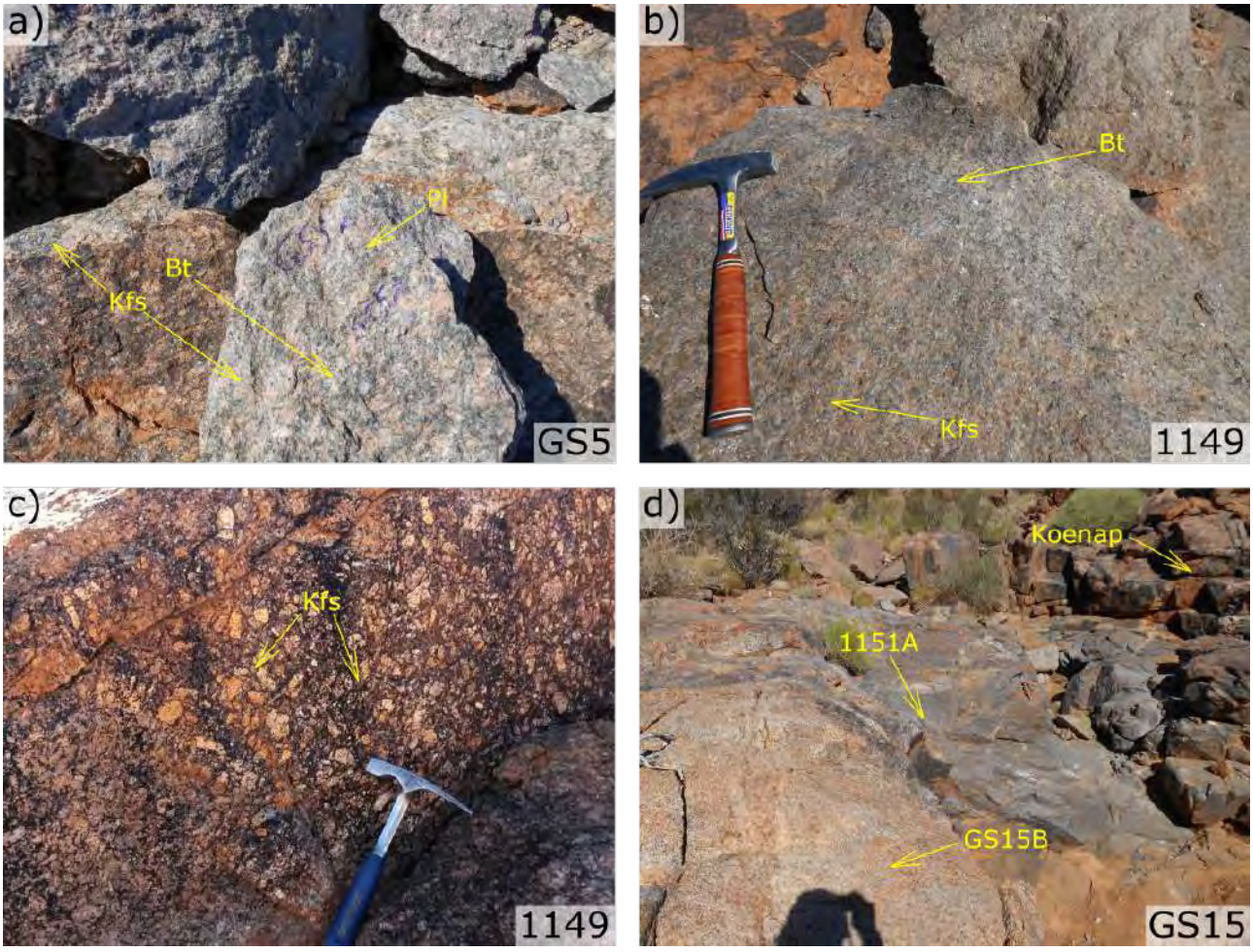

Figure 3.7: *Field photographs of typical Swartoup Pluton rocks. Granite are considered the most typical variety of Swartoup granitoid in the field. They vary in their biotite modes. (a) At locality GS5 the granite has a medium-grey colour. In contrast, the granite at locality 1149 (b) has a grey-green colour, due to its low biotite mode and green-coloured K-feldspar. (c) Lighter-coloured quartz monzonite (sample GS15B) in transitional contact with the darker orthopyroxene-bearing monzodiorite (sample 1151A). An outcrop of Koenap migmatite is seen to the right, and Bysteek Formation outcrops less than 5 m to the left (out of view). (d) Weathering highlights large feldspars typical of Swartoup Pluton. Photographed is a weathered section of the rock in (a).*

Orthopyroxene-bearing Swartoup granitoids

Orthopyroxene bearing granitoids are proximally associated with Bysteek Formation. In all cases where orthopyroxene bearing Swartoup rocks are found, Bysteek Formation outcrops nearby. At locality GS10 a dyke of Swartoup orthopyroxene-bearing monzodiorite (sample GS10B) is exposed less than 10 m from Bysteek Formation rock (including calc-silicates and the hybrid rock, see Section 3.1.4).

Locality GS11 exposes a dome of Swartoup orthopyroxene-bearing monzodiorite, which lies southeast along strike form locality GS10. The sample GS11C was collected from this dome and has very similar modal mineral abundances as the sample GS10B (Table 3.3). This dome is intruded by Polisiehoek Granite-gneiss, shown in Figure 3.14 (sample GS11B, see Section 3.1.5). To the southeast of the area seen in Figure 3.14 lies an outcrop of Bysteek calc-silicate and hybrid rock (Figure 3.12c, Section 3.1.4). Sample GS11A was retrieved about 10 m to east of this Bysteek calc-silicate outcrop, from a mylonitic dyke of Swartoup granitoid.

At locality GS15 (which coincides with 1151), a quartz monzonite with minor orthopyroxene (sample GS15B) shares a transitional contact (2 m) to an orthopyroxene monzodiorite (sample 1151A) (Figure 3.7d). Less than 5 m from these rocks Bysteek Formation outcrops, which forms the eastern side of the valley. The western side of the valley is capped by Koenap migmatite.

Garnet-bearing Swartoup granitoids

Few contacts between the Swartoup Pluton and Koenap migmatites are identified in the field. Commonly, they are lost under scree. At GS15, however, a contact between the Swartoup granitoids and Koenap migmatite was found. The contact at this locality is mylonitised (Figure 3.8a). A vein of garnet-rich material cuts across the mylonite and accumulated in a small body (30 cm across). Material from this body is concordant with the mylonitic layering of the orthopyroxene-bearing monzodiorite. A 15 kg garnetiferous boulder, assumed to be in situ, was collected 3 m along strike from the field of view in Figure 3.8b (sample GS15C).

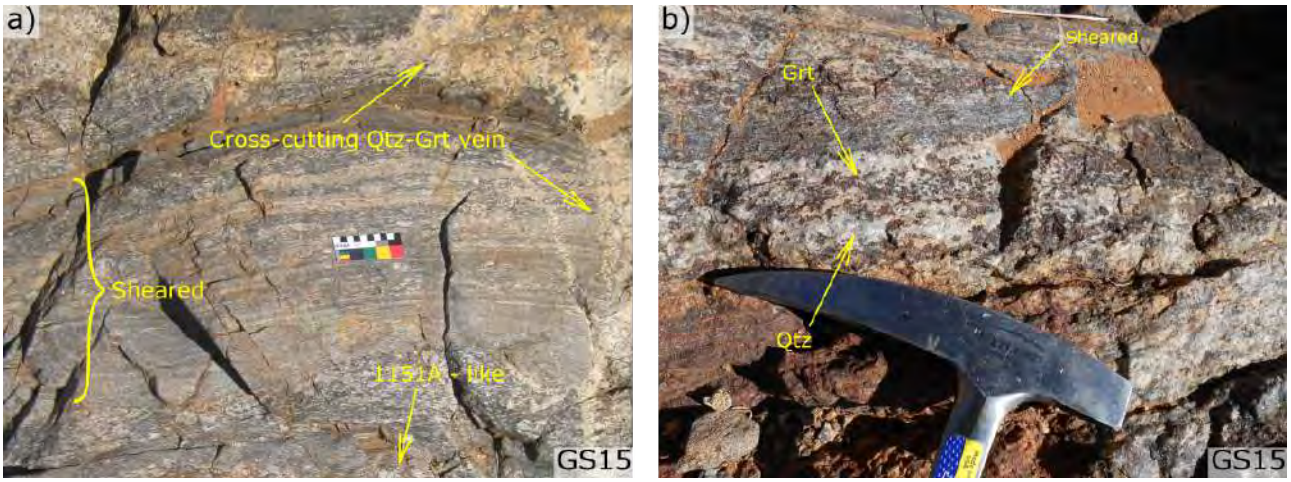

Figure 3.8: *Garnet bearing veins of granitic rock from locality GS15 (same as seen in Figure 3.7c) cross-cutting sheared orthopyroxene-bearing monzodiorite. The vein cross-cuts the layering (right side of the image) with thinner intruding veins as separate features. At the top of the image the vein becomes concordant with the layering/shear plane in the orthopyroxene-bearing monzodiorite. (b) Close-up of the same vein as in (a). The vein containing garnet-rich material here is concordant with the shear plane.*

At locality GS16, multiple veins of garnet-bearing granite outcrop from a ridge of weathered, intercalated Bysteek calc-silicate and metabasite. The western outer margin of the Swartoup Pluton lies about 150 m west of this locality, where large rafts of Koenap migmatites outcrop (Figure 3.6). However, smaller outcrops of Koenap migmatite are also found nearer this locality. These garnet-rich granitic veins host within them large segregation quartz veins and lenses.

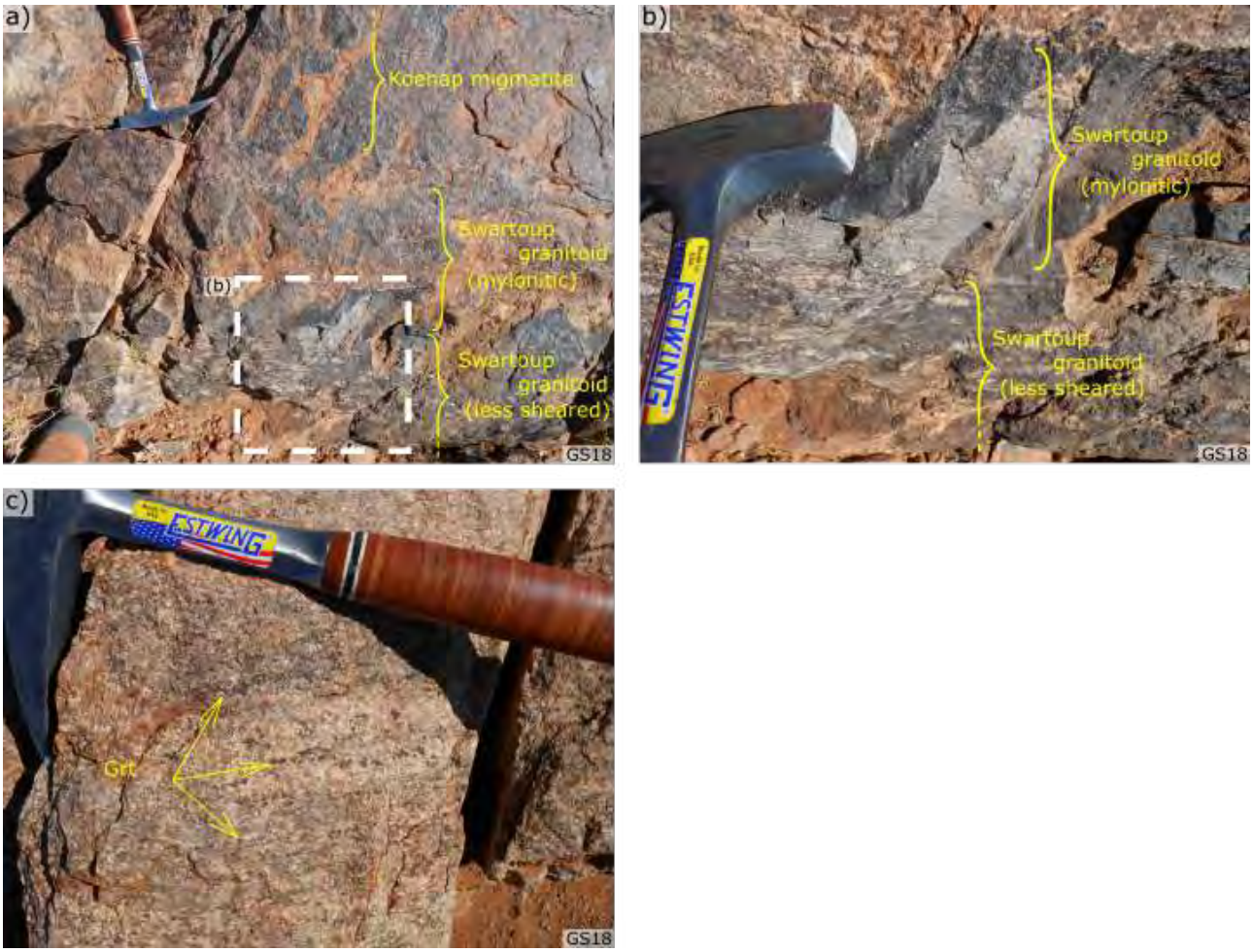

Figure 3.9: *Contacts between Swartoup granitoid and Koenap migmatite are often sheared. At locality GS18 ridges of Koenap migmatite outcrop in the western limb of the Swartoup Pluton. (a) The contact is linear, and the Swartoup material is increasingly sheared towards the contact. The migmatite is not visibly sheared. (b) Close-up of the highlighted area in (a). (c) Layer of garnet-bearing Swartoup granitoid found roughly 3 m away from the Koenap migmatite in (a). This garnet-bearing granitic layer could be tracked laterally for about 10 m.*

At locality GS18, another contact between Swartoup Pluton and Koenap migmatite was found. Locality GS18 lies over Swartoup granitoid, between a ridge of Bysteek calc-silicate to the east and another ridge of Koenap migmatite to the west (Figure 3.2a,b). Figure 3.9 shows the sharp, linear contact. The Swartoup granitoid is mylonitised adjacent to the Koenap migmatite, which appears not to have accommodated any strain. The grain size of the Swartoup granitoid reduces with proximity to the contact from $\sim$ 40 cm away. About 3 m east of this contact (into the Swartoup granitoid) a layer of garnetiferous Swartoup granitoid was found (Figure 3.9c). This

layer could be tracked laterally over about 10 m.

Granitic dyke hosting leucogranitic pods

Figure 3.10 shows a dyke of Swartoup granite from the eastern limb of the Swartoup Pluton (locality GS9). This dyke hosts irregularly shaped pods of leucogranite, one of which is shown in Figure 3.10a. These pods have gradational contacts ($\sim$ 3 cm) to the host granite. Three such dykes were found within 50 m of this locality, along with thinner (5 cm wide) veins of leucogranite. These leucogranitic veins are all mylonitic.

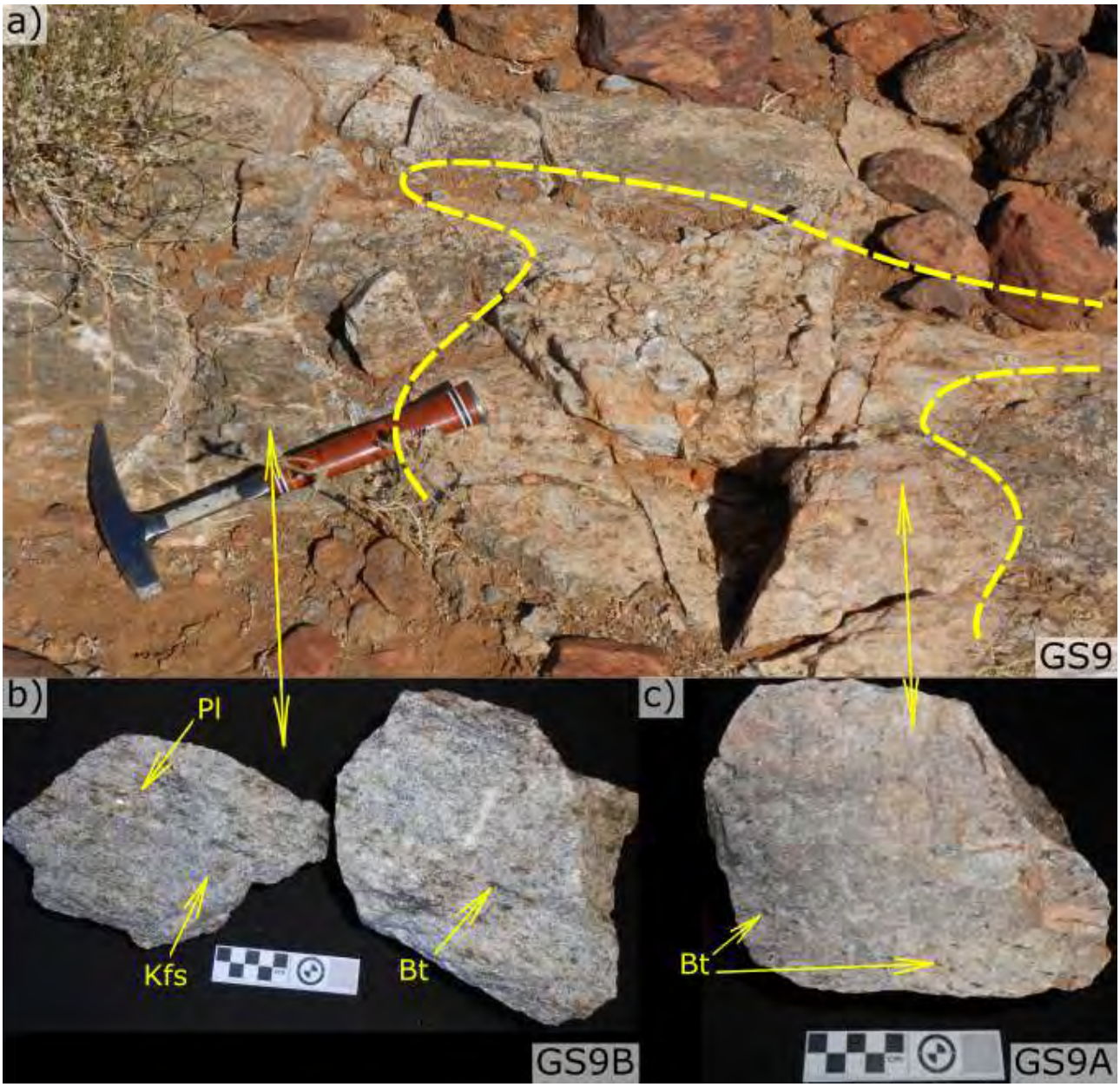

Figure 3.10: *(a) Dyke of Swartoup granite. The granite hosts irregularly shaped pods of leucogranite, which have gradational contacts (3 cm) to the granite. (b) The granite (sample GS9B) is darker coloured and has a strong, pervasive magmatic foliation. (c) In contrast, the leucogranite (sample GS9B) does not display a strong foliation for the lack of abundant biotite.*

Figure 3.10b shows sample GS9B, collected from the Swartoup granite dyke. Figure 3.10c shows sample GS9A, which was collected from one of the largest pods of leucogranite, away from the pod margins.

3.1.4 Hybrid rock field observations

Thin (up to 50 cm) layers of pale-cream to off-white coloured granodioritic rock are found proximally associated with both Bysteek Formation and Swartoup granitoids (Figure 3.12). These are referred to as hybrid rock. This study will demonstrate they result from interaction between Swartoup magma and Bysteek material. Figure 3.11 shows a sample map displaying the sampling localities of the hybrid rock, as well as the Bysteek Formation localities. In addition, locality GS12 has been shown on this map (see Section 3.1.6). Hybrid rock sample petrography is presented in Section 3.2.4.

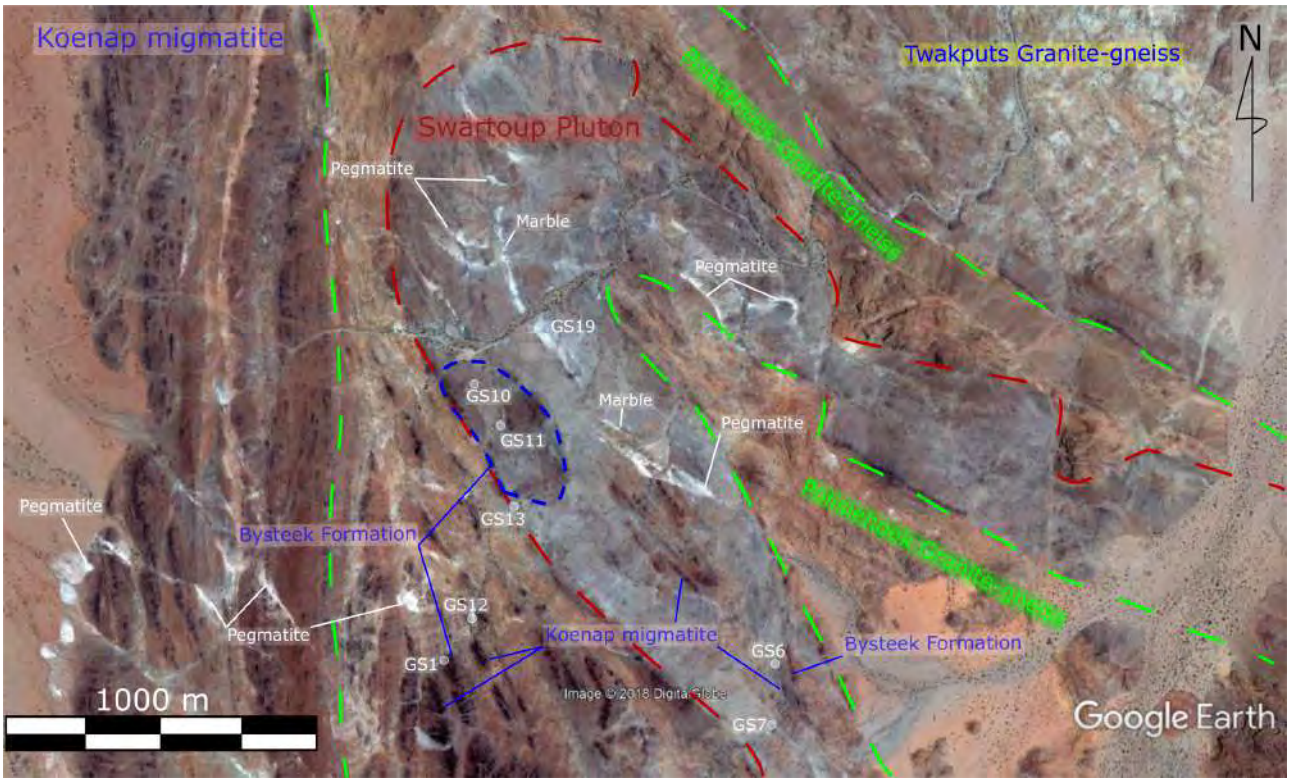

Figure 3.11: *The satellite image shows investigated localities of the Bysteek Formation and an associated hybrid rock. Notice the proximal association of the hybrid rocks (GS1A, GS7A, GS10A, and GS11D) to outcrops of Bysteek Formation and the Swartoup Pluton. The marbles of the Bysteek Formation follow the Pluton around the antiform and can be distinguished from pegmatite which are directed outwards from the Swartoup Pluton. Also shown on this map is the location of a Mafic dyke (GS12, see Section 3.1.6) (image ©2018 Google).*

The hybrid rock are pale, cream-coloured and have prominent mafic minerals. Commonly these mafic minerals are subhedral to euhedral garnet (sample GS7A), or orthopyroxene, clinopyroxene and titanite (samples GS11D, GS13A, GS13B); in a single locality a biotite-rich end-member

is known (sample GS1A). Though only one garnet-rich variety of the hybrid rock has been collected, it together with the pyroxene-rich variety are the typical examples of the hybrid rock. Due to the thin exposures of the rock in the study area (see Figure 3.12), sampling of material sufficiently large for geochemical analyses has proven challenging.

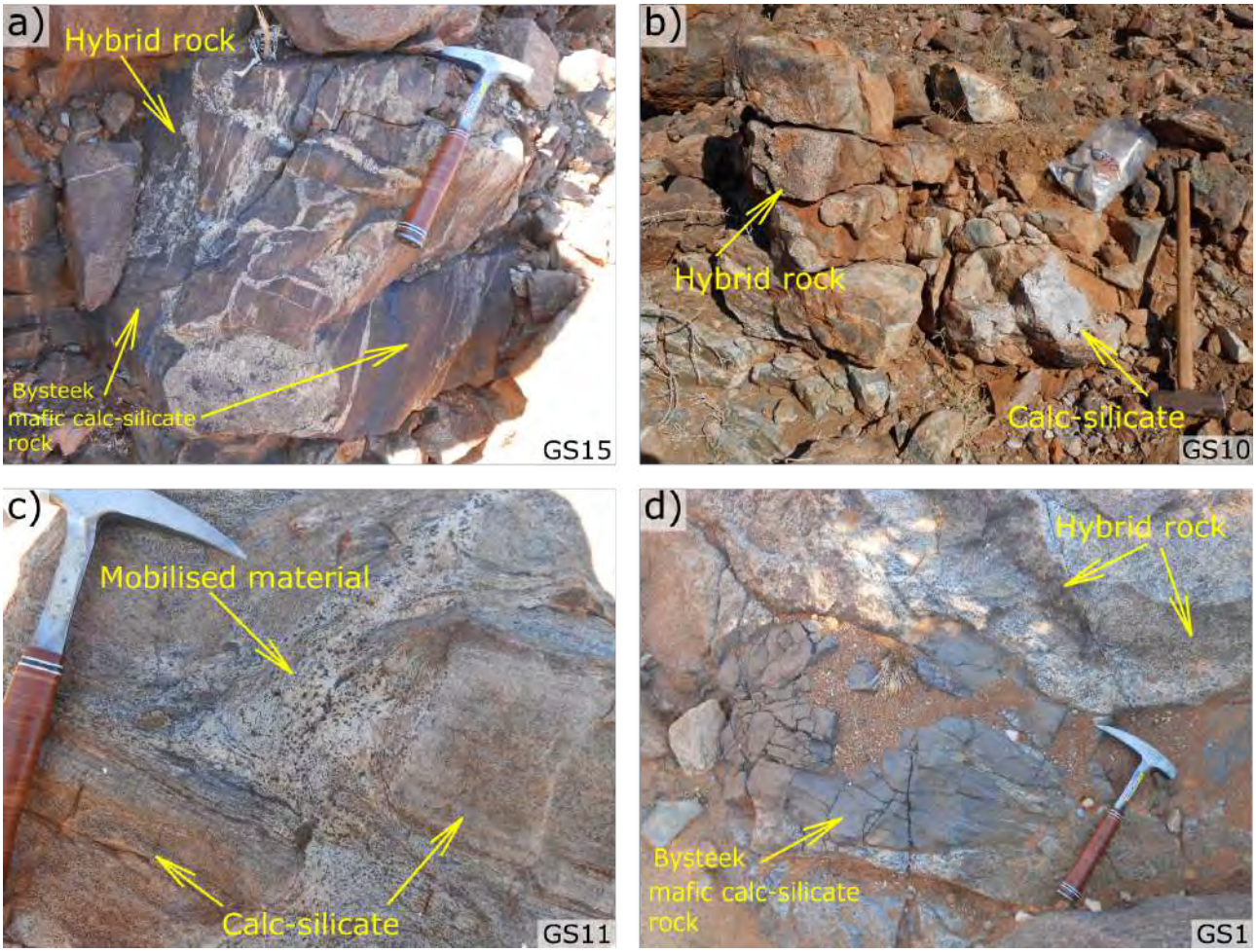

Figure 3.12: *The hybrid rock spatially associated with the Bysteek Formation always is exposed as a thin layer (<0.5 m) contacting Bysteek Formation mafic calc-silicate or calc-silicate. (a) Brecciated mafic calc-silicate with thin veins of hybrid rock. (b) Thin layer of hybrid rock contacting calc-silicate typical of the Bysteek Formation in the study area. (c) An exposure of this Hybrid material mobilised around Bysteek calc-silicate. (d) Xenolith of Bysteek mafic calc-silicate hosted within a large pool (10 m × 30 m) of the hybrid rock. While the hybrid rocks are characteristically pale-coloured, found in small volumes and either garnet or pyroxene rich; this example is the only grey-coloured, biotite rich variety found, and has an unusually large volume; collected as sample GS1A.*

Figure 3.12a–c shows the typical exposures of the hybrid rock. Bysteek mafic calc-silicate, when in contact with the hybrid rock, are commonly brecciated (Figure 3.12a). When the hybrid rock is in contact with Bysteek calc-silicates, it forms a thin layer on the calc-silicate, always facing the nearest the Swartoup granodiorite, such as at locality GS10 (Figure 3.12b). In other occurrences, such as locality GS11, the hybrid rock appears mobilised, cutting through layers of Bysteek calc-silicate (Figure 3.12c). At locality GS11 a large dome of Swartoup monzodiorite

is exposed adjacent to the Bysteek and hybrid rock (about 5 m away). This dome is shown in Figure 3.14b, intruded by Polisiehoek Granite-gneiss (Section 3.1.5). The hybrid rock at locality GS11 is also exposed as a thin layer contacting Bysteek calc-silicate, as at locality GS10. From here the sample GS11D was retrieved, which shows a diffuse contact between the orthopyroxene-clinopyroxene-bearing hybrid rock and Bysteek calc-silicate (see Figure 3.25c, Section 3.2.4).

At locality GS7 layers of a garnet-rich variety of hybrid rock are intercalated with layers of Swartoup granitoid. The contacts between these rock types appear transitional (10 cm), though are commonly mylonitised. Sample GS7A was retrieved from a strain-free layer of hybrid rock. West of this locality is a large dome of Swartoup granitoid, macroscopically similar to the dome at locality GS5. About 7 m northwest of GS7 are layers of blue-grey marble intercalated with dykes of Swartoup granitoid (see Section 3.1.2, Figure 3.5b).

Locality GS13 is located about 30 m south of locality GS5. Here, a ridge of Bysteek calc-silicate outcrops, with Polisiehoek Granite-gneiss intruded on the eastern side of the ridge. At the ridge summit, weathered calc-silicates and blue-grey Bysteek marble is exposed. At the footwall of these Bysteek rocks is a layer comprising irregularly shaped pods of two varieties of hybrid rock. The first is a pegmatitic K-feldspar-rich hybrid rock (sample GS13A). The second variety is finer grained than sample GS13A and has more plagioclase (sample GS13B). These two varieties share sharp contacts in places, and diffuse contacts in others. The pegmatitic K-feldspar-rich variety is found in only one other location in the study area, as a large boulder within the valley containing localities GS6 and GS15/1151.

Figure 3.12d shows a Bysteek mafic calc-silicate xenolith hosted within quartz-biotite-rich hybrid rock (GS1A). This variety of hybrid rock differs from the others in that it has a grey colour and has a much higher biotite mode (see Table 3.4, Section 3.2.3). This locality exposes an unusually large pod of hybrid rock (10 m $\times$ 30 m), which hosts xenoliths of Bysteek mafic calc-silicate (30 cm $\times$ $<$ 1 m), shown in Figure 3.12d. Though the locality is surrounded by outcrops of Koenap migmatite, it is Bysteek Formation which is in direct contact with the pool of hybrid rock. An exposure of Swartoup granitoid lies about 20 m to the southwest. Only one hybrid rock exposure of this variety was found.

3.1.5 Polisiehoek Granite-gneiss field observations

Figure 3.13 shows the Polisiehoek Granite-gneiss sample map. The Polisiehoek Granite-gneisses are characteristically orange-coloured, low biotite mode rocks, commonly with a strong gneissose

fabric. Polisiehoek Granite-gneiss sample petrography is presented in Section 3.2.5.

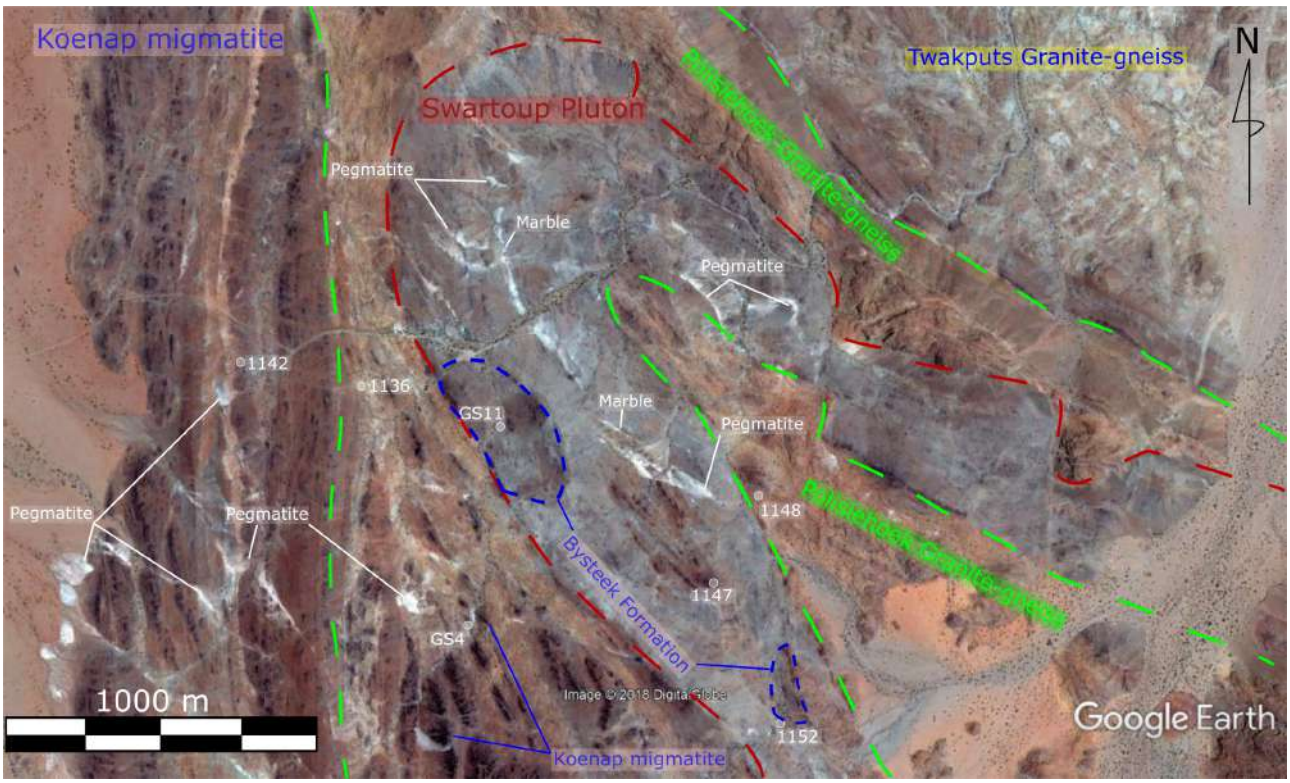

Figure 3.13: *The satellite image shows investigated localities of the Polisiehoek Granite-gneiss. Notice the characteristic orange colour of the rocks, prominent on the satellite image as well as in the field. The Polisiehoek Granite-gneiss form layers stratigraphically above and below the Swartoup Pluton, and also as cross-cutting dykes and veins within the Swartoup Pluton (image ©2018 Google).*

The most sheared Polisiehoek Granite-gneiss specimen collected in the study (sample 1136A) was collected near the Polisiehoek Granite-gneiss–Koenap migmatite contact in the western limb of the antiform. Samples 1148A and 1148B are also mylonitic and were collected near the contact between the Swartoup Pluton and the Polisiehoek Granite-gneiss core of the antiform.

A dyke of Polisiehoek Granite-gneiss intruded at locality 1147, near Koenap and Bysteek outcrops in western limb of the Swartoup Pluton. Sample 1147C was retrieved from here and is a highly sheared LS-tectonite. Locality 1152 lies about 30 m south of the valley containing localities GS6 and GS15. Sample 1152A, however is a granofels, and appears to not have accommodated any strain, possibly due to strain partitioning.

The Polisiehoek white granite specimen, sample 1142A, was collected from a dyke of Polisiehoek material which intruded Koenap migmatite west of the antiform. This sample has a weak, pervasive gneissose fabric.

At locality GS4 lies a sharp, lit-par-lit intrusive contact between Polisiehoek Granite-gneiss and a raft of Koenap migmatite (Figure 3.14a). Stringers of Polisiehoek material intrude the

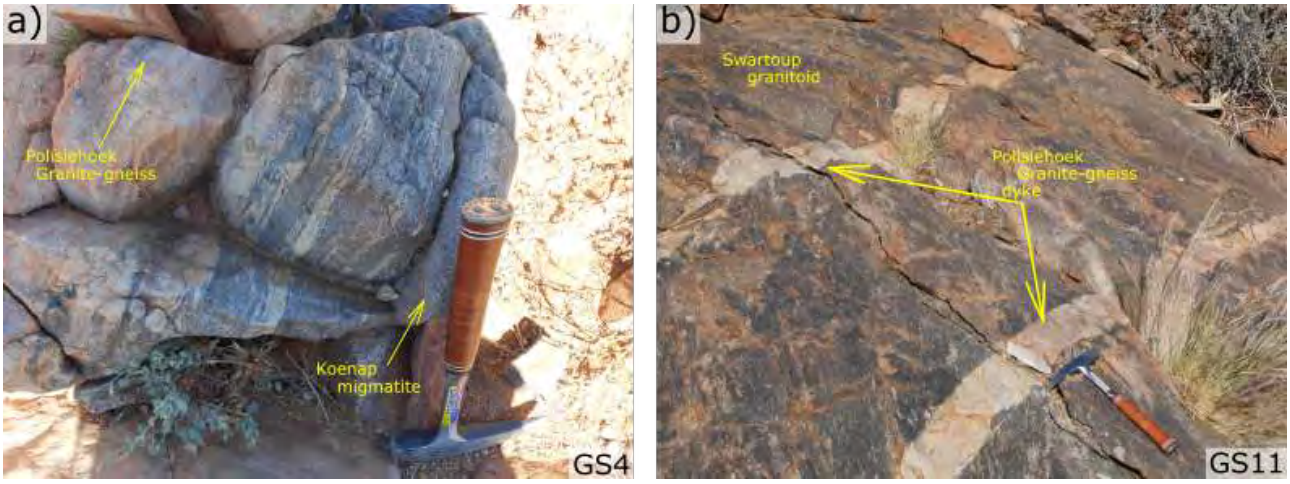

Figure 3.14: *(a) Contact between the Polisiehoek Granite-gneiss and a raft of Koenap migmatite. Veins of Polisiehoek Granite-gneiss intrude into Koenap migmatite concordant to the migmatite metamorphic foliation, defining a transitional contact less than* 0.5 m *wide. (b) Two dykes of Polisiehoek Granite-gneiss intruding a dome of Swartoup monzodiorite along sharp, linear contacts. Each dyke is about* 15 cm *wide, and could be tracked over 100 m south, towards a Polisiehoek Granite-gneiss ridge.*

Koenap migmatite up to about 40 cm, defining the transitional contact. No Koenap material xenoliths are found within the Polisiehoek Granite-gneiss. This contact can be tracked laterally about 15 m, before it is lost under scree from surrounding Koenap migmatite ridges.

Contacts between the Polisiehoek Granite-gneiss and the Swartoup Pluton, *sensu stricto*, are commonly extensively weathered and eroded mylonite zones (up to 20 m wide), confirmed by van Huyssteen (2017). At locality GS11, two veins of Polisiehoek Granite-gneiss (each 20 cm wide) intrude a dome of Swartoup monzodiorite (Figure 3.14b). The veins intrude along sharp, linear contacts. Fragments of Swartoup material (up to 1 cm $\times$ 10 cm) appear to have been ripped from the vein walls and lie up to 7 cm within the veins. The margins of these xenolithic fragments are sharp and linear. The intruded Swartoup monzodiorite was sampled along strike as sample GS10B. No Polisiehoek material appears to intrude the host monzodiorite.

3.1.6 Mafic dyke field observations

A mafic dyke is exposed at locality GS12, where it has intruded Polisiehoek Granite-gneiss. The dyke measures about 3 m $\times$ 20 m in aerial exposure (Figure 3.15a), and a smaller off shoot (about 30 cm $\times$ 1 m) lies about 15 m away to the west. The well-foliated basalt intrudes the Polisiehoek Granite-gneiss along sharp, linear contacts.

The dyke shows brittle deformation features. Two sets of granitic veins cross-cut the dyke. The first are oriented perpendicular to the dyke. These are offset along shear zones which have been filled by granitic material (Figure 3.15b). This second set of veins can be tracked about 15 m

into the surrounding Polisiehoek Granite-gneiss.

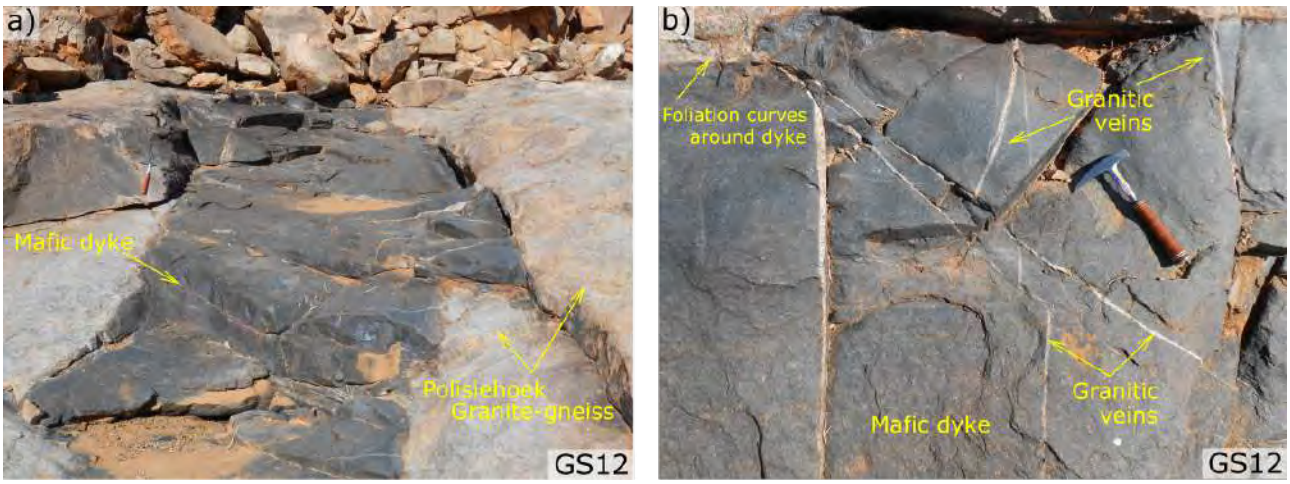

Figure 3.15: *(a) The mafic dyke (3 m × 20 m) shares sharp, linear contacts with Polisiehoek Granite-gneiss. (b) The metamorphic foliation of the Polisiehoek Granite-gneiss curves around the mafic dyke and veins of granitic material cross-cut perpendicular to the mafic dyke. A second set of granitic veins fill shear zones which offset the first set.*

The granitic material is paler-coloured than the Polisiehoek Granite-gneiss and is believed to be related to pegmatite intrusions. A large pegmatite body lies about 200 m west of this locality.

A sample was collected to investigate the mafic material as a possible contaminant of the Swartoup Pluton. Petrography of the collected specimen (sample GS12A) is presented in Section 3.2.6.

3.2 Sample Petrography

A total of 44 rocks (see Table 2.1) were collected from the Koenap Formation (Figure 3.3, 10 migmatite samples, 8 analysed), Swartoup Pluton (Figure 3.6, 16 samples, 14 analysed), Bysteek Formation (Figure 3.11, 3 samples, 2 analysed), hybrid rock (Figure 3.11, 5 samples, 5 analysed), Polisiehoek Granite-gneiss (Figure 3.13, 10 samples, 9 analysed) and the mafic dyke (Figure 3.6) described in the previous section. The igneous rocks of the study are classified using the TAS diagram (Figure 4.1a, after Middlemost, 1994) and the R_1R_2 diagram (Figure 4.1b, after De la Roche et al., 1980). Mineral abbreviations used are those of Whitney and Evans (2010). The abbreviation Ms is used for white mica, though no analyses to confirm muscovite were performed. The modal contents of the specimens were determined visually from thin sections and whole-rock specimens (Tables 3.1–3.3, 3.5, 3.7 and 3.8).

3.2.1 Koenap migmatite

The migmatites of the Koenap Formation generally range from light-brown to dark-grey in colour. They vary in their leucosome/melanosome ratio and the more leucocratic specimens (samples 1137A, 1143A, 1147A and GS4D) commonly have higher modes of alkali feldspar and plagioclase (Table 3.1). In contrast, the more melanocratic specimens (samples 1138A, 1141A, 1141B, 1143B, 1147B and GS4C) commonly have higher garnet and biotite modes.

The Koenap migmatite are commonly structured in four different ways. These, shown in Figure 3.16, are; pod-structured migmatite (a), compositionally layered migmatite (b), stromatically layered migmatite (c) and nebulitic migmatite (b). Table 3.1 shows the mineral abundances of Koenap migmatites.

Table 3.1: *Modal mineral composition of Koenap Formation migmatites (vol%). Modes were determined visually from thin section and macroscopic evaluation. Mineral abbreviations are after Whitney and Evans (2010).*

Sample	Qz	Kfs	Pl	Bt	Grt	Sil	Crd	Ms	Opq	Ttn
1137A	50	10	10	2	9	<1	15	-	3	<1
1138A	56	10	-	2	20	2	8	<1	2	<1
1141A	47	5	<1	2	30	1	15	-	<1	<1
1141B	30	15	15	-	20	-	5	7	4	-
1143A	50	10	10	3	20	1	15	-	2	-
1143B	25	9	9	30	15	≤ 1	9	-	3	-
1147A	37	20	15	9	13	1	5	-	2	-
1147B	38	-	-	26	4	<1	-	30	2	-
GS4C	36	15	5	10	25	1	5	-	3	-
GS4D	50	10	15	5	15	1	2	-	2	-

Pod-structured Koenap migmatite

Figure 3.16a shows sample 1137A, which is representative of a Koenap migmatite variety which comprises pod-like leucosome hosted within melanosome (samples 1137A, 1143B and 1147B). Sample 1137A is one of the more leucocratic migmatites and has a light-brown colour, while 1143B and 1147B are relatively melanocratic and have a dark-brown colour. Irregularly shaped pods of leucosome (1.5 cm–5 cm wide, 5 cm–10 cm long) share gradational boundaries with melanosome, which are slightly smaller in sample 1143B (1 cm–5 cm in width, 1.5 cm–10 cm in length).

The leucosome generally comprises quartz, K-feldspar, plagioclase, garnet, cordierite and biotite. The mineral assemblage of the melanosome is the same as that of the leucosome but with higher

garnet and biotite modes. Garnet are subhedral, and in the leucosome range between 1–2 mm across, while in the melanosome garnet porphyroblasts reach up to 2.5 mm across. Both leucosome and melanosome have a granoblastic texture.

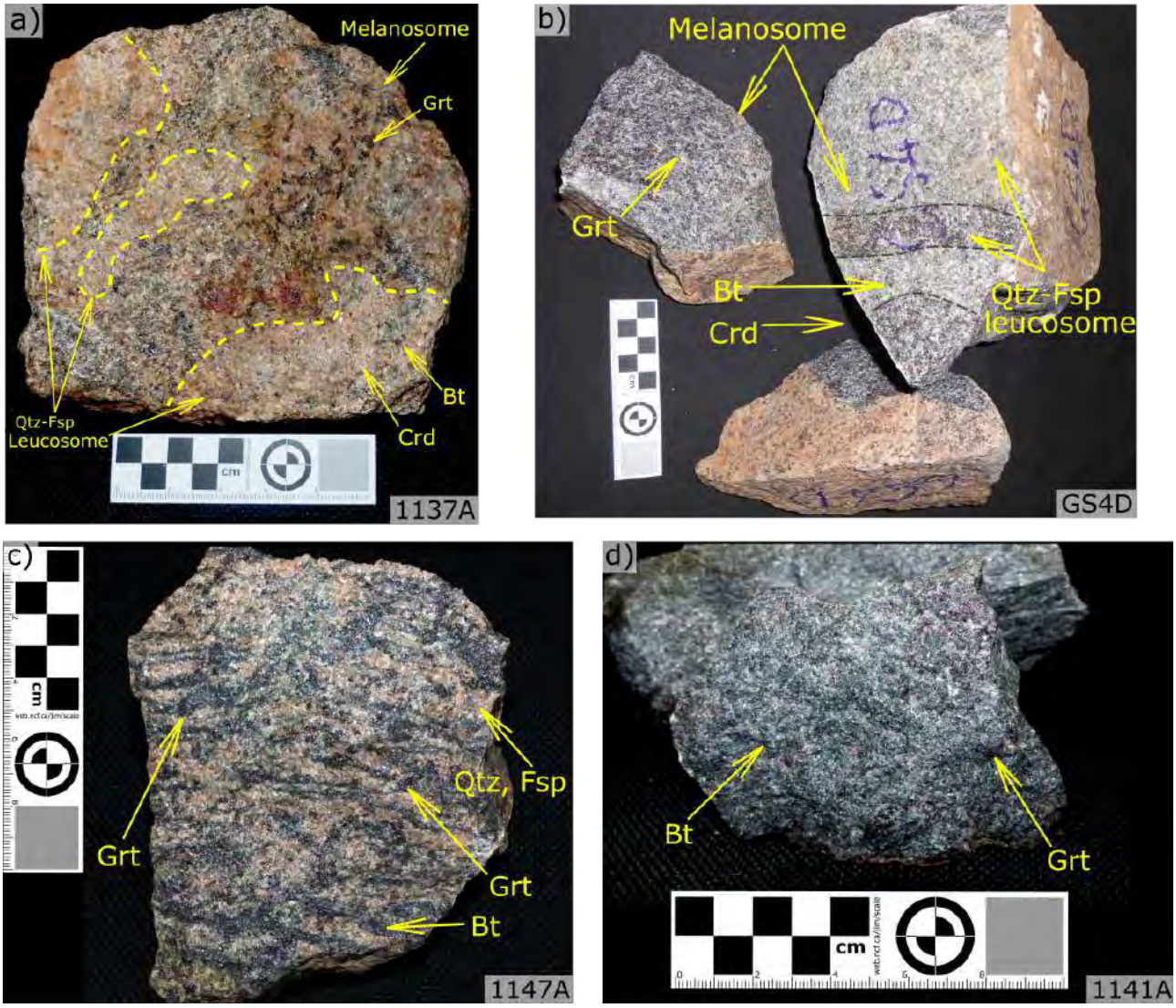

Figure 3.16: *(a) Leucocratic, pod-structured Koenap migmatite. The irregularly shaped, pod-like leucosome share gradational boundaries with the melanosome. (b) The leucosome and melanosome of the compositionally layered migmatite, sample GS4D, are well-segregated into bands. The melanosome of sample 1137A (a) is more felsic than that of (b) sample GS4D. (c) A stromatic migmatite (sample 1147A). The melanosome layers are not uniform and appear to be disrupted by the leucosome. (d) A melanocratic, nebulitic migmatite (sample 1141A). Note the varying amounts of leucosome to melanosome in these representative Koenap migmatites, and the garnet present in both the melanosome and the leucosome.*

Sample 1147B differs from other specimens in that its mineralogy is dominated by biotite, white mica and quartz, with minor garnet. The rock has a continuous schistosity. Aligned with the foliation are segregation quartz lenses up to 2 cm × 2 cm × 8 cm in size. Pod-like bodies of melanosome in this rock are poorly defined by accumulations of biotite clusters (7 mm across).

The pod-structured migmatite of the Koenap Formation generally comprise 25–50 vol% Qz,

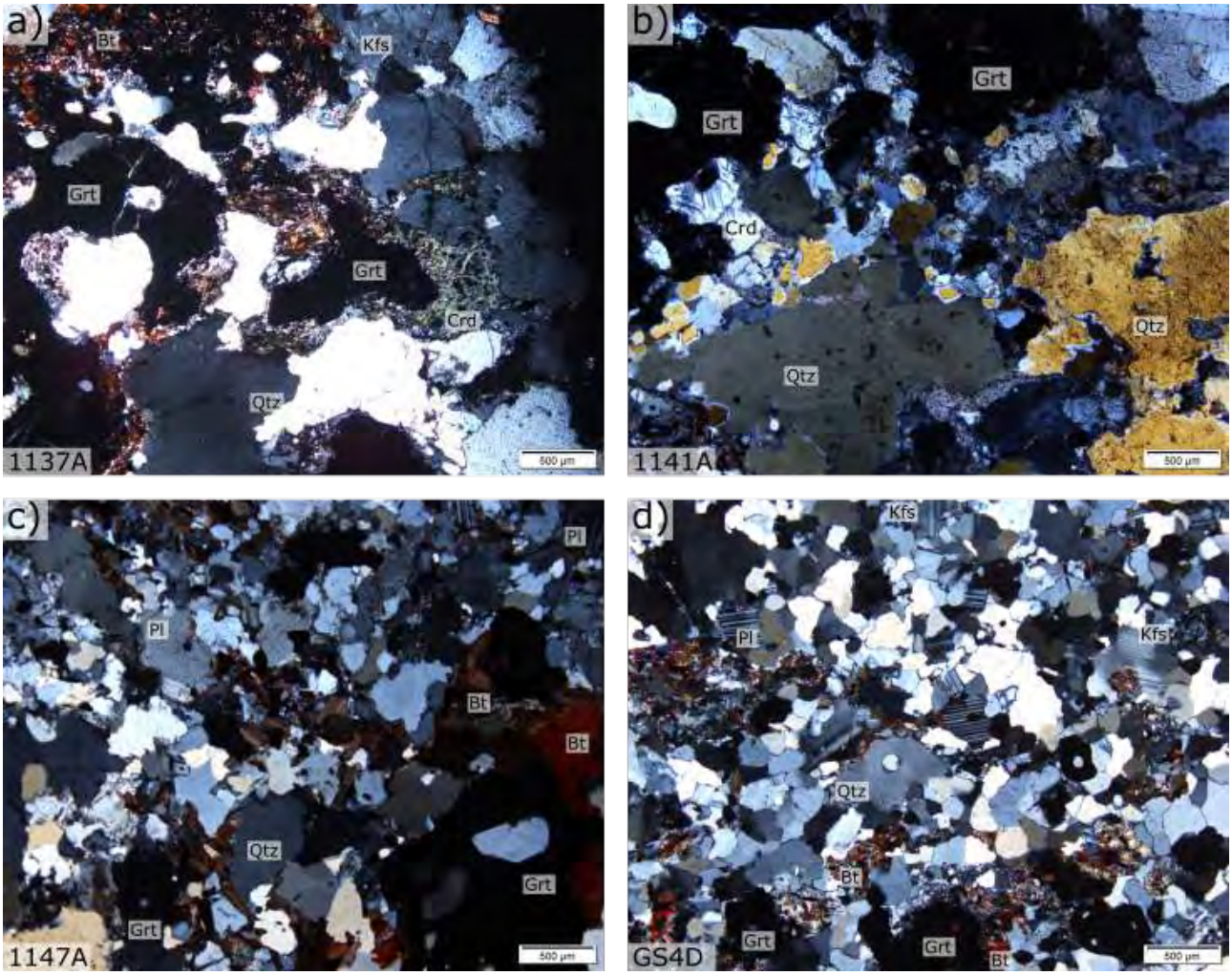

Figure 3.17: *The photomicrographs (crossed polarised light, XPL) are of thin sections prepared from the samples in Figure 3.16. (a) Koenap migmatite garnet typically have a resorbed texture. When present, cordierite is in contact with garnet and is often pinitised. K-feldspar and biotite are spatially associated with garnet, in the more leucocratic migmatite specimens. Compare this to (b). The more melanocratic specimens, such as was seen in Figure 3.17d (sample 1141A), have low biotite and feldspar modes. (c) The photomicrograph shows again the proximal association of biotite and resorbed garnet, typical of the leucocratic migmatites of the study area. (d) The leucosome of sample GS4D has a relatively higher quartz-feldspar mode than other leucosome. Garnet and biotite are proximally associated.*

2–30 vol% Bt, 4–15 vol% Grt, 9–10 vol% Kfs, 9–10 vol% Pl, 9–15 vol% Crd, 2–3 vol% Opq, <1 vol% Sil and trace Ttn. Sample 1147B contains no alkali feldspar, plagioclase or cordierite, but has around 38 vol% Qz, 30 vol% Ms, 26 vol% Bt, 2 vol% Opq and <1 vol% Sil (Table 3.1).

Under the microscope the leucosome and melanosome of samples 1137A and 1143B are distinguished by the proportion of felsic to mafic minerals. The leucosome has higher alkali feldspar and plagioclase modes, while the melanosome has higher biotite and garnet modes, with very little alkali feldspar and plagioclase. The leucosome of sample 1147B comprises alkali feldspar, plagioclase, quartz, white mica, biotite and garnet. The melanosome has more biotite and less quartz than the leucosome and consists of quartz, garnet, white mica and opaque minerals.

Quartz grains of this migmatite variety range in size from 2–8 mm, and form sutured grain boundaries. Quartz porphyroblasts show multiple sub-grain boundaries. Alkali feldspar are anhedral, and about 30 vol% have undergone sericitation. Around 60 vol% of alkali feldspar is microperthitic, showing film-like exsolutions of Na-feldspar in K-feldspar. Plagioclase is anhedral and around 30 vol% has undergone sericitisation. Shared phase boundaries between plagioclase and quartz commonly show symplectitic intergrowths.

Garnet is spatially associated with alkali feldspar, plagioclase, cordierite, biotite, opaque minerals and rare spinel. Garnet have a resorbed texture (Figure 3.17a), and are often poikiloblastic, with quartz, biotite and sillimanite inclusions. Garnet in sample 1137A commonly have a vermicular textured rim of quartz—garnet intergrowths. Sillimanite needles and prismatic laths are always found within or proximal to garnet. Cordierite commonly forms a rim around garnet (Figure 3.17a) and is usually pinitised (that is, replacement by fine grained chlorite and sericite).

Spinel with a translucent green colour in thin section, almost always is found nearby both biotite and garnet and is never found where biotite is absent. Biotite is aligned to the stromatic layering in both leucosome and melanosome. White mica, when present, appears to grow after biotite and shows no preferred orientation. Around 80 vol% of opaque minerals are found proximal to biotite and garnet. They are found in two distinct habits; (i) a larger, anhedral phase and (ii) as an elongated, vermicular texture. The larger opaque mineral was identified by Fisher (2016) using EDS as ilmenite, which commonly contains rutile exsolution lamellae. The smaller, vermicular opaque mineral is magnetite (Fisher, 2016).

Compositionally layered Koenap migmatite

One specimen of compositionally layered migmatite was collected, sample GS4D (Figure 3.16b). This rock has a very high degree of accumulation of leucosome from surrounding migmatite. Compositional bands of leucosome and melanosome vary in thickness from 2–15 cm and are well-segregated from each other along sharp margins.

The leucosome matrix comprises K-feldspar, quartz, and minor plagioclase, which supports garnet. When present, biotite and cordierite are spatially associated with garnet. The melanosome comprises the same mineralogy as the leucosome, but with higher proportions of mafic to felsic phases. The melanosome resembles the nebulitic migmatite, described later (sample 1141A), and supports small volumes of in situ leucosome and within host rootless veins of leucosome.

Sample GS4D consists of 50 vol% Qz, 15 vol% Grt, 15 vol% Pl, 10 vol% Kfs, 5 vol% Bt, 2

vol% Crd, 2 vol% Opq and 1 vol% Sil (Table 3.1). Under the microscope are veinlets of biotite up to 2 mm wide, and up to 3 cm long, aligned subparallel to the layering. Leucocratic veins surrounded by melanosome range in width from 1–15 mm. Leucosome is distinguished in thin section by its higher alkali feldspar and plagioclase modes. The melanosome has a higher biotite mode.

Quartz is foam textured and individual grains are 0.3–0.6 mm across. Alkali feldspar are anhedral, and commonly are around 0.5 mm × 0.5 mm in size. The leucosome layers of sample GS4D are some of the most leucocratic specimens and have a relatively high plagioclase mode (Figure 3.17d). Plagioclase are anhedral and somewhat smaller than K-feldspar, measuring from 0.3 mm × 0.5 mm. Plagioclase porphyroblasts, however, range from 2 mm × 2 mm up to 3 mm × 3 mm.

Garnet crystals have resorbed textures and range in size from about 1–3 mm across. Garnet are always surrounded by biotite and cordierite. Around 15 vol% of cordierite are pinitised. Opaque minerals are rounded, and range in size from 0.01–0.1 mm across. They are found proximal to garnet, or as inclusions to garnet crystals. Sillimanite laths (up to 0.5 mm long) and needles (up to 0.1 mm long) are found proximal to garnet, biotite and cordierite.

Stromatically layered Koenap migmatite

The stromatically layered Koenap migmatite are represented by samples 1138A, 1141B, 1143A, 1147A and GS4C. Figure 3.16c shows sample 1147A, which is representative of these rocks. Samples 1143A and 1147A are relatively leucocratic with well-developed stromatic layering. The other specimens, samples 1138A, 1141B, 1143A and GS4C, are more melanocratic, and have well-developed stromatic layering, except for 1138A which has a weak stromatic structure. Leucosome and melanosome are well-segregated in the more leucocratic specimens and have sharp boundaries, such as sample 1147A (Figure 3.16c). The leucosome in the more melanocratic specimens show diffuse boundaries to the melanosome.

The commonly orange- to light-green-coloured leucosome matrix consists of alkali feldspar, plagioclase and quartz. This matrix supports garnet, cordierite, biotite and elongated lenses of alkali feldspar. When present, cordierite and biotite are always proximal to garnet. Garnet (1–2 mm across) are evenly distributed throughout the leucosome. The commonly dark-grey melanosome comprises the same mineralogy as the leucosome, but with lower modes of felsic phases and higher mafic phase modes. Veins of biotite and opaque minerals up to 1 cm wide and 3 cm long are common and aligned subparallel to the stromatic layering. The garnet in the

melanosome are somewhat larger (2–3 mm across).

The stromatically layered Koenap migmatite generally comprise 30–56 vol% Qz, 13–25 vol% Grt, 10–20 vol% Kfs, 0–15 vol% Pl, 5–15 vol% Crd, 0–10 vol% Bt, 2–4 vol% Opq and 0–2 vol% Sil (Table 3.1). Leucosome and melanosome are generally distinguished under the microscope by their alkali feldspar and plagioclase modes, which are higher in the leucosome. Melanosome have higher modes of biotite and opaque minerals. Quartz in the leucosome of sample 1141B are foam textured, while quartz in the melanosome shows numerous sub-grain boundaries and is not recrystallised. Sample 1138A has the second highest garnet mode of the Koenap migmatite specimens and is relatively melanocratic, along with samples 1141B and GS4C. Samples 1143A and 1147A are more leucocratic. Garnet is evenly distributed throughout the rocks.

Quartz commonly has sutured grain boundaries. Alkali feldspar crystals are anhedral and around 30 vol% are microperthitic. Around 10 vol% of alkali feldspar is recrystallised. Plagioclase are anhedral, and commonly are in equal or lower modes to alkali feldspar.

Figure 3.17c shows a crossed-polarisers photomicrograph of sample 1147A, showing resorbed texture of garnet crystals, common to all specimens. The surrounding matrix consists of quartz and plagioclase (K-feldspar not shown in view). Garnet (2–3 mm) is poikiloblastic, with inclusions of quartz, biotite and sillimanite. Garnet pseudomorph areas are typified by the relict garnet itself, biotite, quartz, alkali feldspar, ilmenite, magnetite and pinitised cordierite. Sample 1138A has an abundance of sillimanite needles as inclusions within garnet, or near the phase boundary of garnet. About 20 vol% of garnet have vermicular quartz-garnet intergrowths around their rims, in sample 1138A.

Biotite commonly is proximally associated with garnet (Figure 3.17c), commonly in direct contact. Veins of biotite and opaque minerals preserve the stromatic foliation in thin section, in samples 1141B and 1143A. These veins can measure up to 1 cm wide and up to 3 cm long. Where present, white mica appears to replace biotite (sample 1141B) and has a random orientation.

The opaque minerals of sample 1138A are found in two distinct habits, like sample 1137A. Larger, anhedral ilmenite and smaller, vermicular magnetite.

Nebulitic Koenap migmatite

Figure 3.16d shows sample 1141A. This rock is one of the most melanocratic Koenap migmatite specimens and is the only collected example of nebulitic migmatite from the Koenap Forma-

tion. The dark-grey, medium–coarse-grained alkali feldspar-cordierite-garnet-quartz granofels is almost isotropic in structure. Very diffuse pods host small (<1 mm across), irregularly shaped volumes of in situ felsic phases and within host rootless veins. These comprise the leucosome, and consist of K-feldspar, quartz and minor plagioclase.

The melanosome consists of garnet, which is spatially associated with cordierite, and interstitial quartz. The melanocratic pods contains about 40 vol% of the garnet, the leucocratic pods 60 vol% of the garnet.

Sample 1141A consists of 4 vol% Qz, 30 vol% Grt, 15 vol% Crd, 5 vol% Kfs, 2 vol% Bt, 1 vol% Sil, <1 vol% Pl and <1 vol% Opq (Table 3.1). This rock is one of the most melanocratic specimens of Koenap migmatite. The small amounts of leucosome are distinguished in thin section by the presence of K-feldspar, which is found only in small veins.

Under the microscope all alkali feldspar is microperthitic. Sericitation of alkali feldspar is advanced, which causes difficulty in distinguishing between alkali feldspar and sericitised plagioclase. Sample 1141A has the highest garnet mode of the collected Koenap migmatites. Garnet have a resorbed texture (Figure 3.17b) and are commonly surrounded by abundant sillimanite needles, cordierite, biotite, alkali feldspar, opaque minerals and rare spinel. Cordierite is always found near garnet and is commonly pinitised. Limited white mica appears after biotite.

3.2.2 Bysteek Formation

Three samples were collected from the Bysteek Formation in this study. The first is a mylonitic Bysteek mafic calc-silicate (sample GS15A) hosting a leucocratic vein, from which a thin section was prepared. The second is a calc-silicate contacting hybrid rock, from which two thin sections were prepared. The calc-silicate portion of the collected sample was crushed and analysed geochemically as sample GS10A. The third specimen is a white marble, from which a thin section was prepared. The rock was crushed and geochemically analysed to investigate the Bysteek marble as a possible contaminant of the Swartoup Pluton. Modal mineral abundances of the collected samples are shown in Table 3.2.

Mylonitic Bysteek mafic calc-silicate

Figure 3.18a and 3.18b show a dark grey-black mylonitic Bysteek mafic calc-silicate (sample GS15A). The LS-tectonite has a pervasive, well-developed tectonic foliation, defined by a roughly 8 mm wide segregation quartz vein and the alignment of flattened and elongated mica

fish (Figure 3.18a). Melanocratic pods of hornblende and biotite are also aligned to the tectonic foliation. The leucosome consists of quartz, K-feldspar and plagioclase.

A leucocratic vein ($\sim$ 1 cm wide) intrudes sub-perpendicular to the tectonic foliation of the rock, along contacts which curve around phenocrysts and pods of host melanosome (Figure 3.18b). The contacts are difficult to distinguish as the vein material and the surrounding leucosome share the same mineralogy.

Under the microscope, the melanocratic pods comprise hornblende, biotite and opaque minerals in equivalent proportions and interstitial quartz. The leucocratic matrix supporting these pods comprise quartz, K-feldspar, plagioclase and minor opaque minerals.

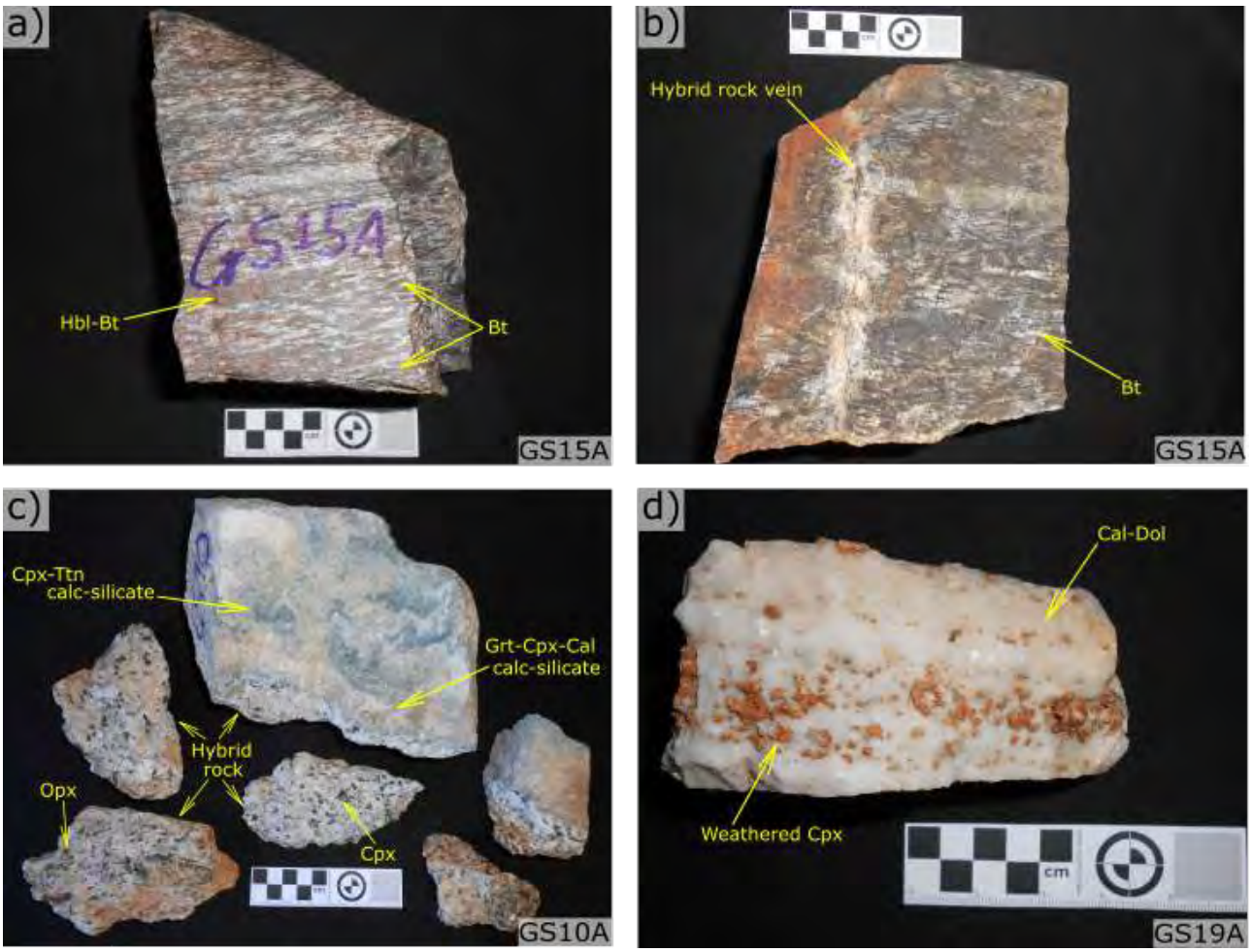

Figure 3.18: *(a) Bysteek Formation mylonite. Aligned to the strong tectonic foliation are melanocratic amphibole–biotite-rich pods and biotite lenses surrounded by leucocratic plagioclase-quartz matrix. Also aligned with the foliation is a segregation quartz vein about 8 mm wide. (b) This specimen is intruded by a vein of the hybrid rock sub-perpendicular to the foliation. (c) The Bysteek calc-silicate collected from locality GS10 (Figure 3.12b). The specimen comprises a dark-grey coloured clinopyroxene-dominant layer, with a sharp contact to an orange-coloured garnet-dominant layer. This garnet-dominant layer pinches and swells along the calc-silicates contact to the pyroxene-rich hybrid rock. (d) Banded white marble collected from one of the Bysteek marble layers within the Swartoup Pluton. The weathered minerals are clinopyroxene (Figure 3.19f).*

Under the microscope, the intrusive vein appears similar to sample GS11D (Section 3.2.4), comprising strain-free quartz and plagioclase as well as recrystallised plagioclase and K-feldspar. Subhedral feldspar within the vein measure up to 3 mm in diameter. Elongated clinopyroxene are aligned sub-parallel to the vein.

Table 3.2: *Modal mineral composition of Bysteek Formation specimens (vol%). Modes were determined visually from thin section and macroscopic evaluation. Mineral abbreviations are after Whitney and Evans (2010).*

Sample	Qz	Kfs	Pl	Bt	Hbl	Grt	Ttn	Cal	Cpx	Chl	Opq
GS10A	-	-	-	-	-	24	6	1	69	-	-
GS15A[a]	68	8	8	8	8	-	-	-	-	-	8
GS15A[b]	40	10	40	3	3	-	-	-	3	-	1
GS19A	-	-	-	-	-	-	-	90	10	<1	<1

GS15A[a] Bysteek mylonitic mineral abundance, ecluding leucocratic vein.
GS15A[b] leucocratic vein mineral abundance.

Bysteek Calc-silicate

Figure 3.18c shows sample GS10A. The collected specimens consist of two layers of calc-silicate and a layer of hybrid rock. The first calc-silicate has a grey colour and is dominated by clinopyroxene and titanite. It shares a sharp, undulating contact to a layer of orange-coloured calc-silicate which pinches and swells up to 5 cm in thickness and is dominated by garnet and clinopyroxene, with minor calcite. The orange-coloured calc-silicate layer has a sharp, linear contact to the hybrid rock. The hybrid rock is a typical clinopyroxene-orthopyroxene bearing variety like sample GS11D (Section 3.2.4). The modal mineral abundance of sample GS10A shown in Table 3.2 excludes the hybrid rock and only considers the calc-silicate layers, as the hybrid rock was removed prior to crushing for analysis. The analysed sample comprised about 60 vol% grey, clinopyroxene–titanite dominated calc-silicate, and about 40 vol% orange-coloured, garnet–clinopyroxene dominated calc-silicate.

The image of sample GS10A from Figure 3.18c has been repeated in Figure 3.19c. Figure 3.19a (PPL) and 3.19b (CPL) are photomicrographs showing the same field of view. They show the clinopyroxene–titanite dominated grey calc-silicate of sample GS10A (Figure 3.19c). This calc-silicate consists of subhedral to anhedral clinopyroxene ($\sim$ 90 vol%) and titanite ($\sim$ 10 vol%), which are randomly distributed throughout the layer.

Figure 3.19d shows a crossed-polarisers photomicrograph of the orange coloured calc-silicate layer. The image shows anhedral clinopyroxene and calcite hosted within large garnet. This

calc-silicate layer consists of garnet (~60 vol%), clinopyroxene (~38 vol%) and calcite (~2 vol%). The contact between the two calc-silicate layers is sharp.

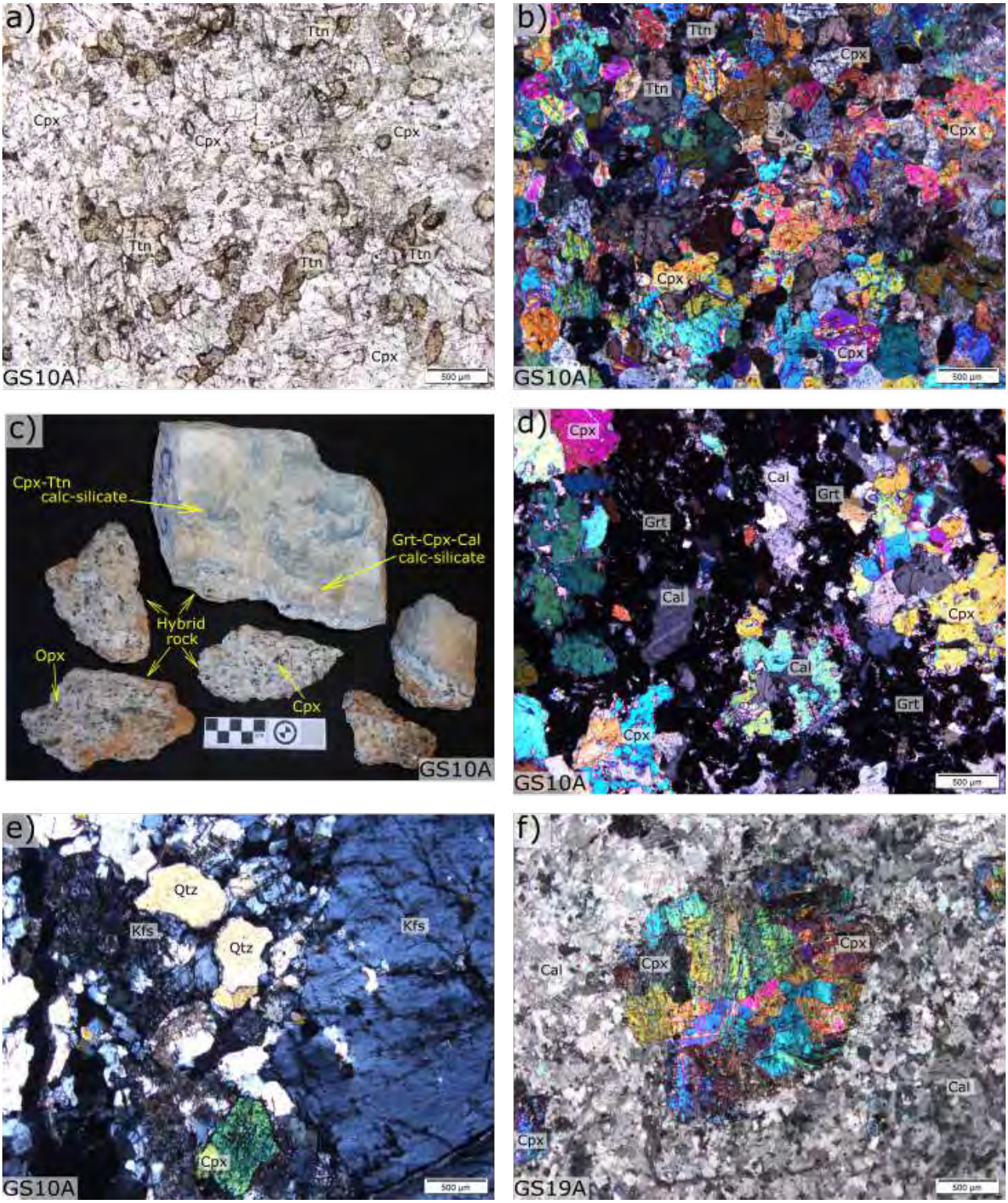

Figure 3.19: *(a) Plane-polarised light (PPL) and (b) Cross-polarised light (XPL) photomicrographs of the same field of view. The images show the clinopyroxene-titanite calc-silicate earlier seen in Figure 3.18c (sample GS10A), here repeated in (c). (d) XPL photomicrograph from the garnet-dominant calc-silicate layer. (e) (XPL) The contact of the calc-silicate portion of sample GS10A to the hybrid rock is marked by K-feldspar. (f) Clinopyroxene surrounded by calcite groundmass, from the Bysteek marble sample, GS19A (XPL).*

The contact between the orange-coloured calc-silicate and the hybrid rock is sharp. It is marked by the appearance of quartz, microperthitic K-feldspar, plagioclase and clinopyroxene (see Section 3.2.4). Figure 3.19e shows a K-feldspar, quartz and clinopyroxene from the contact with hybrid rock. The calc-silicate rock is to the left of view in the image.

Bysteek marble

Sample GS19A is a banded white marble, shown in Figure 3.18d. The weathered phases visible in Figure 3.18d are clinopyroxene. Bands of clinopyroxene vary from about 0.2 cm–2.3 cm wide.

Under the microscope clinopyroxene is supported in a calcite matrix (Figure 3.19f). Clinopyroxene are subhedral and range from 1–4 mm in diameter. When present, trace amounts of chlorite are found in the silicate layer containing the clinopyroxene. Chlorite is associated with the clinopyroxene.

3.2.3 Swartoup granitoids

Five varieties of granitoid; granodiorite, granite, orthopyroxene-bearing granitoids, garnet-bearing granitoids and leucogranite are associated with the Swartoup. These have been classified (Table 3.4) using mineral modes (Tables 3.3, 3.4) and the TAS (Figure 4.1a; after Middlemost, 1994) and R_1R_2 diagrams (Figure 4.1b; after De la Roche et al., 1980). A geochemical classification scheme based on the Fe-number, modified alkali-lime index and aluminium saturation index (see Figure 4.2), as proposed by Frost et al. (2001), was also used, although the rock names as classified by this scheme have not been adhered to (see Section 4.2). Orthopyroxene-bearing igneous rocks are named by adding the modifier 'orthopyroxene-bearing', as per the proposal of Frost and Frost (2008).

The five granitoid varieties are subdivided into two groups, Swartoup group 1 and 2. Within the sampled collection, granodiorites are the most common rocks, constituting Swartoup group 1. These are represented by the samples 1139A, 1140A, 1144A, 1145A and 1146A. These were collected near the hinge of the antiform (Figure 3.6). Samples 1139A and 1140A were taken from a dyke surrounded by Koenap migmatite to the west of the Swartoup Pluton (Figure 3.6). These two samples are garnet-bearing, but they plot with the rest of the Swartoup granodiorite samples on chemical variation diagrams. These five granodiorite samples form Swartoup group 1, which are geochemically and petrographically uniform.

In contrast, Swartoup group 2 is compositionally and geochemically more variable than Swartoup

group 1. Swartoup group 2 includes the samples 1149A, 1151A, GS5A, GS9A, GS9B, GS10B, GS11A, GS11C, GS15B, GS15C and GS16A. Swartoup group 2 includes granites, orthopyroxene-bearing monzodiorites, orthopyroxene-bearing quartz monzonite, garnet-bearing granitoids and a leucogranite sample. Most of these rocks were collected from the western limb of the antiform. Only samples GS9A and GS9B were taken from the eastern limb. Swartoup group 2 are geochemically and petrogenetically variable.

Table 3.3: *Modal mineral composition of Swartoup Pluton granitoids (vol%). Modes were determined visually from thin section and macroscopic evaluation. Mineral abbreviations are after Whitney and Evans (2010).*

	Sample	Qz	Kfs	Pl	Bt	Grt	Sil	Opx	Cpx	Opq	Ttn
Typical granodiorites	1139A	50	15	15	10	7	<1	-	-	5	-
	1140A	35	30	20	13	<1	<1	-	-	2	-
	1144A	20	50	10	20	-	-	-	-	≤ 1	-
	1145A	30	30	24	15	-	-	-	-	1	<1
	1146A	22	28	33	12	-	-	-	-	5	-
Typical granites	1149A	48	38	10	2	-	-	-	-	2	-
	GS5A	40	34	20	5	-	-	-	-	1	-
	GS9B	35	40	20	5	-	-	-	-	<1	-
	GS11A	55	5	32	3	-	-	-	-	2	-
Opx-bearing granitoids	1151A	20	5	40	15	-	<1	15	-	5	-
	GS10B	20	25	20	10	-	-	15	-	10	-
	GS11C	25	35	20	5	-	-	10	-	5	-
	GS15B	15	50	20	10	-	-	<1	-	5	-
Grt-bearing granitoids	GS15C	30	20	15	15	15	<1	-	-	5	-
	GS16A	50	5	25	5	25	-	-	-	2	-
Leucogranite	GS9A	35	35	25	2	-	-	1	1	<1	-

Swartoup group 2 granites (samples 1149A, GS5A) were considered the most abundant type within the Swartoup Pluton. However, as outlined in Section 3.1.3, the intense weathering prevents a reliable estimation of the abundance of subtypes in the Swartoup Pluton. Sample GS9B is classified as a granite on both the TAS (Figure 4.1a; after Middlemost, 1994) and R_1R_2 (Figure 4.1b; after De la Roche et al., 1980) diagrams. As such, sample GS9B has been included here, along with sample GS11A. Sample GS11A was not analysed but is macroscopically similar to the rest of the granite samples and has a similarly low biotite mode (Table 3.3).

Samples 1151A and GS10B are orthopyroxene-bearing monzodiorites that both contain 15 vol% orthopyroxene. Sample GS15B is a quartz monzonite (Table 3.4), which contains <1 vol% orthopyroxene. Sample GS11C is included here as it has almost the same modal mineral abundance as sample GS10B (Table 3.3) and was collected along strike from locality GS10. Sample GS11C has not been geochemically analysed. These rocks were all collected near

outcrops of Bysteek Formation (see Figure 3.7).

Table 3.4: *Igneous Swartoup Pluton rock names as classified by the TAS diagram (Figure 4.1a Middlemost, 1994) and the R_1R_2 diagram (Figure 4.1b De la Roche et al., 1980). As per the proposal by Frost and Frost (2008), the modifier 'Opx-bearing' is added to orthopyroxene-bearing rocks. Where the classification schemes name the same rock specimens differently, the name in brackets is not used in this study.*

Variety	Sample	Classification scheme		
		TAS diagram (Middlemost, 1994)	R_1R_2 diagram (De la Roche et al., 1980)	Frost et al. (2001)
Typical granodiorites	1139A	Granodiorite	Granodiorite	(Two-mica granite)
	1140A	Granodiorite	Granodiorite	(Two-mica granite)
	1144A	Granodiorite	Granodiorite	Granodiorite
	1145A	Granodiorite	Granodiorite	(Two-mica granite)
	1146A	(Quartz monzonite)	Granodiorite	(Two-mica granite)
Typical granites	1149A	Granite	Granite	(Diorite)
	GS5A	Granite	Granite	(Diorite)
	GS9B	Granite	Granite	(Diorite)
Opx-bearing granitoids	1151A	Opx-bearing monzodiorite	Opx-bearing monzodiorite	(Opx-bearing ferrodiorite)
	GS10B	(Opx-bearing monzonite)	Opx-bearing monzodiorite	(Opx-bearing ferrodiorite)
	GS15B	Opx-bearing quartz monzonite	Opx-bearing quartz monzonite	([a])
Grt-bearing granitoids	GS15C	(Granodiorite)	Granite	(Two-mica granite)
	GS16A	(Quartzolite)	Granite	(Diorite)
Leucogranite	GS9A	Granite	Granite	Granite

[a] Rock not classified by this scheme as it is alkalic and peraluminous, see Section 4.2.

Garnet-bearing granitoids from the Swartoup Pluton are proximally associated with the Koenap Formation (Section 3.1.3). Samples GS15C and GS16A are layered and were both collected near Koenap migmatite outcrops (Figure 3.6).

Pods of leucogranite, hosted within granitic dykes, are present at locality GS9 (Section 3.1.3). The leucogranite specimen (sample GS9A) was shown in Figure 3.10c.

Swartoup granodiorites (samples 1139A, 1140A, 1144A, 1145A and 1146A)

Figure 3.20a shows sample 1144A, which is representative of the Swartoup granodiorites. They vary in colour from medium- to dark-grey and are medium- to coarse-grained. A pervasive magmatic layering is present in all samples and varies from weak to strong. The leucocratic layers comprise grey-coloured K-feldspar (2 mm × 3 mm–1 cm × 2 cm) and cream-coloured plagioclase (0.5 cm × 1 cm) set in a matrix of biotite and interstitial quartz. The melanocratic layers comprise the same mineralogy, but have much higher biotite modes, and the feldspar crystals are generally smaller (2–3 mm across). Leucocratic and melanocratic layers range

in thickness from 0.3 cm to 7 cm. The crushed volume of sample 1145A contains a larger melanocratic proportion of rock than the other specimens.

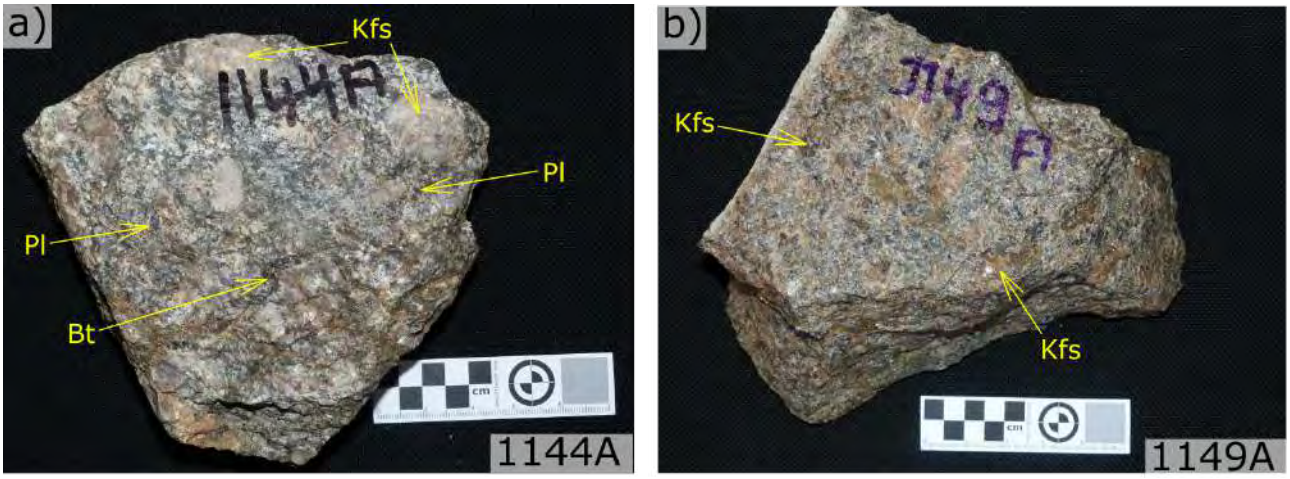

Figure 3.20: *(a) A moderately well-layered Swartoup granodiorite, sample 1144A. The specimen is representative of the geochemically distinct Swartoup group 1. Notice the large, prominent K-feldspar phenocrysts, which aid in distinguishing the Swartoup granitoids in the field. Also visible are black coloured plagioclase. (b) Sample 1149A, a typical granite encountered on the Swartoup Pluton. Notice the lower biotite mode of (b) relative to (a).*

The K-feldspar and plagioclase phenocrysts commonly have cream-coloured, recrystallised rims. Sample 1146A has the largest K-feldspar phenocrysts (up to 2 cm × 4 cm) of any rock in the study area. Sample 1144A contains black-coloured plagioclase phenocrysts (0.5 cm × 1 cm to 1 cm × 2 cm) in addition to grey- (K-feldspar) and cream-coloured (plagioclase) phenocrysts.

Samples 1139A has 7 vol% garnet and 1140A has <1 vol% garnet. Garnet are anhedral and range in size from 1–3 mm across. They are found mostly in the melanocratic layers and always proximal to biotite.

Under the microscope, elongated phases are always aligned subparallel to the layering of the Swartoup granodiorites. Commonly, quartz have sutured grain boundaries. K-feldspar are usually anhedral and around 80 vol% show simple twinning and 20 vol% show microcline twinning. Commonly, K-feldspar phenocrysts are recrystallised along their phase margins. The recrystallised grains are usually microcline. Sericitic alteration has affected 20–30 vol% of both K-feldspar and plagioclase. Around 20 vol% of K-feldspar crystals are microperthitic, while some of the largest feldspar phenocrysts are antiperthitic. Symplectitic intergrowths are common at grain boundaries between K-feldspar and plagioclase in sample 1140A. Figures 3.21c and 3.21d show the typical biotite-quartz matrix surrounding K-feldspar and plagioclase phenocrysts.

Figures 3.21a and 3.21b show a garnet crystal from sample 1140A. Garnet crystals, found in samples 1139A and 1140A, have resorbed textures and are always near biotite, K-feldspar and

opaque grains. When present, embayments in garnet crystals are filled by biotite or quartz. Around 70 vol% of opaque grains are found near biotite.

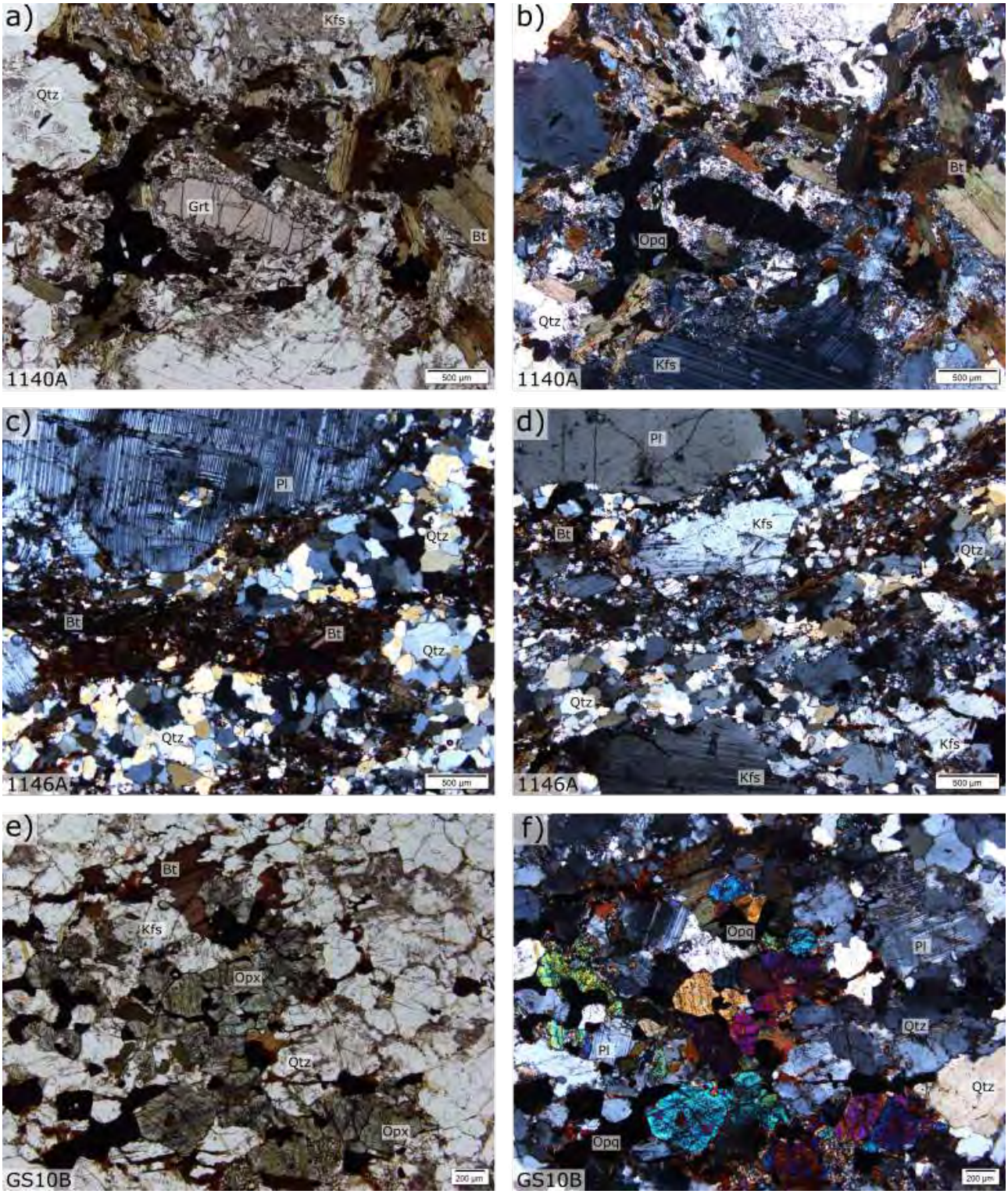

Figure 3.21: *(a) PPL and (b) XPL photomicrographs of the same field of view of garnet from sample 1140A. The garnet is surrounded by K-feldspar, biotite and opaque grains. (c,d) (XPL) The typical biotite-quartz-feldspar matrix surrounding K-feldspar and plagioclase phenocrysts from sample 1146A. (e) (PPL) and (f) (XPL) The same field of view of subhedral orthopyroxene, biotite and opaque phases from sample GS10B, an orthopyroxene-bearing monzodiorite.*

Typical Swartoup granites (Samples 1149A, GS5A, GS9B and GS11A)

Figure 3.20b shows sample 1149A, a granite specimen which, along with sample GS5A, are the typical variety of Swartoup Pluton rock (Figure 3.7). Sample GS9B was collected from a granitic dyke which hosts pods of leucogranite (Figure 3.10). Sample GS11A was retrieved from a mylonitic dyke, though is otherwise macroscopically similar to the Swartoup granites.

This variety of Swartoup rocks are characterised by their relatively low biotite modes (Table 3.3), and so they are lighter in colour than the Swartoup granodiorites. Samples GS5A, GS9B and GS11A are medium-grey in colour, while sample 1149A (Figure 3.20b) has a grey-green colour, imparted to it by green-coloured K-feldspar phenocrysts.

The Swartoup granites are medium- to coarse-grained and sample 1149A has no readily discernible leucocratic and melancratic layers. Sample GS5A has a pervasive, weak magmatic layering, defined by alignment of elongated grains. Samples GS9B and GS11A are sheared and have well developed tectonic foliation. Veinlets of biotite and interstitial quartz surround K-feldspar (0.3 cm × 0.5 cm to 1.5 cm × 2 cm) and plagioclase phenocrysts (0.3 cm × 0.5 cm).

The foliation of the rocks are readily discernible under the microscope. This is due to alignment of elongated feldspar and quartz grains. Quartz in samples 1149A and GS5A are almost completely foam textured (∼95 vol% of quartz). K-feldspar is anhedral to subhedral and ranges in size from 0.5–2 cm across, while plagioclase varies from 1–4 mm across and is also anhedral. K-feldspar phenocrysts of sample 1149A are commonly microperthitic and recrystallised along their grain boundaries. The recrystallised grains of sample 1149A usually show microcline twinning. Microcline twinning is visible in around 95 vol% of K-feldspar in sample GS5A. Retrograde sericitisation has affected 10–30 vol% of K-feldspar and around 20–40 vol% of plagioclase.

Sample 1149A has a very low biotite mode (2 vol%, Table 3.3) and what biotite there is, is evenly distributed throughout the specimen. In samples GS5A and GS11A biotite is also evenly distributed throughout and opaque phases are spatially associated with biotite. The opaque phases are anhedral, and commonly range in size from 0.2 mm × 1 mm to 0.5 mm × 1 mm.

Orthopyroxene-bearing Swartoup granitoids (Samples 1151A, GS10B, GS11C, GS15B)

Four orthopyroxene-bearing Swartoup granitoids are identified in this study. These rocks are generally much darker in colour than other Swartoup rocks. Samples 1151A, GS10B and GS11C are dark-brown in colour, while sample GS15C is much lighter in colour, due to its high K-feldspar and plagioclase modes. Figure 3.22a shows sample GS10B, which is one of two orthopyroxene-bearing monzodiorites. The other orthopyroxene-bearing monzodiorite is sample 1151A and both contain 15 vol% Opx. Sample GS15B, an orthopyroxene-bearing quartz monzonite (Figure 3.22b), contains minor orthopyroxene ($<$ 1 Opx). Samples 1151A and G15B were collected from bodies in contact with each other (Section 3.1.3). The fourth orthopyroxene-bearing granitoid is sample GS11C, which has not been geochemically analysed. This rock was collected from a dome of Swartoup monzodiorite, along strike from sample GS10B, which was collected from a Swartoup dyke which intruded Bysteek calc-silicates and mafic calc-silicates. Though less sheared, sample GS11C is macroscopically similar to sample GS10B. As sample GS11C also shares similar mineral modes (Table 3.3), it is assumed to be an orthopyroxene-bearing monzodiorite like sample GS10B.

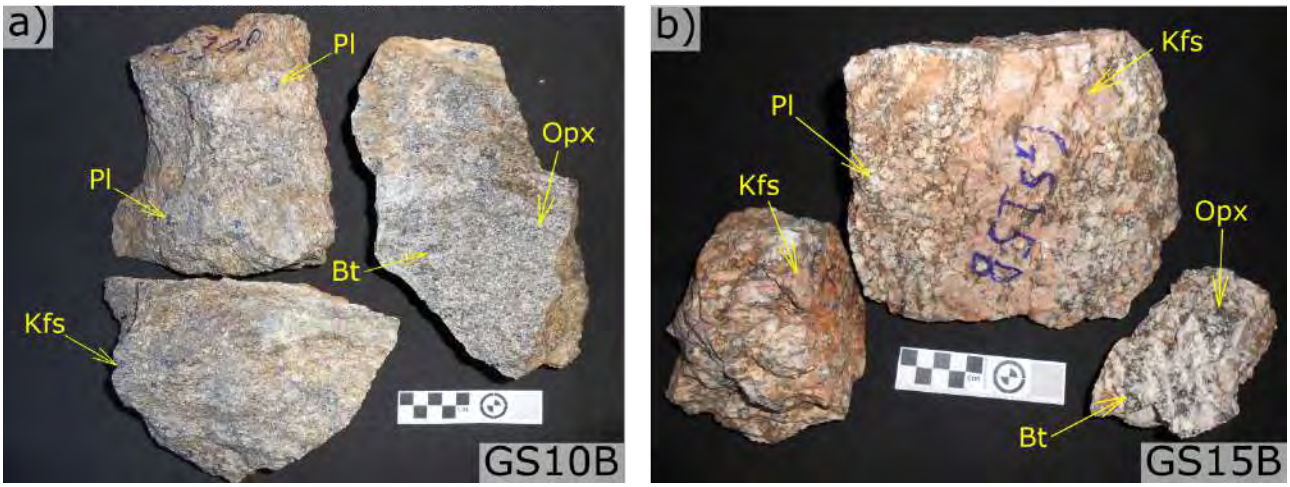

Figure 3.22: *(a) Sample GS10B, an orthopyroxene bearing monzodiorite. Notice the black coloured plagioclase, and prominent black orthopyroxene. (b) Sample GS15B, an orthopyroxene-bearing quartz monzonite. Notice the pink-coloured layer of subhedral K-feldspar, and cream-coloured plagioclase.*

These rocks are generally dark-grey in colour and are medium- to coarse-grained. Sample GS15B has larger K-feldspar and plagioclase phenocrysts so is lighter-coloured than the others. The rocks have a pervasive layering, weak in samples GS10B and GS11C, and strong in samples 1151A and GS15B. Leucocratic layers comprise K-feldspar (up to 2 cm across), plagioclase (up to 1 cm across), biotite and interstitial quartz. In sample GS10B and GS11C, subhedral,

black-coloured plagioclase phenocrysts (Figure 3.22a) measure 0.4 cm × 1 cm in size. They are identified in hand specimen by the well-developed cleavage, and the twinning visible on cleavage planes. The melanosome consists of the same mineralogy as the leucosome, but has much higher biotite modes, in addition to orthopyroxene (anhedral to subhedral, less than 4 mm across). K-feldspar and plagioclase are smaller in the melanosome than the leucosome. In sample GS15B, plagioclase is commonly found in melanocratic biotite-rich layers, while the leucosome consists of pink-coloured K-feldspar layers (Figure 3.22b).

The layering and tectonic foliation of these rocks are well preserved in thin section by alignment of melanocratic lenses of orthopyroxene, biotite and opaque minerals. Leucosomes consist of K-feldspar, plagioclase and quartz.

K-feldspar is anhedral, and ranges in size from 0.5 mm × 1 mm–1 mm × 2.5 mm. Up to 15 vol% of K-feldspar and 50 vol% of plagioclase have undergone retrograde sericitisation. Plagioclase (1 mm × 1 mm–1.5 mm × 2.5 mm) is found as both subhedral prismatic laths and anhedral grains. Sample GS15B has a higher K-feldspar mode (50 vol% Kfs) and similar plagioclase mode to sample GS10B (20 vol% Pl). Sample 1151A has a high plagioclase mode (40 vol% Pl) and a lower K-feldspar mode than the others (5 vol% Kfs, Table 3.3). Symplectitic plagioclase-quartz intergrowths are common in sample 1151A, between plagioclase and K-feldspar phenocrysts.

Garnet-bearing Swartoup granitoids (Swartoup group 2, samples GS15C and GS16A)

Figure 3.23 shows samples GS15C and GS16A. These are medium grained garnetiferous Swartoup granites. These rocks have pervasive, well developed layering. The leucosome and melanosome layers of both samples are poorly segregated. The layering is enhanced, in sample GS15C, by shearing and grain size reduction of the more leucocratic, less garnet-rich layers. The more garnet-rich melanocratic layers are less sheared. Sample GS16A contains multiple quartz segregation veins (0.7–1.2 cm thick) that are parallel to leucocratic and melanocratic layers.

The leucocratic layers consist of grey-coloured K-feldspar (2–4 mm across), cream-coloured plagioclase (2–4 mm across) and grey-coloured quartz lenses (up to 0.2 cm × 2 cm). The melanocratic layers consist of subhedral garnet (1–3 mm across), biotite and opaque minerals set in a matrix of K-feldspar, plagioclase and quartz.

Figure 3.24 shows CPL photomicrographs of sample GS15C. Samples GS15C and GS16A have

a well-developed foliation, pronounced by alignment of quartz and feldspar lenses (1.5 mm × 4 mm). Quartz is almost completely foam textured. Plagioclase and K-feldspar measure 1 mm × 1 mm–1.5 mm × 4 mm in size and commonly have undergone retrograde sericitisation. K-feldspar phenocrysts (up to 1 cm long) of sample GS15C are anhedral and microperthitic.

Samples GS15C and GS16A contain 15–25 vol% garnet. All biotite is associated with garnet (< 1–6 mm), as seen in Figure 3.24. Garnet is anhedral, and commonly has a resorbed texture. They also usually have quartz and biotite inclusions. Fractures within garnet crystals are always filled by biotite. Opaque minerals measuring 0.1–0.2 mm across are commonly sub-rounded, and angular grains are somewhat larger, measuring up to 0.3 mm × 0.5 mm.

The contacts from melanocratic to leucocratic layers in thin section are marked by an increase in grain size and decrease in mafic mineral modes.

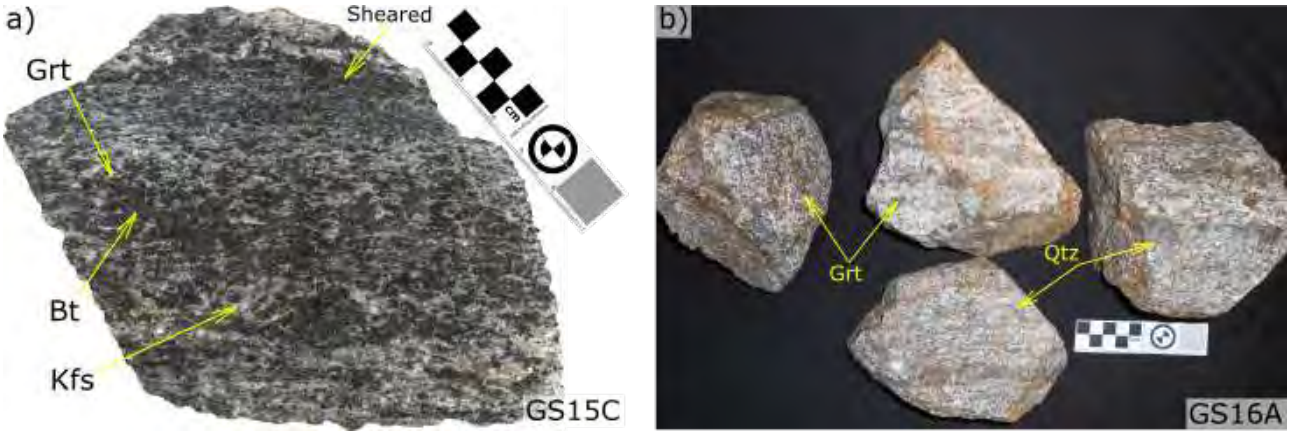

Figure 3.23: *(a) Scan of a cut surface of sample GS15C, a garnet-bearing granite. The rock is sheared near the contacts of its layers. Each layer comprises quartz, K-feldspar, biotite and garnet. (b) Sample GS16A, a garnet-bearing granite. Note the prominent quartz segregation veins.*

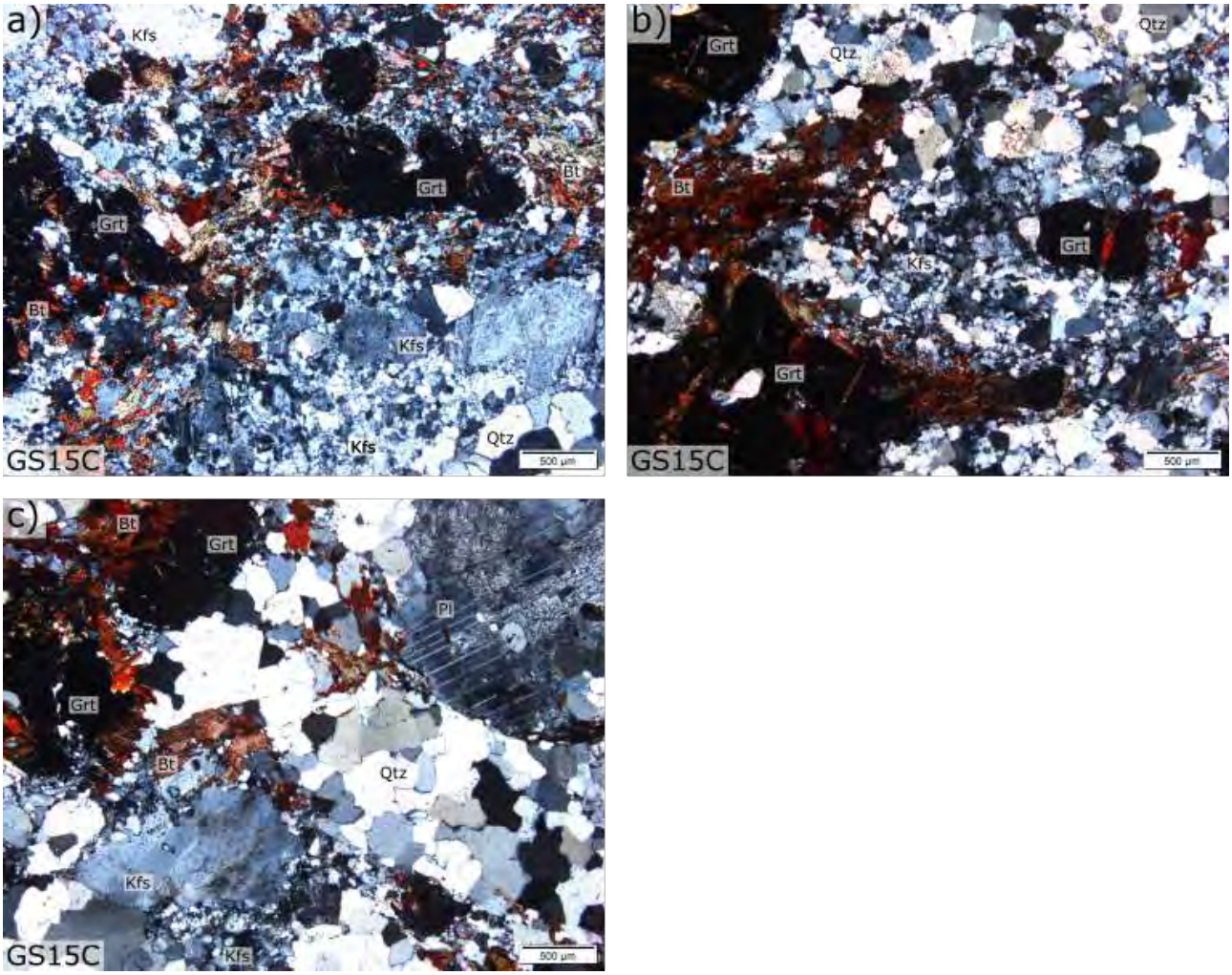

Figure 3.24: *(a-c) XPL photomicrographs from the garnet-bearing Swartoup granite, sample GS15C. The images show the typical plagioclase and K-feldspar phenocrysts characteristic of the Swartoup rocks. Where present, biotite is proximally associated with garnet.*

Swartoup leucogranite (sample GS9A)

Figure 3.10c shows the Swartoup leucogranite, sample GS9A, collected from pods of leucogranite hosted in a granitic dyke. The pale, cream-coloured specimen contains melanocratic pods, poorly segregated from the melanocratic host, with diffuse contacts. The leucocratic layers comprise K-feldspar (0.6 cm × 1 cm), plagioclase (0.6 cm × 1 cm) and quartz. The melanocratic layers consist of the same mineralogy but have a higher mode of translucent grey-coloured quartz, giving these pods a slightly darker colour. The rock contains elongated lenses of quartz and K-feldspar, defining a weak foliation. Lenses of a biotite (up to 2 mm wide, 1 cm long) are found randomly distributed throughout the specimen. These biotite lenses are visible in the field and are found with increasing frequency towards the host granite.

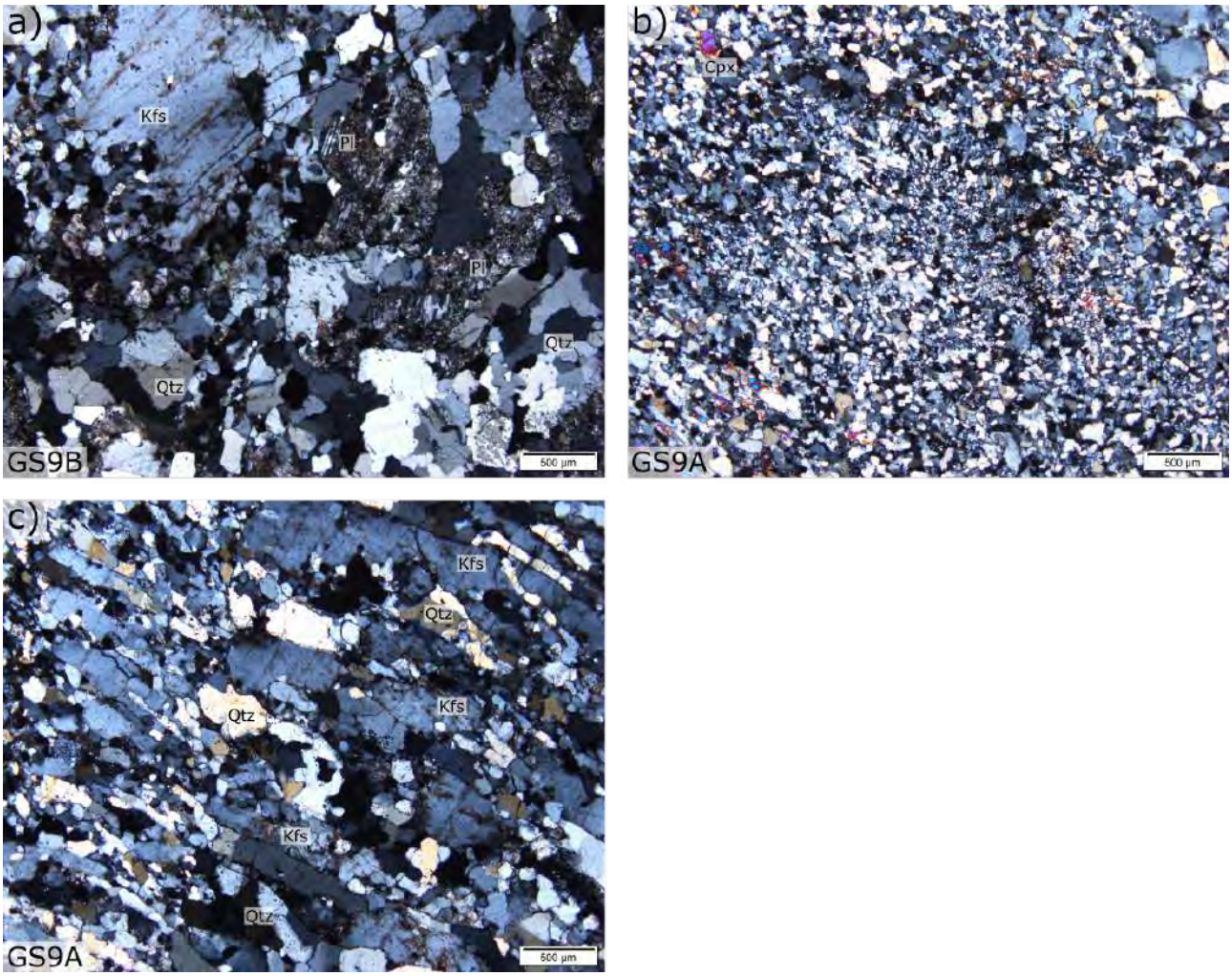

Figure 3.25: *(a) (XPL) K-feldspar and plagioclase phenocrysts from a Swartoup granodiorite (sample GS9B). The granodiorite was collected from a dyke hosting pods of leucogranite (sample GS9A) (Figure 3.10). The leucogranite (b, XPL) consists of a fine-grained quartz—K-feldspar matrix. (c, XPL) Sheared contact zone between the granodiorite and leucogranite. Quartz and K-feldspar phenocrysts characteristic of the granodiorite are intercalated with finer-grained quartz and K-feldspar characteristic of the leucogranite, suggesting a transitional boundary between these rock types.*

The specimen shows a contact to the host granite. This contact is transitional over about 2 cm. It is marked by interlayered phenocrysts of K-feldspar and quartz. The granitic host contains large K-feldspar and plagioclase phenocrysts typical of Swartoup granitoids.

Figure 3.25 shows CPL photomicrographs of sample GS9A, the Swartoup leucogranite. The rock consists mostly of K-feldspar, plagioclase and quartz (0.6 cm × 1 cm), all almost completely recrystallised (Figure 3.25b). Few lenses remain which are not recrystallised, and these define the tectonic foliation in thin section.

Within the quartzofeldspathic groundmass, minor, small clinopyroxene grains (1 vol%) are randomly distributed. The contact zone from the leucogranite to its host granite (Figure 3.25a) is marked by a graphic intercalation of quartz and K-feldspar phenocrysts, shown in Figure 3.25c. The granite host contains K-feldspar and plagioclase phenocrysts typical of Swartoup granitoids.

3.2.4 Hybrid rocks

The hybrid rocks of this study are shown in Figure 3.26. They are identified by their leucocratic nature and field associations (see Section 3.1.4). Petrography of the four varieties of hybrid rock found in the study area follows. First is presented the quartz-biotite-dominated variety, sample GS1A (Figure 3.26a). Only one locality exposing this rock type was found in the study area. A garnet-bearing variety (Figure 3.26b, sample GS7A) and an orthopyroxene-clinopyroxene-bearing variety were also sampled (Figure 3.26c, sample GS11D). Together, these two samples represent the typical hybrid rocks. Samples GS13A and GS13B (Figures 3.26d and 3.26e) comprise the K-feldspar-rich variety of hybrid rock. Sample GS13A has porphyroclastic K-feldspar and sample GS13B has the highest K-feldspar mode of the hybrid rocks. Table 3.5 shows the modal mineral composition of the hybrid rocks, and Table 3.6 shows their names, as classified by the TAS (Figure 4.1a; after Middlemost, 1994) and R_1R_2 diagrams (Figure 4.1b; after De la Roche et al., 1980). Like for the Swartoup Pluton, the geochemical classification scheme proposed by Frost et al. (2001), was also used but has again not been adhered to, in favour of the aforementioned schems Orthopyroxene-bearing igneous rocks are named by adding the modifier 'orthopyroxene-bearing', as per the proposal of Frost and Frost (2008).

Quartz-biotite variety (sample GS1A)

Shown in Figure 3.26a, sample GS1A is a medium-grey coloured granodiorite, with a well-developed magmatic layering. The layering is defined by melanocratic biotite-rich pods, up to 0.3 cm × 2 cm × 5 cm in size.

The S-tectonite consists of elongated, grey-coloured quartz lenses (up to 1 cm long) and anhedral, off-white-coloured K-feldspar (≤ 0.5 cm) and plagioclase (≤ 0.5 cm) phenocrysts. The biotite-rich pods consist mostly of biotite, with minor anhedral garnet (up to 2 mm) and opaque minerals.

Sample GS1A consists of approximately 40 vol% Qz, 35 vol% Kfs, 20 vol% Bt, 5 vol% Pl, 5 vol% Grt and 2 vol% Opq. Under the microscope we can see the leucocratic layers consist of quartz, K-feldspar and plagioclase. Quartz lenses are recrystallised to a foam texture and are up to 1 cm in length. K-feldspar and plagioclase are anhedral, and phenocrysts of both measure up to 0.5 cm across. Elongated minerals are aligned to the magmatic layering.

The melanocratic pods consist mostly of biotite, with minor garnet. Garnet crystals are anhedral and always associated with biotite. Figure 3.27a shows a crossed-polariser photomicrograph of typical garnet crystals from sample GS1A. Minor opaque grains are found within the melanocratic pods.

Table 3.5: *Modal mineral composition of hybrid rock (vol%). Modes were determined visually from thin section and macroscopic evaluation. Mineral abbreviations are after Whitney and Evans (2010).*

Sample	Qz	Kfs	Pl	Bt	Grt	Sil	Opx	Cpx	ttn	Opq
GS1A	40	35	5	20	5	-	-	-	-	2
GS7A	20	30	35	<1	15	<1	-	-	-	<1
GS11D	30	10	40	-	-	-	10	10	2	-
GS13A	25	25	43	<1	-	-	2	5	-	<1
GS13B	20	55	10	2	-	-	10	2	-	1

Table 3.6: *Hybrid rock names as classified by the TAS (Figure 4.1a; Middlemost, 1994) and R_1R_2 (Figure 4.1b; De la Roche et al., 1980) diagrams. Rock names based on the classification scheme of Frost et al. (2001) are also shown. Where the classification schemes name the same rock specimen differently, the name in brackets is not used in this study.*

Variety	Sample	Classification scheme		
		TAS diagram (Middlemost, 1994)	R_1R_2 diagram (De la Roche et al., 1980)	Frost et al. (2001)
Qz-Bt-rich	GS1A	Granodiorite	(Granite)	(Diorite)
Grt-bearing	GS7A	Granodiorite	Granodiorite	(Two-mica granite)
Opx-Cpx-rich	GS11D	Px-bearing Granodiorite	(Px-bearing Tonalite)	(Px-bearing diorite)
Kfs-rich	GS13A	Px-bearing Granite	Px-bearing Granite	(Px-bearing diorite)
Kfs-rich	GS13B	(Px-bearing Granite)	Px-bearing Granodiorite	(Px-bearing diorite)

Samples GS11D, GS13A and GS13B contain both orthopyroxene and clinopyroxene, so the modifier Px-bearing is used.

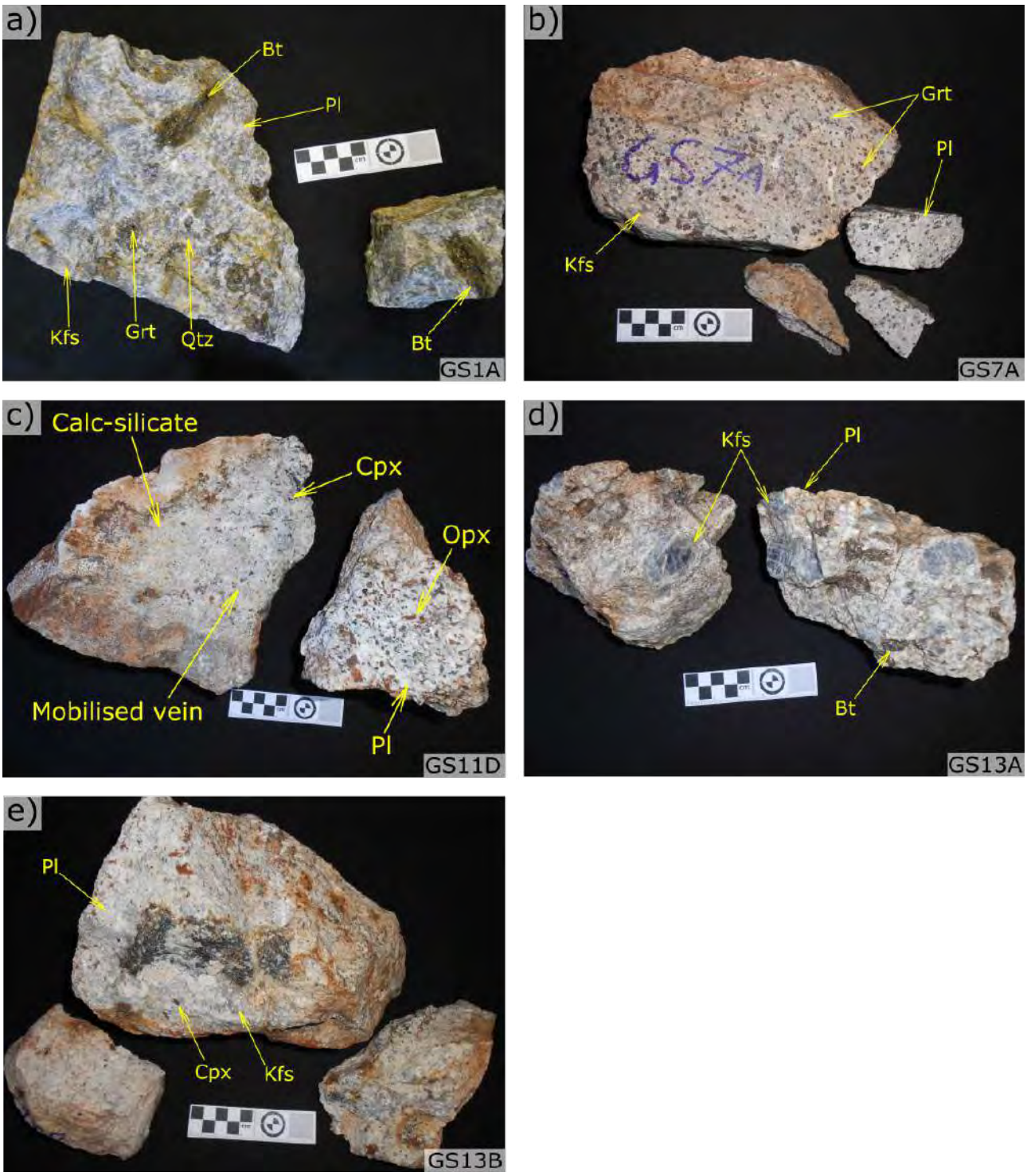

Figure 3.26: *The various types of hybrid rock encountered in the study area. (a) Grey-coloured granodiorite, sample GS1A. One occurrence of this quartz-biotite-dominant variety was found in the study area. (b) Garnet-rich granodiorite, sample GS7A. (c) The specimen on the right is a pyroxene-rich granodiorite. This specimen was crushed and analysed as sample GS11D. The specimen on the left is a Bysteek calc-silicate, similar to sample GS10A (Figure 3.18c), contacting part of the same rock as sample GS11D. The calc-silicate becomes increasingly granitic towards the upper right of the photograph, and a mobilised vein of Hybrid-type material is visible. (d) The pyroxene-bearing granite contains large blue-grey K-feldspar phenocrysts not typical of the hybrid rock. Such rock was found only in two localities of the study area, GS13 and within 10 m of GS6. (e) The pyroxene bearing granite, sample GS13B, was collected from a pod in the same hybrid rock layer as sample GS13A. This specimen, sample GS13B, lacks the large K-feldspar phenocrysts but has a higher feldspar and pyroxene mode.*

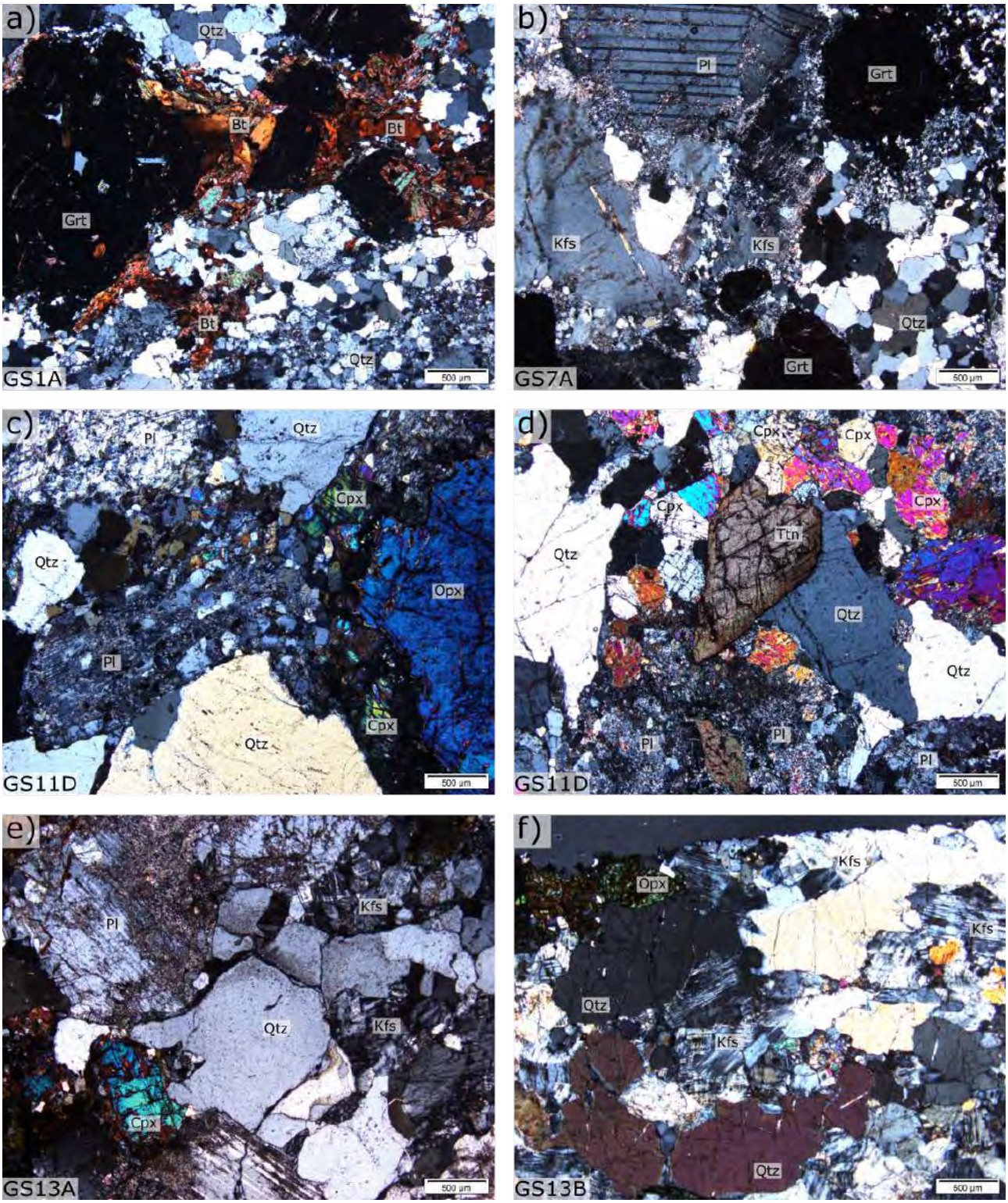

Figure 3.27: *The hybrid rock specimens (CPL). (a) Garnet from the quartz-biotite-dominant Hybrid variety. Garnet is always in contact with biotite. (b) The garnet-rich granodiorite sample GS7A is dominated by K-feldspar, plagioclase, quartz and rounded garnet. (c) and (d) are both from sample GS11D. (c) Recrystallised plagioclase-quartz clast. (d) The pyroxene-rich granodiorite, sample GS11D, comprises subhedral orthopyroxene, subhedral to euhedral clinopyroxene, subhedral to euhedral titanite, subhedral plagioclase and magmatic quartz. (e) K-feldspar (strained) and plagioclase phenocrysts typical of sample GS13A. Also visible are clinopyroxene and quartz. (f) The pyroxene-bearing granodiorite, sample GS13B, generally has a finer grain size than sample GS13A. The rock also has higher orthopyroxene and clinopyroxene modes than sample GS13A*

Garnet-bearing variety (sample GS7A)

Figure 3.26b, shows sample GS7A, a garnet-bearing variety of hybrid rock. This rock, together with sample GS11D, are the typical hybrid rock varieties encountered in the study area.

The rock is a cream-coloured, garnet-bearing granodiorite. The rock is moderately-well segregated into leucocratic and melanocratic pods. This is believed to result from inhomogeneous melt compositions, due to the limited distance between source materials (that is, Swartoup magma and its Bysteek calc-silicate wall-rock). The leucocratic pods consist of quartz, plagioclase, K-feldspar and garnet (< 1–3 mm). K-feldspar and plagioclase phenocrysts are commonly 0.6 cm to 1 cm in length. The melanocratic pods comprise the same mineralogy as the leucocratic pods, but with the addition of biotite and higher modes of quartz and garnet. Garnet crystals of the melanocratic pods are somewhat larger than those in the leucocratic pods (1.5–7 mm).

Sample GS7A consists of approximately 35 vol% Pl, 30 vol% Kfs, 20 vol% Qz, 15 vol% Grt, <1 vol% Opq and <1 vol% Sil. In thin section a very diffuse layering of garnet-richer and -poorer layers defines the magmatic foliation. Quartz, K-feldspar and plagioclase commonly measure 0.6 cm to 1 cm in length. They, along with anhedral garnet (< 1–3 mm), comprise the leucocratic pods (Figure 3.27b). Quartz lenses are foam textured and both K-feldspar and plagioclase are anhedral. The melanocratic pods have higher quartz and garnet modes.

Orthopyroxene-clinopyroxene variety (sample GS11D)

Sample GS11D is shown in Figure 3.26c. The sample crushed and analysed as sample GS11D is the right hybrid rock specimen shown in the figure. The left specimen is a Bysteek calc-silicate, macroscopically similar to GS10A. Visible in Figure 3.26c is a diffuse contact from calc-silicate to hybrid rock. The rock becomes increasingly granitic towards the contact on the right of the specimen. 'Stringer' veins of the hybrid rock are visible in the calc-silicate. These are believed to result from melting of the calc-silicate rock after introduction of and mixing with Swartoup magma (see Section 5.3.3).

Sample GS11D is an orthopyroxene-clinopyroxene-bearing granodiorite. The rock is almost isotropic in structure and contains 0.3 cm to 1.5 cm subhedral to euhedral, brown-coloured orthopyroxene and 0.2 cm to 0.5 cm anhedral to subhedral, green-black coloured clinopyroxene. Euhedral titanite (< 1–1.5 mm in length) are evenly distributed and randomly oriented along with the pyroxenes in a white plagioclase-K-feldspar-quartz matrix. This rock variety has the

whitest leucocratic matrix of the hybrid rocks and is the most plagioclase-rich (Table 3.5).

Sample GS11D consists of approximately 40 vol% Pl, 30 vol% Qz, 10 vol% Cpx, 10 vol% Opx, 10 vol% Kfs and 2 vol% Ttn. This pyroxene-bearing granodiorite has the highest plagioclase, orthopyroxene and clinopyroxene modes of the hybrid rocks and is isotropic.

Figures 3.27c and 3.27d show two CPL photomicrographs of sample GS11D. The rock contains subhedral to euhedral orthopyroxene which are up to 0.5 cm in diameter (Figure 3.27c). Clinopyroxene is found in two habits within the thin section specimen. The first are subhedral grains, up to 1 mm in length, though subhedral to euhedral clinopyroxene much larger are found in hand specimen. Clinopyroxene are also found in irregularly shaped veinlets, which are recrystallised to a foam texture (Figure 3.27d).

Subhedral K-feldspar and plagioclase grains measure up to 1.5 mm in length. Plagioclase are also found in a second habit, whereby anhedral to subhedral plagioclase (Figure 3.27c,d) are recrystallised. These grains are commonly in contact with large, strain-free quartz. When altered, the recrystallized plagioclase grains have undergone higher degrees of retrograde sericitisation than non-recrystallised plagioclase. Euhedral titanite (0.2–0.7 mm) is commonly found throughout the sample (Figure 3.27d).

K-feldspar-rich variety (samples GS13A and GS13B)

Figures 3.26d (sample GS13A, pyroxene-bearing granite) and 3.26e (sample GS13B, pyroxene-bearing granodiorite) show two pyroxene-bearing granitoids. These specimens were collected from two adjacent pods in a layer of hybrid rock.

Sample GS13A is a pyroxene-bearing granite (Table 3.6). The rock is characterised by blue-grey phenocrystic K-feldspar up to 3 cm in length (Figure 3.26d), seen only in one other locality in the study area (see Section 3.1.4). The rock has been included as one of the K-feldspar-rich varieties of hybrid rock, due to this porphyritic structure. However, the rock has the second lowest K-feldspar mode of the hybrid rocks. Sample GS13A is relatively isotropic. Elongated masses of weathered biotite, similar to those in sample GS1A, show no preferred orientation. K-feldspar and plagioclase are off-white in colour, except for the large blue-grey K-feldspar phenocrysts. Clinopyroxene and orthopyroxene are randomly distributed throughout the rock matrix and are not localised to the biotite masses.

Sample GS13B is also a pyroxene-bearing granodiorite. The rock, in contrast to sample GS13A, has the highest K-feldspar mode of the hybrid rocks, though it lacks the phenocrystic K-feldspar

of sample GS13A. The pyroxene-bearing granodiorite has a well-developed magmatic foliation. K-feldspar and plagioclase crystals are off-white in colour, in contrast to quartz which has a translucent grey colour. Pyroxene-rich pods (2 cm × 4 cm) host minor biotite.

Sample GS13A consists of approximately 38 vol% Pl, 25 vol% Kfs, 25 vol% Qz, 5 vol% Bt, 5 vol% Cpx, 2 vol% Opx and <1 vol% Opq. Under the microscope, the rock contains subhedral, foam-textured plagioclase and K-feldspar surrounded by almost strain-free quartz, very similar to sample GS11D (Figure 3.27e). Larger, strain-free plagioclase phenocrysts are also common. Figure 3.27e shows somewhat sericitic plagioclase in contact with quartz and K-feldspar. The K-feldspar is recrystallised to a much higher degree than the quartz grain. Clinopyroxene is commonly in contact with orthopyroxene and both are anhedral to subhedral.

Sample GS13B consists of approximately 55 vol% Kfs, 20 vol% Qtz, 10 vol% Pl, 10 vol% Opx, 2 vol% Cpx, 2 vol% Bt and 1 vol% Opq (Figure 3.27f). Visible in thin section is a single 1.5 mm × 4.5 mm foam-textured clinopyroxene surrounded by foam-textured K-feldspar. These are adjacent to 3.5 mm × 5.5 mm strain-free quartz. The rest of the specimen appears as Figure 3.27f, which shows foam-textured K-feldspar and a small, relict orthopyroxene crystal. Sample GS13B has more orthopyroxene and clinopyroxene combined than sample GS13A, though sample GS13A has a higher clinopyroxene mode.

3.2.5 Polisiehoek Granite-gneiss

The Polisiehoek Granite-gneisses are divided into three varieties for descriptive purposes; sheared (samples 1136A, 1147C, 1148A and 1148B), non-sheared (sample 1152A) and granitic (sample 1142A). Additionally, two samples are described separately as they show contacts from Polisiehoek Granite-gneiss to (i) Koenap migmatite (sample GS4E) and (ii) Swartoup monzodiorite (sample GS11B). Table 3.7 shows the modal mineral abundances of the collected specimens.

Typical sheared Polisiehoek Granite-gneiss (samples 1136A, 1147C, 1148A, 1148B and GS4B)

Figure 3.28a shows sample 1136A, a typical LS-tectonite of the Polisiehoek Granite-gneiss. The rock is a biotite-K-feldspar-plagioclase-quartz gneiss. The sheared gneisses of the Polisiehoek Granite-gneiss vary in colour from orange-pink to dark pink-brown. They are quartzofeldspathic and, if present, biotite and garnet modes are low. Sample 1147C is a biotite-K-feldspar-

Table 3.7: *Modal mineral composition of Polisiehoek Granite-gneisses (vol%). Modes were determined visually from thin section and macroscopic evaluation. Mineral abbreviations are after Whitney and Evans (2010).*

Sample	Qz	Kfs	Pl	Bt	Grt	Sil	Ms	Opq
1136A	35	25	30	5	-	-	2	3
1142A	52	37	10	-	-	-	1	-
1147C	34	32	34	<1	-	-	-	-
1148A	39	58	-	2	<1	-	-	<1
1148B	45	50	-	3	-	-	-	2
1152A	38	48	10	<1	5	-	-	<1
GS4B	55	32	10	-	-	3	-	<1
GS4E	58	30	10	-	-	2	-	<1
GS11B	45	50	5	-	-	-	-	<1

plagioclase-quartz gneiss and samples 1148A and 1148B are quartz-K-feldspar gneisses.

Layers of leucosome and melanosome have broad, gradational transitions between them. Leucosomes have higher feldspar modes than melanosomes, which are more quartz-rich (and have more biotite, if present). Commonly the gneisses are fine to medium-grained, and biotite crystals (1 × 3 × 5 mm) define the tectonic foliation, if present. Sample 1136A shows the highest biotite mode of all the Polisiehoek Granite-gneiss specimens. Elongated streaky lenses of quartz (1–7 mm wide, up to 5 cm long) and K-feldspar (3 mm wide, up to 5 cm long) are aligned to this foliation and help distinguish the foliation in the absence of biotite.

The gneissose structure of samples 1148A and 1148B are enhanced by modal layering and grain size variations between quartz-rich (3 mm Qtz, 5 mm Fsp) and feldspar-rich layers (interstitial Qtz, < 1 mm Fsp). The boundaries between layers are sharp and linear. The gneisses commonly have rotated porphyroblasts of K-feldspar and plagioclase. These ϕ- and σ-clasts (see Passchier and Trouw, 2005) of K-feldspar and plagioclase commonly have subhedral prismatic lath cores, 0.5 cm × 2 cm in cross-section.

Figures 3.29a (PPL) and 3.29b (CPL) show the same photomicrograph field of view of sample 1136A. In thin section we see the typical sheared Polisiehoek Granite-gneisses are dominated by quartz, K-feldspar and lesser plagioclase. They contain approximately 34–45 vol% Qz, 25–58 vol% Kfs, 0–30 vol% Pl, <1–5 vol% Bt, < 1–3 vol% Opq and some have 2 vol% Ms and <1 vol% Grt (Table 3.7).

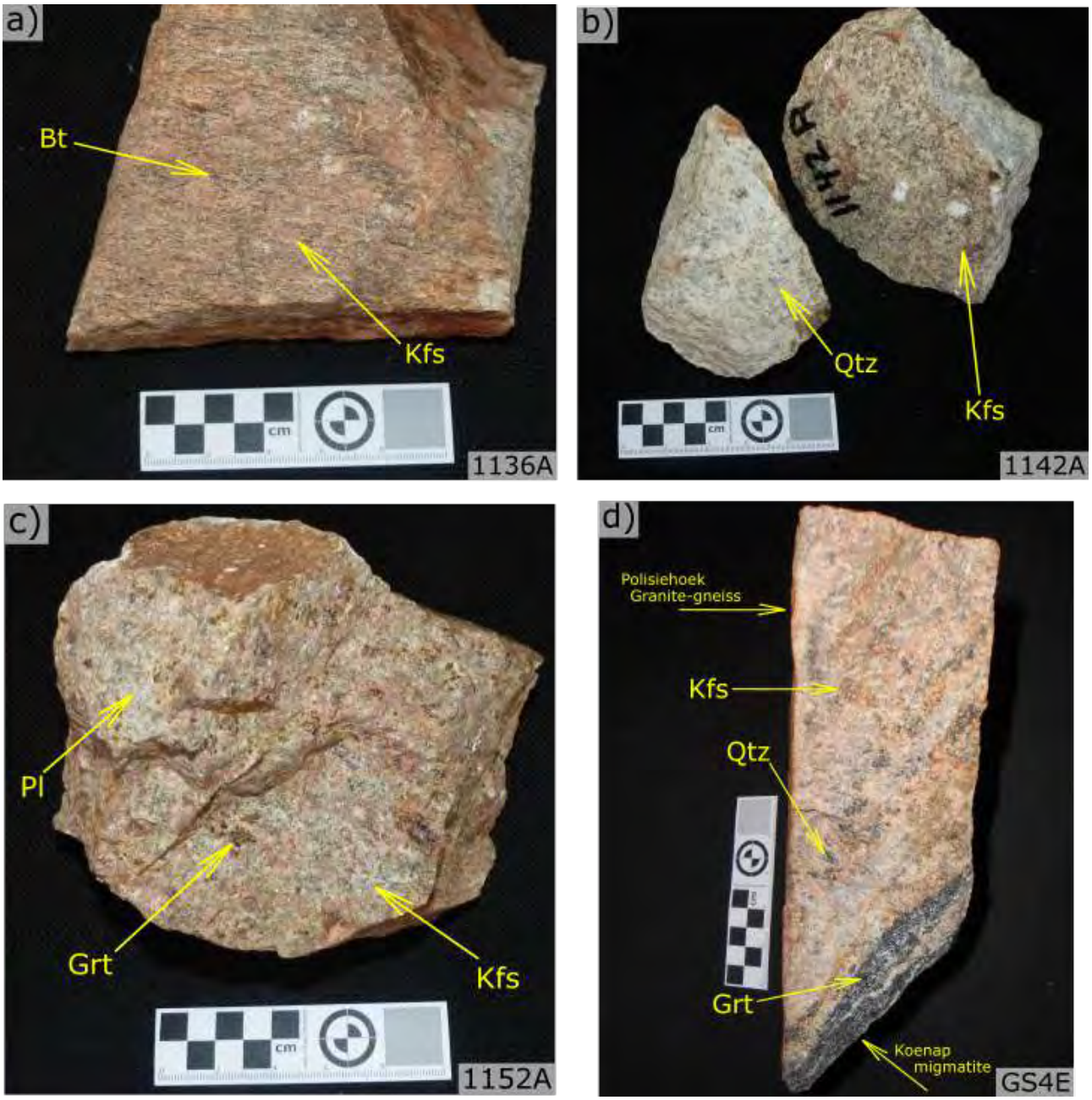

Figure 3.28: *The figures show typical varieties of the Polisiehoek Granite-gneiss found in the study area. Note the characteristic orange-colour of the rocks, which only the leucogranite does not share. (a) Typical pencil gneiss of the Polisiehoek Granite-gneiss. The strong tectonic foliation is defined by elongated biotite and quartz lenses. (b) While the leucogranite does not have the orange-colour characteristic of the Polisiehoek Granite-gneiss, it does share its characteristically low biotite mode which differentiates it from the igneous rocks associated with the Swartoup Pluton. (c) This granofels represents one of the least sheared Polisiehoek Granite-gneiss rocks and has the highest garnet mode of the collected Polisiehoek Granite-gneiss samples. Garnet are found in clusters (0.5 cm across) which border the leucosomes. (d) This specimen shows a section of the contact between Polisiehoek Granite-gneiss and a raft of Koenap migmatite (see Section 3.1.5, Figure 3.14a). The contact is transitional as veins of Polisiehoek material intrude into the Koenap migmatite.*

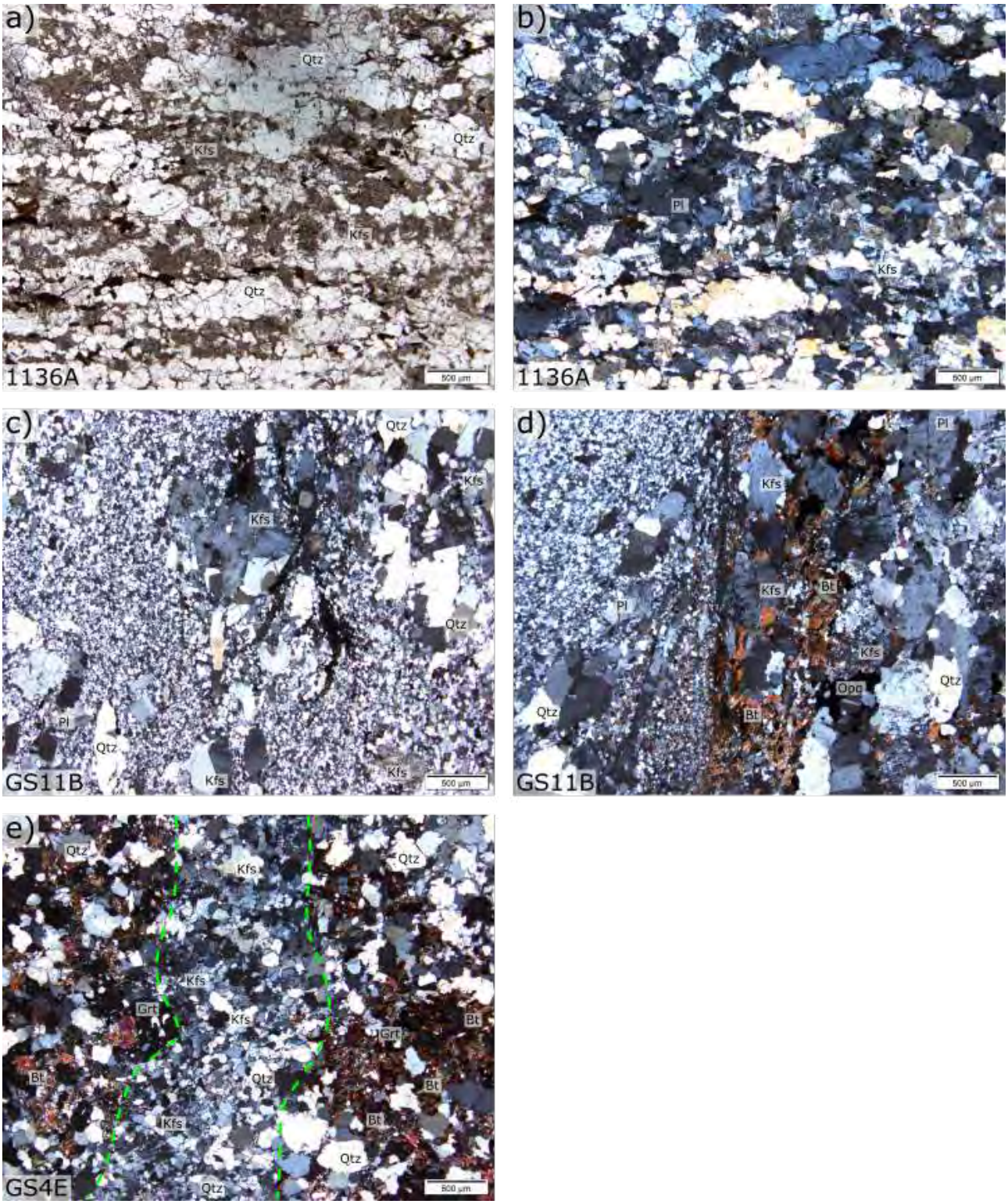

Figure 3.29: *(a) (PPL) and (b) (XPL) show the same field of view of a thin section from sample 1136A, the pencil gneiss in Figure 3.28. Note the low biotite mode, and elongated K-feldspar and quartz lenses. (c) K-feldspar phenocrysts set in a quartz-K-feldspar groundmass, sample GS11B. This specimen was collected from a dyke intruding a Swartoup granitoid (see Figure 3.14b). (d) Contact of this sample GS11B (Polisiehoek Granite-gneiss, left of image) to Swartoup monzodiorite (right of image). Note the sharp, linear contact marked by an increase in grain size and biotite mode. (e, XPL) A stringer vein of Polisiehoek Granite-gneiss which intruded Koenap migmatite lit-par-lit. Note the low biotite mode of the Polisiehoek vein, central in the photomicrograph, and the sharp, curved contacts to the Koenap material. The contacts are marked by an increase in grain size and the modal abundances of biotite and opaque minerals towards the Koenap migmatite host.*

The layering of these rocks is shown in thin section by alignment of biotite and opaque minerals, when present. Lenses of quartz, K-feldspar and plagioclase are also aligned with the foliation. Higher quartz modes are generally associated with melanocratic layers, and leucocratic layers with slightly higher K-feldspar and plagioclase modes.

About 70 vol% of quartz in these rocks is foam-textured. Commonly 70 vol% of plagioclase (up to 90 vol%) and up to 50 vol% of K-feldspar have undergone sericitisation. The relatively advanced alteration of these rocks helps distinguish them in thin section from other rock types.

Sample 1148A contains trace amounts of garnet, which appears to be breaking down. Garnet here is surrounded by dark-green spinel and biotite. Biotite and opaque grains are always found near each other in these rocks, when present.

Non-sheared, garnet-bearing variety (sample 1152A)

Sample 1152A is a medium-grained, orange-coloured garnet-plagioclase-quartz-K-feldspar granofels. The specimen is shown in Figure 3.28c. Alignment of prismatic feldspar lath porphyroblasts defines a very weak layering within leucocratic pods. The leucosomes comprise orange-coloured K-feldspar, grey quartz and cream-coloured plagioclase. Also found within the leucosome are grey K-feldspar porphyroblast laths, 0.5 cm to 1 cm in length.

Small pods (0.5 cm) of melanosome are present between leucocratic pods. The melanosomes consist of quartz, K-feldspar, garnet and biotite. Garnet (1–2 mm across) are subhedral and have depletion haloes. This sample has the highest garnet mode of the specimens collected from the Polisiehoek Granite-gneiss.

Sample 1152A consists of approximately 48 vol% Kfs, 38 vol% Qz, 10 vol% Pl, 5 vol% Grt, <1 vol% Bt and <1vol% Opq (Table 3.7). Under the microscope, quartz grains are foam-textured and K-feldspar crystals are also recrystallised, in contrast, plagioclase is not. K-feldspar and plagioclase have both undergone sericitisation. About 60 vol% of K-feldspar porphyroblasts (0.5–1 cm) are microperthitic. Alignment of quartz and feldspar porphyroblasts defines the layering of the leucosome in thin section. Biotite is commonly found near garnet, and opaque minerals are almost always found adjacent to biotite. Opaque minerals generally have a granular habit and measure 0.2 mm across.

Polisiehoek white granite (sample 1142A)

Shown in Figure 3.28b, sample 1142A is a white granite. On the TAS diagram (after Middlemost, 1994) the rock is classified as a granite. The R_1R_2 diagram (after De la Roche et al., 1980) classifies the rock as an alkali granite. However, the classification scheme of Frost et al. (2001) names this rock a diorite (classification not used, see Section 4.2). The rock is equigranular and medium-grained. A gneissic foliation is poorly-developed, along which elongated, grey-coloured quartz lenses are aligned. Individual quartz grains measure 1–8 mm across. Both K-feldspar and plagioclase are anhedral, and measure 3–10 mm across. Sample 1142A consists of approximately 52 vol% Qz, 37 vol% Kfs, 10 vol% Pl, 3 vol% Opq and 1 vol% Ms (Table 3.7).

In thin section about 70 vol% of quartz, K-feldspar and plagioclase crystals are foam-textured. Quartz and feldspar lenses define the foliation in thin section. The rock contains about 1 vol% white mica, which is proximally associated with K-feldspar which has undergone sericitisation.

Polisiehoek Granite-gneiss–Koenap migmatite contact specimen (sample GS4E)

Figure 3.28d shows sample GS4E. This specimen shows part of a lit-par-lit intrusive contact between Polisiehoek Granite-gneiss and Koenap migmatite. Figure 3.14a shows the contact in field (Section 3.1.5). The crushed and analysed sample of this specimen contains around 5 vol% of Koenap migmatite. This was done to investigate any possible genetic relationships between the two rock-types and have a Polisiehoek-Koenap 'intermediate' specimen.

The Polisiehoek section of the specimen is a medium-grained, orange-coloured plagioclase-K-feldspar-quartz gneiss. The rock is sheared parallel to the contact and has a well-developed tectonic foliation. Grain size variations enhance this foliation. Layers of quartz and K-feldspar porphyroblasts alternate with layers of interstitial quartz and smaller K-feldspar grains. K-feldspar is orange-coloured while quartz is translucent grey-green in colour and plagioclase is off-white.

The Koenap material is identical to Koenap migmatite sample GS4C (Section 3.2.1). Stringers of Polisiehoek material intrude between Koenap migmatite layers lit-par-lit, and they anastomose around garnet porphyroblasts (< 0.5 cm).

Under the microscope, Polisiehoek material intrudes along sharp contacts that curve around garnet porphyroblasts (0.2–5 mm). Figure 3.29e shows a photomicrograph (CPL) of one of these Polisiehoek stringers, central in the image, bounded by yellow dashed lines. The contact

is marked by an increase in grain size of K-feldspar, plagioclase and quartz in the host Koenap migmatite. The modal abundances of garnet, biotite and opaque minerals also increase at the contact.

The Polisiehoek material part of the specimen is a sillimanite-bearing plagioclase-K-feldspar-quartz gneiss. The rock consists of approximately 58 vol% Qz, 30 vol% Kfs, 10 vol% Pl, 2 vol% Sil, <1 vol% Opq (Table 3.7). Quartz (0.5 mm), K-feldspar (0.2 mm) and plagioclase (0.3 mm) are all foam-textured. The layering of the rock is defined in thin section by alignment of quartz lenses in quartz-rich layers.

The rock has an abundance of prismatic laths and needles of sillimanite, up to 0.5 mm long. These are distributed randomly throughout the Polisiehoek Granite-gneiss matrix. Opaque crystals have an angular habit and are less than 0.01 mm across.

The intruded Koenap migmatite is identical to sample GS4C, which was sampled 3 m from the Polisiehoek Granite-gneiss-Koenap migmatite contact (Figure 3.14a, Section 3.1.5). The stromatic layering of the migmatite is defined in thin section by melanocratic garnet-biotite-opaque mineral layers.

Quartz has sutured grain boundaries. K-feldspar is anhedral and microperthitic. Plagioclase is anhedral. Garnet has a resorbed texture, and is poikiloblastic, with inclusions of sillimanite, quartz and biotite. Garnet is commonly surrounded by biotite, K-feldspar, cordierite and opaque minerals.

Polisiehoek Granite-gneiss–Swartoup monzodiorite contact specimen (sample GS11B)

The plagioclase-quartz-K-feldspar gneiss (sample GS11B) was retrieved from a 20 cm-wide vein intruding a dome of Swartoup monzodiorite (Figure 3.14b, Section 3.1.5). The contacts are sharp and linear. The collected sample contains part of the contact and Swartoup material at the contact was removed prior to crushing for geochemical analysis. No Swartoup xenoliths were found in the crushed material.

Sample GS11B is fine-grained and has a pale-orange colour. The rock is sheared parallel to the contact and has a well-developed tectonic foliation. K-feldspar porphyroblasts and quartz lenses are aligned in the foliation. The rock has no mafic phases visible in hand specimen.

Sample GS11B consists of approximately 50 vol% Kfs, 45 vol% Qz, 5 vol% Pl and <1 vol%

Opq (Table 3.7). Under the microscope (Figure 3.29c,d) the rock is sheared parallel to the vein contact along multiple layers. These layers are distinguished in thin section by grain-size variations. Layers of fine-grained, recrystallised quartz and K-feldspar are interlayered with layers of the same recrystallised quartzofeldspathic groundmass, but also have quartz, K-feldspar and plagioclase porphyroblasts aligned sub-parallel to the layers (Figure 3.29c).

Figure 3.29d shows a crossed-polariser photomicrograph of a section of the contact from Polisiehoek vein (left in view) to the host Swartoup monzodiorite (right in view). The tectonic foliation of the Polisiehoek Granite-gneiss lies at an acute angle to the contact, which is sharp and linear. The contact to host Swartoup is marked by an increase in biotite and plagioclase modes as well as an increase in grain-size.

3.2.6 Mafic dyke

The mafic dyke specimen, sample GS12A, was collected to investigate the possibility of the Swartoup Pluton having a mantle component. The sample was collected from locality GS12, shown in Figure 3.15, Section 3.1.6. The mafic dyke is cross-cut by veins of granitic material that are likely to have been sourced from a nearby pegmatite. These have not been considered in determining the modal mineral composition of the rock, shown in Table 3.8. The rock is classified by the TAS diagram (Figure 4.1a, after Middlemost, 1994) as an olivine-gabbro, while the R_1R_2 chemical variation diagram (Figure 4.1b, after De la Roche et al., 1980) classifies the rock as a pyroxenite.

The rock is a black coloured metabasalt (Figure 3.30a), and has a very well-developed foliation, defined by alignment of orthopyroxene. Interstitial plagioclase and K-feldspar are translucent and have a light-grey colour in hand specimen.

The rock consists of 60 vol% Opx, 32 vol% Pl, 10 vol% Kfs, 5 vol% Cpx and 3 vol% Opq. Under the microscope, the metabasalt is adcumulate textured and the foliation is defined by alignment of elongated grains (Figure 3.30b). Orthopyroxene is anhedral to subhedral while the other minerals are anhedral. No quartz is present in thin section. All minerals are evenly distributed throughout the sample.

The sample shows one of the granitic veins that intruded the mafic dyke (Figure 3.30a). This granitic material comprises quartz (0.2–1.5 cm), K-feldspar (4 mm), plagioclase (1.5–3 mm) and biotite (up to 2 mm × 3 mm clusters) which are all aligned with the vein. Biotite occurs mostly at the contact between the two rock-types.

Table 3.8: *Modal mineral composition of the mafic dyke sample (vol%). Modes were determined visually from thin section and macroscopic evaluation. Mineral abbreviations are after Whitney and Evans (2010).*

Sample	Opx	Cpx	Pl	Kfs	Opq
GS12A	60	5	32	10	3

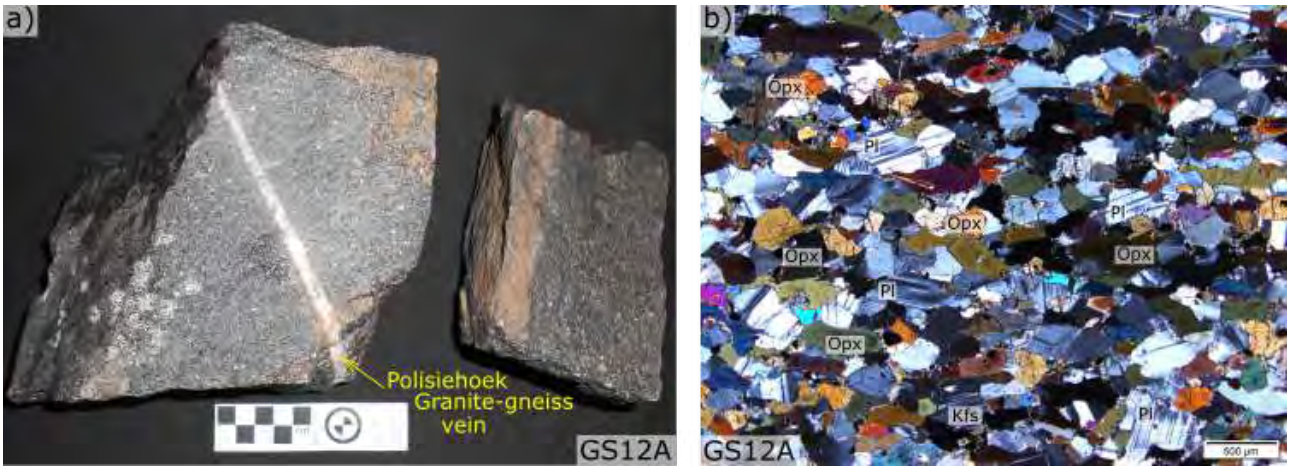

Figure 3.30: *(a) Specimens of the mafic dyke at locality GS12 (Section 3.1.6). The specimen is intruded by a vein of granitic material (4 mm wide). The contacts of this vein are sharp and linear. (b) The cumulate textured pyroxenite has a strong, pervasive magmatic foliation and comprises orthopyroxene, plagioclase, minor K-feldspar and excess quartz.*

3.3 Summary

The sample map from Figure 3.1 is repeated in Figure 3.31. Most of the rock types are readily distinguished in the satellite image. The Swartoup Pluton has a grey colour and forms an antiform. Red-brown coloured Polisiehoek Granite-gneisses over- and under-lie the Swartoup Pluton, stratigraphically. This is a result of Polisiehoek material intruding the overlying Koenap and Bysteek metasediments as well as intruding below the Swartoup Pluton. Subsequent folding resulted in Polisiehoek Granite-gneiss appearing around the outer margins and within the core of the antiform (see Figure 1.3). Koenap migmatite has a darker weathering colour than Polisiehoek Granite-gneiss, and generally lies west of the antiform, but is also exposed as outcrop within Polisiehoek Granite-gneiss and the Swartoup Pluton. The Koenap migmatites often form a dark coloured 'desert varnish'. Bysteek mafic calc-silicate and calc-silicate also are commonly exposed within both Polisiehoek Granite-gneiss and the Swartoup Pluton but are not readily distinguishable from Koenap migmatite in Figure 3.31. Bysteek marble are exposed near the stratigraphic middle of the Swartoup Pluton and can be seen curving with the antiform near the hinge (Figure 3.31). Pegmatites are also found in the area, and generally intrude perpendicular

to the strike of the Bysteek marble when within the Pluton, and form dykes with large scree areas outside the Pluton (Figure 3.31).

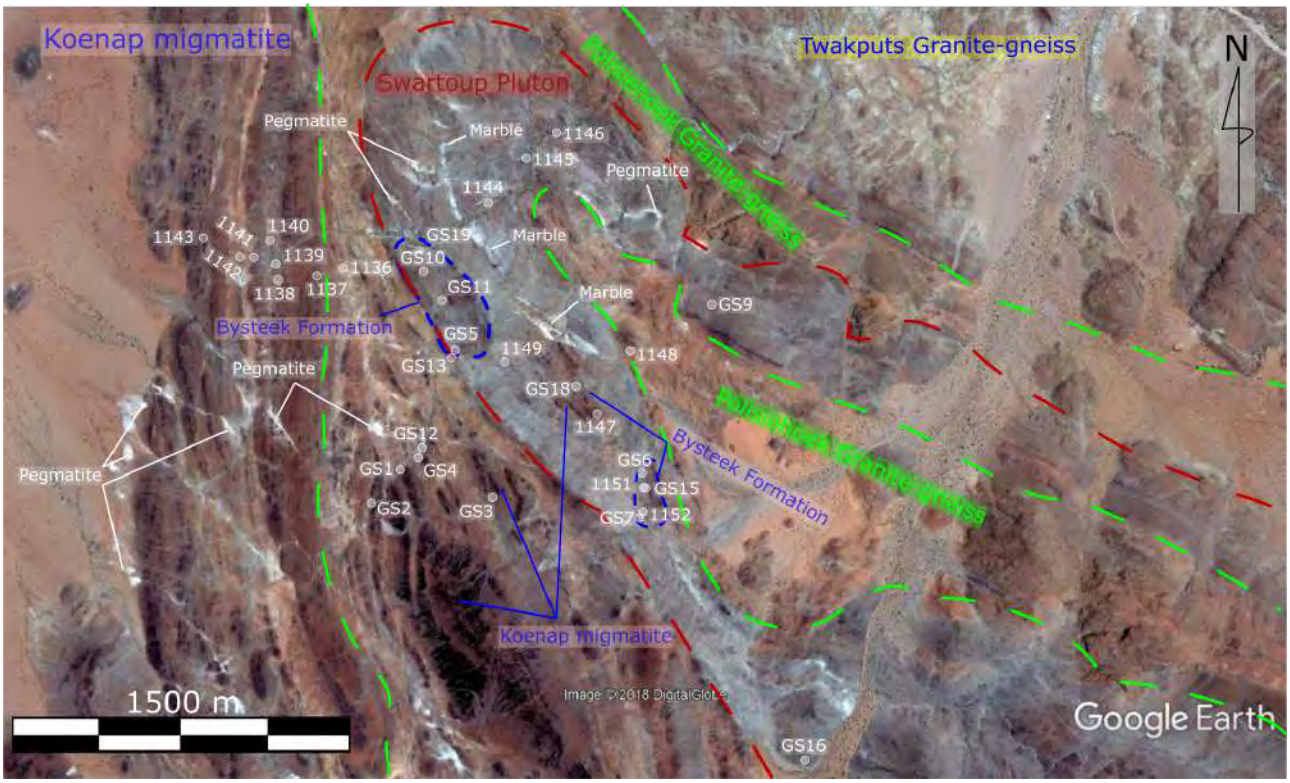

Figure 3.31: *The sample map from Figure 3.1 is repeated for reference. Hosted in an antiformal structure are the Swartoup Pluton (bounded in red) and its Polisiehoek Granite-gneiss core (bounded in green). Stratigraphically upward from the Swartoup Pluton is another Polisiehoek Granite-gneiss layer. West of the antiform are migmatites of the Koenap Formation and calc-silicates of the Bysteek Formation. These metasediments are also exposed within the Swartoup Pluton itself. Rafts of Koenap migmatite outcrop within the Polisiehoek Granite-gneiss on the western limb of the antiform. Pegmatites (left of view, and also near the hinge of the antiform) intrude throughout the sequence (image ©2018 Google).*

Koenap migmatite

These anatexites are often jointed and weathered with a black 'desert varnish'. This aides in their identification from a distance. Few contacts could be found in the field, as they are often adjacent to ridges of Koenap migmatite and buried under scree slopes (Section 3.1.1). However, at locality GS18, rafts of Koenap migmatite crop out within the western limb of the Swartoup Pluton (Section 3.1.3). Here, the contact is linear and mylonitic. The Koenap migmatite appears relatively unstrained, unlike the Swartoup granitoid which shows grain size reduction towards the contact (Figure 3.9a). Parallel to this contact are garnet-bearing granitoid layers.

In contrast, west of the Swartoup Pluton at locality GS4, a raft of Koenap migmatite shares a lit-par-lit, transitional intrusive contact with Polisiehoek Granite-gneiss (Section 3.1.5). Stringers

of Polisiehoek material intrude up to about 40 cm into Koenap migmatite along sharp contacts (Figure 3.14a).

Koenap migmatites vary in their leucosome to melanosome proportions as well as the degree to which these have segregated (Section 3.2.1). Samples 1138A, 1141A, 1143B, 1147B and GS4C are the more restitic, melanocratic specimens. Samples 1137A, 1143A, 1147A and GS4D are more leucocratic.

The Koenap migmatites have strong, pervasive, migmatitic fabrics that can be divided into four types. These are pod-structured (samples 1137A, 1143B and 1147B), compositionally layered (sample GS4D), stromatically layered (samples 1138A, 1141B, 1143A, 1147A and GS4C) and nebulitic migmatites (sample 1141A). Pod-structured migmatites have gradational boundaries between leucosomes and melanosomes. In contrast, compositionally layered migmatites show sharp boundaries between leucosomes and melanosomes, which have a high degree of segregation. Compositional layers vary from 2–15 cm thick. Stromatically layered migmatites often have well-developed stromatic layering which has been disrupted by leucosomes. The margins between leucosomes and melanosomes vary from sharp to gradational. Nebulitic migmatites are almost isotropic and resemble the melanocratic bands of the compositionally layered migmatites. Nebulitic migmatites host small volumes of *in-situ* leucosomes and within host leucocratic, rootless veins.

Under the microscope, leucosomes generally comprise quartz, K-feldspar, plagioclase, garnet, cordierite and biotite. Melanosomes comprise the same minerals but have somewhat greater proportions of garnet, biotite and opaque minerals. They also have lower K-feldspar and plagioclase modes than the leucosomes. Melanosomes also often have somewhat larger garnet porphyroblasts.

Garnet always has a resorbed texture and is often poikiloblastic, with inclusions of biotite, quartz and sillimanite. K-feldspar, plagioclase, quartz and biotite are proximally associated with garnet, as are cordierite, spinel and opaque minerals, when present. Cordierite commonly form rims around garnet and is usually pinitised.

Bysteek Formation

Typical Bysteek Formation outcrops (Figures 3.2a and 3.5a) are dark coloured and jointed (Section 3.1.2). They are also more angular, helping to distinguish them from Koenap migmatite. At locality GS7, blue-grey coloured Bysteek marble was intruded by sheared Swartoup granitoid

layers along sharp, linear contacts (Figure 3.5b). This marble hosts folded clasts of calc-silicate rock and hybrid rock (Figure 3.5b).

At locality GS6, Bysteek mafic calc-silicate is intruded, lit-par-lit, by Swartoup granitoids (Figure 3.5c). The mafic calc-silicate layers share sharp, curved contacts to the Swartoup material. Nearby, a boulder of mafic calc-silicate (Figure 3.5d) hosts folded veins of hybrid rock. In contrast, at locality GS15, Bysteek mafic calc-silicate is brecciated and has been intruded by hybrid rock (Figure 3.12a).

Sample GS10A is a Bysteek calc-silicate rock. The specimen consists of grey coloured, clinopyroxene-titanite-dominated calc-silicate rock which shares a sharp, undulating contact with orange-coloured, garnet-clinopyroxene-dominated calc-silicate rock (Figures 3.18c and 3.19a,b,d). The orange-coloured calc-silicate layers have pinches and swells up to 5 cm wide. The crushed and analysed portion of the specimen comprises about 60 vol% grey and 40 vol% orange-coloured calc-silicate. Both calc-silicate rock layers share sharp, undulating contacts with hybrid rock.

The mylonitic Bysteek mafic calc-silicate, sample GS15A, comprises hornblende, biotite, quartz, K-feldspar, plagioclase and opaque minerals. The L-S tectonite hosts mica fish supported in a leucocratic matrix of quartz, K-feldspar and plagioclase. This specimen was intruded by a vein of hybrid rock, containing recrystallised plagioclase clasts in contact with large, strain-free quartz grains, much like sample GS11D (Section 3.2.2).

Sample GS19A is a banded white Bysteek marble (Figure 3.18d). The rock was collected from a Bysteek marble layer near the stratigraphic centre of the Swartoup Pluton (Figure 3.31). Clinopyroxene (1–4 mm across) are hosted in pervasive, linear layers 0.2–2.3 cm wide and supported in a calcite matrix (Figure 3.19d).

Swartoup granitoids

Swartoup granitoids typically have a grey-colour when fresh that together with higher biotite modes, helps distinguish them from other rock types in the field (Figure 3.7a). They also often have larger feldspar phenocrysts than the other rock types, which are most helpful in identification of weathered outcrops (Figure 3.7b,c). Sampling was conducted with a focus on collecting fresh material, due to intense weathering (Section 3.1.3). As such, though the majority of the Swartoup sample set are granodiorites, the relative proportions of granitoids in the sample set do not reflect their proportions in the Pluton. The typical Swartoup rock type granite, such as in samples 1149A and GS5A.

Swartoup group 1 comprises the five typical Swartoup granodiorite specimens, samples 1139A, 1140A, 1144A, 1145A and 1146A (Table 3.4). The Swartoup group 1 specimens are somewhat compositionally and geochemically homogeneous but they are distinct from Swartoup group 2 (see Chapter 4). Swartoup group 2 consist of typical Swartoup granites (samples 1149A, GS5A and GS9B), orthopyroxene-bearing monzodiorites (samples 1151A and GS10B), orthopyroxene-bearing quartz monzonite (sample GS15B), garnet-bearing granites (samples GS15C and GS16A) and a leucogranite (sample GS9A).

Most of Swartoup group 1, the Swartoup granodiorites, were taken from near the hinge of the antiform (samples 1144A, 1145A and 1146A, Figure 3.6). Samples 1139A and 1140A are garnet-bearing and were taken from a dyke intruded into Koenap migmatite, to the west of the Pluton. However, they are still more geochemically similar to the rest of Swartoup group 1 than Swartoup group 2, and are classified as granodiorites in both classification schemes (Table 3.4).

Swartoup group 1 generally vary from medium- to dark-grey in colour and are medium- to coarse-grained (Section 3.2.3). They have a pervasive magmatic layering. Leucocratic layers comprise K-feldspar and plagioclase supporting biotite and quartz matrix. Melanocratic layers comprise the same minerals but with higher biotite modes and somewhat lower feldspar modes.

Samples 1149A and GS5A are the typical Swartoup granites (Figure 3.7). Sample GS9B was taken from a dyke (Figure 3.10) which hosts pods of leucogranite (sample GS9A). These granitic specimens have been geochemically analysed, but sample GS11A has not. Sample GS11A is macroscopically similar to these previously mentioned granites but was taken from a mylonitic dyke. It has therefore not been geochemically analysed due to concerns over possible mass transfer.

The Swartoup granites are characterised by relatively lower biotite modes (Table 3.3) than the Swartoup granodiorites and orthopyroxene-bearing monzodiorites. As such, they are lighter-coloured than the rest of the Swartoup granitoids. The Swartoup granites are medium- to coarse-grained, and show pervasive, weak magmatic layering.

The four orthopyroxene-bearing Swartoup granitoids identified in this study are samples 1151A, GS10B, GS11C and GS15B. At locality GS10, sample GS10B (orthopyroxene-bearing monzodiorite, Figure 3.21a) was collected from a dyke less than 10 m from the Bysteek calc-silicate, sample GS10A (Section 3.1.2, 3.1.3). A similar situation exists at locality GS11, where sample GS11C was collected from a dome of Swartoup monzodiorite near to Bysteek calc-silicate (Section 3.1.3). Sample GS11C has almost the same modal composition as sample GS10B (Table 3.3) but this specimen has not been geochemically analysed. Orthopyroxene-bearing quartz mon-

zonite (sample GS15B) shares a transitional contact with orthopyroxene-bearing monzodiorite (sample 1151A, Figure 3.7d). The orthopyroxene-bearing quartz monzonite has only minor orthopyroxene (<1 vol%, Table 3.3), in contrast to the orthopyroxene-bearing monzodiorites, samples 1151A and GS10B, which both have around 15 vol% orthopyroxene.

Samples 1151A, GS10B and GS11C are generally much darker in colour than other Swartoup granitoids, due to their relatively higher biotite modes and orthopyroxene contents. Sample GS15B (Figure 3.21b) is much lighter in colour than the other orthopyroxene-bearing rocks, due to its large K-feldspar and plagioclase phenocrysts. They are all medium- to coarse-grained rocks with a pervasive, magmatic layering. Leucocratic layers comprise K-feldspar, plagioclase, biotite and interstitial quartz. The melanocratic layers consist of the same mineralogy, but have much higher biotite modes, in addition to orthopyroxene. K-feldspar and plagioclase are finer-grained in the melanocratic layers.

Under the microscope, sample GS15B has a higher K-feldspar mode and similar plagioclase mode as sample GS10B. However, sample 1151A has a high plagioclase mode and a lower K-feldspar mode than the others (Table 3.3).

At locality GS18, garnet-bearing granitic layers are parallel to a mylonitic contact between Swartoup granitoid and Koenap migmatite (Figure 3.9). The garnet-bearing granites, samples GS15C and GS16A (Figure 3.23), were also collected near Koenap migmatite. However, Bysteek Formation also crops out at locality GS15.

Samples GS15C and GS16A are medium-grained and have pervasive, well developed layering, though the leucocratic and melanocratic layers of both samples are poorly segregated. The layering of sample GS15C is enhanced by shearing and grain size reduction. In contrast, the layering of sample GS16A is enhanced by multiple quartz segregation veins that are parallel to leucocratic and melanocratic layers. The leucocratic layers consist of K-feldspar, plagioclase and quartz. The melanocratic layers contain garnet, biotite and opaque grains set in a matrix of K-feldspar, plagioclase and quartz.

Hybrid rocks

The hybrid rocks are typically exposed as thin layers of off-white to pale-cream coloured granodioritic rock hosting subhedral to euhedral garnet or pyroxene (Section 3.1.4). They are always found in contact with Bysteek Formation (Figure 3.12) and Swartoup granitoids usually are also nearby, typically within about 10 m.

Hybrid rock is almost always in contact with either Bysteek mafic calc-silicate or calc-silicate rock. Bysteek mafic calc-silicate is often brecciated when in contact with hybrid rock, which often comprises the matrix supporting the breccia (Figure 3.12a). When in contact with Bysteek calc-silicate, hybrid rock usually faces towards nearby Swartoup granitoid (Figure 3.12b). It is likely the hybrid rock is usually physically eroded, along with Bysteek calc-silicate, leaving behind only thin layers. Where calc-silicate rock and hybrid rock layers are eroded completely, the more resistant Bysteek mafic calc-silicate protects the intruded hybrid rock.

Four varieties of hybrid rock have been identified (Section 3.2.4). These are quartz-biotite-rich (sample GS1A), garnet-bearing (sample GS7A), orthopyroxene-clinopyroxene-bearing (sample GS11D) and K-feldspar-rich (samples GS13A and GS13B). Of these, the garnet- and orthopyroxene-clinopyroxene-rich are the typical varieties.

Sample GS1A was collected from a pod of hybrid rock, which is surrounded by Bysteek mafic calc-silicate, and also hosts Bysteek mafic calc-silicate xenoliths (Figure 3.12d). This hybrid rock is further away from the Swartoup Pluton than the other specimens. The specimen is a medium-grey coloured granodiorite with a well-developed magmatic layering, defined by melanocratic biotite-rich pods and elongated quartz lenses. These pods are supported by leucocratic layers comprising quartz, K-feldspar and plagioclase. The melanocratic layers consist mostly of biotite, with minor garnet and opaque minerals.

Sample GS7A was collected from layers of garnet-rich hybrid rock intercalated with layers of Swartoup granitoid, about 7 m away from Bysteek marble. The cream-coloured, garnet-bearing granodiorite is moderately-well segregated into melanocratic and leucocratic pods. The leucocratic pods comprise quartz, plagioclase, K-feldspar and garnet. Melanocratic pods consist of these same minerals but with the addition of biotite and a higher garnet mode.

Sample GS11D is an orthopyroxene-clinopyroxene-bearing granodiorite. This rock was collected from a hybrid rock layer in contact with Bysteek calc-silicate rock, less than 5 m from a dome of Swartoup monzodiorite. Figure 3.26c shows the hybrid rock in diffuse contact with Bysteek calc-silicate rock. Stringers of hybrid rock are present within the calc-silicate and the specimen overall becomes more 'granitic' towards the hybrid rock.

This almost isotropic rock is one of the typical varieties of hybrid rock. It is rich in orthopyroxene, clinopyroxene and titanite, which are randomly distributed throughout a plagioclase-K-feldspar-quartz matrix.

Under the microscope, clinopyroxene is found in two habits. The first are subhedral to euhedral

grains and the second are as foam-textured, irregularly shaped veinlets (Figure 3.27d). There are also largely strain-free plagioclase and quartz in contact with strained clasts of plagioclase and quartz (Figure 3.27c).

At locality GS13 a layer of hybrid rock lies at the footwall of Bysteek calc-silicate rock. This calc-silicate rock was intruded by a nearby dyke of Polisiehoek Granite-gneiss. The hybrid rock layer comprises pods of phenocrystic K-feldspar-rich hybrid rock (sample GS13B) and finer-grained, K-feldspar-pyroxene-richer pods of hybrid rock (sample GS13A). These pods share both sharp and diffuse contacts with each other. Under the microscope, sample GS13A shows recrystallised plagioclase and K-feldspar grains in contact with strain-free quartz and plagioclase (Figure 3.27 3.27e), similar to sample GS11D.

Polisiehoek Granite-gneiss

A characteristic red-brown weathering colour distinguishes Polisiehoek Granite-gneiss form other rock types. When fresh, they have a typically orange colour, with few exceptions. This, along with their relatively low biotite and higher K-feldspar modes, helps distinguish them from Swartoup granitoids. These rocks appear to have accommodated the most strain in the study area, and vary from pencil gneisses to granofelses (Figure 3.28a,c).

Most Polisiehoek Granite-gneiss specimens are sheared (samples 1136A, 1147C, 1148A, 1148B and GS4B) biotite-K-feldspar-plagioclase-quartz gneisses or quartz-K-feldspar gneisses (Table 2.1). They vary form orange-pink to dark pink-brown in colour and are fine- to medium-grained.

Leucosomes have higher feldspar modes than melanosomes, which have higher quartz and biotite modes. Layers of leucosome and melanosome share gradational boundaries. These layers, along with elongated biotite lenses, and quartz and K-feldspar lenses define strong tectonic foliation in the rocks.

Sample 1152A is a medium-grained garnet-plagioclase-quartz-K-feldspar granofels (Figure 3.28c). This orange-coloured rock is the least sheared Polisiehoek Granite-gneiss specimen and has the highest garnet mode (Table 3.7). The rock comprises pods of leucosome and melanosome which are internally weakly layered. Leucosomes contain K-feldspar, quartz and plagioclase. However, melanosomes contain quartz, K-feldspar, garnet and biotite.

Sample 1142A differs from the rest of the Polisiehoek Granite-gneisses with respect to its colour. The rock is a white granite, with less than 1 vol% mica minerals (Table 3.7). The equigranular

rock has a poorly developed gneissic foliation, along which streaky quartz lenses that are aligned. Under the microscope antiperthite exsolutions are common in plagioclase, and larger than in other rocks.

Few contacts between Polisiehoek Granite-gneiss and other rock-types could be investigated in detail (Section 3.1.5). They are often buried under scree slopes of ridges of Koenap migmatite or are highly mylonitised when in contact with Swartoup granitoid, confirmed by van Huyssteen (2017).

At locality GS4, Polisiehoek Granite-gneiss shares a lit-par-lit intrusive, transitional contact with Koenap migmatite (Figure 3.14a). Stringers of Polisiehoek material intrude Koenap migmatite up to about 40 cm and anastomose around garnet porphyroblasts. In contrast, no Koenap xenoliths were found in the Polisiehoek Granite-gneiss body.

Sample GS4E is a medium-grained, sillimanite-bearing plagioclase-K-feldspar-quartz gneiss (Figure 3.28d). The orange-coloured rock shows part of the contact with Koenap migmatite and is sheared parallel to this. Under the microscope, the rock differs from other Polisiehoek Granite-gneisses in that it has an abundance of sillimanite needles and prisms randomly distributed throughout. The crushed and analysed specimen includes a portion of the Koenap material, to investigate any relationship between the Polisiehoek Granite-gneiss and the Koenap Formation.

At locality GS11, contacts between Polisiehoek Granite-gneiss and Swartoup monzodiorite are exposed. Here, two veins of Polisiehoek Granite-gneiss intrude a Swartoup monzodiorite dome along sharp, linear contacts (Figure 3.14b). Xenoliths of elongated, angular Swartoup material are found within the intrusive veins.

Sample GS11B is a fine-grained, plagioclase-quartz-K-feldspar gneiss. The rock has a pale orange colour, like most other Polisiehoek Granite-gneiss specimens and has no mafic minerals visible in hand specimen or thin section. Under the microscope, the rock comprises layers of fine-grained quartz, K-feldspar and plagioclase (Figure 3.29c). The contact is marked by the appearance of biotite and an increase in grain size (Figure 3.29d).

Mafic dyke

At locality GS12 a well-foliated basaltic dyke is exposed (Section 3.1.6). The body has a north-northwest–south-southeast strike (Figure 3.15), somewhat parallel to the orientation of the Hartebees River Shear Zone (Figure 1.2). The mafic dyke intruded Polisiehoek Granite-gneiss along sharp, linear contacts, which appear to have been offset during brittle deformation

(Figure 3.15). The rock is easily distinguished by its black-colour and high orthopyroxene mode. Contrasting with its black colour, two sets of pale coloured granitic veins intruded the dyke. These could be tracked about 15 m into the Polisiehoek Granite-gneiss host, towards a large pegmatite body. This pegmatite is located about 200 m west of locality GS12.

Sample GS12A has a very well-developed foliation defined by alignment of orthopyroxene (Figure 3.30). Under the microscope, the specimen comprises mostly orthopyroxene and plagioclase, with lesser K-feldspar and clinopyroxene and opaque minerals. All phases are evenly distributed throughout.

The sample shows one of the granitic veins which intruded the mafic dyke. This felsic material comprises quartz, K-feldspar, plagioclase and biotite. Biotite occurs mostly at the contact between the two rock-types.

CHAPTER 4

Geochemistry

Major, minor and trace element analyses were conducted on thirty-nine samples (eight Koenap migmatites, three Bysteek Formation rocks, fourteen Swartoup Pluton rocks, five hybrid rocks, nine Polisiehoek Granite-gneisses, and one mafic dyke; Table 2.1) at the University of Stellenbosch's Central Analytical Facilities. The results of the analyses are found in Tables 4.1-4.5. The analytical procedures are found in Section 2.3.

Total-Alkali versus Silica (Figure 4.1a; after Middlemost, 1994) and R_1R_2 (Figure 4.1b; after De la Roche et al., 1980) diagrams were used to classify the igneous rocks of this study, shown in Section 4.1. Section 4.2 also presents classification diagrams, namely the Fe-number, Modified Alkali-lime Index and Aluminium Saturation Index (Figure 4.2). Section 4.3 explores the I-, S- and A-type granitoid characteristics of the igneous rocks of the study, using diagrams of P_2O_5, Ce, Y and La against Rb and SiO_2 (Figure 4.3).

Section 4.4 shows various chemical variation diagrams. These include major and minor oxide plots against silica (Figures 4.4–4.5), molar titanium and zirconium against maficity (Figure 4.6) and chondrite normalised rare-earth diagrams (Figure 4.7). The geochemical compositions of the analysed samples are compared to published pelite and greywacke compositions (Section 2.1, Tables 2.2–2.4). Pelites are considered the most likely protolith of the Koenap Formation (Moen and Toogood, 2007, Section 1.3), however, greywackes are considered more fertile protoliths of granitoids (Clemens, 2012). Melt segregation from such protoliths should produce discernible trends of depletion or enrichment in specific chemical components. Light-grey fields are used to indicate greywacke compositions and light-brown ones for pelitic compositions. The rare-earth

plots of Section 4.4.3 have been normalised using CI carbonaceous chondrite of McDonough and Sun (1995).

Section 4.5 contains the results of the Sm/Nd and Rb/Sr isotope analyses (Tables 4.9, 4.8; Figure 4.8) of selected samples (Table 2.1). The analytical procedures are found in Section 2.3.3. At the end of Sections 4.1 to 4.5 are summary and interpretation subsections. These interpretations consider field relationships and sample petrography (Chapter 3) but mostly concern the data of only their respective geochemistry sections. Chapter 5 presents a discussion which brings all available data into consideration. Section 4.6 presents results of U/Pb zircon age dating (Figure 4.9) done on rocks from the study area; the analytical procedures of which are found in Section 2.4.

4.1 Rock classification schemes

The igneous rocks of the sample set (Swartoup granitoids, hybrid rocks, Polisiehoek Granite-gneisses and the mafic dyke specimen) have been plotted on a Total-Alkali versus Silica (TAS) diagram, after Middlemost (1994) (Figure 4.1a). This diagram, along with the R_1R_2 chemical variation diagram of De la Roche et al. (1980) (Figure 4.1b), was used to classify the igneous rocks of this study (see Tables 2.1, 3.4 and 3.6). The Koenap migmatite and Bysteek Formation specimens are plotted for comparison only.

The silica contents of the sample set are also described in the following subsection. However, they are not described again in detail except for when it is appropriate. The silica contents of the rocks are however, repeated in Section 4.4.1 for convenience, as many of the data plots are against silica.

4.1.1 Total-alkali versus silica diagram

A detailed description of the TAS diagram is shown in Appendix A.1.1.1. The TAS diagram shows the Swartoup group 1 rocks (samples 1139A, 1140A, 1144A, 1145A and 1146A) have similar silica and alkali contents as each other. Most of the Swartoup group 1 specimens plot in the upper portion of the Granodiorite field (6–7 wt% K_2O + Na_2O). Sample 1146A has somewhat more alkalis (about 8 wt% K_2O + Na_2O) and plots in the Quartz Monzonite field. In contrast, Swartoup group 2 specimens show greater variation in their SiO_2 contents (52 to 84 wt% SiO_2). These rocks plot in the Monzodiorite (sample 1151A), Monzonite (sample GS10B), Quartz Monzonite (sample GS15B), Granodiorite (sample GS15C) and Granite fields

Table 4.1: *Major, minor and trace element data of collected Koenap migmatite specimens. The XRF analyses have been normalised to 100 wt% anhydrous. The Fe-contents of the rocks have been expressed as* FeO^{T} *(*$FeO^{T} = 0.89 \times Fe_2O_3$*).*

Sample	1137A	1138A	1141A	1143A	1143B	1147B	GS4C	GS4D
wt.%								
SiO_2	66.72	64.18	64.05	67.94	68.83	65.36	66.50	65.61
TiO_2	1.09	1.17	1.20	1.04	1.03	1.08	1.24	1.26
Al_2O_3	14.71	14.42	15.10	15.00	14.70	14.77	15.66	14.89
Cr_2O_3	0.01	0.01	0.01	0.01	0.01	*bdl*	0.01	*bdl*
FeO^{T}	7.55	12.78	12.36	7.53	7.30	9.21	8.92	9.04
MnO	0.10	0.15	0.10	0.14	0.11	0.14	0.10	0.14
MgO	2.32	3.24	3.55	2.65	2.63	2.82	3.71	2.43
CaO	1.86	0.50	0.44	1.70	1.65	0.46	0.54	1.69
Na_2O	2.07	0.43	0.30	1.30	1.21	0.55	0.67	1.67
K_2O	2.65	1.53	1.44	1.72	1.69	3.96	1.48	1.79
P_2O_5	0.07	0.04	0.04	0.07	0.05	0.07	0.03	0.04
ppm								
Ba	843.41	594.08	551.43	419.97	390.87	892.87	381.85	776.50
Ce	106.67	79.51	87.76	108.84	93.17	104.77	120.79	97.75
Co	18.25	17.92	13.90	17.97	16.01	23.00	21.66	22.97
Cr	75.11	89.86	91.55	88.30	86.62	78.36	112.85	91.55
Cs	0.48	0.51	1.41	1.05	1.16	3.85	1.49	0.71
Cu	20.03	14.37	19.40	5.06	9.85	23.53	22.02	31.50
Dy	10.10	11.18	10.50	8.47	8.27	9.13	11.20	11.12
Er	6.49	6.77	6.47	5.13	5.11	5.56	6.70	6.13
Eu	1.89	1.27	1.04	1.45	1.26	1.87	1.33	2.20
Gd	9.26	9.99	9.36	8.88	8.23	9.52	11.10	8.98
Hf	8.35	9.90	9.96	8.28	8.22	9.00	10.41	7.90
Ho	2.31	2.37	2.22	1.75	1.74	1.89	2.22	2.25
La	53.46	38.91	43.08	52.28	46.88	51.53	56.35	49.45
Lu	0.82	0.94	0.90	0.70	0.76	0.84	0.93	0.82
Mo	0.77	1.04	0.99	0.77	0.95	1.15	0.77	0.85
Nb	12.45	14.60	12.55	12.02	11.71	13.11	17.33	15.91
Nd	49.82	38.56	42.40	53.13	44.33	49.76	57.34	43.25
Ni	37.59	26.72	37.68	52.22	29.65	38.82	59.10	57.10
Pb	15.72	9.85	4.84	18.16	15.59	10.83	3.41	7.34
Pr	12.74	9.76	10.84	13.17	11.00	12.65	14.38	11.14
Rb	74.26	41.85	52.37	59.99	56.24	146.06	60.65	46.96
Sc	25.40	28.68	26.85	24.02	22.16	24.91	28.20	28.88
Sm	9.96	8.86	8.77	10.34	8.57	9.84	11.33	7.64
Sr	135.17	37.84	26.27	58.05	68.20	66.64	36.42	108.60
Ta	0.65	0.92	0.66	0.63	0.65	0.69	0.73	0.76
Tb	1.49	1.78	1.62	1.33	1.32	1.47	1.66	1.69
Th	16.07	14.14	16.27	19.42	16.33	19.80	17.44	11.70
Tm	0.93	0.96	0.91	0.73	0.72	0.79	0.99	0.87
U	1.00	1.37	0.82	1.55	1.15	1.35	0.93	0.93
V	148.82	156.25	157.70	128.15	125.31	131.55	140.15	148.50
Y	60.35	63.24	58.33	48.06	47.25	51.31	60.45	58.75
Yb	6.13	6.67	6.24	5.11	5.18	5.23	6.52	5.87
Zn	106.92	142.28	80.71	156.72	135.28	120.18	56.60	86.85
Zr	308.29	367.51	367.10	299.70	290.46	329.88	369.95	266.20

Major and minor analyses conducted using XRF; trace element analyses conducted using LA-ICP-MS.
bdl = below detection limit.

Table 4.2: *Major, minor and trace element data of Swartoup granitoids (continued on page 93). The XRF analyses have been normalised to 100 wt% anhydrous. The Fe-contents of the rocks have been expressed as* FeO^{T} *(*$FeO^{T} = 0.89 \times Fe_2O_3$*).*

Sample	1139A	1140A	1144A	1145A	1146A	1149A	1151A
wt%							
SiO_2	66.63	65.93	65.55	63.65	65.56	75.36	53.04
TiO_2	1.04	1.03	0.96	1.26	0.88	0.37	2.01
Al_2O_3	14.11	14.32	15.39	14.68	15.38	12.35	17.57
Cr_2O_3	0.01	0.01	0.01	0.01	0.01	*bdl*	0.01
FeO^T	6.42	6.38	5.15	6.59	4.50	1.91	10.27
MnO	0.09	0.10	0.08	0.10	0.05	0.03	0.18
MgO	1.32	1.30	1.50	1.76	1.10	0.47	2.77
CaO	2.69	2.51	3.33	3.56	2.83	1.93	6.11
Na_2O	2.50	2.73	2.99	2.71	2.73	2.29	3.45
K_2O	3.72	4.20	3.75	3.84	5.46	4.63	1.86
P_2O_5	0.36	0.36	0.30	0.39	0.25	0.09	0.75
ppm							
Ba	1098.88	1137.68	1291.77	1477.60	1727.87	917.03	852.74
Ce	176.81	114.26	86.81	89.59	81.94	115.41	138.70
Co	9.14	9.44	10.49	13.91	9.48	3.96	21.76
Cr	21.45	23.33	27.23	28.10	22.26	11.76	45.15
Cs	0.65	0.77	0.54	0.47	1.26	1.30	1.85
Cu	20.24	14.98	19.07	17.48	14.27	11.60	28.50
Dy	10.31	8.58	5.37	4.89	4.42	2.17	9.36
Er	5.05	4.26	2.83	2.54	2.13	0.96	4.93
Eu	3.17	2.98	2.54	2.85	2.71	2.05	3.90
Gd	14.08	10.20	6.87	6.88	6.05	3.71	12.40
Hf	12.88	13.49	11.05	10.66	11.33	4.17	20.62
Ho	2.00	1.67	1.03	0.97	0.86	0.38	1.83
La	89.43	57.32	46.92	46.39	43.83	68.07	67.61
Lu	0.55	0.50	0.33	0.35	0.28	0.10	0.61
Mo	1.06	1.25	0.88	0.95	0.84	0.75	1.03
Nb	19.91	18.93	13.67	13.24	11.15	6.23	25.52
Nd	80.40	56.20	40.42	42.87	37.73	40.80	70.04
Ni	9.96	11.40	14.82	15.26	11.94	6.05	23.96
Pb	20.87	18.14	23.44	20.31	25.26	25.18	14.89
Pr	20.71	13.92	10.25	10.87	9.57	11.76	17.08
Rb	132.86	151.43	96.17	88.39	157.46	124.28	55.51
Sc	16.89	16.46	13.81	16.58	12.86	7.55	24.15
Sm	15.29	11.17	7.82	8.11	7.08	5.05	13.45
Sr	179.35	191.88	220.45	263.75	248.65	146.64	339.36
Ta	0.59	0.73	0.64	0.63	0.45	0.32	1.32
Tb	1.88	1.45	0.92	0.93	0.75	0.44	1.61
Th	21.57	10.50	3.17	0.78	2.80	23.33	1.23
Tm	0.63	0.56	0.38	0.33	0.28	0.13	0.67
U	1.14	0.65	0.58	0.46	0.87	0.78	1.61
V	63.73	63.40	85.99	119.20	72.36	33.02	149.11
Y	52.57	43.02	27.38	25.57	22.39	10.03	49.18
Yb	3.93	3.46	2.25	2.20	1.85	0.87	4.48
Zn	118.61	111.60	94.60	122.21	78.01	38.11	190.08
Zr	528.25	547.00	438.31	442.41	448.31	159.32	880.94

Major and minor analyses conducted using XRF; trace element analyses conducted using LA-ICP-MS.
bdl = below detection limit.

Table 4.3: *Major, minor and trace element data of collected Swartoup granitoids (continued from page 92). The XRF analyses have been normalised to 100 wt% anhydrous. The Fe-contents of the rocks have been expressed as* FeO^{T} *(*$FeO^{T} = 0.89 \times Fe_2O_3$*).*

Sample	GS5A	GS9A	GS9B	GS10B	GS15B	GS15C	GS16A
wt%							
SiO_2	72.98	74.76	76.80	57.52	65.65	63.26	83.82
TiO_2	0.61	0.12	0.22	2.22	0.61	0.96	0.26
Al_2O_3	12.77	13.05	11.79	13.90	17.01	14.23	7.03
Cr_2O_3	0.00	0.00	0.00	0.00	0.00	*bdl*	0.01
FeO^T	2.67	0.69	1.19	9.69	2.28	10.74	3.62
MnO	0.03	0.01	0.02	0.12	0.02	0.18	0.14
MgO	0.68	0.00	0.30	2.30	0.81	2.83	0.68
CaO	1.94	1.54	1.27	5.23	1.87	1.05	1.59
Na_2O	2.33	1.72	1.88	2.97	2.84	1.72	1.21
K_2O	4.70	7.13	5.67	3.44	7.57	3.60	0.43
P_2O_5	0.14	0.01	0.03	0.59	0.09	0.06	0.02
ppm							
Ba	688.50	2685.50	1741.00	1243.50	1840.00	488.25	168.50
Ce	219.20	35.20	19.34	161.05	638.70	81.65	17.40
Co	5.12	0.94	2.97	24.61	5.83	20.80	6.98
Cr	17.86	17.40	11.80	14.82	13.57	77.60	44.43
Cs	1.29	12.82	3.52	0.36	2.30	1.76	0.23
Cu	29.47	9.50	17.58	17.16	18.53	21.90	29.80
Dy	3.62	3.21	0.33	8.53	4.89	24.78	12.52
Er	1.22	2.01	0.29	4.64	1.20	12.02	11.59
Eu	1.69	0.59	1.82	3.07	2.79	1.32	0.67
Gd	7.62	2.69	0.53	10.86	15.75	14.18	4.55
Hf	7.59	7.96	3.73	10.16	4.26	9.28	4.95
Ho	0.54	0.64	0.10	1.63	0.62	4.71	3.46
La	116.77	16.41	15.50	77.92	338.25	40.55	9.34
Lu	0.10	0.44	0.04	0.55	0.13	1.31	2.16
Mo	0.92	0.97	0.36	1.23	0.51	0.74	0.88
Nb	13.32	14.66	4.37	23.13	16.01	32.11	8.52
Nd	78.65	15.23	4.46	71.00	228.90	35.28	6.56
Ni	13.00	33.00	6.10	11.85	12.20	45.95	29.35
Pb	29.08	23.45	27.24	22.04	52.60	19.05	5.63
Pr	22.86	4.51	1.57	18.88	66.13	9.23	1.90
Rb	161.20	499.20	156.50	93.50	311.10	166.20	19.83
Sc	10.40	8.09	5.99	23.83	8.34	32.70	24.71
Sm	11.28	3.34	0.68	12.82	27.86	8.47	2.13
Sr	124.10	588.85	261.00	337.80	195.25	58.75	53.02
Ta	0.23	2.23	0.06	1.14	0.77	2.04	0.20
Tb	0.79	0.44	0.06	1.50	1.27	3.29	1.25
Th	42.00	78.45	1.34	2.28	167.95	16.07	2.25
Tm	0.14	0.34	0.04	0.54	0.15	1.51	1.84
U	1.06	6.74	0.42	0.30	2.90	1.28	0.43
V	37.87	14.32	27.70	205.20	40.15	104.90	43.85
Y	13.57	17.32	2.31	43.92	15.89	135.70	91.83
Yb	0.79	2.36	0.30	3.69	0.85	9.63	13.46
Zn	57.10	17.20	24.60	120.15	51.90	107.60	26.65
Zr	278.10	191.40	124.25	395.85	148.35	324.30	165.25

Major and minor analyses conducted using XRF; trace element analyses conducted using LA-ICP-MS.
bdl = below detection limit.

Table 4.4: *Major, minor and trace element data of the Bysteek Formation marble and calc-silicate, hybrid rocks and the mafic dyke specimen. The XRF analyses have been normalised to 100 wt% anhydrous. The Fe-contents of the rocks have been expressed as* FeO^{T} *(*$FeO^{T} = 0.89 \times Fe_2O_3$*).*

	Bysteek marble		hybrid rock					Mafic dyke
Sample	GS19A	GS10A	GS1A	GS7A	GS11D	GS13A	GS13B	GS12A
wt.%								
SiO_2	6.60	50.53	71.36	64.44	68.27	75.59	71.74	44.56
TiO_2	0.05	2.22	0.91	0.73	0.71	0.04	0.32	1.15
Al_2O_3	0.02	9.14	11.90	16.28	16.65	13.17	13.00	15.52
Cr_2O_3	0.00	*bdl*	0.01	*bdl*	*bdl*	*bdl*	*bdl*	*bdl*
FeO^{T}	0.56	3.94	6.76	6.85	1.09	0.55	1.42	14.22
MnO	0.02	0.15	0.09	0.15	0.03	0.01	0.03	0.24
MgO	13.13	3.98	1.81	1.56	0.28	0.12	0.35	8.34
CaO	80.92	29.13	1.10	2.32	8.19	1.63	3.66	11.47
Na_2O	0.00	0.04	1.52	2.69	2.27	2.30	1.92	1.69
K_2O	0.00	0.20	2.92	3.61	1.87	5.88	6.44	0.58
P_2O_5	0.02	0.04	0.05	0.06	0.09	0.02	0.10	0.11
[a]LOI	40.30	4.25	0.18	0.29	1.04	0.45	0.57	0.15
ppm								
Ba	3.10	103.40	927.90	975.00	386.40	1424.00	864.00	29.70
Ce	0.92	156.10	41.38	129.82	189.25	15.80	116.70	6.71
Co	0.69	7.98	17.68	11.00	2.84	1.63	2.85	62.35
Cr	15.59	16.00	74.32	26.09	11.38	16.63	15.93	81.25
Cs	0.27	0.19	1.65	1.47	15.14	2.32	10.52	0.31
Cu	11.20	14.19	21.73	33.45	27.75	13.42	19.67	95.20
Dy	0.16	19.65	11.45	21.34	11.86	0.93	5.63	4.12
Er	0.21	9.92	7.32	9.40	5.94	0.55	3.12	2.60
Eu	*bdl*	2.69	1.51	2.59	1.77	1.28	0.83	0.93
Gd	0.00	21.57	7.06	13.62	12.58	0.86	6.70	3.29
Hf	*bdl*	11.11	5.49	11.62	3.25	3.66	2.74	1.17
Ho	0.04	3.75	2.38	3.83	2.18	0.21	1.13	0.83
La	0.43	50.49	21.67	63.87	67.20	11.62	53.82	2.49
Lu	0.04	1.01	0.86	0.92	0.64	0.13	0.40	0.40
Mo	0.31	8.60	0.72	0.78	2.97	0.59	2.03	0.51
Nb	1.16	80.80	15.56	22.55	39.77	1.69	20.30	3.05
Nd	0.44	101.30	17.33	53.42	85.05	4.52	44.45	6.22
Ni	9.25	14.20	49.35	17.75	8.75	10.65	11.25	100.70
Pb	3.24	9.29	8.92	27.64	20.00	25.02	29.21	2.22
Pr	0.09	23.28	4.62	14.70	23.80	1.45	12.87	1.14
Rb	0.62	9.28	94.15	137.55	204.65	236.70	304.60	12.89
Sc	0.47	11.48	26.37	22.63	6.77	5.74	7.64	49.36
Sm	*bdl*	23.03	4.23	10.45	15.98	0.96	7.77	2.33
Sr	271.90	64.50	100.05	150.65	175.20	291.05	323.40	85.22
Ta	*bdl*	8.30	0.74	0.74	4.07	0.07	1.58	0.11
Tb	*bdl*	3.22	1.46	2.90	1.85	0.17	1.00	0.55
Th	0.07	19.83	5.80	27.07	33.72	1.15	19.49	0.06
Tm	0.04	1.31	0.98	1.21	0.86	0.08	0.45	0.39
U	0.27	13.40	0.87	1.55	5.25	0.30	3.67	0.03
V	13.95	81.85	120.25	55.85	25.35	14.53	22.29	306.50
Y	2.08	91.22	67.08	106.25	60.57	5.28	33.01	23.05
Yb	0.16	7.96	6.58	7.07	4.94	0.52	2.63	2.55
Zn	14.95	154.55	76.85	58.90	39.65	12.95	44.20	117.80
Zr	1.12	286.05	187.05	439.15	76.10	152.10	74.70	34.70

Major and minor analyses conducted using XRF; trace element analyses conducted using LA-ICP-MS.
bdl = below detection limit.
[a]LOI not normalised.

Table 4.5: *Major, minor and trace element data of Polisiehoek Granite-gneisses. The XRF analyses have been normalised to 100 wt% anhydrous. The Fe-contents of the rocks have been expressed as* FeO^{T} *(*$FeO^{T} = 0.89 \times Fe_2O_3$*).*

Sample	1136A	1142A	1147C	1148A	1148B	1152A	GS4B	GS4E	GS11B
wt%									
SiO_2	75.71	78.84	73.70	76.65	77.47	73.16	78.10	80.79	74.38
TiO_2	0.22	0.04	0.22	0.06	0.12	0.21	0.01	0.02	0.10
Al_2O_3	12.44	12.47	13.91	12.31	11.89	14.12	12.37	10.63	13.15
Cr_2O_3	*bdl*	*bdl*	*bdl*	*bdl*	*bdl*	*bdl*	*bdl*	*bdl*	*bdl*
FeO^{T}	2.09	0.23	1.99	1.09	1.28	2.25	1.35	1.31	1.31
MnO	0.04	0.01	0.03	0.04	0.04	0.06	0.02	0.02	0.04
MgO	0.37	0.04	0.29	0.05	0.05	0.27	0.09	0.11	0.12
CaO	0.82	0.79	0.88	0.33	0.45	1.37	0.62	0.54	0.94
Na_2O	2.97	4.68	3.21	2.62	2.75	2.81	2.61	2.03	3.10
K_2O	4.68	2.70	5.32	6.00	5.38	5.09	4.31	3.75	5.81
P_2O_5	0.08	0.11	0.09	0.13	0.05	0.06	0.10	0.09	0.06
ppm									
Ba	756.20	153.61	326.93	396.06	458.12	627.52	69.45	186.20	110.90
Ce	64.72	16.90	103.90	39.94	52.27	78.78	10.28	14.98	60.48
Co	4.19	0.71	2.73	1.04	2.11	3.50	0.61	1.53	1.25
Cr	12.65	9.50	12.07	9.40	8.23	14.00	13.65	16.20	10.55
Cs	0.60	0.36	3.34	0.90	0.68	1.07	0.69	0.44	6.29
Cu	12.29	4.67	7.98	9.16	7.28	15.01	33.00	29.40	4.70
Dy	8.72	0.97	8.39	7.76	9.18	6.70	2.00	0.51	9.55
Er	6.84	0.63	5.28	6.70	7.27	7.12	1.67	0.31	5.98
Eu	0.98	0.15	0.66	0.49	0.68	1.51	*bdl*	0.25	0.30
Gd	6.40	0.85	8.11	4.12	6.43	3.81	0.95	0.53	7.14
Hf	4.19	1.73	5.16	2.70	3.76	5.67	2.05	1.92	3.18
Ho	2.06	0.22	1.77	1.93	2.22	1.93	0.38	0.07	1.80
La	31.88	6.68	48.16	18.97	25.45	48.60	4.19	9.08	23.41
Lu	0.95	0.08	0.77	1.27	1.17	1.32	0.39	0.10	0.97
Mo	0.71	0.58	0.75	1.60	0.73	0.74	0.37	0.55	0.58
Nb	3.14	0.28	19.49	1.83	14.73	3.45	4.36	1.13	33.78
Nd	29.44	6.25	46.65	16.54	23.47	25.40	4.03	4.16	27.81
Ni	7.28	6.47	5.74	6.96	5.87	6.30	8.10	17.95	4.80
Pb	21.89	11.57	32.69	32.30	21.99	31.53	12.37	15.40	31.96
Pr	7.47	1.91	12.33	4.61	6.27	7.88	1.23	1.41	7.56
Rb	131.18	51.06	331.65	216.99	242.94	171.20	187.35	160.45	423.20
Sc	12.36	5.67	7.89	15.42	14.22	11.28	12.76	7.12	9.50
Sm	6.16	1.14	9.87	4.20	5.88	3.52	1.05	0.77	8.15
Sr	81.31	34.53	47.11	30.71	16.09	65.15	19.33	26.25	31.75
Ta	0.08	0.05	1.68	0.09	0.94	0.31	*bdl*	*bdl*	2.84
Tb	1.15	0.16	1.29	0.89	1.24	0.74	0.20	0.10	1.44
Th	14.44	0.21	34.22	5.23	8.75	7.85	*bdl*	0.16	23.10
Tm	1.01	0.11	0.82	1.06	1.13	1.15	0.27	0.05	1.01
U	0.65	0.42	5.50	1.04	1.12	0.81	0.21	0.27	13.12
V	25.81	12.90	23.28	13.98	13.05	28.18	8.62	13.92	11.85
Y	58.03	5.45	51.56	53.70	58.42	53.50	10.74	2.11	54.43
Yb	6.63	0.69	5.36	8.31	7.83	8.94	2.92	0.42	7.05
Zn	26.95	12.11	41.05	23.48	29.72	25.98	38.15	78.00	27.35
Zr	131.98	37.52	156.15	53.01	81.29	202.40	29.33	35.15	64.50

Major and minor analyses conducted using XRF; trace element analyses conducted using LA-ICP-MS.
bdl = below detection limit.

(samples 1149A, GS5A, GS9A, GS9B). The total alkali contents of Swartoup group 2 rocks show somewhat more variation than those of Swartoup group 1. Sample GS16A lies away from the rest of the Swartoup granitoids, at a much lower total alkali content of 2 wt% K_2O + Na_2O. This rock plots in the Quartzolite field. The hybrid rocks plot in the Granodiorite (samples GS1A, GS7A and GS11D) and Granite (samples GS13A and GS13B) fields.

The Polisiehoek Granite-gneisses plot in the Granite field. Their SiO_2 contents are higher than those of Swartoup group 1, but are comparable to the granitic Swartoup group 2 specimens (samples 1148A, GS5A and GS9A). The total alkali contents of the Polisiehoek Granite-gneisses are, on average, higher than those of the Swartoup group 1 specimens. The mafic dyke specimen plots in the Olivine-gabbro field.

Shown for reference, the Koenap migmatites plot in the Granodiorite field, at similar total alkali, but lower SiO_2 contents than Swartoup group 1. Samples 1137A, 1143A and GS4D are the most leucocratic Koenap migmatites (Section 3.2.1). They lie at somewhat higher total alkali contents (<3 wt% K_2O + Na_2O) than the more melanocratic specimens, samples 1138A, 1141A, 1143B and GS4C. However, sample 1147B is melanocratic and has a relatively high alkali content (around 4 wt% K_2O + Na_2O), which is likely due to its white mica mode (Table 3.1).

The Bysteek calc-silicate (sample GS10A) plots in the Gabbro field, at a much higher silica content (48 wt% SiO_2) compared to the Bysteek marble, which has 3.9 vol% SiO_2 and no detectable K_2O or Na_2O. Their low alkali contents are expected as these specimens are dominated by calcite, clinopyroxene and garnet (Section 3.2.2, Table 3.2).

4.1.2 R_1R_2 plutonic rock classification

The R_1R_2 chemical variation diagram (Figure 4.1b; after De la Roche et al., 1980) was used in conjunction with the TAS diagram to further classify the igneous rocks of this study (Tables 2.1, 3.4 and 3.6). The parameters R_1 and R_2 are defined as;
R_1 = 4Si – 11(Na + K) - 2(Fe + Ti),
R_2 = 6Ca + 2Mg + Al. These parameters have been calculated from oxide percentages converted to millications (De la Roche et al., 1980). A detailed description of the R_1R_2 diagram is shown in Appendix A.1.1.2.

Figure 4.1b is in general agreement with the TAS diagram (Figure 4.1a). The R_1R_2 diagram classifies all the Swartoup group 1 specimens as granodiorites, whereas the TAS diagram classifies them all as granodiorites with the exception of sample 1146A (quartz monzonite). Both

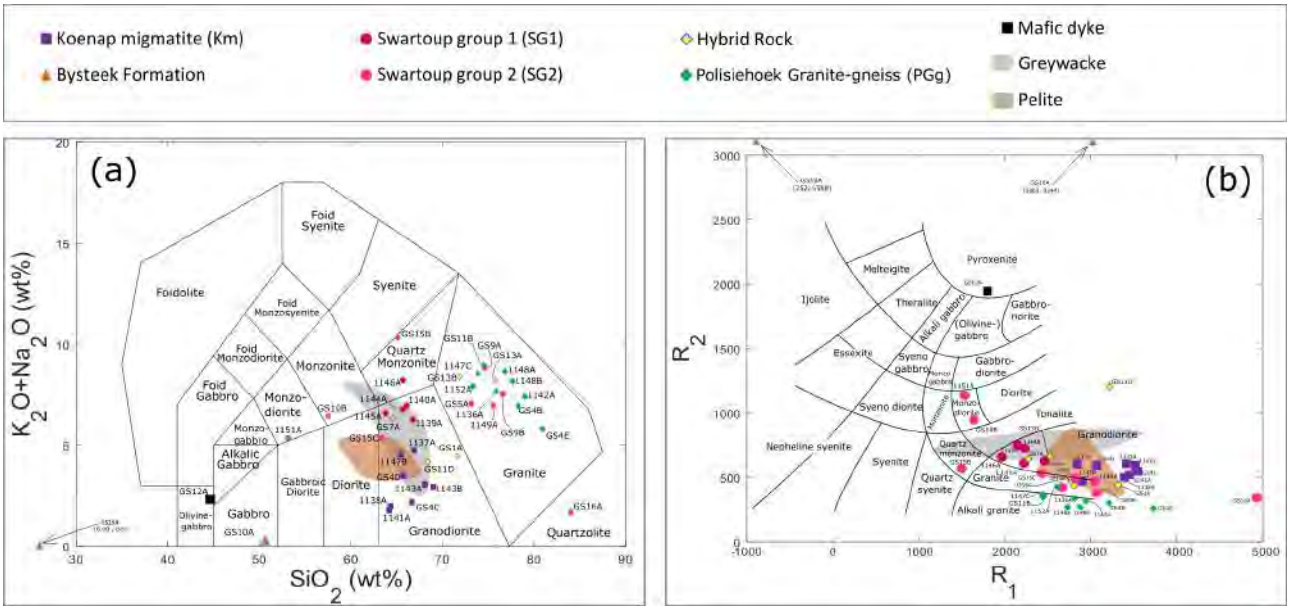

Figure 4.1: *(a) Total-Alkali versus Silica (TAS) diagram (after Middlemost, 1994), used in conjunction with the R_1R_2 diagram (after De la Roche et al., 1980) to classify the igneous specimens of this study. These include the Swartoup granitoids, hybrid rocks, Polisiehoek Granite-gneisses and the mafic dyke specimen, sample GS12A. Koenap Formation migmatites and the Bysteek calc-silicate and marble are plotted for comparison only. Published greywacke and pelite compositions (Section 2.1, Tables 2.2–2.4) are included for comparison. (b) R_1R_2 diagram (after De la Roche et al., 1980) used in conjunction with the Total-alkali versus silica (TAS) diagram (after Middlemost, 1994), to classify the igneous specimens of this study. Koenap Formation migmatites and the Bysteek calc-silicate and marble specimens are plotted for comparison only, as well as published greywacke and pelite compositions (Section 2.1, Tables 2.2–2.4).*
$R_1 = 4Si - 11(Na + K) - 2(Fe + Ti)$,
$R_2 = 6Ca + 2Mg + Al$.

Figures 4.1a and 4.1b classify samples 1149A, GS5A, GS9A and GS9B as granites. Samples 1151A (monzodiorite) and GS15B (quartz monzonite) are classified the same by these two diagrams as well. However, as per Frost and Frost (2008), the modifier 'orthopyroxene-bearing' is added as a prefix to these specimens. Sample GS10B also receives this modifier as it is orthopyroxene-bearing (Table 3.3). However, the R_1R_2 diagram classifies this specimen as a monzodiorite and by the TAS diagram it is a monzonite. Both samples GS15C and GS16A are classified as granites by the R_1R_2 diagram but the TAS diagram classifies them as a granodiorite and a quartzolite, respectively.

Two hybrid rock specimens, samples GS1A and GS13A, plot in the Granite field. Samples GS7A and GS13B plot in the Granodiorite field. In contrast to the other hybrid rock specimens, sample GS11D plots at a much higher R_2 value (around 1250 millications). Sample GS11D plots outside of the fields defined by De la Roche et al. (1980) but it does plot within an extended Tonalite field. The R_1R_2 diagram is in poor agreement with the TAS diagram in classification of the hybrid rock specimens. The TAS diagram classifies samples GS1A, GS7A and GS11D as

granodiorites and samples GS13A and GS13B as granites (Section 4.1.1). However, the R_1R_2 diagram classifies samples GS7A and GS13B as granodiorites, sample GS11D as a tonalite and sample GS13A as a granite.

Sample GS12A, the mafic dyke specimen, plots in the Pyroxenite field. This is not strictly in agreement with the TAS diagram (Figure 4.1a). The TAS diagram classifies the specimen as a Peridot-gabbro. However, sample GS12A plots near the Gabbro field of the TAS diagram, though, and plots near the (Olivine-) gabbro field of the R_1R_2 diagram, so perhaps there is some agreement.

The Koenap migmatites, also shown for reference, plot mostly in the Granodiorite field (samples 1137A, 1138A, 1141A, 1143A, 1143B GS4C and GS4D). Sample 1147B plots within this range but falls outside the Granite field, plotting in the Alkali granite field. This is in good agreement with the TAS diagram. Also, like the TAS diagram, the R_1R_2 diagram shows the more leucocratic Koenap migmatite specimens, samples 1137A and GS4D, along with the melanocratic sample 1147B, separated from the melanocratic ones.

The Bysteek calc-silicate (sample G10A) and marble (sample GS19A) specimens plot well off the diagram at very high R_2 values, caused by their high CaO contents (see Section 4.4.1). Like the TAS diagram (Figure 4.1a), the R_1R_2 diagram does not accommodate the Bysteek marble in any defined field. This can be expected as this diagram is intended for use with igneous plutonic rocks. Likely for this same reason, sample GS10A, the Bysteek calc-silicate, also plots outside the defined fields of the diagram. However, as the calc-silicate comprises relatively less calcium-rich phases, such as calcite, and more silica-rich ones, such as garnet and clinopyroxene, it plots at relatively higher R_1 and lower R_2 values than the marble specimen.

The pelite compositions, shown for reference, have typically higher R_1 and lower R_2 contents than the greywacke compositions. Three of the Koenap migmatites (samples 1137A, 1147B and GS4D) show overlap with the pelite field. All the Koenap migmatites plot at lower R_2 values than the greywacke field but are within its R_1 range.

4.1.3 Summary and interpretation of the TAS and R_1R_2 diagram classifications

Preference for classification of igneous rocks was given to the R_1R_2 chemical variation (Figure 4.1b) diagram over the TAS diagram (Figure 4.1a). This is because the R_1R_2 diagram takes into consideration eight elements (Si, Na, K, Fe, Ti, Ca, Mg and Al) of the whole-rock

compositions in contrast to the TAS diagram which considers only the three oxides Na_2O, K_2O and SiO_2. However, there are two exceptions. Samples GS1A and GS11D plot within extensions of the granite and tonalite fields, respectively, of the R_1R_2 diagram. As they do not plot strictly within the boundaries used by (De la Roche et al., 1980), the TAS diagram is used, which classifies them both as granodiorites. However, sample GS16A also plots outside the fields of the R_1R_2 diagram but the TAS diagram classification (quartzolite) has not been used in this case. This is because the high value of the sample is likely caused by its high silica content. This is likely a result of a 'nugget effect', caused by segregation quartz veins in the collected specimen (Section 3.2.3). Crushing and homogenisation of a larger volume of this rock may mitigate this effect. Granite, after the R_1R_2 diagram, is therefore more representative of the rock-type than quartzolite. The results of the classification are found in Tables 2.1, 3.4 and 3.6.

The Swartoup group 1 samples plot well within the Granodiorite fields of both classification diagrams. The Swartoup group 2 specimens, in contrast, vary from low silica and alkali contents (sample 1151A, Monzodiorite field), to Swartoup group 1, then to higher silica and alkalis in the Granite field. This pattern is seen in both diagrams (Figures 4.1a, 4.1b). Sample GS15C, a garnet-bearing granite, plots between Swartoup group 1 and the Koenap migmatites in both the TAS and R_1R_2 diagrams. Garnet-bearing granitoids of the Swartoup Pluton are spatially associated with Koenap migmatite and crop out less than 15 m from the contact (Section 3.1, Figure 3.1). This may suggest that the garnet could be xenocrystic, entrained in magma extracted from nearby migmatite, in which garnet is common as a part of a peritectic assemblage. However, though sample GS16A is also garnet-bearing, the rock has a high silica content. This pulls the sample to high SiO_2 and values in Figures 4.1a and 4.1b, respectively, so it does not plot with sample GS15C.

Most Koenap migmatite specimens plot within the greywacke composition field of the TAS diagram. This diagram shows two Koenap migmatites, samples 1147B and GS4D, plot in the pelite and greywacke fields. Another three specimens, samples 1137A, 1143A and 1143B, show overlap with the greywacke field and the rest of the Koenap migmatites plot below the pelite and greywacke composition fields. In contrast, the R_1R_2 diagram shows some Koenap migmatites overlap with the pelite composition field. The R_1R_2 diagram shows three Koenap migmatites, samples 1137A, 1147B and GS4D overlapping with the pelite field and the rest have higher R_2 values. Most of the Swartoup group 1 rocks (samples 1139A, 1140A, 1144A, 1145A) show overlap with the greywacke composition field of the TAS diagram. Only samples 1140A, 1144A and 1145A show overlap with the greywacke field in the R_1R_2 diagram and sample 1139A plots within the pelite field. Sample GS15B is the only Swartoup group 2 specimen to show overlap

with the greywacke composition field in the TAS diagram. Though the rest of the Swartoup group 2 rocks have similar total alkali contents as the greywacke field, they show higher and lower SiO_2 contents. All the hybrid rock specimens show total alkali contents which are similar as the greywacke field in the TAS diagram but only samples GS7A and GS11D show overlap, with the greywacke field. The R_1R_2 diagram shows samples GS7A and GS13B overlapping the greywacke field and samples GS1A and GS13A overlapping the pelite field. The Polisiehoek Granite-gneisses do not show overlap with the pelite and greywacke fields. In the TAS diagram they, like Swartoup group 2 specimens, show total alkali contents similar to the greywacke composition field. However, they plot at higher SiO_2 contents than the greywacke field. The R_1R_2 diagram shows them at lower R_2 values than the pelite and greywacke composition fields. However, most Polisiehoek Granite-gneiss specimens show similar values as the pelite field, with sample GS4E plotting at higher , though still within greywacke field–like contents.

The Koenap migmatites show similar patterns in the TAS and R_1R_2 diagram. The more melanocratic specimens (samples 1141A, 1143A, 1143B and GS4C) plot at lower alkali and higher values, in contrast to the more leucocratic specimens (samples 1137A and GS4D) which plot at higher alkali and higher R_2 values. Sample 1147B lies nearer the leucocratic samples in these diagrams. This rock is dark in colour due to its low K-feldspar and plagioclase modes, and high white mica mode. The white mica likely formed during retrograde alteration, whereby white mica was more stable in the lower amphibolite facies and grew after alkali feldspar. The rock is low in garnet and high in biotite modes relative to the other Koenap migmatites.

Both Figures 4.1a and 4.1b show a general trend where Swartoup group 1 specimens overlap the greywacke composition field, and between this and the more melanocratic Koenap migmatites, plots the pelite composition field, which shows overlap with the more leucocratic Koenap migmatites. This, together with the spatial relationships of Koenap migmatite and the Swartoup Pluton (Section 3.1, Figure 3.1) may be interpreted as a possible genetic relationship between the Swartoup group 1 rocks and the Koenap migmatites. The Koenap protolith may have had either a pelitic composition, which fits particularly well with Figure 4.1b, or a pelitic composition with some greywacke components, which fits well with Figure 4.1a. Mobilisation of melt formed during anatexis should produce enrichment/depletion trends in chemical variation diagrams. This can be seen if we consider the Swartoup group 1 specimens to represent possible mobilised material, and the melanocratic Koenap migmatites as representative of the restite left behind after partial melt extraction. The more leucocratic Koenap migmatites plot between these two groups, as would be expected if they have undergone lower degrees of partial melt extraction relative to the melanocratic ones. This will be revisited in the Discussion, Section 5.3.1.

The hybrid rocks appear to vary from Swartoup group 1 specimens to the Koenap migmatites and on to the granitic Swartoup group 2 rocks in both diagrams, particularly in the R_1R_2 diagram. This, together with the spatial associations of these rocks in the field (see Figures 3.1, 3.12, Sections 3.1.4, 3.3), may be interpreted as a possible genetic relationship between the hybrid rocks with Koenap migmatite and Swartoup groups 1 and 2. However, there are only a few data concerning the hybrid rock specimens, and no correlation between them and the Bysteek specimens (samples GS10A and GS19A) is evident in the TAS diagram. Calc-silicate rocks of the Bysteek Formation show the strongest spatial association with hybrid rock in the field (Section 3.1.4, 3.3). Sample GS11D does, though, lie at higher R_2 values than other hybrid rock specimens in the R_1R_2 diagram, as does the Bysteek calc-silicate, sample GS10A. However, one would expect a high R_2 value from sample GS11D, given the rocks high plagioclase, pyroxene and titanite modes (Section 3.2.4). More data is needed to further investigate any relationships involving the hybrid rocks, and they will be revisited in the Discussion, Section 5.3.2.

The TAS and R_1R_2 diagrams show somewhat of a trend where the Polisiehoek Granite-gneisses plot opposite the Koenap migmatites, with the pelite composition field between them. This, along with their spatial relationship with Koenap migmatite in the field (Section 3.1, Figure 3.1) may be interpreted as a possible genetic relationship between the two. If the melanocratic Koenap migmatite specimens are regarded as restite after extraction of Polisiehoek melt, then the Koenap protolith composition is restricted in Figure 4.1b to the high R_1–low R_2 portion of the pelite composition field. This would then necessitate no greywacke component in the Koenap protolith, otherwise restite with more tonalitic or dioritic compositions should result. This too, will be revisited in the Discussion, Section 5.3.1.

4.2 Fe-number, MALI and ASI classification

Frost et al. (2001) propose a classification scheme for granitic rocks based on three parameters, namely; Fe-number, Modified Alkali-Lime Index (MALI) and the Aluminium Saturation Index (ASI) (Figure 4.2). These three parameters are then used in succession to determine the rock-type (Frost et al., 2001). Table 4.6 shows the rock names as classified by this scheme. Table A.7 (Appendix A.1.1.3) shows the classification table of Frost et al. (2001).

Fe-number

The Fe-number is defined as,

$$\text{Fe} - \text{number} = \frac{\text{FeO}}{(\text{FeO} + \text{MgO})},$$

which conveys information regarding the differentiation history of the granitic magma (Frost et al., 2001). However, many geochemical analyses make no distinction between ferric and ferrous iron, so the authors defined the parameter Fe* as a substitute. Frost et al. (2001) define Fe* as,

$$\text{Fe}* = \frac{\text{FeO}^{\text{tot}}}{(\text{FeO}^{\text{tot}} + \text{MgO})}.$$

Frost et al. (2001) also propose the terms ferroan and magnesian, as opposed to the terms tholeiitic and calc-alkaline, as the Fe-number is unrelated to the alkalinity of the rock.

Figure 4.2a shows Swartoup group 1 plotting mostly within the field of various A-type granites determined by Frost et al. (2001). These all lie in the ferroan field. Only one Swartoup group 1 analysis plots in the magnesian field. Swartoup group 1 shows overlap with the greywacke composition field and some overlap is also seen with the lower Fe* value pelite compositions. Most of the Fe* ratios of Swartoup group 2 show a similar Fe* range as Swartoup group 1. However, due to silica variation they vary off these ranges. Four samples plot in the ferroan field, three of which show overlap with the A-type granite field. Five Swartoup group 2 analyses plot in the magnesian field. Sample GS15B shows an Fe* ratio of 0.73, plotting below the rest of the Swartoup granitoids. Four of the magnesian Swartoup group 2 rocks show overlap with the Cordilleran granite field of Frost et al. (2001), the fifth rock, sample GS16A, has a high silica content and plots to the right of the rest of Swartoup group 2.

The hybrid rock samples vary between the Swartoup group 1 cluster and the higher silica content, granitic Swartoup group 2 analyses (64–75 wt% SiO_2), showing a similar range in Fe* values as the Swartoup granitoids, Fe* = 0.78–0.81. Most analyses plot in the magnesian field, with only sample GS7A plotting in the ferroan field (Fe* = 0.81).

The Polisiehoek Granite-gneisses plot in the ferroan field, between Fe* = 0.84 and 0.96, and show some overlap with the Cordilleran granitoids. However, they are in better agreement with the A-type field. The Polisiehoek Granite-gneisses have higher silica contents than the pelite and greywacke composition fields and so show no overlap with them. However, two analyses show Fe* ratios which are comparable with the upper greywacke field, and the lower five Polisiehoek samples have Fe* values which range over the upper pelite field. The other four specimens have higher Fe* ratios than the published sediment compositions.

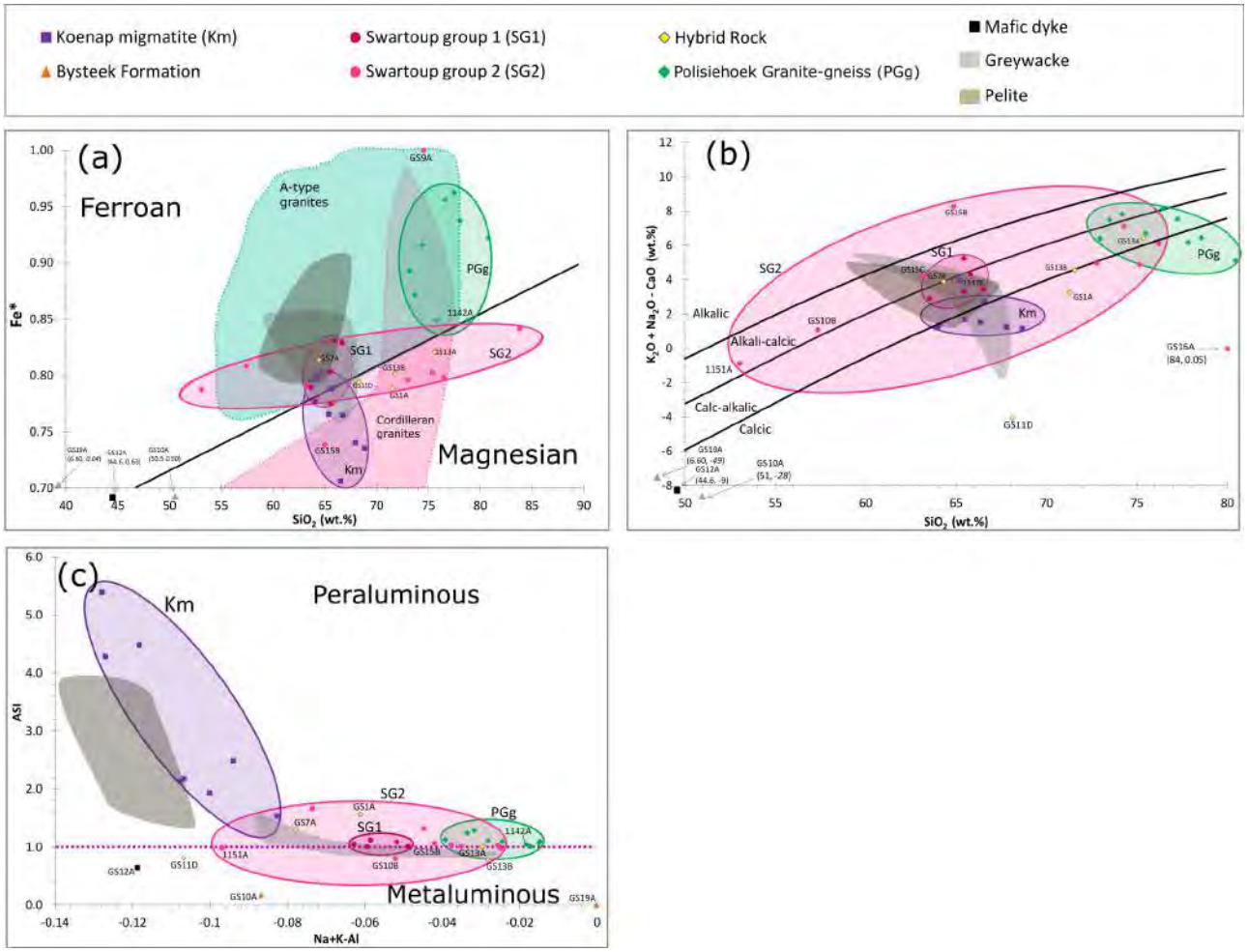

Figure 4.2: *Diagrams used for the granitic classification scheme of Frost et al. (2001). (a) Fe* plotted against SiO_2 (wt%), where* $\mathrm{Fe*} = \mathrm{FeO^{tot}}/(\mathrm{FeO^{tot}} + \mathrm{MgO})$ *(after Frost et al., 2001). (b) Modified Alkali-Lime Index (MALI) against SiO_2 (wt%), where $MALI = K_2O + Na_2O - CaO$ (after Frost et al., 2001). (c) The Aluminium Saturation Index (ASI) is shown against* $\mathrm{Na_2O + K_2O - Al_2O_3}$*, where* $ASI = \mathrm{Al_2O_3}/(\mathrm{CaO} - 1.67\mathrm{P_2O_5} + \mathrm{Na_2O} + \mathrm{K_2O})$ *(Frost et al., 2001). Rocks with $ASI > 1.0$ are termed peraluminous, while those with $ASI < 1.0$ and* $\mathrm{Na_2O + K_2O} > \mathrm{Al_2O_3}$ *are peralkaline and when $ASI < 1.0$ and* $\mathrm{Na_2O + K_2O} < \mathrm{Al_2O_3}$*, the rock is metaluminous (Frost et al., 2001). Koenap migmatite are circled in blue, Swartoup group 1 in red, Swartoup group 2 in magenta and the Polisiehoek Granite-gneisses in green.*

The mafic dyke specimen, sample GS12A, is shown for reference and plots in the magnesian field, with an Fe* ratio of 0.63.

The Koenap migmatites are only shown for reference, as this plot is designed for granitoid classification. They plot mostly in the magnesian field below Swartoup group 1, at similar silica contents but somewhat lower Fe* values, between Fe* = 0.70 and 0.81. Three Koenap migmatites show overlap with Swartoup group 1, and one of them plots in the ferroan field. On average, they have lower Fe* ratios than the greywacke compositions, though four analyses show overlap with this field. Only one Koenap migmatite shows overlap at the pelite composition field.

The Bysteek marble (Fe* = 0.00) and calc-silicate (Fe* = 0.50) specimens are also shown only

for reference. These samples plot in the magnesian field outside the field of view of Figure 4.2a.

Modified Alkali-Lime Index (MALI)

The MALI is defined as the sum (Frost et al., 2001),

$$\text{MALI} = K_2O + Na_2O - CaO.$$

This is used to separate out four classes of suites based upon the silica content at which K_2O + Na_2O equals CaO. The MALI is based upon the alkali-lime classification of Peacock (1931). Similar trends should be shown by comagmatic suites in the MALI versus silica diagram (Frost et al., 2001).

Figure 4.2b shows Swartoup group 1 mostly in the calc-alkalic field (four samples, MALI = 3.0–4.5 wt%). These analyses show overlap with the pelite and greywacke composition fields. One analysis plots at a higher MALI (MALI = ∼5.5 wt%), in the alkali-calcic field. Swartoup group 2 shows a large range in MALI values, mostly between 4.0 and 8.5 wt%. These vary between all four fields, from alkalic to calcic. The Swartoup group 2 rocks show a MALI range similar to the greywacke composition field, but plot around it due to silica variations. Three Swartoup group 2 samples show relatively lower MALI values than the rest of them, from about -1 to +1 wt%. Sample GS16A plots in the calcic field and has the highest silica contents of the Swartoup granitoids. In contrast, the two lowest silica contents are shown by samples 1151A and GS10B, which plot in the alkali-calcic field at MALI values below Swartoup group 1.

Most hybrid rock samples show MALI values between about 3.5 and 6.5 wt%, varying between Swartoup group 1 and the granitic (high silica) Swartoup group 2 rocks. One sample plots in the alkali-calcic field (sample GS7A, 4.0 wt% MALI) and two plot in each of the calc-alkalic and calcic fields. Sample GS11D shows the lowest MALI value of the hybrid rocks at -4 wt%. This is expected form the rocks relatively high plagioclase and pyroxene modes (Section 3.2.4).

The Polisiehoek Granite-gneisses show somewhat higher MALI values than Swartoup group 1. They vary in MALI values from about 5 to 8.5 wt% and are somewhat evenly distributed between the alkali-calcic (three samples), calc-alkalic (three samples) and calcic fields (two samples). On average, the Polisiehoek Granite-gneisses have higher MALI value than the pelite and greywacke composition fields.

The mafic dyke specimen, again shown for reference, has a MALI value of -9 wt%, plotting in the calcic field as expected from its plagioclase and pyroxene modes (Section 3.2.6).

The Koenap migmatites are shown only for reference, and plot at slightly lower MALI values than Swartoup group 1. Most plot in the calcic field between 1.0 and 3.0 wt% MALI. One sample shows a higher MALI value, 4.0 wt%, plotting in the alkali-calcic field. Some overlap is shown with the lower MALI and higher silica pelite and greywacke compositions.

The Bysteek calc-silicate and marble samples are also shown for reference and plot well into the calcic field, at MALI values below -25 wt%.

Aluminium Saturation Index (ASI)

Frost et al. (2001) define the Aluminium Saturation Index (ASI) as the molar oxide ratio,

$$\text{ASI} = \frac{\text{Al}_2\text{O}_3}{(\text{CaO} - 1.67\text{P}_2\text{O}_5 + \text{Na}_2\text{O} + \text{K}_2\text{O})}.$$

With this, rocks with ASI > 1.0 are termed peraluminous. However, when ASI < 1.0, the rocks are metaluminous if (the molar oxides) $\text{Na}_2\text{O} + \text{K}_2\text{O} < \text{Al}_2\text{O}_3$ but peralkaline if (the molar oxides) $\text{Na}_2\text{O} + \text{K}_2\text{O} > \text{Al}_2\text{O}_3$ (Frost et al., 2001).

Peraluminous granites must have more Al than can be accommodated by feldspars, so must include other aluminous phases. In weakly peraluminous rocks those phases may be aluminous biotite, but in strongly peraluminous rocks those phases may be muscovite, cordierite, garnet or an aluminosilicate such as sillimanite (Frost et al., 2001). Metaluminous granites would likely contain excess Ca after feldspar accommodates Al. Such rocks would contain calcic phases such as augite or hornblende and a lack of sodic ferromagnesian phases (Frost et al., 2001). Peralkaline granites, however, contain more alkalis than necessary to produce feldspar. Some of these alkalis would then need accommodation in ferromagnesian silicates such as hornblende, in weakly peralkaline rocks, or sodic pyroxenes and amphiboles, in strongly peralkaline rocks (Frost et al., 2001).

Figure 4.2c shows the ASI plotted against molar $\text{Na}_2\text{O} + \text{K}_2\text{O} - \text{Al}_2\text{O}_3$, so that, for all samples below an ASI of 1.0; they are metaluminous when molar $\text{Na}_2\text{O} + \text{K}_2\text{O} - \text{Al}_2\text{O}_3$ is negative and peralkaline when molar $\text{Na}_2\text{O} + \text{K}_2\text{O} - \text{Al}_2\text{O}_3$ is positive. All the analyses have negative molar $\text{Na}_2\text{O} + \text{K}_2\text{O} - \text{Al}_2\text{O}_3$ values.

Swartoup group 1 specimens are all peraluminous. They have a narrow range of ASIs, between 1.00 and 1.12 and have molar $\text{Na}_2\text{O} + \text{K}_2\text{O} - \text{Al}_2\text{O}_3$ values between -0.049 and -0.063. Swartoup group 1 shows overlap with the published greywacke composition field. The majority of Swartoup group 2 are also peraluminous. These rocks have a wider range of ASIs as Swartoup group 1, from 0.80–1.66. Samples GS9A, GS10B and 1151A are metaluminous. Swartoup group 2 rocks

have a large range in molar $Na_2O + K_2O - Al_2O_3$ values, from about 0.025 to 0.097. Swartoup group 2 show overlap with the greywacke composition field, having a similar range of molar $Na_2O + K_2O - Al_2O_3$ values, though a somewhat wider range in ASI values.

Three of the hybrid rocks are peraluminous (samples GS1A, GS7A and GS13A) and two are is metaluminous (samples GS11D and GS13B). The hybrid rocks have a similar range of ASI values as Swartoup group 2, varying between 0.78 and 1.57. Their molar $Na_2O + K_2O - Al_2O_3$ contents also show overlap with Swartoup group 2 and range from -0.028 to -0.107.

The Polisiehoek Granite-gneisses have ASI values ranging between 1.01 to 1.29. These rocks show molar $Na_2O + K_2O - Al_2O_3$ values between -0.014 and -0.039, overlapping with the highest molar $Na_2O + K_2O - Al_2O_3$ content Swartoup group 2 samples. Though the Polisiehoek Granite-gneisses do not overlap directly with the greywacke composition field, they have a similar range in ASIs as the greywackes, and show some overlap with the highest molar $Na_2O + K_2O - Al_2O_3$ value greywackes.

The mafic dyke specimen is shown on Figure 4.2 for reference. This rock has one of the lowest ASI (ASI = 0.64) and molar $Na_2O + K_2O - Al_2O_3$ values (-0.119). Like in previous diagrams, the Koenap migmatites are also shown for reference. They are all peraluminous, with ASIs ranging between 1.9 and 5.4. Low Ca, P, Na and K contents in the Koenap migmatites drive up their ASIs with decreasing molar $Na_2O + K_2O - Al_2O_3$ (Figure 4.4a,b,c). This ASI range is similar to that shown by the pelite composition field (1.3–3.8), but at somewhat elevated molar $Na_2O + K_2O - Al_2O_3$ values (-0.106 to -0.138).

The Bysteek specimens are plotted for reference and have the lowest ASIs. Sample GS10A, the Bysteek calc-silicate, has an ASI of 0.17 and the marble, sample GS19A, has an ASI of $\sim$0. Sample GS19A has a molar $Na_2O + K_2O - Al_2O_3$ value of 'sim0. The molar $Na_2O + K_2O - Al_2O_3$ value of sample GS10A, -0.087, is within the molar $Na_2O + K_2O - Al_2O_3$ ranges of Swartoup group 2 and the hybrid rocks.

Rock classification using the Fe*, MALI and ASI diagrams

The classification scheme of Frost et al. (2001) lists a number of possible rock names for each geochemical subset (shown in Table A.7, Appendix A.1.1.3). For example, granitoids that are magnesian, calc-alkalic and peraluminous can be either diorites, monzodiorites or granodiorites (see Frost et al., 2001).

A summary of the results of this classfication scheme are shown in Table 4.6 (Table A.6 shows

the Fe8, MALI and ASI values as well as all possible rock names for each rock). This scheme does not agree with the TAS and R_1R_2 classification diagrams (see Tables 3.4 and 3.6). Few samples are given the same rock names by this scheme and the previous two. Only samples 1144A (granodiorite) and GS9A (granite) are given the same rock-names by this scheme and either of the TAS and R_1R_2 diagrams. Sample GS15B is unclassified by the scheme of Frost et al. (2001), as the specimen is both alkalic and peraluminous.

Table 4.6: *Geochemical classification of granitoids using the Fe*, modified alkali-lime index and aluminium saturation index, after Frost et al. (2001). This classification scheme lists a number of possible rock names for each geochemical subset (see Table A.7).*

Rock unit	Sample	Fe*	MALI	ASI	Rock type
Swartoup group 1	1139A	Ferroan	Calc-alkalic	Peraluminous	Two-mica granite
	1140A	Ferroan	Calc-alkalic	Peraluminous	Two-mica granite
	1144A	Magnesian	Calc-alkalic	Peraluminous	Granodiorite
	1145A	Ferroan	Calc-alkalic	Peraluminous	Two-mica granite
	1146A	Ferroan	Alkali-calcic	Peraluminous	Two-mica granite
Swartoup group 2	GS5A	Magnesian	Calcic	Peraluminous	Diorite
	GS9A	Ferroan	Calc-alkalic	Metaluminous	Granite
	GS9B	Magnesian	Calcic	Peraluminous	Diorite
	GS10B	Ferroan	Alkali-calcic	Metaluminous	Ferrodiorite
	GS15B	Magnesian	Alkalic	Peraluminous	[a]
	GS15C	Ferroan	Alkali-calcic	Peraluminous	Two-mica granite
	GS16A	Magnesian	Calcic	Peraluminous	Diorite
	1149A	Magnesian	Calcic	Peraluminous	Diorite
	1151A	Ferroan	Alkali-calcic	Metaluminous	Ferrodiorite
Hybrid rock	GS1A	Magnesian	Calcic	Peraluminous	Diorite
	GS7A	Ferroan	Calc-alkalic	Peraluminous	Two-mica granite
	GS11D	Magnesian	Calcic	Metaluminous	Diorite
	GS13A	Magnesian	Calc-alkalic	Peraluminous	Diorite
	GS13B	Magnesian	Calcic	Metaluminous	Diorite
Polisiehoek Granite	1142A	Magnesian	Calcic	Peraluminous	Diorite

[a] Rock not classified by this scheme as it is alkalic and peraluminous.

Though Swartoup group 1 vary between ferroan and magnesian (Figure 4.2a), they are all peraluminous (Figure 4.2c, Table 4.6) and either calc-alkalic or alkali-calcic (Figur 4.2b). As such, Swartoup group 1 are named as two-mica granites, except for sample 1144A, a granodiorite by this classification scheme.

Swartoup group 2 rocks vary from ferroan to magnesian, calcic to alkalc and peraluminous to metaluminous. Table 4.6 shows they are classified mostly as diorites (samples GS5A, GS9B, GS16A and 1149A) and ferrodiorites (samples GS10B and 1151A) with one granite (sample GS9A) and a two-mica granite (sample GS15C).

Of the hybrid rocks, most are magnesian and vary form calcic to calc-alkalic and peraluminous

to metaluminous. The classification scheme of Frost et al. (2001) name these rocks diorites, except for sample GS7A, a two-mica granite.

The Polisiehoek Granite-gneisses are all peraluminous and ferroan, and vary from alkali-calcic to calcic (Figure 4.2). Only sample 1142A, the Polisiehoek white granite (Section 3.2.5) is named a diorite by the Frost et al. (2001) granitoid classification scheme (all other Polisiehoek Granite-gneisses show metamorphic fabrics, and so were named accordingly; Section 3.2.5).

Geochemical classification of granitoids by the TAS and R_1R_2 diagrams (Figure 4.1) has been favoured over this scheme as proposed by Frost et al. (2001), as the aforementioned schemes show better agreement with each other than they do with the latter scheme (see Tables 3.4 and 3.6).

4.3 I-, S- and A-type granitoid characteristics

Diagrams of P_2O_5, Ce, Y and La against Rb or SiO_2 (Figure 4.3) are useful to distinguishing I- and S-type characteristics in granitoids, especially in leucogranitic rocks (Chappell and White, 1992; Chappell, 1999; Zhang et al., 2019) such as the Polisiehoek Granite-gneiss. However, as can be seen in the ASI diagram (Figure 4.2c), the Swartoup granitoids, Polisiehoek Granite-gneisses and hybrid rocks have ASIs close to 1. This makes distinctions between I- and S-type granitoids difficult (Chappell, 1999). Figure 5.2 (Section 5.3.1) shows diagrams of (a) $(Na_2O + K_2O)/CaO$ and (b) FeO^T/MgO versus Zr + Nb + Ce + Y, and also (c) $(Al_2O_3 + CaO)/(FeO^T + Na_2O + K_2O)$ versus $100 \times (MgO + FeO^T + TiO_2)/SiO_2$. These are used to distinguish A-, I- and S-type granitoids as well as fractionated I- and S-type granitoids (e.g. Whalen et al., 1987; Sylvester, 1989; Zhang et al., 2019). The $(Al_2O_3 + CaO)/(FeO^T + Na_2O + K_2O)$ versus $100 \times (MgO + FeO^T + TiO_2)/SiO_2$ diagram (Figure 5.2c) can also be used to distinguish alkaline from peraluminous rocks. However, these results do not agree well with the ASI classification used by Frost et al. (2001). This diagram is instead used to confirm classification of fractionated I- and S-type granitoids made by the $(Na_2O + K_2O)/CaO$ and FeO^T/MgO versus Zr + Nb + Ce + Y diagrams.

4.3.1 P_2O_5 against Rb

Figure 4.3a shows P_2O_5 (wt%) against Rb (ppm). Peraluminous melts, which generally result in S-type granitoids, show positive correlation between P_2O_5 and Rb (and also with SiO_2, Figure 4.5d) due the high solubility of apatite in them (Chappell and White, 1992; Chappell, 1999;

Zhang et al., 2019). In contrast, highly fractionated I-type granitoids, which are commonly weakly peraluminous to metaluminous, generally have low P_2O_5 contents that decrease with Rb (and SiO_2). This is generally thought to be due to low solubility of apatite in such melts and the presence of a restite that includes apatite crystals (Chappell and White, 1992; Chappell, 1999).

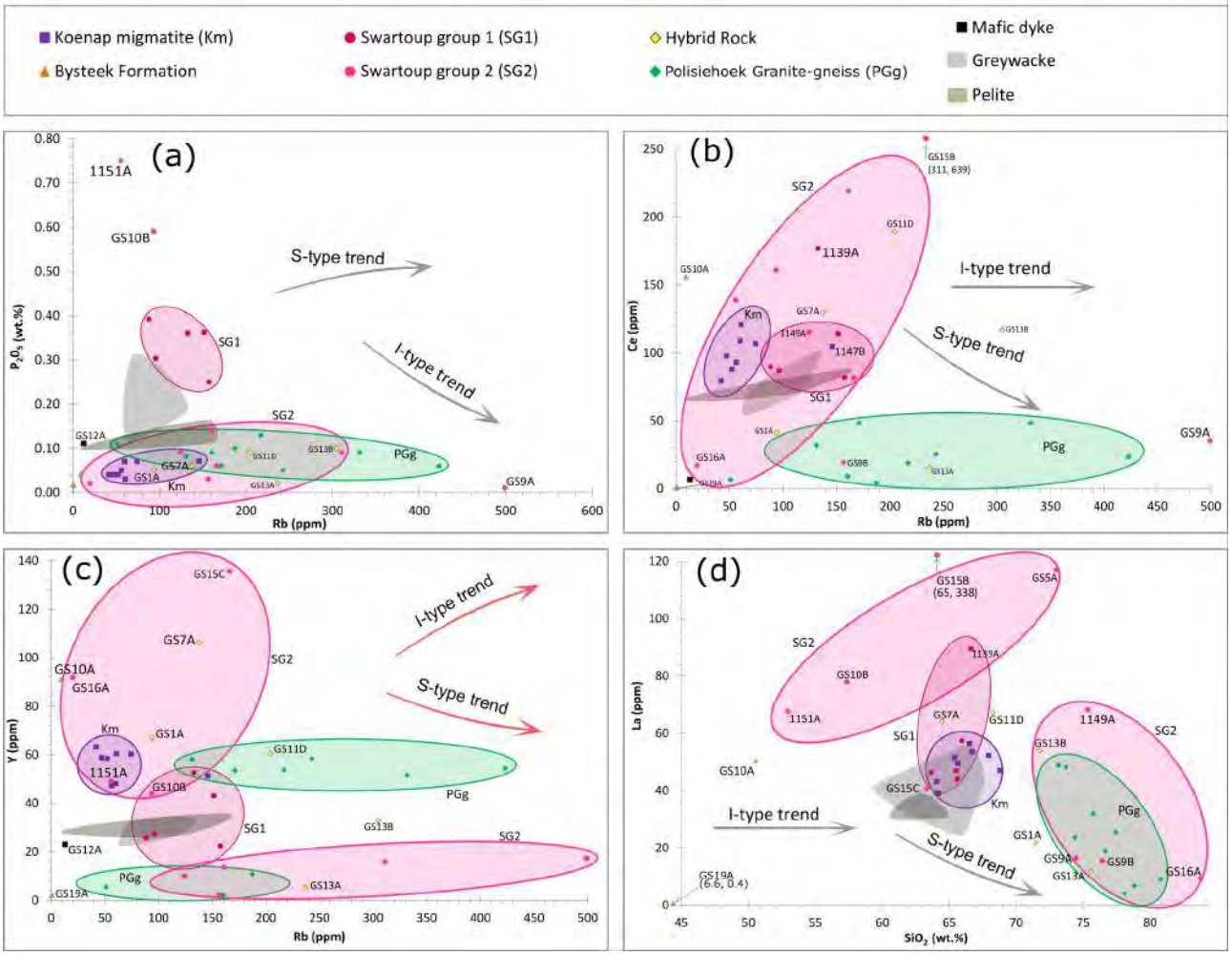

Figure 4.3: *Diagrams of (a) P_2O_5, (b) Ce and (c) Y against Rb and (d) La versus SiO_2 are useful for distinguishing I- and S-type characteristic granitoids from each other. The differing trends shown by such granitoids is attributed to the different solubilities of apatite in I- and S-type melts (Chappell and White, 1992; Chappell, 1999). Koenap migmatite are circled in blue, Swartoup group 1 in red, Swartoup group 2 in magenta and the Polisiehoek Granite-gneisses in green.*

Figure 4.3a shows Swartoup group 1 with relatively high P_2O_5 contents, from 0.25 to 0.39 wt%. There is some overlap of both the P_2O_5 and Rb (∼90–160 ppm) contents of Swartoup group 1 with the published greywacke compositions (0.12–0.31 wt% P_2O_5; 70–130 ppm Rb). The high P_2O_5 contents of the granodiorites, relative to both the published greywacke and pelite (0.10–0.16 wt% P_2O_5; ∼10–170 ppm Rb) compositions are generally compatible with S-type granitoids.

The P_2O_5 versus Rb diagram does not show clear distinction of Swartoup group 2 between an

I- or S-type granitoids. While high P_2O_5 contents are an S-type characteristic, both S- and I-type granitoids can have low P_2O_5 contents. Two analyses from Swartoup group 2, samples 1151A and GS10B, show high P_2O_5 contents around 0.60–0.75 wt% P_2O_5. However, the rest of Swartoup group 2 appear to show an increase in P_2O_5 content (0.02–0.10 wt%) with Rb (20–310 ppm), mostly at lower P_2O_5 contents than the published pelite compositions. One outlier, sample GS9A, shows low P_2O_5 contents (0.01 wt%) at high Rb (500 ppm).

The hybrid rock specimens show a similar range of P_2O_5 (0.02–0.10 wt%) and Rb (90–300 ppm) contents as the majority of Swartoup group 2, and also increase in P_2O_5 with Rb. Though the increasing P_2O_5 with Rb suggests an S-type affinity, the low P_2O_5 contents, again similar to Swartoup group 2, indicate an I-type trend cannot be ruled out by this diagram.

The Polisiehoek granite-gneisses show low P_2O_5 contents (0.05–0.013 wt%) which appear to decrease with increasing and Rb (50–420 ppm); suggestive of an I-type characteristic. Their P_2O_5 contents are, on average, lower than both the published greywacke and pelite compositions.

The mafic dyke sample shows 0.11 wt% P_2O_5 and 13 ppm Rb.

The Koenap migmatites (∼0.03–0.07 wt% P_2O_5; ∼40–150 ppm Rb) are included in the P_2O_5 versus Rb diagram for reference. They show almost the same Rb ranges as the published greywacke and pelite compositions. However, they show much lower P_2O_5 contents, consistent with removal or fractionation of phosphorous-bearing phases such as apatite and monazite to a melt fraction.

The Bysteek marble (0.01 wt% P_2O_5; 0.6 ppm Rb) and calc-silicate (0.04 wt% P_2O_5; 9 ppm Rb) specimens are also shown for reference. They have the two lowest Rb contents of the sample set, and two of the lowest P_2O_5 contents.

4.3.2 Ce against Rb

Figure 4.3b shows Ce (ppm) against Rb (ppm). Generally, I-type granitoids display slightly positive- to no-correlation between Ce with increasing Rb, while S-type granitoids show somewhat negative trends (Chappell and White, 1992; Chappell, 1999; Zhang et al., 2019).

The Ce versus Rb diagram (Figure 4.3b) shows Swartoup group 1 with somewhat more Ce (∼80–110 ppm; one exception, sample 1139A, at 180 ppm Ce) than published pelite (∼60–80 ppm) and greywacke compositions (∼50–90 ppm), though the data show much overlap. While this diagram may indicate an I-type affinity of Swartoup group 1, it does not rule out an S-type characteristic, as the data are relatively close to each other.

Swartoup group 2 show wide variation in Ce contents, form ∼20–220 ppm, with one exception at ∼640 ppm Ce (two samples at low Ce and one at high Ce have not been circled in Figure 4.3b). The large range in Ce concentrations of Swartoup group 2 is probably an indicator of source/protolith differences (Chappell and White, 1992; Chappell, 1999; Zhang et al., 2019). This may suggest an I-type affinity for Swartoup group 2, as sediment compositions are generally more constrained.

The hybrid rocks show a similar range in Ce contents as Swartoup group 2, ranging from about 20–190 ppm Ce. Again, as for Swartoup group 2, this wide range in Ce contents is characteristic of some I-type granitoids.

The Polisiehoek Granite-gneisses show Ce contents (∼10–100 ppm) lower than the published greywacke and pelite compositions. This may indicate they have an S-type affinity. However, they also appear to show no correlation with Rb, a I-type granitoid trend. This can result from a low-Ce igneous protolith.

The mafic dyke specimen, sample GS12A, shows a low Ce content of 6.7 ppm.

The Koenap migmatites (∼40–60 ppm La; ∼80–120 ppm Ce) are included for reference. They show almost the same range in Ce compositions as Swartoup group 1, at somewhat lower Rb contents.

The Bysteek marble (0.9 ppm Ce) shows one of the lowest Ce contents of the sample set. The calc-silicate specimen (160 ppm), however, shows a similar Ce content as Swartoup group 2 and the hybrid rocks.

4.3.3 Y against Rb

Figure 4.3c shows Y (ppm) versus Rb (ppm). Chappell (1999) refers to the contrasting behaviour of Y in felsic I- and S-type granitoids as one of the most distinctive features of these two rock types; along with the behaviour of P_2O_5. Up to about 75 wt% SiO_2, both I- and S-type rocks show similar Y abundances, which continues at about the same level for S-type granitoids (Chappell, 1999). In diagrams against Rb, like Figure 4.3c, the S-type rocks show slight negative correlation (see Zhang et al., 2019). For I-type granites, they show up to 5 times the amount of Y as the S-type rocks (Chappell, 1999). The explanation for this given by Chappell (1999) is that Y behaves as a strongly incompatible element in the high-Y I-type rocks, with no Y-bearing accessory phase fractionating. The fractionating S-type haplogranites have a bulk partition coefficient for Y close to one, therefore an Y-bearing accessory mineral would be consistently

present (Chappell, 1999).

Only the granitic Swartoup group 2 rocks and the Polisiehoek Granite-gneisses have SiO_2 contents above 75 wt%.

The Y versus Rb diagram (Figure 4.3c) shows Swartoup group 1 as having Y contents (22–53 ppm Y) with much overlap with the published pelite (27–35 ppm Y) and greywacke (24–33 ppm Y) compositions. Due to overlap in the Rb contents of these analyses, no clear affinity towards either I- or S-type trends can be distinguished form this diagram.

Swartoup group 2, however, show a greater range in Rb contents than Swartoup group 1. They also show two distinct groups of analyses in the Y versus Rb diagram. One group (4 samples, ∼45–135 ppm Y, ∼20–170 ppm Rb) shows higher Y contents than the published sediment compositions and the other shows somewhat lower Y contents (5 samples, ∼2–20 ppm Y, 120–500 ppm Rb). These five analyses at low Y contents include the granitic Swartoup group 2 rocks ($<$ 75 wt% SiO_2), samples 1149A, GS5A, GS9A and GS9B, as well as sample GS15B (∼65 wt% SiO_2). The high silica rock, sample GS16A (84 wt% SiO_2) has the lowest Rb content of Swartoup group 2 (∼20 ppm Rb) and around 90 ppm Y, and so lies with the upper Y Swartoup group 2 analyses. No explanation is given for the high-Y contents of the upper Y Swartoup group 2 analyses, though this may be due to source differences or local concentrations of Y. The low Y group, however, shows a strong S-type characteristic as they have lower-Y contents than the published sediment compositions.

The hybrid rock specimens show a wide range of Y contents (∼5–110 ppm Y), similar to the total range in Y-contents shown by Swartoup group 2. One sample, GS13A (∼5 ppm Y), lies with the lower-Y Swartoup group 2 analyses. However, sample GS13B (∼35 ppm Y) has a similar Y content as the published sediment compositions and the rest of the hybrid rocks (3 samples, ∼60–110 ppm Y) have similar Y contents as the higher Swartoup group 2 analyses. This indicates the hybrid rocks include both I- and S-type characteristics.

The Polisiehoek Granite-gneiss show two distinct groups of Y contents. The lower group has lower Y contents, from ∼2–10 ppm Y (3 samples), than the published pelite and greywacke compositions, indicating these rocks have an S-type affinity. In contrast, the upper group shows ∼50–60 ppm Y (6 samples), more than the published sediment compositions, suggesting an I-type affinity for these rocks.

The mafic dyke sample has a moderate-Y content of around 25 ppm Y.

As was done in the P_2O_5 and Ce versus Rb diagrams, the Koenap migmatites are shown in

the Y-diagram (Figure 4.3c) for reference as well. These rocks have Y-contents ranging from around 50–60 ppm Y, more than what was shown by the published sediment compositions.

The Bysteek Formation samples are also shown for reference on the Y versus Rb diagram. The Bysteek marble, sample GS19A, shows around 2 ppm Y, while the calc-silicate, sample GS10A, specimen has ∼90 ppm Y. This range is somewhat similar to that shown by the hybrid rock analyses.

4.3.4 La against SiO_2

Figure 4.3d shows La (ppm) against SiO_2 (wt%). This diagram should show similar trends as the Ce versus Rb diagram, with regard to I and S-type granitoids. Generally, I-type granitoids display little correlation between La with increasing SiO_2, while S-type granitoids show somewhat negative trends, especially in leucogranites (Chappell and White, 1992; Chappell, 1999; Zhang et al., 2019). Above 73 wt% SiO_2, La is expected to show a marked decease with increasing SiO_2 in S-type granitoids, corresponding to fractional crystallisation of leucogranite liquids (Chappell, 1999). I-type compositions show this decrease to a lesser degree, and some may retain high La contents (Chappell, 1999). This behaviour of La in S-type granitoids is due to fractional crystallisation of monazite from felsic liquids (Chappell, 1999). Low La contents are possible in some I-type leucoogranites. This can be attributed to either monazite as a fractionating phase, despite low P contents, or allanite was instead fractionating (Chappell, 1999).

The La versus SiO_2 diagram (Figure 4.3d) shows Swartoup group 1 with around ∼40–60 ppm La (one exception, sample 1139A, at 90 ppm La). They show somewhat more La than the published pelite compositions (∼30–40 ppm La) and some overlap with the published greywackes (∼25–55 ppm La). Like the Y versus Rb diagram, the La against SiO_2 diagram shows no clear distinction of Swartoup group 1 between I- and S-type characteristics.

Swartoup group 2 shows two distinct groups in the La versus SiO_2 diagram, like what was seen in the Y versus Rb diagram (Figure 4.3c). The relatively higher SiO_2 content, granitic Swartoup group 2 rocks show decreasing La with SiO_2 (∼10–70 ppm La), a strong S-type characteristic. The rest of Swartoup group 2 show more La (∼70–120 ppm La; one exception, GS15B, at ∼390 ppm La) than the published sediment compositions. Due to the similar SiO_2 contents of these Swartoup group 2 rocks and the sediment compositions, the rocks show no I- or S-type affinities in this diagram.

The hybrid rock specimens show decreasing La with increasing SiO_2 (∼10–70 ppm La). Their La contents have the same range in values as that of the granitic Swartoup group 2 analyses (<75 wt% SiO_2), though at somewhat lower SiO_2 contents (∼65–75 wt% SiO_2). Their decreasing La contents with silica are more typical of S-type granitoids than I-type granitoids, however this diagram is also compatible with the latter rock type.

Polisiehoek Granite-gneiss analyses show strong negative correlation between La and SiO_2. Their La contents decrease from ∼50 ppm to 5 ppm La, over a silica range of about 75–80 wt% SiO_2. As previously stated, this characteristic is more common to S-type, rather than I-type granitoids, especially in haplogranites.

The mafic dyke specimen, sample GS12A shows about 2 ppm La, one of the lowest La contents of the sample set.

Like in previous diagrams, the Koenap migmatites (∼40–55 ppm La) are included for reference. They show somewhat more La than the published pelite compositions. However, they show overlap with the published greywacke compositions (∼25–55 ppm La) at similar SiO_2 contents.

Again, the Bysteek Formation analyses are included for reference. The Bysteek marble, GS19A, shows the lowest La concentration in the sample set, <1 ppm La. In contrast the Bysteek calc-silicate, sample GS10A, shows a moderate La content of 50 ppm La.

4.4 Further chemical variation diagrams

Variation diagrams against silica, as proposed by Harker (1909), are shown in Figures 4.4–4.5c. Figure 4.6d shows a plot of molar $Al_2O_3/(MgO + FeO^T)$ versus molar $CaO/(MgO + FeO^T)$, which is used to help determine the source rocks from which partial melts are produced (see Altherr et al., 2000). Diagrams showing maficity (molar Fe + Mg), as used by Clemens et al. (2011) and Clemens (2012), are found in Section 4.4.2 (Figure 4.6). Chondrite normalised rare earth diagrams are presented in Section 4.4.3, Figure 4.7.

4.4.1 Major and minor element oxide plots

Figures 4.3d and 4.4 show either oxide or elemental contents against silica oxide. The SiO_2 contents were already presented with the TAS diagram (Section 4.1.1, Figure 4.1a). However, as SiO_2 are the basis for most of the diagrams shown in this section the silica variations are summarised for the main rock types.

The Koenap migmatites show 64 to 69 wt% SiO_2. The Bysteek calc-silicate (sample GS10A) shows less silica, around 48 wt% SiO_2. However, the Bysteek marble, which has 3.9 vol% SiO_2, shows the lowest silica content of the sample set, as expected from the calcite dominated marble (Section 3.2.2, Table 3.2.

Swartoup group 1 show similar SiO_2 (63–66 wt% SiO_2) values as the Koenap migmatites. However, Swartoup group 2 vary from above to below this range (53–84 wt% SiO_2). The Swartoup group 2 rocks often referred to as granitic have SiO_2 contents from 73–84 wt% and comprise samples 1149A, GS5A, GS9A, GS9B and GS16A.

The hybrid rocks show SiO_2 concentrations which vary from 64–75 wt% SiO_2. Their SiO_2 contents generally overlap with Swartoup group 1 and the granitic Swartoup group 2 rocks.

The Polisiehoek granite-gneisses have similar silica contents as the granitic Swartoup group 2 rocks (73–81 wt% SiO_2). Published greywacke (59–68 wt% SiO_2) and pelite (59–67 wt% SiO_2) compositions have similar SiO_2 contents compared to each other and also to Swartoup group 1 and the Koenap migmatites.

K_2O against SiO_2

Most of the Koenap migmatite specimens show a narrow range in K_2O contents from 1.4–1.8 wt% (Figure 4.4a). These samples plot at lower K_2O concentrations than the published greywacke composition field (2.0–4.5 wt%). The pelite composition field shows overlap with the upper portion of the greywacke field. Sample 1137A plots at a higher K_2O content (2.7 wt% K_2O) than the main Koenap migmatite cluster and overlaps the greywacke field. Similarly, sample 1147B also plots at a higher K_2O concentration (3.9 wt% K_2O). However, the sample has a K_2O content compatible with both the pelite and greywacke fields, but due to SiO_2 variations only shows overlap with the pelite field.

The Bysteek marble has no detectable K_2O and the calc-silicate specimen has 0.2 wt% K_2O. This correlates with the lack of potassium-rich phases in these specimens (Section 3.2.2).

Most Swartoup group 1 samples form a cluster which shows overlap with the greywacke and pelite fields, close to the most K_2O-rich Koenap migmatite, sample 1147B, between 3.7 and 4.2 wt% K_2O. Only sample 1146A plots above the greywacke and pelite fields, at 5.5 wt% K_2O.

Swartoup group 2 specimens show a broad, positive K_2O—SiO_2 trend. At the lower end of this trend, sample 1151A shows 1.9 wt% K_2O ($\sim$53 wt% SiO_2), similar to the Koenap migmatites. The Swartoup group 2 K_2O concentrations then increase towards the granitic samples which

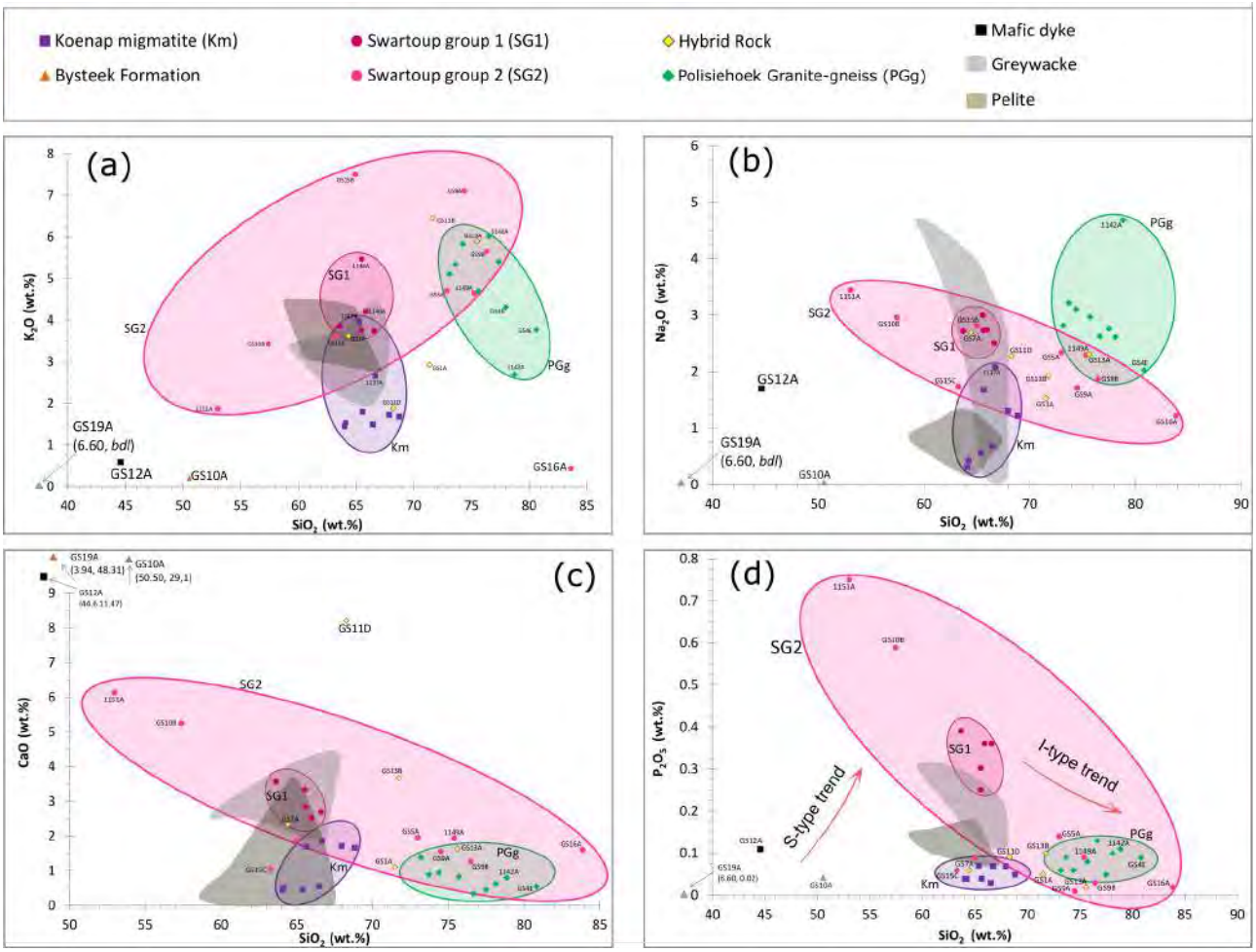

Figure 4.4: *Harker diagrams showing (a) K_2O, (b) Na_2O, (c) CaO, and (d) P_2O_5 against SiO_2 (wt%). Koenap migmatite are circled in blue, Swartoup group 1 in red, Swartoup group 2 in magenta and the Polisiehoek Granite-gneisses in green. See text for context of I- and S-type trends in (d).*

show between 4.5 and 7.5 wt% K_2O, at around 75 wt% SiO_2.

The hybrid rocks are widely scattered, showing no clear trends or clustering. Their K_2O concentrations vary from near those of the Koenap migmatites at 1.9 wt% K_2O (sample GS11D), to 5.9–6.4 wt% K_2O, plotting near the Polisiehoek Granite-gneisses and some of the granitic Swartoup group 2 rocks.

The Polisiehoek Granite-gneiss specimens show a negative K_2O–SiO_2 trend, at moderate to high K_2O contents (2.7–6.0 wt% K_2O). The lower K_2O content Polisiehoek Granite-gneisses show overlap with the K_2O compositions of the pelite and greywacke fields. However, due to the higher silica contents of the Polisiehoek samples, they all plot away from these fields. The mafic dyke has a relatively low K_2O content of 0.6 wt% K_2O, consistent with its moderately low K-feldspar mode (10 vol%, Section 3.2.6).

Na_2O against SiO_2

The Na_2O contents of all rocks in the sample set are compatible with published greywacke compositions (Figure 4.4b), which show a full range of ∼0.0 to 4.7 wt% Na_2O. Most samples show less than about 3.5 wt% Na_2O. The majority of the Swartoup group 2 specimens, hybrid rocks and Polisiehoek Granite-gneisses plot outside the greywacke field itself due to variations in SiO_2 contents.

The four most melanocratic Koenap migmatites (samples 1138A, 1141A, 1147B and GS4C, Section 3.2.1) have $<$ 1 wt% Na_2O wt% Na_2O and show overlap with the published pelite composition field (0.2–1.2 wt% Na_2O). The other three, relatively more leucocratic, Koenap migmatites plot at higher Na_2O contents, up to about 2.1 wt% Na_2O, showing overlap with the greywacke field.

The Bysteek marble (below detection limit Na_2O) and calc-silicate (0.04 wt% Na_2O) show very little Na_2O. This correlates with their absence of sodium-bearing phases (Section 3.2.2).

Swartoup group 1 shows overlap with the greywacke field, at Na_2O contents between 2.5 and 3.0 wt% Na_2O. However, Swartoup group 2 show a well-defined negative Na_2O–SiO_2 trend, from 3.7 wt% Na_2O (sample 1151A) to 1.2 wt% Na_2O (sample GS16A), with one exception, sample GS15C, which shows slightly less Na_2O. Swartoup group 1 lies within this well-defined trend.

Samples GS7A and GS11D show overlap with the greywacke field (1.2–2.7 wt% Na_2O). These two specimens and sample GS13B show negative correlation between Na_2O and SiO_2, much like that shown by the Swartoup granitoids. One outlier, sample GS1A, plots slightly below this trend at a lower Na_2O content (∼1.5 wt%).

The Polisiehoek Granite-gneisses show overlap with the Na_2O contents of the greywacke composition field but at higher SiO_2 contents. Most plot between 2.0 and 3.2 wt% Na_2O and show negative correlation between Na_2O and SiO_2. Sample 1142A is an outlier at 4.7 wt% Na_2O, but the rock still shows overlap with the published greywacke Na_2O compositions. The mafic dyke specimen shows a moderate Na_2O content around 1.7 wt%.

CaO against SiO_2

The Koenap migmatites show two somewhat distinct groups of CaO contents (Figure 4.4c). Samples 1138A, 1141A, 1147B and GS4C show low CaO contents around 0.5 wt% CaO and are some of the most melanocratic Koenap migmatites (Section 3.2.1) and show overlap with the

published pelite composition field (∼0.03–3.7 wt% CaO). Samples 1137A, 1143A, 1143B and GS4D show higher CaO contents, plotting from 1.6 to 1.9 wt% CaO with some overlap with the pelite composition field. These specimens are more leucocratic, except for sample 1143B which is somewhat melanocratic (Section 3.2.1).

The Bysteek marble (48 wt% CaO) and calc-silicate (28 wt% CaO) specimens show the two highest CaO concentrations of the sample set. This is expected as the Bysteek marble is dominated by calcite and the Bysteek calc-silicate comprises mostly clinopyroxene, garnet and titanite (Section 3.2.2, Table 3.2).

Swartoup group 1 specimens cluster reasonably well between 2.5 and 3.5 wt% CaO, showing higher CaO contents than the Koenap migmatites and overlap with the published greywacke compositions (∼2.0–4.3 wt% CaO). In contrast, the Swartoup group 2 specimens shows more variation than those of Swartoup group 1. They vary from samples 1151A (6.1 wt% CaO) and GS10B (5.2 wt% CaO), which have the highest CaO amounts of the Swartoup granitoid specimens, to sample GS15C, which has the lowest, at about 1.1 wt% CaO. Samples GS15B, GS16A and the Swartoup group 2 granites (samples 1149A, GS5A, GS9A and GS9B) have CaO contents closer to those of the upper Koenap migmatite group (1.3 to 2.0 wt% CaO). The CaO versus SiO_2 diagrams shows a negative correlation trend from samples 1151A and GS10B (Swartoup group 2), to the Swartoup group 1 analyses and then on to the granitic Swartoup group 2 rocks.

The hybrid rocks show CaO amounts between 1.1 and 8.1 wt% CaO, which overlap with the majority of both the Swartoup granitoid and Koenap migmatite specimens. Only sample GS11D (8.1 wt% CaO) shows a significantly higher CaO content, which is even higher than the Swartoup group 2 outliers, samples 1151A and GS10B (6.1, 5.1 wt%). This probably resulted from the high plagioclase and clinopyroxene modes of sample GS11D (Section 3.2.4, Table 3.5).

The Polisiehoek Granite-gneisses show uniformly low CaO amounts, not exceeding 1.5 wt% CaO. They show lower CaO concentrations than greywacke compositions. Their low CaO contents correlate with their low plagioclase modes and general lack of calcium-rich phases (Section 3.2.5).

The mafic dyke specimen (11.5 wt% CaO) plots at CaO contents higher than the rest of the sample set, except for the two Bysteek Formation rocks. This is consistent with the high plagioclase and clinopyroxene modes of the specimen (Section 3.2.6).

P_2O_5 against SiO_2

The Koenap migmatites show a narrow range in P_2O_5 between 0.03 and 0.07 wt% P_2O_5 (Figure 4.4d). They plot at lower P_2O_5 contents than the published pelite and greywacke composition fields, with only three samples plotting near the lowest portion of the pelite field. This pelite field shows 0.07–0.17 wt% P_2O_5 and has some overlap with the greywacke composition field (0.12–0.31 wt% P_2O_5). The Bysteek marble (0.01 wt% P_2O_5) and calc-silicate specimens (0.04 wt% P_2O_5) have low of P_2O_5 contents.

The rocks of Swartoup group 1 define a relatively loose cluster of analyses between 0.25 and 0.39 wt% P_2O_5. They plot above the greywacke field, except for sample 1146A, which lies within this field. Swartoup group 2 vary greatly, in contrast. Samples 1151A (0.75 wt% P_2O_5) and GS10B (0.59 wt% P_2O_5) have much higher P_2O_5 than Swartoup group 1 and the greywacke and pelite compositions. The rest of Swartoup group 2 have P_2O_5 contents that are comparable to the Koenap migmatites and pelites (0.01–0.14 wt% P_2O_5), but at higher SiO_2 contents. If all Swartoup group 2 specimens are considered, as well as Swartoup group 1, then all the Swartoup Pluton analyses show a negative correlation between P_2O_5 and SiO_2. However, if only the lower-P_2O_5 Swartoup group 2 samples are considered, Swartoup group 2 shows no correlation other than consistently low P_2O_5 contents.

The hybrid rocks show low P_2O_5 values which range from 0.02–0.10 wt% P_2O_5. These P_2O_5 values are similar to those of the Koenap migmatite specimens as well as most of the Swartoup group 2 samples. Sample GS13A has the least P_2O_5 and sample GS13B has the most. Sample GS7A plots with the Koenap migmatites.

The Polisiehoek Granite-gneiss has P_2O_5 contents which range between 0.05 and 0.13 wt% P_2O_5, somewhat higher than those shown by the Koenap migmatites and similar to the pelites. However, due to their higher SiO_2 contents, the Polisiehoek Granite-gneisses form a separate cluster. No P_2O_5–SiO_2 correlation is evident amongst them. The mafic dyke specimen has a moderate P_2O_5 content of 0.11 wt% P_2O_5.

FeO^T against SiO_2

Figure 4.5a shows that the Koenap migmatites appear to define a negative FeO^T–SiO_2 trend. Six analyses have FeO^T contents (9–10 wt% FeO^T) lower than those of the published pelite compositions (11–17 wt% FeO^T). Two outliers show higher FeO^T concentrations (around 14 wt% FeO^T) that show overlap with the published pelite and greywacke (9–14 wt% FeO^T) composition

fields. These high FeO^T samples are the most melanocratic Koenap migmatites (Section 3.2.1).

The Bysteek marble specimen has a very low FeO^T content (∼0.6 wt%), which corresponds with its general lack of iron-rich phases (Section 3.2.2) and suggests that its clinopyroxene mode is comprised predominantly of diopside (see the MgO content, below). The Bysteek calc-silicate sample has a moderate iron content, with around 4 wt% FeO^T.

Swartoup group 1 have lower FeO^T contents (∼5–7 wt% FeO^T) than the Koenap migmatite specimens. Swartoup group 2, in contrast have much greater variation. Two orthopyroxene-bearing and one garnet-bearing samples (1151A, GS10B and GS15C) have relatively high iron contents, around 11–12 wt% FeO^T, similar to Koenap migmatite. The rest of Swartoup group 2 all contain less FeO^T than Swartoup group 1, with 1–4 wt% FeO^T.

The hybrid rocks show somewhat less variation than that of Swartoup group 2. Two samples (GS1A and GS7A) have ∼6.8 wt% FeO^T, similar to that shown by Swartoup group 1. The rest of the hybrid rock analyses have 0.6–1.4 wt% FeO^T, slightly less than the granitic Swartoup group 2 rocks, on average.

The Polisiehoek Granite-gneisses show a narrow range of FeO^T contents, which decrease slightly with increasing silica, from around 2 to <1 wt% FeO^T. The mafic dyke specimen, sample GS12A, has the highest FeO^T concentration of the sample set at 14 wt% FeO^T.

MgO against SiO_2

The Koenap migmatites have a range of MgO contents, from 2.3 to 3.7 wt% MgO (Figure 4.5b). They show overlap with the published greywacke compositions (2.0–3.5 wt% MgO). The pelite composition field shows overlap with both Koenap migmatite and the greywacke field and extends to lower MgO values, varying from 1.1 to 3.9 wt% MgO.

The Bysteek calc-silicate, sample GS10A, has a relatively high MgO content of 3.8 wt% MgO. The Bysteek marble specimen, GS19A, however, has the second highest MgO content of the sample set, at 7.8 wt MgO. These high MgO concentrations are consistent with predominantly diopside-rich clinopyroxene modes in the calc-silicate sample and a large dolomitic component to the marble specimen (Section 3.2.2).

Swartoup group 1 have lower MgO concentrations than Koenap migmatite and show overlap with pelite compositions between 1.1 and 1.8 wt% MgO. Similar to the Fe_2O_3 diagram, three Swartoup group 2 analyses have higher MgO contents than the rest of Swartoup group 2. Samples 1151A and GS10B, both Opx-bearing, have 2.8 and 2.3 wt% MgO and sample GS15C,

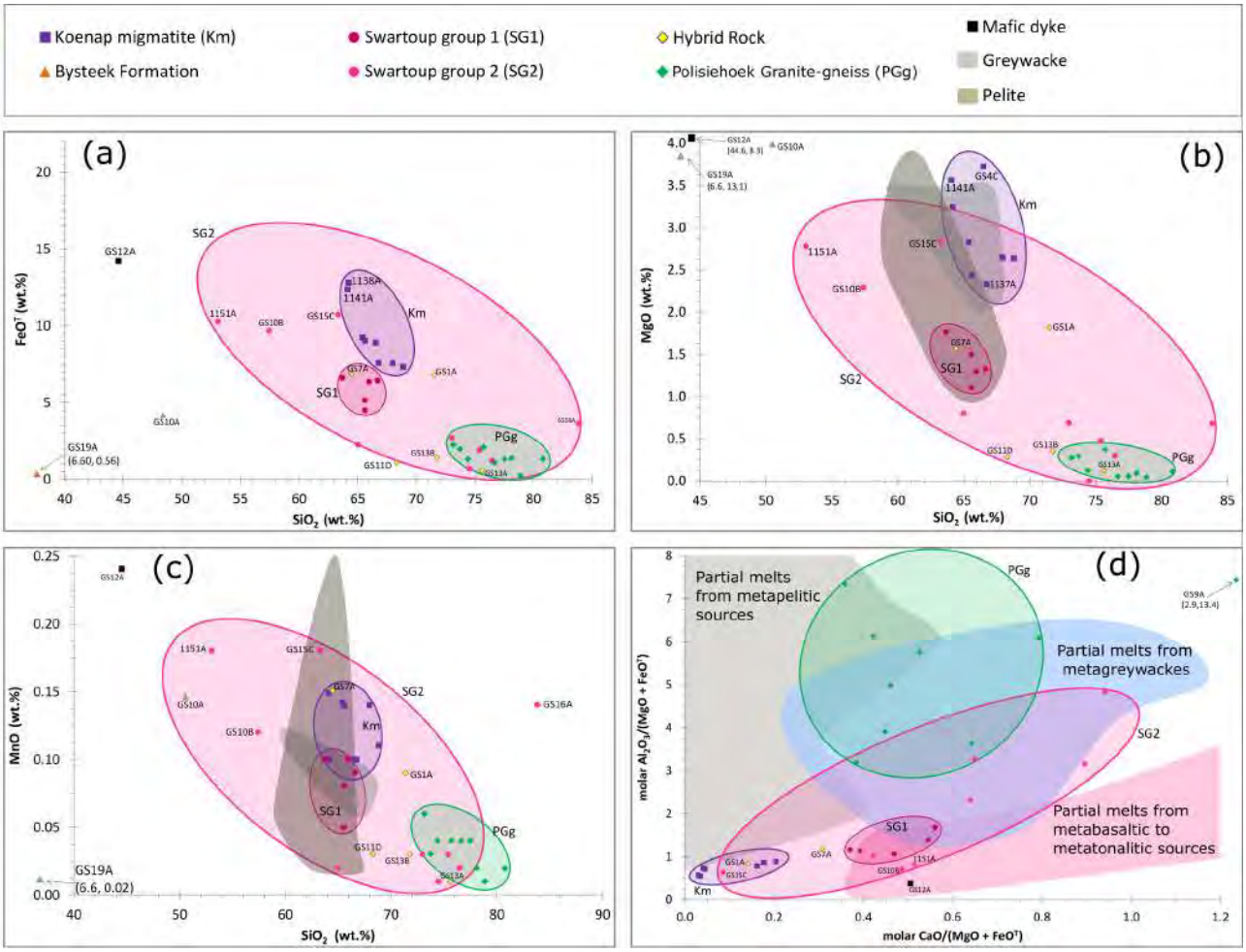

Figure 4.5: *Harker diagrams showing (a) FeO^T, (b) MgO and (c) MnO against SiO_2 (wt%). (d) Molar $Al_2O_3/(MgO + FeO^T)$ against molar $CaO/(MgO + FeO^T)$ (modified after Altherr et al., 2000), which suggests Swartoup group 1 samples are derived from partial melting of metagreywacke to metabasaltic/metatonalitic sources. Swartoup group 2 appear to be chiefly derived from both metagreywacke and metatonalitic/metabasaltic sources. The Polisiehoek Granite-gneisses appear to derive chiefly from a metagreywacke protolith, with some metapelitic component. Koenap migmatite are circled in blue, Swartoup group 1 in red, Swartoup group 2 in magenta and the Polisiehoek Granite-gneisses in green.*

Grt-bearing, also has 2.8 wt% MgO. The rest of Swartoup group 2 have lower MgO contents than the pelites, from 0–0.8 wt% MgO.

Two hybrid rocks, samples GS1A (1.8 wt% MgO) and GS7A (1.6 wt% MgO), have similar MgO contents as Swartoup group 1. Samples GS11D, GS13A and GS13B have lower MgO, comparable to the lower Swartoup group 2 cluster. These samples have between 0.1 and 0.4 wt% MgO.

The Polisiehoek Granite-gneisses have, on average, less MgO than Swartoup group 2, ranging between 0.05 and 0.37 wt% MgO. The mafic dyke, sample GS12A, has 8.3 wt% MgO, the highest of the sample set, consistent with the rock's high Opx mode (~60 vol%, Section 3.2.6).

MnO against SiO_2

The Koenap migmatites have 0.10–1.15 wt% MnO (Figure 4.5c). The high MnO contnets are probably due to high garnet modes (Table

The Bysteek calc-silicate specimen has a similar MnO content as the Koenap migmatites (0.14 wt% MnO), however the Bysteek marble shows one f the lowest MnO concentrations, at 0.01 wt% MnO.

Swartoup group 1 have somewhat lower MnO contents (0.05–0.10 wt% MnO) than the Koenap migmatites. They have overlap with both the published pelite and greywacke composition fields. Two Opx-bearing Swartoup group 2 rocks (samples 1151A and GS10B) and the two Grt-bearing analyses (samples GS15C and GS16A) have higher MnO contents (0.12–0.18 wt% MnO) than Swartoup group 1. The rest of the Swartoup group 2 specimens have lower MnO contents than the greywacke compositions, between 0.01 and 0.03 wt% MnO. The Swartoup group 2 analyses define a negative trend between MnO and SiO_2, except for sample GS16A, which lies off the trend, due to its high SiO_2 content.

The hybrid rocks show almost as much variation in MnO contents as Swartoup group 2. Sample GS7A has 0.15 wt% MnO and lies with the upper Swartoup group 2 analyses and the Koenap migmatites. Sample GS1A has slightly less MnO than the Koenap migmatites, with 0.09 wt% MnO, similar to Swartoup group 1. The rest of the hybrid rocks have between 0.01 and 0.03 wt% MnO, the same as the lower MnO content Swartoup group 2 rocks.

The Polisiehoek Granite-gneisses show a decrease in MnO with SiO_2 contents from 0.06 to 0.01 wt% MnO, mostly below the published greywacke composition field.

The mafic dyke sample has the highest MnO content of the sample set, 0.18 wt% MnO.

Molar $Al_2O_3/(MgO + FeO^T)$ against molar $CaO/(MgO + FeO^T)$

Figure 4.5d shows a molar $Al_2O_3/(MgO + FeO^T)$ against molar $CaO/(MgO + FeO^T)$ diagram. Altherr et al. (2000) produced the diagram from published compositions of experimentally produced partial melts formed by dehydration melting of various bulk compositions.

Figure 4.5d shows Swartoup group 1 between molar $Al_2O_3/(MgO + FeO^T)$ values of ∼1.1–1.4, and molar $CaO/(MgO + FeO^T)$ values of 0.37–0.56. Four Swartoup group 1 analyses show overlap with the field of partial melts from metabasaltic to metatonalitic sources. Two of these

analyses show overlap with the field of Partial melts from metagreywackes as well. One sample lies slightly away from the metabasaltic-metatonalitic partial melt field, at a slightly lower molar $CaO/(MgO + FeO^T)$ value. This diagram suggests that Swartoup group 1 were chiefly derived from a tonalitic source, possibly with some greywacke component.

Swartoup group 2 show molar $Al_2O_3/(MgO + FeO^T)$ ratios ranging mostly from 0.6–4.8 and their molar $CaO/(MgO + FeO^T)$ values range mostly between 0.09 and 0.90. Sample GS9A is an outlier, due to its lack of MgO, and so plots off the diagram with a molar $Al_2O_3/(MgO + FeO^T)$ value of 13.4 and a molar $CaO/(MgO + FeO^T)$ value of 2.9. However, three Swartoup group 2 analyses show overlap with the metagreywacke partial melt field, and three analyses show overlap with the metabasaltic–metatonalitic partial melt field. Three samples show no overlap with any field, likely due to molar $CaO/(MgO + FeO^T)$ variations. Figure 4.5d appears to show that Swartoup group 2 is derived from partial melts sourced from either a heterogeneous protolith comprising both greywacke and tonalitic components, or the Swartoup group 2 rocks were derived from multiple protoliths of greywacke and tonalitic/metabasaltic compositions.

The hybrid rock analyses show molar $Al_2O_3/(MgO + FeO^T)$ ratios between 0.8 and 12.1 and molar $CaO/(MgO + FeO^T)$ values from 0.14 to 6.57. Two analyses are shown on Figure 4.5d, samples GS1A and GS7A, which do not show overlap with any fields on the diagram. These two samples have moderate CaO contents, and two of the highest FeO^T and MgO contents of the hybrid rocks. The high molar ratios of the rest of the samples are likely due to high CaO and low FeO^T and MgO contents. These analyses plot within an extended field of Partial melts from metabasaltic—metatonalitic sources. The Polisiehoek Granite-gneiss analyses range between 3.2–7.3 molar $Al_2O_3/(MgO + FeO^T)$ and 0.36–0.79 molar $CaO/(MgO + FeO^T)$. Six analyses show overlap with the Partial melts from metagreywackes field, and three show overlap with the field of partial melts from metapelitic sources. These two fields do themselves show some overlap, and some samples plot in both fields. Figure 4.5d appears to indicate the Polisiehoek Granite-gneiss samples are derived from partial melts of metagreywacke sources, with at least some local metapelitic component.

The mafic dyke specimen shows 0.4 molar $Al_2O_3/(MgO + FeO^T)$ and 0.51 molar $CaO/(MgO + FeO^T)$. The analysis shows overlap with the field of partial melt from metabasaltic—metatonalitic sources. This is consistent with a mantle derived rock. However, the metabasalt did not result from partial melting of a basalt.

Koenap migmatite are shown for reference. They show 0.5–0.9 molar $Al_2O_3/(MgO + FeO^T)$ ratios and their molar $CaO/(MgO + FeO^T)$ are between 0.03 and 0.20. They show slightly

lower molar $Al_2O_3/(MgO + FeO^T)$ values than the metapelitic partial melt field.

The Bysteek Formation samples are not shown on Figure 4.5d due to their high molar $CaO/(MgO + FeO^T)$ contents, 4.33 for the Bysteek marble and 3.38 for the calc-silicate sample. The molar $Al_2O_3/(MgO + FeO^T)$ ratio of the Bysteek marble is less than 0.1 and that of the calc-silicate specimen is around 0.6. They would appear to lie somewhat below an extended field of partial melts from metabasaltic–metatonalitic sources. However, these are calcium-rich metasediments and are not partial melt derivatives.

Summary

The Koenap migmatites show overlap with the published pelite field in the CaO and MnO diagrams, and with the greywacke composition field in the K_2O and Fe_2O_3 diagrams. The Na_2O and MgO diagrams show the Koenap migmatites overlapping both the pelite and greywacke composition fields. However, in the P_2O_5 diagram, they contain less P_2O_5 than both sediment composition fields. The more melanocratic Koenap migmatites have lower CaO and higher Fe_2O_3 contents than the relatively more leucocratic Koenap migmatites. This agrees with the lower plagioclase and higher garnet and biotite modes of the melanosome as compared to the leucosome (Section 3.2.1).

The Bysteek Formation marble shows low SiO_2, K_2O, P_2O_5, Na_2O, Fe_2O_3 and MnO contents and high amounts of CaO and MgO. This is consistent with the rock's dominant calcite mode, with lesser clinopyroxene, and suggests some dolomitic component to the marble. The Bysteek calc-silicate sample has low K_2O, P_2O_5 and Na_2O contents similar to the marble, but it also has moderate amounts of SiO_2, Fe_2O_3 and MnO. The rock also has high CaO and MgO concentrations. This is typical of a calc-silicate dominated by clinopyroxene and garnet, with minor titanite SiO_2 (Section 3.2.2). Swartoup group 1 has higher K_2O, Na_2O and CaO than the Koenap migmatites. However, they also have lower Fe_2O_3, MgO and MnO contents than Koenap migmatite. Swartoup group 1 has higher P_2O_5 contents than Koenap migmatite and also the published pelite and greywacke compositions. This is a characteristic common to S-type granitoids (Chappell and White, 1992; Chappell, 1999), which agrees with the P_2O_5 versus Rb diagram (Figure 4.3a). In all these Harker diagrams published pelite and greywacke compositions appear geometrically between Swartoup group 1 and the Koenap migmatite compositions.

Swartoup group 2 show positive correlation with silica only in the K_2O Harker diagram, all others in this section (Na_2O, CaO, P_2O_5, Fe_2O_3, MgO and MnO) show negative correlation with silica. The low and decreasing P_2O_5 contents with increasing SiO_2 is a characteristic

often exhibited by I-type granitoids (Chappell and White, 1992; Chappell, 1999). This is only somewhat consistent with the trend displayed by Swartoup group 2 in the P_2O_5 versus Rb diagram (Figure 4.3a), which shows low P_2O_5, an I-type granitoid characteristic, and increasing P_2O_5 with increasing Rb, an S-type characteristic. Swartoup group 2 shows greater range in compositions above and below Swartoup group 1, in all the diagrams.

The hybrid rocks appear to follow the Swartoup group 2 analyses in all Harker diagrams. Samples GS1A and GS7A have oxide contents similar to either Swartoup group 1 or the Koenap migmatites, likely resulting in their comparable biotite and garnet modes (Section 3.2.4). Samples GS13A and GS13B always plot with the granitic Swartoup group 2 analyses. Sample GS11D usually has similar oxide contents to samples GS13A and GS13B, but at lower SiO_2, the exceptions being the K_2O and CaO diagrams. The K_2O diagram shows sample GS11D with a low K_2O content, which agrees with its low K-feldspar mode. However, samples GS13A and GS13B have higher K_2O contents, consistent with their higher K-feldspar modes (Section 3.2.4). The CaO diagram shows sample GS11D with a high amount of CaO, consistent with its high plagioclase mode, and samples GS13A and GS13B have much lower CaO.

The Polisiehoek Granite-gneisses show negative correlations between SiO_2 and K_2O, Na_2O, Fe_2O_3, MgO and MnO, and they have uniformly low CaO and P_2O_5 contents. Low P_2O_5 contents are a characteristic of I-type granitoids, though they often also exhibit negative correlation with SiO_2 (Chappell and White, 1992; Chappell, 1999). This agrees with the I-type affinity shown by the Polisiehoek Granite-gneiss analyses in P_2O_5 against Rb diagram (Figure 4.3a). The Polisiehoek Granite-gneisses have lower K_2O and greater Na_2O contents than the granitic Swartoup group 2 specimens. This may indicate a higher albite component in their alkali-feldspars, compared with those of Swartoup group 2.

The mafic dyke sample, GS12A, appears to show no relationship with any other rock type in these diagrams. Its low K_2O, high CaO, Fe_2O_3, MgO and MnO contents are consistent with the rocks low mode of K-bearing phases and high orthopyroxene and plagioclase modes (Section 3.2.6).

4.4.2 Plots against maficity

Stevens et al. (2007), Clemens et al. (2011), Clemens (2012) and Clemens and Stevens (2012) use diagrams of elemental and molar concentrations against maficity, molar Fe + Mg per 100 g of rock. The maficity of a rock is easier to relate to mineralogical and chemical influences on magma composition than traditional indices, such wt% SiO_2 (Clemens et al., 2011; Clemens,

2012). These diagrams are shown in Figure 4.6. Though these diagrams are not designed for metamorphic or sedimentary rocks, the Koenap migmatites, Bysteek Formation specimens and published pelite and greywacke compositions have been included for comparison. The spatial relationships between the different rock types shown in the Ti (Figure 4.6a) and Zr (Figure 4.6b) against Fe + Mg diagrams are similar.

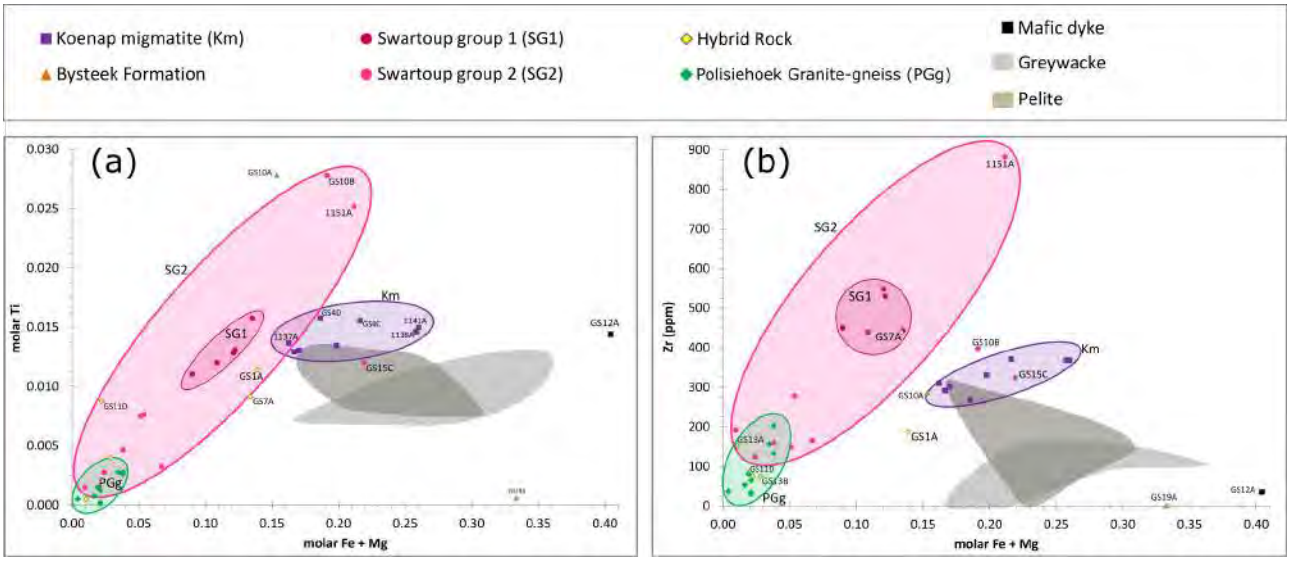

Figure 4.6: *Diagrams of (a) Molar Ti and (b) Zr (ppm) against molar Fe + Mg per 100 g of rock (maficity) (Clemens et al., 2011). Koenap migmatite are circled in blue, Swartoup group 1 in red, Swartoup group 2 in magenta and the Polisiehoek Granite-gneisses in green.*

Molar titanium against maficity

Figure 4.6a shows the Koenap migmatites with 0.17–0.26 mol Fe + Mg and 0.013–0.016 mol Ti. The Koenap migmatites show some overlap with the published pelite composition field (0.17–0.31 mol Fe + Mg). The more leucocratic specimens (samples 1137A, 1143A and GS4D), as well as sample 1143B (somewhat melanocratic, Section 3.2.1), plot at lower maficities around than the more melanocratic Koenap migmatites (samples 1138A and 1141A). The greywacke composition field (0.17–0.35 mol Fe + Mg) shows overlap with the higher maficity–lower Ti portion of the pelite field and does not appear compatible with any analyses of the sample set.

The Bysteek marble has a very low titanium content (0.0004 mol Ti) and has around 0.20 mol Fe + Mg. In contrast, the calc-silicate sample plots near the top of the diagram at 0.027 mol Ti and shows around 0.15 mol Fe + Mg. The higher maficity of the marble specimen relative to the calc-silicate sample is probably due to a strong dolomitic component of its calcite-dominated mineralogy (Section 3.2.2).

The Swartoup group 1 samples define a somewhat linear, positive trend between Ti and Fe + Mg. They have similar titanium contents (0.011–0.016 mol Ti) as the Koenap migmatite

specimens but show lower maficities (0.090–0.013 mol Fe + Mg). Most Swartoup group 2 rocks (samples GS9A, GS9B, 1149A, GS15B, GS5A and 1151A) lie on the same linear trend as the Swartoup group 1 analyses. Most of Swartoup group 2 show lower titanium and Fe + Mg contents than Swartoup group 1 and plot towards the bottom left of the diagram. However, two analyses, samples 1151A and GS10B, show higher contents, around 0.2 mol Fe + Mg and above 0.025 mol Ti. Sample GS15C is an outlier and plots below the trend shown by other Swartoup granitoid specimens. Sample GS15C is the only Swartoup granitoid analysis that plots within the pelite field.

The Polisiehoek Granite-gneiss samples plot in the bottom left of the diagram, at low titanium (below 0.0028 mol Ti) and Fe + Mg contents (0.004–0.038 mol Fe + Mg). They define a short, positive Ti–Fe + Mg trend. Two hybrid rocks, samples GS13A and GS13B show low titanium (0.0005–0.004 mol Ti) and maficities (0.011–0.028 mol Fe + Mg) values. However, sample GS11D has more titanium (0.008 mol Ti) and plots above this. Samples GS1A and GS7A show similar titanium contents as sample GS11D, but due to their Fe + Mg contents (∼0.135 mol Fe + Mg) they plot closer to, but not within, the pelite and greywacke fields.

The mafic dyke has the highest maficity (∼0.4 mol Fe + Mg) of the sample set, and a moderate titanium content (0.014 mol Ti). The sample also has the highest maficity of the sample set, ∼0.40 mol Fe + Mg. This is consistent with its abundance of iron- and magnesium-rich phases (Section 3.2.6).

Zirconium against maficity

The Koenap migmatites show a positive trend between Zr and molar Fe + Mg (Figure 4.6b). The more leucocratic specimens (samples 1137A, 1143A and GS4D), as well as sample 1143B (somewhat melanocratic, Section 3.2.1), plot at the bottom left of this trend at around 290 ppm Zr and 0.17 mol Fe + Mg. These specimens show overlap with the upper portion of the pelite composition field. The most melanocratic Koenap migmatites (samples 1138A and 1141A) plot at the top right of the previously mentioned trend, around 0.26 mol Fe + Mg and 370 ppm Zr. The rest of the Koenap migmatites have higher Zr contents than the pelites. However, all the Koenap migmatite samples have maficities compatible with the pelite field. The greywacke field shows overlap with the lower zirconium content portion of the pelite field.

The Bysteek marble has very little zirconium (around 1 ppm Zr). In contrast, the Bysteek calc-silicate specimen has much more zirconium, about 290 ppm Zr.

Swartoup group 1 specimens have higher zirconium contents (440–530 ppm Zr) than the Koenap migmatites (290–370 ppm Zr). The majority of Swartoup group 2 show low zirconium contents, from around 120 to 280 ppm Zr. Samples GS10B and GS15C (∼320–400 ppm Zr) have similar zirconium concentrations to the Koenap migmatites. Sample 1151A has a similar Fe + Mg content as sample GS15C, but with much more zirconium, 880 ppm Zr. These specimens, with the rest of Swartoup group 2, define a positive zirconium–maficity trend. Swartoup group 1 is compatible with this trend. None of the Swartoup granitoid specimens plot within the greywacke or pelite fields.

The hybrid rocks show a similar range of values as Swartoup group 2. Three specimens plot at low zirconium and Fe + Mg contents and two others plot at higher zirconium and Fe + Mg amounts. Samples GS11D, GS13A and GS13B lie near the lower Fe + Mg Swartoup group 2 rocks, from 75–150 ppm Zr and 0.01–0.03 mol Fe + Mg. Sample GS1A has a similar zirconium content (190 ppm Zr) to sample GS13A but is nearer the Bysteek calc-silicate and Koenap migmatites with respect to Fe + Mg (0.14 mol Fe + Mg). Sample GS7A has more zirconium (440 ppm Zr) and plots with Swartoup group 1.

The Polisiehoek Granite-gneiss samples have low zirconium contents, below ∼200 ppm Zr. These rocks show overlap with some of the Swartoup group 2 rocks and also some of the hybrid rocks. The Polisiehoek Granite-gneiss samples define a positive zirconium–maficity trend. The mafic dyke specimen has one of the lowest zirconium contents of the samples, at around 30 ppm Zr.

Summary and interpretation

Here a summary of key features of the previous data is presented, with potential interpretations based on the maficity diagrams, field observations and petrography. First presented are the Koenap migmatites, then the Swartoup Pluton rocks are discussed. The Swartoup granitoids and Koenap migmatites are discussed together in relation to each other, and afterwards the Bysteek Formation and Swartoup granitoids are elaborated on, as there are relatively few samples. The hybrid rocks are discussed after the Bysteek Formation, then the Polisiehoek Granite-gneiss and the mafic dyke are discussed.

Koenap migmatites

In the Ti and Zr versus maficity diagrams (Figure 4.6), the more melanocratic Koenap migmatites, samples 1138A, 1141A, 1147B and GS4C, plot at higher maficities than the more leucocratic ones, samples 1137A, 1143A and GS4D (Section 3.2.1). The more leucocratic samples also have

lower zirconium amounts and their titanium concentrations are somewhat lower as well. These define a positive correlation trend of zirconium and Fe + Mg and perhaps a somewhat-positive trend with titanium and Fe + Mg. Sample 1143B plots at the lower maficity end of the Koenap migmatite trends, even though the rock appears melanocratic. It has one of the highest biotite and lowest quartz modes of the Koenap migmatites (Table 3.1, Section 3.2.1). The rest of the melanocratic Koenap migmatites have, on average, more quartz, garnet and biotite, so have higher maficities. In contrast, the more leucocratic ones have relatively more K-feldspar and plagioclase, and so they have lower maficities.

Swartoup granitoids

As stated earlier, the maficity diagrams are designed to form linear arrays originating at the origin (e.g. Clemens et al., 2011). Plots of Zr (ppm) against Fe + Mg (mol) usually form less well-defined linear trends than those of Ti (mol) against Fe + Mg (mol) (Clemens et al., 2011; Clemens, 2012). This is evident when comparing the Ti diagram, where most igneous samples appear to lie along a single, well defined linear trend, to the Zr diagram, where both Swartoup groups 1 and 2 form clusters defining a wide-ranging linear trend. These trends are referred to here as the Swartoup granitoid trends.

Swartoup group 1 plots at maficities intermediate between the majority of Swartoup group 2 (low maficity, typical Swartoup granites) and the Koenap migmatites (discussed below).

Swartoup group 2 are somewhat more variable in both zirconium and titanium contents than Swartoup group 1. Samples 1149A, GS5A, GS9A, GS9B and GS15B (Swartoup group 2) plot in the bottom left of both maficity diagrams. Sample 1151A plots beyond Swartoup group 1 in both diagrams, as does sample GS10B but only in the Ti diagram. Samples GS10B and GS15C plot nearer the pelite fields in the Zr diagram and sample GS15C plots within that in the Ti one. These higher titanium contents may indicate that samples 1151A and Swartoup group 1 share a common source with the majority of Swartoup group 2 (typical Swartoup granites), but are more evolved than them. The outliers of this trend, samples GS10B, GS15C and GS16A are discussed below.

Bysteek Formation, Swartoup Pluton and Koenap migmatite

The Bysteek marble (sample GS19A) has almost the same maficity as sample GS10B, and very little titanium and zirconium. Sample GS10B lies at higher titanium contents and lower zirconium and maficities than the Swartoup granitoid trend. This specimen was collected

from a dyke of Swartoup orthopyroxene-bearing monzodiorite, less than 10 m away from the Bysteek calc-silicate, sample GS10A. The Bysteek calc-silicate sample shows Ti, Zr and Fe + Mg characteristics as sample GS10B, regarding its position relative to the Swartoup granitoid trend in Figures 4.6a and 4.6b. These two rocks plot on the same side, either above or below, of the previously discussed trend in each diagram.

The Swartoup orthopyroxene-bearing monzodiorite may be genetically related to the Bysteek Formation, though there are few geochemical data supporting this. Field evidence supporting this is the proximal association of Bysteek Formation, particularly calc-silicates, to the orthopyroxene-bearing granitoids (Section 3.1.3). Sample GS10B may have a different source compared to the rest of Swartoup group 2. Or, it may share the same or a geochemically similar source rock to the rest of Swartoup group 2, but was contaminated by Bysteek wall-rock material prior to its emplacement. The orthopyroxene-bearing monzodiorite (sample GS10B) and the Bysteek marble (sample GS19A) do share similar maficities. However, it is the Bysteek calc-silicate sample which has zirconium and titanium contents more like those of sample GS10B. The titanium content of sample GS10B is higher than that of the calc-silicate, however.

As previously mentioned, Swartoup group 1 specimens plot between the typical Swartoup granites (Swartoup group 2), the Koenap migmatites and the Bysteek Formation specimens. Swartoup group 1 has a similar titanium content as the Koenap migmatites. We may consider Swartoup group 1 as a less evolved, more mafic version of Swartoup group 2. However, we could also consider the two Bysteek Formation specimens in the data set. These have comparable maficities as the Koenap migmatites, but the calc-silicate has much more titanium. It could be possible that a mixture between Bysteek marble and calc-silicate could contaminate typical Swartoup granitic magma sufficiently to bring both the titanium content and the maficity of the package above that of Swartoup group 2 to where they are in Figure 4.6a. In addition, Bysteek marble units are found throughout the Swartoup Pluton, especially near the hinge of the antiform, where the Swartoup granodiorites (Swartoup group 1) were collected (Figure 3.6). However, the Zr diagram does not support this, as both Bysteek specimens have lower zirconium contents than the Swartoup group 1 samples. Although, it may also be possible that the two Bysteek specimens in the sample set have unusually low zirconium contents.

Hybrid rocks

Sample GS7A is representative of one of the typical varieties of hybrid rock encountered in the field. This garnet-rich sample was collected near blue-grey coloured Bysteek marble and a

Swartoup granitoid dome (Section 3.1.4). In the Zr diagram, sample GS7A lies with Swartoup group 1, the Swartoup granodiorites. However, in the Ti diagram, the hybrid rock specimen lies somewhat between Swartoup group 1 and the Bysteek marble. This garnet-rich variety of hybrid rock may be the result of a mixture between Bysteek marble and Swartoup granodiorite, i.e. Swartoup group 1-like material, if it is assumed the blue-grey Bysteek marble is analogous to the white Bysteek marble specimen. It should be remembered, however, only one specimen of this variety of hybrid rock has been collected.

Sample GS11D is a pyroxene-rich hybrid rock representative of the other typical variety of hybrid rock encountered in the field. This variety of hybrid rock is always found in contact with Bysteek calc-silicate and facing Swartoup granitoids (Section 3.1.4). This particular specimen was collected along strike from locality GS10 (Sections 3.1.3 and 3.1.4), where the Bysteek calc-silicate sample GS10A was collected. Sample GS11D was collected in contact with Bysteek calc-silicate, and the calc-silicate portion of the rock contains stringers of Hybrid material within the calc-silicate (Figure 3.26c, Section 3.2.4). Sample GS11D, like sample GS10A, plots above the Swartoup granitoid trend in the Ti diagram. Sample GS11D may have formed after hybridisation of Bysteek calc-silicate by granitic Swartoup magma, which would otherwise have solidified to a typical Swartoup group 2 granite composition. Alternatively, sample GS11D may simply be the result of anatexis of Bysteek calc-silicate, as early stage, eutectic compositions should plot nearer the origins of these types of diagrams. It should be remembered only one specimen of this variety of hybrid rock has been collected.

Compared to the Ti diagram, the Zr diagram shows sample GS1A further away from Swartoup group 2 and the rest of the hybrid rocks, nearer Koenap migmatite and the published pelite compositional field. In the Ti diagram, sample GS1A plots below the previously discussed Swartoup granitoid trend, as do the Koenap migmatites, Bysteek marble sample and the pelite field. The rock also has a similar maficity to some Swartoup group 1 specimens. Considering these geochemical spatial relationships and the spatial associations of the hybrid rock and these other rock types in the field (Figure 3.1, Section 3.3), there may be a genetic link between sample GS1A and Swartoup group 1, Koenap migmatite, Bysteek marble or pelite. Sample GS1A was collected form a large pool of hybrid rock which hosts large xenoliths of Bysteek metabasite (Section 3.1.4). Though this pool is in contact with Bysteek Formation rocks, Koenap migmatite surrounds the locality at a greater distance and a Swartoup granitoid is also situated nearby (Section 3.1.4). Sample GS1A may be a hybrid between Swartoup group 1-like material (Swartoup granodiorite) and either Koenap migmatite or Bysteek marble. The Koenap and Bysteek Formations are intercalated, both part of the Arribees Group. A localised

pocket of marble may have mixed with intruding Swartoup melt, forming the hybrid rock pod and leaving the competent metabasite rafts intact. It should be noted that only one outcrop of this variety of hybrid rock was found.

Samples GS13A and GS13B were collected from a layer of hybrid rock in contact with Bysteek marble units (Section 3.1.4). This hybrid rock variety has relatively high K-feldspar and plagioclase modes (Table 3.5, Section 3.2.4). Sample GS13A contains coarse K-feldspar and sample GS13B has a relatively high K-feldspar mode. Both specimens lack the clinopyroxene content of the pyroxene-rich variety like sample GS11D. These specimens (samples GS13A and GS13B) lie near the origins of both Figures 4.6a and 4.6b. This is due to their relatively high feldspar modes, and comparatively low mafic contents. They may represent a hybrid between Swartoup group 2 granites and Bysteek Formation marble. Or, perhaps they were more similar to sample GS11D, and have undergone metasomatism after intrusion of relatively K-feldspar-rich Polisiehoek magma, which crops out nearby (Section 3.1.4).

Polisiehoek Granite-gneisses

These analyses all lie near the origins of the maficity diagrams and show relatively less variation as compared to Swartoup group 2. With regard to these two diagrams, the Polisiehoek Granite-gneisses could be considered the late stage, more evolved result of anatexis of the Koenap migmatites. They could have been early stage unevolved, low-temparature melts. However, such melts are usually small in volume, and the Polisiehoek Granite-gneiss is laterally extensive (Section 1.2). Also, field observations show Polisiehoek magma intruded after intrusion of the Swartoup Pluton (Section 3.1.5).

Mafic dyke

This single, basaltic specimen lies at a relatively high maficity, as would be expected. The titanium content is like that of the Koenap migmatites and Swartoup group 1. However, considering field observations there is likely no genetic link between this rock and the Koenap migmatites or the Swartoup Pluton. The mafic dyke most likely post-dates intrusion of the Polisiehoek Granite-gneiss, which, in turn post-dates intrusion of the Swartoup Pluton (Sections 3.1.6, 4.6).

4.4.3 Chondrite normalised rare-earth diagrams

Figure 4.7 shows rare-earth diagrams of the various rock types, normalised to CI carbonaceous chondrite of McDonough and Sun (1995). Figure 4.7a shows Koenap migmatite and the

Swartoup group 1 and 2 analyses are shown separately on Figures 4.7b and 4.7c, and together on 4.7d. The hybrid rocks are shown in Figure 4.7e along with the Bysteek Formation and mafic dyke analyses, as there are relatively few data. Figure 4.7f shows the Polisiehoek Granite-gneiss specimens. Table 4.7 shows the $[La/Yb]_N$, Eu/Eu*, $[La/Sm]_N$ and $[Gd/Yb]_N$ ratios as well as the La and Yb concentrations relative to chondritic values.

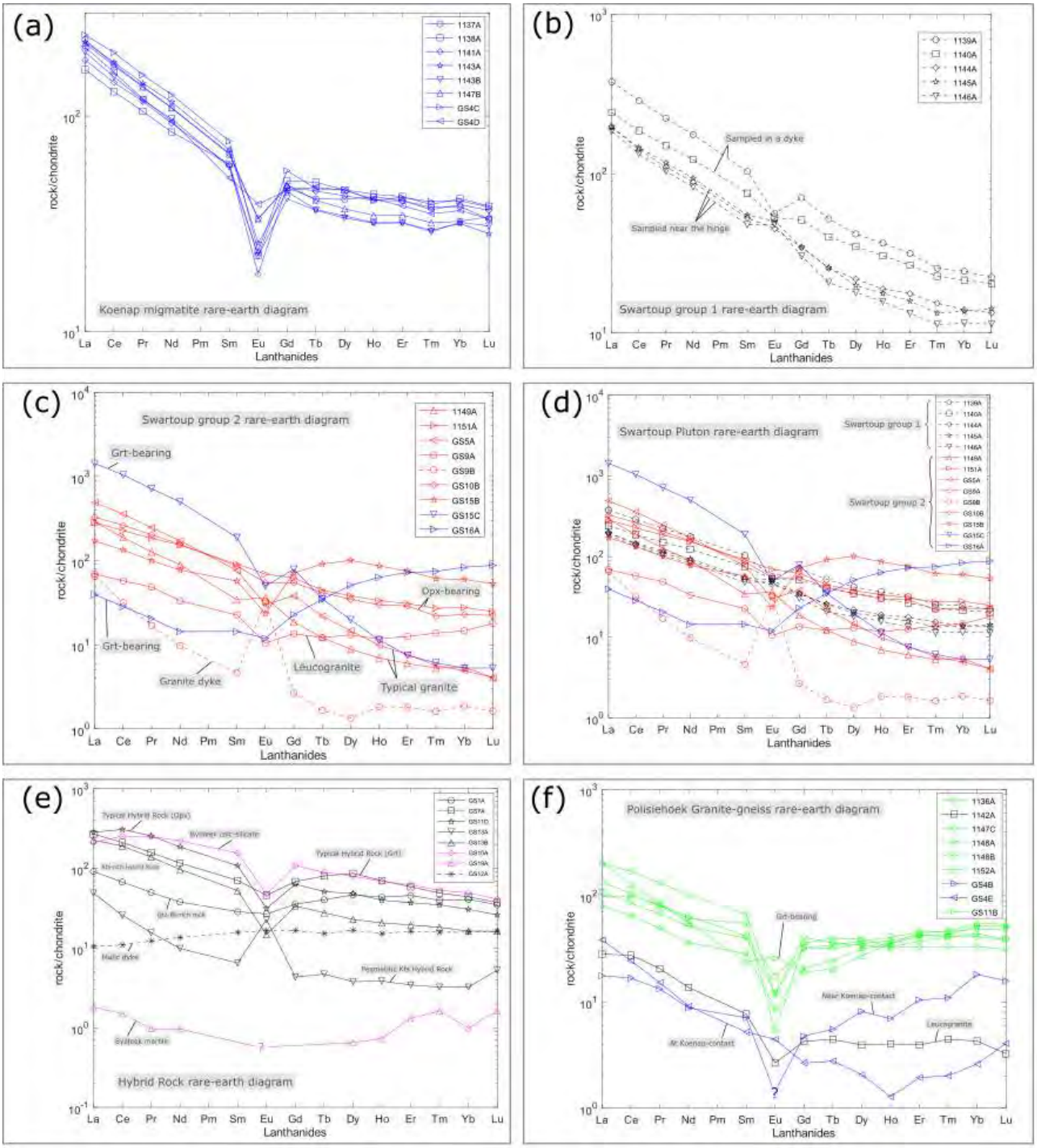

Figure 4.7: *Chondrite normalised rare-earth diagrams are shown for (a) Koenap migmatite, (b) Swartoup group 1, (c) Swartoup group 2, (d) all Swartoup granitoid (Swartoup groups 1 and 2), (e) the Bysteek Formation, hybrid rock and mafic dyke specimens and (f) shows the Polisiehoek Granite-gneiss rare-earth diagram.*

Table 4.7: *Shown are the $[La/Yb]_N$ ratios of the rock types as well as their Eu*/Eu ratios. Eu*/Eu is defined as $[(0.5 \times (Sm + Gd))/Eu]_N$. Samples GS19A (Bysteek marble specimen) and GS4B (Polisiehoek Granite-gneiss) contain no detectable Eu. Normalisation is done against CI carbonaceous chondrite of McDonough and Sun (1995).*

Rock unit	$[La/Yb]_N$	Eu*/Eu	$[La/Sm]_N$	$[Gd/Yb]_N$	La conc.	Yb conc.
Koenap migmatite	4.2–7.5	1.2–2.9	2.7–4.0	1.2–1.5	164–237	31.7–41.4
Swartoup group 1	11.0–16.0	0.8–1.5	3.2–3.9	2.4–2.9	196–377	13.7–24.4
Swartoup group 2	0.5–240.0	0.7–2.7	2.7–14.2	0.3–15.0	65.4–1430	1.86–59.8
Hybrid rock	2.3–15.0	0.2–2.9	2.6–7.6	0.9–2.0	49.0–284	3.23–43.9
Polisiehoek Granite-gneiss	1.0–14.7	0.8–8.5	1.8–8.6	0.3–1.2	17.7–205	2.6–55.5

Concentration ranges given relative to chondritic values (and not ppm).
Eu*/Eu > 1 corresponds to a positive Eu anomaly, while Eu*/Eu < 1 is a negative Eu anomaly.

Summary

A summary of the geometric relationships of these data are presented with some interpretations based on this data, field observations (Section 3.1) and sample petrography (Section 3.2). The Swartoup granitoids are compared to the Koenap migmatites as well as the Bysteek Formation and hybrid rocks in the Discussion Chapter. Rock profiles can be evaluated in terms of mineralogical controls, based on petrographic evidence and REE profiles of relevant minerals. This will be done in the Discussion Chapter.

The Koenap migmatites (Figure 4.7a) show strong negative europium anomalies and are more enriched in light rare-earth elements than they are heavy rare-earth elements.

Swartoup group 1 show uniform trends across the lanthanides (Figure 4.7b). Most show weak, positive europium anomalies.

Swartoup group 2 show multiple REE-profile patterns (Figure 4.7c) that are largely distinct from those of Swartoup group 1. The REE-profiles of samples 1149A, GS5A (typical Swartoup granites) and GS15C (garnet-bearing granite) appear similar to each other. Those of the orthopyroxene-bearing monzodiorites (samples 1151A and GS10B) show very similar REE-profiles and rock/chondrite ratios. Samples GS9A and GS9B, which were collected from the same dyke, show similar lanthanum contents but their REE profiles are different to each other. That of the leucogranite (sample GS9A) shows moderate overall REE depletion ($[La/Yb]_N = 5.0$). However, the REE-profile of sample GS9B shows marked REE depletion ($[La/Yb]_N = 40.4$) with a large positive europium anomaly (Eu*/Eu = 0.1).

The two Bysteek Formation calc-silicate specimens (Figure 4.7e) show two distinct REE-profiles. The calc-silicate, sample GS10A, shows REE enrichment up to praseodymium and depletion thereafter. The Bysteek marble, sample GS19A, has a relatively flat REE-profile with near-

chondritic abundances, though many elements are missing from the diagram as their concentrations were below detection limits.

The hybrid rock specimens (Figure 4.7e) show considerable variation in their REE abundances and profile shapes but remain below the Bysteek calc-silicate in terms of REE abundances, on average. Samples GS11D and GS13B, both pyroxene-bearing granodiorites, show similar REE-profiles to calc-silicate sample GS10A. Sample GS7A also shows an REE-profile somewhat similar to samples GS10A, GS11D and GS13B, with similar La/Yb ratios but different europium anomalies.

Most of the Polisiehoek Granite-gneiss specimens show LREE depletion, a strong negative europium anomaly and a somewhat flat or slight enrichment in, the HREE profile (Figure 4.7f).

The mafic dyke specimen (Figure 4.7e) is enriched in REEs relative to the chondrite standard, and the profile is relatively flat at about ten times chondritic values. Such a flat profile is consistent with mantle-derived rock if it has not experienced any later alteration or melting events. The sample has not been considered further in this regard, as field evidence and U/Pb Concordia ages suggest the dyke post-dates the Polisiehoek Granite-gneiss (Sections 3.1.6, 4.6).

4.5 Isotope diagrams

Figures 4.8a (Sm/Nd) and 4.8b (Rb/Sr) show the results of isotope analyses (Tables 4.8 and 4.9) done at the University of Cape Town's Department of Geological Sciences, Rondebosch, South Africa. Analytical procedures are shown in Section 2.3.3.

4.5.1 Sm/Nd isotope diagram

Figure 4.8a shows $^{143}Nd/^{144}Nd$ against $^{147}Sm/^{144}Nd$. Regression lines are included in the diagram, where applicable. These lines are interpreted as mixing lines, and not necessarily isochrons.

The Koenap migmatites form a cluster (samples 1137A, 1143B and 1147B) near $^{143}Nd/^{144}Nd = 0.511962$ and $^{147}Sm/^{144}Nd = 0.116$, sample 1138A lies away from this, at $^{143}Nd/^{144}Nd = 0.512061$ and $^{147}Sm/^{144}Nd = 0.138$. The Bysteek marble has a $^{143}Nd/^{144}Nd$ ratio of 0.512197, higher than the Koenap migmatites and the marble has no detectable samarium ($^{147}Sm/^{144}Nd = 0.000$).

Samples 1145A and 1146A (Swartoup group 1) lie almost on top of each other in Figure 4.8a

Table 4.8: *Whole-rock Sm-Nd isotope data for Koenap migmatites, the Bysteek marble, Swartoup Pluton, hybrid rocks, Polisiehoek Granite-gneiss and the mafic dyke specimen.*

Rock type	Sample	Nd (ppm)	Sm (ppm)	$^{143}Nd/^{144}Nd$	$^{147}Sm/^{144}Nd$	2σ	ϵ_{Nd} at 1134 Ma
Koenap migmatite	1137A	49.82	9.96	0.51972	12	0.120421	−1.93
	1138A	38.56	8.86	0.512061	14	0.138331	−2.79
	1143B	44.33	8.57	0.511962	17	0.116448	−1.53
	1147B	49.76	9.84	0.511940	15	0.119040	−2.35
Bysteek marble	GS19A	0.44	0.00	0.512197	23	0.000000	20.03
Swartoup group 1	1145A	40.08	5.05	0.512007	10	0.113953	−0.23
	1146A	70.04	13.45	0.512010	11	0.113034	−0.10
Swartoup group 2	1149A	80.40	15.29	0.511792	9	0.074471	1.24
	1151A	56.20	11.17	0.512032	14	0.115617	−0.05
	GS5A	40.42	7.81	0.511807	28	0.114535	−4.29
	GS9A	42.86	8.11	0.511758	202	0.119071	−6.00
	GS9B	37.72	7.08	0.511831	22	0.116371	−4.09
	GS10B	40.08	5.04	0.512171	13	0.113970	2.91
	GS15B	70.40	13.45	0.511731	21	0.113042	−5.55
	GS15C	17.33	4.22	0.512219	15	0.074404	9.60
	GS16A	53.42	1.45	0.512492	19	0.115673	8.94
Hybrid Rock	GS1A	85.05	15.98	0.512182	15	0.146669	−1.63
	GS7A	4.52	0.96	0.512052	17	0.117821	0.02
	GS11D	44.45	7.77	0.512017	15	0.127922	−1.07
	GS13A	29.44	6.16	0.512071	15	0.127922	−1.07
	GS13B	6.25	1.14	0.512015	17	0.105283	1.12
Polisiehoek Granite-gneiss	1136A	16.54	4.20	0.512101	11	0.12026	−0.22
	1142A	25.40	3.52	0.511993	16	0.109945	0.01
	1148A	27.81	8.15	0.512239	16	0.152994	−1.45
	1152A	6.22	2.33	0.511851	23	0.083362	1.11
	GS11B	40.80	5.05	0.512405	12	0.176524	2.87
Mafic dyke	GS12A	70.04	13.45	0.513000	13	0.225670	2.87

and are near the analyses of samples GS11D and 1151A. Swartoup group 1 lie near $^{143}Nd/^{144}Nd$ = 0.114and $^{147}Sm/^{144}Nd$ = 0.512010, at somewhat higher $^{143}Nd/^{144}Nd$ ratios than the main Koenap migmatite cluster. Swartoup group 2 show extensive variation in their $^{143}Nd/^{144}Nd$ ratios. As a result, their regression line has a negative gradient. Samples GS5A, GS9A, GS9B and GS15B lie at lower $^{143}Nd/^{144}Nd$ (0.511731–0.511831) but similar $^{147}Sm/^{144}Nd$ (0.113–0.116) ratios as the main Koenap migmatite cluster. Sample 1149A lies at a similar $^{143}Nd/^{144}Nd$ (0.511792), but lower $^{147}Sm/^{144}Nd$ ratio (0.074) as the previously described Swartoup group 2 cluster. Sample GS15C lies at the same $^{147}Sm/^{144}Nd$ ratio (0.074), but a much higher $^{143}Nd/^{144}Nd$ ratio (0.512219), as sample 1149A. Sample GS10B ($^{143}Nd/^{144}Nd$ = 0.512171, $^{147}Sm/^{144}Nd$ = 0.114) lies between samples GS16A ($^{143}Nd/^{144}Nd$ = 0.512492, $^{147}Sm/^{144}Nd$ = 0.116) and 1151A ($^{143}Nd/^{144}Nd$ = 0.512032, $^{147}Sm/^{144}Nd$ = 0.116).

The hybrid rocks lie above the Koenap migmatites. Their linear trend goes from sample GS13B

Table 4.9: *Whole-rock Rb-Sr isotope data for Koenap migmatites, the Bysteek marble, Swartoup Pluton, hybrid rocks, Polisiehoek Granite-gneiss and the mafic dyke specimen.*

Rock type	Sample	Rb (ppm)	Sr (ppm)	$^{87}Rb/^{86}Sr$	$^{87}Sr/^{86}Sr$	2σ	$^{87}Sr/^{86}Sr$ at 1134 Ma
Koenap migmatite	1137A	74.26	135.17	1.5490	0.74403	15	0.71889
	1138A	41.85	37.84	3.1183	0.76847	20	0.71785
	1143B	56.24	68.20	2.3248	0.75723	9	0.71949
	1147B	146.06	66.64	6.1801	0.82536	11	0.72504
Bysteek marble	GS19A	0.62	271.90	0.0064	0.70660	10	0.70649
Swartoup group 1	1145A	88.39	263.75	0.94488	0.72345	13	0.70811
	1146A	157.46	248.65	1.78549	0.73661	15	0.70763
Swartoup group 2	1149A	124.146	146.64	2.38946	0.74727	14	0.70848
	1151A	55.51	339.36	0.46119	0.71459	13	0.70710
	GS5A	132.86	179.35	2.08863	0.76766	13	0.73375
	GS9A	151.43	191.88	2.22510	0.74523	12	0.70911
	GS9B	96.16	220.44	1.22991	0.73342	13	0.71345
	GS10B	88.39	263.75	0.94488	0.71245	13	0.69711
	GS15B	157.46	248.64	1.78553	0.78548	11	0.75649
	GS15C	124.28	146.64	2.38955	0.85903	14	0.82024
	GS16A	55.51	339.36	0.46119	0.73472	13	0.72723
Hybrid Rock	GS1A	94.15	100.05	2.6532	0.75988	10	0.71681
	GS7A	137.55	150.65	2.57430	0.75649	10	0.71470
	GS11D	204.65	175.20	3.29341	0.75712	11	0.70366
	GS13A	236.70	291.05	2.2927	0.74540	11	0.70818
	GS13B	304.60	323.40	2.65557	0.74952	10	0.70641
Polisiehoek Granite-gneiss	1136A	131.18	81.31	4.54857	0.80462	14	0.73079
	1142A	51.06	34.53	4.16980	0.78507	24	0.71738
	1148A	216.99	30.71	19.92455	1.08293	41	0.75949
	1152A	171.20	65.15	7.40874	0.85279	25	0.73252
	GS11B	423.20	31.75	0.42646	0.71262	11	0.70569
Mafic dyke	GS12A	12.89	85.22	0.42646	0.71262	11	0.70569

at $^{143}Nd/^{144}Nd = 0.512015$ and $^{147}Sm/^{144}Nd = 0.105$ to sample GS1A at $^{143}Nd/^{144}Nd = 0.512182$ and $^{147}Sm/^{144}Nd = 0.147$.

The Polisiehoek Granite-gneisses show slightly less variation in their $^{143}Nd/^{144}Nd$ ratios than Swartoup group 2, however their range of $^{147}Sm/^{144}Nd$ ratios is somewhat wider.

The mafic dyke has the highest $^{143}Nd/^{144}Nd$ (0.513000) and $^{147}Sm/^{144}Nd$ (0.225) ratios of the sample set.

4.5.2 Rb/Sr isotope diagram

Figure 4.8b shows $^{87}Sr/^{86}Sr$ against $^{87}Rb/^{86}Sr$. Regression lines are included in the diagram, where applicable. These lines are mixing lines, and not isochrons.

The Koenap migmatites (samples 1137A, 1138A, 1143B and 1147B) lie very close to their

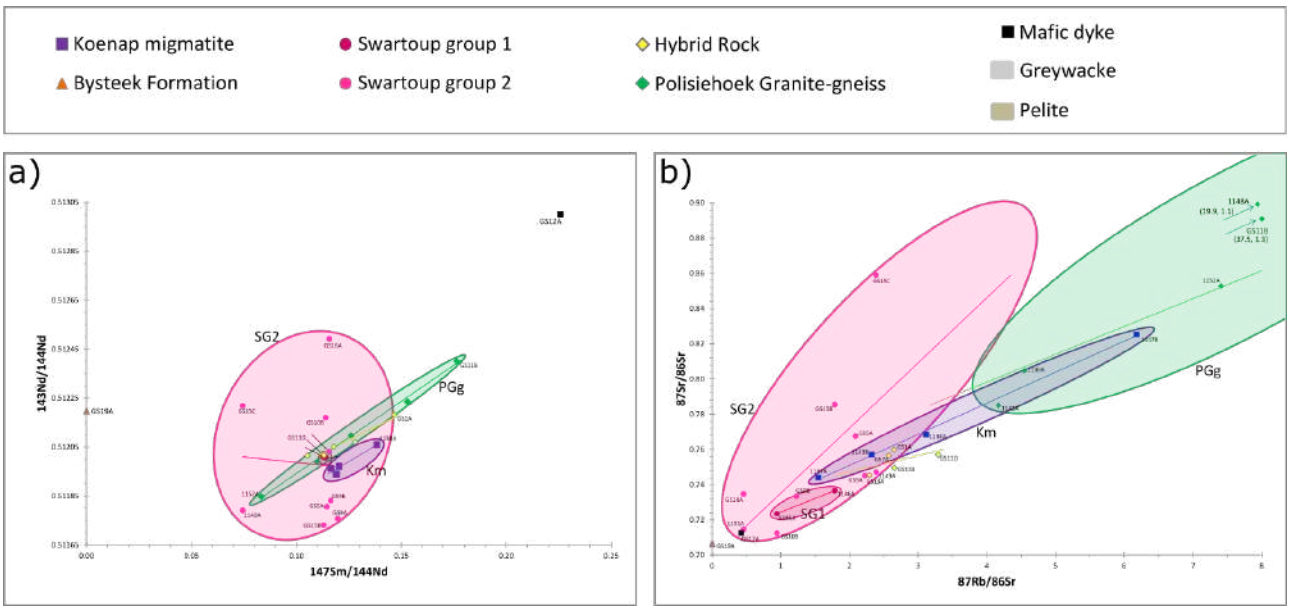

Figure 4.8: *(a) Sm/Nd diagram. The plotted lines are regression lines. The samples define mixing lines and not isochrons. The Koenap migmatites form a main cluster (samples 1137A, 1143B and 1147B) and sample 1138A lies at higher $^{143}Nd/^{144}Nd$ and $^{147}Sm/^{144}Nd$ ratios. The Bysteek marble has no detectable samarium but it has a higher $^{143}Nd/^{144}Nd$ than the Koenap migmatites. The Swartoup group 1 specimens, samples 1145A and 1146A, lie together st slightly higher $^{143}Nd/^{144}Nd$ and lower $^{147}Sm/^{144}Nd$ ratios than the main Koenap migmatite cluster. Swartoup group 2 varies mostly along the $^{143}Nd/^{144}Nd$ axis, form well-below to well-above the Koenap migmatites, at similar or lower $^{147}Sm/^{144}Nd$ ratios as the main Koenap migmatite cluster. The hybrid rocks lie above the Koenap migmatite trend, near sample 1151A (Swartoup group 2) and extending to higher $^{143}Nd/^{144}Nd$ and $^{147}Sm/^{144}Nd$ ratios. The Polisiehoek Granite-gneisses define a trend which lies near that of the hybrid rocks, though it is slightly steeper and has greater lateral extent. The mafic dyke specimen has the highest $^{143}Nd/^{144}Nd$ and $^{147}Sm/^{144}Nd$ ratios of the sample set.*
(b) Rb/Sr isotope diagram. The plotted lines are regression lines. The samples define mixing lines and not isochrons. The Koenap migmatites lie somewhat in the middle of the sample set. The Bysteek marble and mafic dyke specimens lie at the lowest $^{87}Rb/^{86}Sr$ and $^{87}Sr/^{86}Sr$ ratios. Swartoup group 1 rocks, samples 1145A and 1146A, lie below the Koenap migmatites, as do the hybrid rocks. Samples GS1A and GS7A (hybrid rocks) lie closer to the Koenap migmatites than the rest of the hybrid rocks (samples GS11D, GS13A and GS13B). In contrast, the Swartoup group 2 regression line lies above that of the Koenap migmatites. However, Swartoup group 2 varies above and below their regression line. Samples 1149A, GS5A, GS9A and GS9B all lie nearer the Koenap migmatites. Samples GS15B, GS15C and GS16A lie above the Swartoup group 2 line, and samples 1151A and GS10B lie nearer it's base. The Polisiehoek granite-gneisses vary over large $^{87}Rb/^{86}Sr$ and $^{87}Sr/^{86}Sr$ ratios, though samples 1136A, 1142A and 1152A lie much nearer the rest of the sample set than samples 1148B and GS11B do.

regression line in Figure 4.8b, ranging from sample 1137A at $^{87}Rb/^{86}Sr = 1.5$ and $^{87}Sr/^{86}Sr = 0.744$ up to sample 1147B at $^{87}Rb/^{86}Sr = 6.2$ and $^{87}Sr/^{86}Sr = 0.825$. The Bysteek marble has the lowest $^{87}Rb/^{86}Sr$ (0.0, to 1 decimal place) and $^{87}Sr/^{86}Sr$ (0.707) ratios of the sample set.

Only two Swartoup group 1 specimens have been isotopically analysed. Samples 1145A and 1146A lie at lower $^{87}Sr/^{86}Sr$ and $^{87}Sr/^{86}Sr$ ratios than the Koenap migmatites. Sample 1145A lies at 0.9 $^{87}Rb/^{86}Sr$ and 0.723 $^{87}Sr/^{86}Sr$ and sample 1146A is at 1.8 $^{87}Rb/^{86}Sr$ and 0.737 $^{87}Sr/^{86}Sr$. Swartoup group 2 is much more variable, though they mostly lie above the Koenap migmatites. Sample 1151A ($0.5 < ^{87}Rb/^{86}Sr$, $0.715 < ^{87}Sr/^{86}Sr$) lies at the base of the regression line of all Swartoup group 2 specimens. Samples GS15B, GS15C and GS16A lie at either higher $^{87}Sr/^{86}Sr$ or lower $^{87}Rb/^{86}Sr$ ratios than the Swartoup group 2 regression line. In contrast, samples GS5A and GS9A lie at slightly lower $^{87}Sr/^{86}Sr$ or higher $^{87}Rb/^{86}Sr$ ratios than this line and samples 1149A and GS9A do so to a greater extent, lying opposite the Koenap migmatite trend line. Sample GS10B plots at a similar $^{87}Sr/^{86}Sr$ ratio (0.712) as sample 1151A, but at higher $^{87}Rb/^{86}Sr$ (0.9).

The hybrid rocks all lie below the Koenap migmatites, and sample GS13A lies near samples 1149A and GS9A (Swartoup group 2). Samples GS11D, GS13A and GS13B appear to form a linear trend from 2.3–3.3 $^{87}Rb/^{86}Sr$ and 0.745–7.57 $^{87}Sr/^{86}Sr$. The hybrid rock regression line sits above this and samples GS1A and GS7A lie above (around 2.6 $^{87}Rb/^{86}Sr$ and 0.758 $^{87}Sr/^{86}Sr$), slightly below the Koenap migmatites.

The Polisiehoek Granite-gneisses show the most variation of the sample set. Sample 1142A (4.2 $^{87}Rb/^{86}Sr$ and 0.785 $^{87}Sr/^{86}Sr$) lies below the Polisiehoek Granite-gneiss regression line and samples 1136A and 1152A lie reasonably near it. However, samples 1148A (19.9 $^{87}Rb/^{86}Sr$ and 1.1 $^{87}Sr/^{86}Sr$) and GS11B (37.5 $^{87}Rb/^{86}Sr$ and 1.3 $^{87}Sr/^{86}Sr$) lie far outside the range of values shown by the rest of the sample set.

The mafic dyke specimen lies near sample 1151A, at relatively lower $^{87}Rb/^{86}Sr$ (0.5) and $^{87}Sr/^{86}Sr$ (0.713) ratios.

4.5.3 Summary and interpretation

Here we discuss and interpret the Rb/Sr and Sm/Nd isotope data with reference to field observations and sample petrography (Chapter 3).

Rb/Sr and Sm/Nd diagrams

The Koenap migmatites lie reasonably close to their Rb/Sr regression line (Figure 4.8b) and less so to their Sm/Nd one (Figure 4.8a). These regression lines do not define isochrons in either diagram. Their variations are most likely to have been caused by mobility of Rb and Sr in fluids during hydrothermal alteration or weathering (e.g., Waight, 2013). Alternatively, these variations may reflect an inhomogeneous initial isotopic composition of the pelitic Koenap protolith.

The Bysteek marble (sample GS19A) has very little rubidium (0.62 ppm) and no detectable samarium (Table 4.8). The rock then has the lowest $^{87}Rb/^{86}Sr$, $^{87}Sr/^{86}Sr$ and $^{147}Sm/^{144}Nd$ ratios of the sample set. The low rubidium content may be expected as the marble shows very few K-bearing phases; comprising calcite, clinopyroxene and minor chlorite and opaque minerals (Section 3.2.2). Note the Bysteek calc-silicate, sample GS10A, was not isotopically analysed.

The two Swartoup group 1 specimens (samples 1145A and 1446A) appear to produce a trend line of comparable gradient to the Koenap migmatites, suggesting they share similar ages. However, two data points cannot be used to define a line, and in the Sm/Nd diagram the samples lie very close to each other, defining a very short, negative trend. This would not be expected in an Sm/Nd diagram and is most likely an indication of protolith heterogeneity.

Swartoup group 2 is much more variable than Swartoup group 1. In Figure 4.8b, samples 1151A, 1149A and GS9A appear to define a somewhat linear trend almost concordant with the line previously mentioned between the two Swartoup group 1 specimens. This may suggest these Swartoup groups 1 and 2 specimens are derivatives of the same homogenous protolith and share similar ages. However, they may also share a common, homogeneous protolith, and received contamination from different sources. This fits with the observation that sample GS9B lies at slightly lower $^{87}Rb/^{86}Sr$ and higher $^{87}Sr/^{86}Sr$ ratios than these five Swartoup granitoids' trend, on average. Field evidence suggests samples GS9A and GS9B may be cogenetic, as sample GS9B was collected from a granite dyke hosting pods of leucogranite (sample GS9A, Section 3.2.3). Then, sample GS9B would have been contaminated by some material (such as calcium-rich Bysteek rock), raising its $^{87}Sr/^{86}Sr$ and lowering its $^{87}Rb/^{86}Sr$ ratios, relative to the rest of these Swartoup group 2 rocks. The Swartoup group 1 samples should then have been contaminated by some other material, lowering its $^{87}Sr/^{86}Sr$ and raising its $^{87}Rb/^{86}Sr$ ratios. In contrast, though no linear relationship between samples 1151A, 1149A and GS9A is seen in Figure 4.8a. Swartoup group 2 vary greater with respect to $^{143}Nd/^{144}Nd$ than $^{147}Sm/^{144}Nd$. This suggests the Swartoup Pluton was fed from (i) multiple sources, or (ii) a heterogenous

source-rock that did not homogenise prior to anatexis.

Samples 1151A, GS10B and GS16A lie at lower $^{87}Sr/^{86}Sr$ ratios than the rest of Swartoup group 2 and Swartoup group 1 (Figure 4.8b). These three rocks plot near the mafic dyke and Bysteek marble, suggesting there may be some genetic relationship between them and the Swartoup granitoids. Figure 4.8a, in contrast, shows samples 1151A, GS10B and GS16A lying at almost the same $^{147}Sm/^{144}Nd$ ratios as the Koenap migmatites, therefore no such relationship concerning the mafic dyke specimen is seen in the Sm/Nd diagram. Relationships concerning the Swartoup Pluton can be dismissed as far the mafic dyke is concerned, as field evidence and U/Pb Concordia ages suggest the dyke post-dates the Polisiehoek Granite-gneiss (Sections 3.1.6, 4.6).

Samples GS15B, GS15C and GS16A are more radiogenic than the Swartoup group 2 regression line (Figure 4.8b). This may indicate they share a different protolith to the rest of Swartoup group 2 or they experienced a different degree of contamination. Note that, in Figure 4.8b, samples 1149A, GS5A and GS15B form a linear trend sub-perpendicular to the regression lines of the sample set. It may be that these specimens, a granite, granodiorite and quartz monzonite, represent varying degrees of contamination. Or perhaps they are three progressively older rocks, with sample 1149A the youngest and sample GS15B the oldest. In contrast, though no linear relationship between samples GS15B, GS15C and GS16A is seen in Figure 4.8a. A line connecting samples GS15C and GS16A would be almost parallel to the rest of the regression lines of the sample set. However, two samples only cannot define a line. Also, sample GS15B lies at the lowest $^{143}Nd/^{144}Nd$ ratio and its $^{147}Sm/^{144}Nd$ ratio is comparable to the Koenap migmatites. This again suggests contamination of Swartoup material or mixing of multiple sources.

Three hybrid rocks, samples GS11D, GS13A and GS13B, define a somewhat linear trend in Figure 4.8b. This trend is almost concordant with the previously discussed trend of Swartoup group 1 and samples 1149A, 1151A and GS9A (Swartoup group 2). This may suggest these eight rocks share very similar protolith and are of similar ages. Samples GS1A and GS7A lie closer to the Koenap migmatites, possibly suggesting these two samples are older than the other three hybrid rocks. However, given the proximity of samples GS1A and GS7A to Koenap and Bysteek Formation rocks (Section 3.1.4), it is more likely that this indicates contamination of Hybrid melt by either Koenap or Bysteek Formation. Alternatively, these two hybrid rocks may have been formed by hybridisation of calc-silicate with Swartoup granitoid more akin to sample GS5A. In contrast, samples GS1A and GS7A lie with the rest of the hybrid rocks in

Figure 4.8a, defining a somewhat linear trend which includes Swartoup group 1 (samples 1145A and 1146A) and sample 1151A from Swartoup group 2. This supports samples GS1A and GS7A having undergone mixing or contamination, as they appear not to be temporally separated in Figure 4.9a.

The Polisiehoek Granite-gneisses lie above and below their regression line in Figure 4.8b but are reasonably close to theirs in Figure 4.8a. These diagrams suggest that the Polisiehoek Granite-gneiss formed from a heterogenous source rock. However, they may also have been subjected to contamination by hydrothermal fluids mobilising Rb and Sr (or meteoric fluids, during weathering). Their regression line is shallower than those of the Koenap Formation and Swartoup group 2. If this is taken as an indication of their isochron(s), this would suggest the Polisiehoek granite-gneisses are younger than the Koenap Formation and Swartoup group 2, on average. This is supported by field evidence (Section 3.1.5) and U/Pb zircon ages (Section 4.6). However, the Sm/Nd diagram shows a different pattern. Here, the Polisiehoek Granite-gneiss' regression line is slightly steeper, suggesting the reverse scenario. However, it should be stated again, that these regression lines are not isochrons.

The mafic dyke specimen has the second lowest $^{87}Sr/^{86}Sr$ and $^{87}Rb/^{86}Sr$ ratios. As there is only one data point, no inferences can be made regarding the dykes age. However, we could consider the material as a contaminant to the Swartoup Pluton. This would lower the $^{87}Sr/^{86}Sr$ and $^{87}Rb/^{86}Sr$ ratios, compared to the Koenap migmatites. However, field relationships do not support this (Section 3.1.6).

4.6 U/Pb zircon ages

This data (Tables A.8 and A.8, Appendix A.4) was provided by Professor Dirk Frei, University of the Western Cape. The analyses were done on samples collected during previous field work in the same study area, and the analytical procedures are as in Bial et al. (2015a)(Section 2.4).

Figure 4.9 shows two Wetherill Concordia diagrams. Sample J37A is a Koenap migmatite and shows two concordia ages of 1235.0 ± 5.2 Ma and 1232.6 ± 5.1 Ma (Figure 4.9a). Sample 980 shows a concordia age of 1229.0 ± 8.9 Ma and is believed to be a Swartoup granitoid (Figure 4.9b).

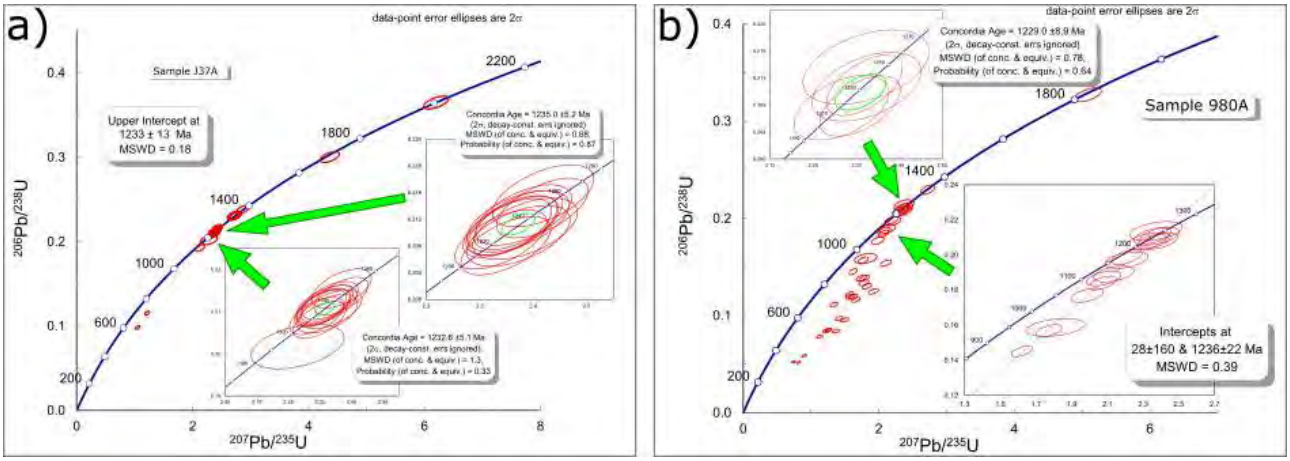

Figure 4.9: *Wetherill Concordia diagrams of samples (a) J37A and (b) 980A. Data and analyses provided by Prof Dirk Frei (University of the Western Cape).*

CHAPTER 5

Discussion

5.1 Summary of characteristics

5.1.1 Koenap migmatite

Petrography

Koenap Formation migmatite are mostly granulite facies granofelses, with some samples showing gneissic fabric. The rocks show variation in their leucosome-melanosome proportions as well as the degree to which these have segregated (Section 3.2.1). The rocks generally comprise quartz, K-feldspar, plagioclase, garnet, cordierite, biotite and opaque minerals (Section 3.2.1). Leucosomes contain somewhat higher K-feldspar and plagioclase proportions than the melanosomes, which contains somewhat higher proportions of garnet, biotite and opaque minerals as well as relatively larger garnet porphyroblasts (Section 3.2.1).

Geochemistry

The Koenap migmatites are generally magnesian, calcic and peraluminous (Figure 4.2). These rocks appear somewhat compatible with a (meta-)pelitic protolith, likely with some greywacke components (e.g., TAS diagram, Figure 4.1a; R_1R_2 diagram, Figure 4.1b; Aluminium Saturation Index, Figure 4.2c; CaO versus SiO_2, Figure 4.4c; molar $Al_2O_3/(MgO + FeO^T)$ against molar $CaO/(MgO + FeO^T)$, Figure 4.5d; and Ti-, Zr versus molar Fe + Mg, Figures 4.6a,b).

5.1.2 Swartoup Pluton

Petrography

Swartoup group 1 comprise typical Swartoup granodiorite (Section 3.2.3). These granodiorites are somewhat compositionally and geochemically homogeneous and are distinct from Swartoup group 2. The granodiorite (Swartoup group 1) is pervasively magmatically layered with K-feldspar-plagioclase-rich leucocratic layers and melanocratic layers with higher biotite modes. Swartoup group 2 is comprised of all other Swartoup granitoids, including typical Swartoup granites, orthopyroxene-bearing monzodiorite, orthopyroxene-bearing monzonite, garnet-bearing granite and leucogranite (Section 3.2.3). These rocks usually comprise the same mineralogy as Swartoup group 1, but with somewhat lower biotite modes (Table 3.3). Swartoup group 2 show weak though pervasive magmatic layering (Section 3.2.3).

Existence of hybrid facies (calc-silicate contamination by Bysteek Formation)

These feldspar-rich granodioritic rocks contain prominent subhedral to euhedral garnet/pyroxene and titanite. They are always in contact with Bysteek Formation rocks and within ~ 10 m of Swartoup granitoid outcrop (e.g. Figure 3.2, Section 3.1). Typical occurrences of hybrid rock are shown in Figure 3.12, Section 3.1.4. The rock are often exposed as thin layers in contact with Bysteek calc-silicate rocks, facing towards the nearest Swartoup granitoid. Elsewhere, the rock appears as veins intruding competent Bysteek mafic calc-silicate (Figure 3.12a) and also as folded veins (Figure 3.5d) intruding Bysteek mafic calc-silicate.

One exception to the typical hybrid rock occurrence is the biotite-rich variety of hybrid rock. This is crops out as a large pod that is surrounded by Bysteek mafic calc-silicate, and the pod also hosts a Bysteek mafic calc-silicate xenolith (Figure 3.12d).

The field evidence suggests these thin hybrid rocks formed by contamination of (possibly granodioritic) Swartoup Pluton material with its wall-rock, that is, the calc-silicates of the Bysteek Formation. The presence of folded hybrid rock veins within Bysteek mafic calc-silicate rock suggests the Bysteek rocks must have been hot and ductile for some time after crystallisation of the hybrid rocks. This is consistent with long-lasting high-heat flows typical of a continental back-arc setting (see Section 1.2.1) as proposed for the NMC by Bial et al. (2015a,b, 2016).

Geochemistry

Swartoup group 1 are mostly ferroan, calc-alkalic granodiorites. They show a clear S-type trend in the P_2O_5 versus Rb diagram (Figure 4.3a). However, S-type trends are shown in the Ce and Y versus Rb diagrams (Figures 4.3b,c) if the Koenap migmatite specimens are considered to be the Swartoup protolith rather than the literature metasediments. The $(Na_2O + K_2O)/CaO$ (Figure 4.4a) and FeO^T/MgO (Figure 4.4b) versus Zr + Nb + Ce + Y diagrams are consistent with Swartoup group 1 as having an S-type affinity, though with somewhat elevated Zr + Nb + Ce + Y contents, likely due to high apatite or monazite contents.

Swartoup group 2 vary from monzodiorite to granite, due to variations in SiO_2 content. They also all vary from ferroan to magnesian and alkalic to calcic geochemistries. The Swartoup group 2 rocks show an I-type trend in the P_2O_5-Rb diagram, in contrast to Swartoup group 1. Both I- and S-type trends are shown in the Y-Rb diagram by Swartoup group 2.

The Swartoup group 2 granites are most representative of the Swartoup Pluton. Swartoup group 1 granodiorite is overrepresented in the data set due to sampling bias, which targeted fresh material. Orthopyroxene- and garnet-bearing granitoids are anomalous, found only in a few localities within the study area. Swartoup group 2 comprises rocks that show (i) S- and (ii) I-type affinity rock as well as (iii) small volumes of highly fractionated S-type material (see Section 5.3.1).

5.1.3 Polisiehoek Granite-gneiss

Petrography

Most Polisiehoek Granite-gneiss specimens are sheared biotite-K-feldspar-plagioclase-quartz gneisses or quartz-K-feldspar gneisses (Figure 3.28, Section 3.2.5). They show strong tectonic foliation, defined by leucosome and melanosome layers, quartz and K-feldspar lenses, and elongated biotite lenses. Leucosomes have higher feldspar modes than melanosomes, which have higher quartz, biotite and garnet modes. These layers share gradational boundaries.

Geochemistry

All Polisiehoek Granite-gneiss specimens are ferroan. However, they vary from alkali-calcic to calcic and peraluminous to peralkaline (Figure 4.2). The Polisiehoek Granite-gneiss shows I-type trends in P_2O_5, Ce and Y against Rb diagrams (Figure 4.3a,b,c) and S-type trends in

the Y against Rb and La against SiO_2 diagrams (Figure 4.3c,d). The Polisiehoek Granite-gneiss analyses comprise highly fractionated I- and S-type granites (Section 4.1.3).

5.2 Age and isotopic evidence for origin of Swartoup Pluton

5.2.1 Zircon ages

The Koenap migmatites show two concordia ages of 1235.0 ± 5.2 Ma and 1232.6 ± 5.1 Ma (Figure 4.9a). These ages are somewhat younger than those given by the 1.3 and 1.35 Ga Kenhardt Formation (Pettersson et al., 2007), also a part of the Kakamas Domain, but preceding the associated putonic and gneissic rocks included in this study.

Detrital zircon cores from the Kenhardt Formation (Kakamas Domain) have pre-tectonic ages of 1.3 and 1.35 Ga (Pettersson et al., 2007). These are believed to show that the Kenhardt Formation is an early, syn-tectonic sedimentary unit (Pettersson et al., 2007). The data here show that the Koenap Formation (∼ 1230 Ma, also part of the Kakamas Domain) post-date the Kenhardt Formation somewhat, but are still consistent with the timing of the Namaquan Orogeny as a whole (∼ 1.3–1.0 Ga, Chapter 1).

U/Pb zircon analyses from the Swartoup Pluton show a Concordia age of 1229.0 ± 8.9 Ma (*pers. comm.,* D. Frei, 2018). This new age is consistent with, and within imprecision of, an early magmatic component of the 1110–1210 Ga age range found by Pettersson et al. (2009). Their study involved ion-probe zircon dating of plutonic rocks of the Kakamas Domain and found slightly younger ages, overall, than the data presented in this study.

The Polisiehoek Granite-gneiss shares lit-par-lit, transitional intrusive contacts with Koenap migmatite (Sections 3.1.5, 3.2.5). Contacts between the Polisiehoek Granite-gneiss and Swartoup Pluton are extensively weathered and eroded mylonite zones (Section 3.1.5). However, veins of Polisiehoek material have sharp, linear contacts with Swartoup monzodiorite and also host xenolithic fragments of the monzodiorite (Section 3.1.5). As such, the Polisiehoek Granite-gneiss must post-date formation of Koenap migmatite and intrusion of the Swartoup Pluton.

U/Pb zircon analyses yield a Concordia age of 1134 ± 4 Ma for the Polisiehoek Granite-gneiss (*pers. comm.,* D. Frei, 2018). This is consistent with field evidence, which shows clear cross-cutting relationships between the older Koenap migmatite (1235.0 ± 5.2 Ma and 1232.6 ± 5.1 Ma) and Polisiehoek Granite-gneiss (Section 3.1.5). This means that the Swartoup Pluton

would represent one of the earliest magmatic phases of this area, preceding the Polisiehoek event.

It is worth noting Pettersson et al. (2009) gave a somewhat anomalously old 2244 Ma TDM age for the Polisiehoek Granite-gneiss and a T_{CHUR} age of 1420 Ma. Pettersson et al. (2009) note the true crustal residence age of the Polisiehoek Granite-gneiss sample relies on the mantle source, due to the high Sm/Nd ratio (0.1683) of their sample. Pettersson et al. (2009) suggest that the Kakamas Domain crust was extracted from a single depleted-mantle-like source between 1.6 and 1.2 Ga, with Palaeoproterozoic crustal components, as suggested by their Polisiehoek Granite-gneiss analysis, and then melted to form 1.2–1.1 Ga magmatic granitoids.

5.2.2 Isotopic relationships

Figure 5.1 shows ϵ_{Nd} plotted against $^{87}Sr/^{86}Sr$, at time, t = 1230 Ma.

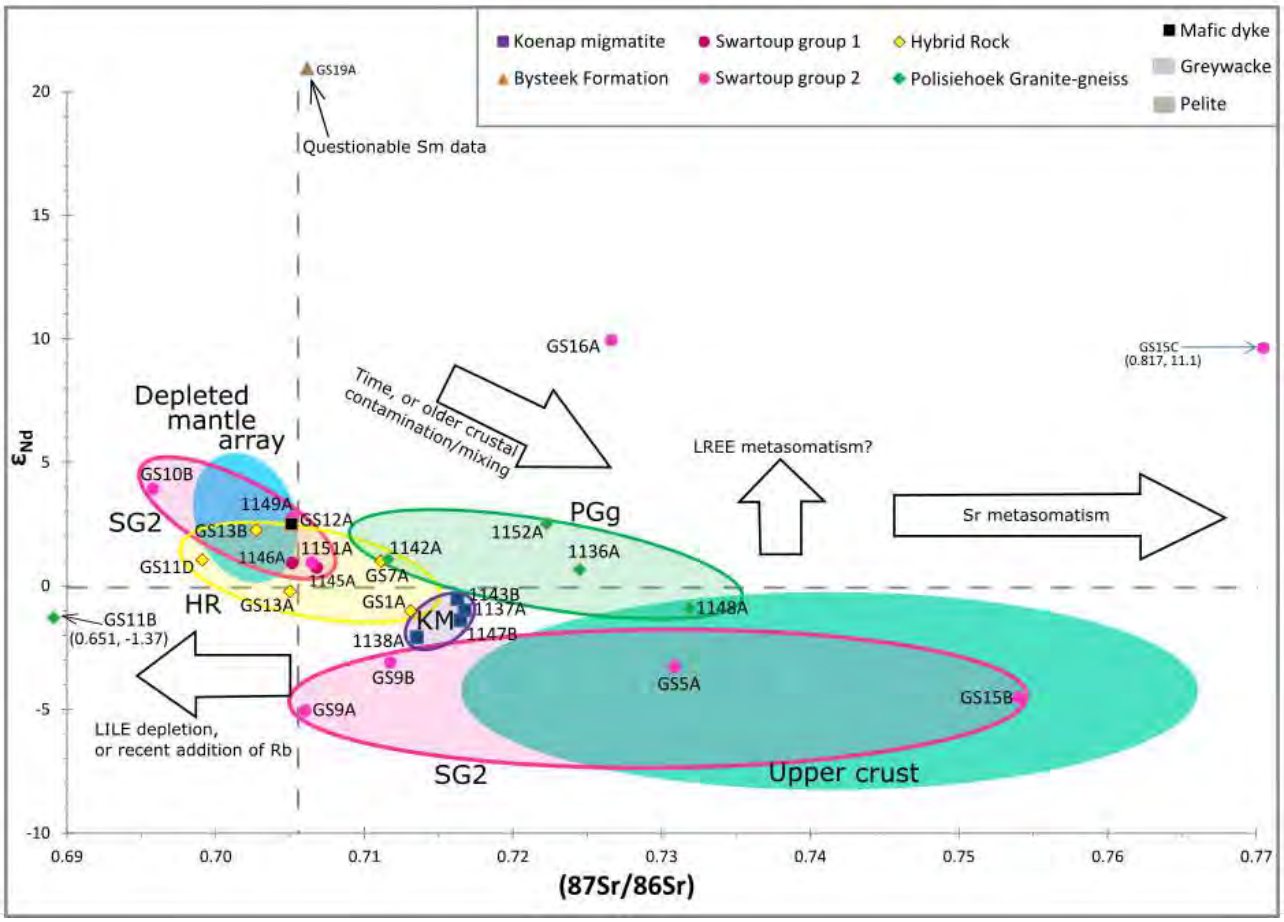

Figure 5.1: *ϵ_{Nd} plotted against $^{87}Sr/^{86}Sr$, at time, t = 1230 Ma, for the Swartoup Pluton, Koenap migmatite, hybrid rock, Polisiehoek Granite-gneiss and mafic dyke. The Bysteek marble, sample GS19A, has a very high ϵ_{Nd} value of 20, caused by its low samarium content.*

Koenap migmatites and Bysteek marble

The Koenap migmatites lie at typical upper crustal compositions, consistent with them being metasedimentary rocks (Figure 5.1). The Koenap migmatites appear to be relatively homogeneous as they cluster well. In contrast, the Bysteek marble lies far above all other rocks in the sample set, at $\epsilon_{Nd} = 20$. This is most likely an artefact of the mathematics of ϵ_{Nd}, as the marble has no detectable samarium, so division by a very small number has caused ϵ_{Nd} to be large.

Swartoup granitoids

Samples 1145A and 1146A (Swartoup group 1) have isotopic compositions between bulk earth and those of the Koenap migmatites. Swartoup group 2 are much more variable. However, samples 1149A and 1151A also lie between bulk earth and the Koenap migmatite compositions, forming a cluster with the Swartoup group 1 rocks (sample 1145A and 1146A). In contrast, sample GS10B has a lower $^{87}Sr/^{86}Sr$ ratio than depleted mantle and a similar ϵ_{Nd} value. This is consistent with samples GS5A and GS15B (Swartoup group 2) resulting from anatexis of Koenap migmatite and they may be considered end-members of the Swartoup Pluton. The Swartoup granitoids which lie closer to bulk earth must then have mixed with, or been contaminated by, components which lie near isotopic bulk earth or in the depleted mantle array. Samples GS9A and GS9B have lower ϵ_{Nd} values than the Koenap migmatites but have $^{87}Sr/^{86}Sr$ ratios somewhat between those of the Koenap migmatites and the previously mentioned Swartoup granitoid cluster. This suggests they are older than the Swartoup granitoids that plot nearer bulk earth compositions. However, they may also have resulted from mixing or contamination of Koenap derived material with lower crustal rocks, which are expected to have lower ϵ_{Nd} values than bulk earth and lower $^{87}Sr/^{86}Sr$ ratios than upper crustal rocks.

Samples GS10B, GS15C and GS16A have higher ϵ_{Nd} values than the rest of the rocks, except for the Bysteek marble specimen. Sample GS10B plots near the depleted mantle field. Though this rock may have been contaminated by mantle components, it is more plausible that this rock experienced depletion of LILEs, such as by fluid loss, lowering its $^{87}Sr/^{86}Sr$ ratio. Samples GS15C and GS16A lie at relatively high ϵ_{Nd} values, caused by high $^{143}Nd/^{144}Nd$ ratios, possibly due to metasomatism. Sample GS15C also has a high $^{87}Sr/^{86}Sr$ ratio, possibly due to Sr-metasomatism. However, their high ϵ_{Nd} values may also have been caused by contamination with a low samarium-rock, such as the Bysteek marble, sample GS19A. However, these two Swartoup granites are garnet-bearing and are proximally associated with Koenap migmatite in

the field (Section 3.1.3).

Hybrid rocks, Bysteek rocks and Swartoup granitoids

The Bysteek marble lies at $^{87}Sr/^{86}Sr = 0.706$ and the pyroxene-rich hybrid rock, sample GS11D, lies at $^{87}Sr/^{86}Sr = 0.704$. This hybrid rock was collected in contact with GS10A-like calc-silicate rock that contains stringer veins of hybrid rock (Sections 3.1.4, 3.2.4). Though the Bysteek calc-silicate (sample GS10A) was not isotopically analysed, it may have an $^{87}Sr/^{86}Sr$ ratio between those of the marble and calc-silicate rock. In any case, as sample GS11D was in contact with Bysteek calc-silicate and lies at the lowest $^{87}Sr/^{86}Sr$ ratio of the hybrid rocks, it can be considered a hybrid rock end-member. The rest of the hybrid rock specimens lie at somewhat higher ϵ_{Nd} values than the Koenap migmatites, but are between sample GS11D and the Koenap migmatites with respect to their $^{87}Sr/^{86}Sr$ ratios. Their similar ϵ_{Nd} values provide strong evidence for the hybrid rocks having been formed by *in situ* anatexis of Bysteek calc-silicate. An influx of felsic material, carrying LILEs (especially, potassium and rubidium), may then increase the $^{87}Sr/^{86}Sr$ ratios of the hybrid rocks. Such felsic material is likely to be Swartoup granitoid (Section 3.1.3). Also, note that sample GS7A, the garnet-rich hybrid rock, has the same ϵ_{Nd} value as the pyroxene-rich hybrid rock, sample GS11D. In contrast, sample GS1A has the lowest ϵ_{Nd} and highest $^{87}Sr/^{86}Sr$ values of the hybrid rocks, plotting near the Koenap migmatites. This suggests that sample GS7A, with its high garnet mode, has little association with the Koenap migmatites, unlike sample GS1A which may have the greatest Koenap component of the hybrid rocks. However, this data set has few samples and more specimens are needed to confirm such relationships.

Polisiehoek Granite-gneisses

The Polisiehoek Granite-gneisses show a wide range of $^{87}Sr/^{86}Sr$ ratios (Figure 5.1), though a narrower range than that of Swartoup group 2. They generally have higher ϵ_{Nd} values than the rest of the rocks. Sample GS11B has a particularly low $^{87}Sr/^{86}Sr$ ratio (0.651), and $\epsilon_{Nd} = -1.37$. This is probably caused by exsolution of fluids, leading to loss of LILEs. Sample GS11B was collected from a dyke intruding a Swartoup monzodiorite dome (Section 3.1.5). This dome is along strike from the dyke where sample GS10B was collected from. In Figure 4.8b, samples GS10B and GS11B have the two lowest $^{87}Sr/^{86}Sr$ ratios. An alternative explanation for the low $^{87}Sr/^{86}Sr$ ratio of sample GS11B would be contamination of the Polisiehoek Granite-gneiss by the host monzodiorite. However, the dyke intrudes along sharp, linear contacts and contains xenoliths of Swartoup granitoid which also have sharp, linear contacts to the host Polisiehoek

material (Section 3.1.5). This suggests the dyke intruded after the Swartoup granitoid was at least partially solidified and probably did not assimilate any host material.

Mafic dyke

The mafic dyke specimen has ϵ_{Nd} and $^{87}Sr/^{86}Sr$ values that are expected for a mafic, mantle derived body. The isotopic composition of the specimen is compatible as a possible contaminant of Swartoup melts. However, field evidence does not support this, as the dyke appears to have intruded after the Polisiehoek Granite-gneiss, which, in turn was emplaced after the Swartoup Pluton (Sections 3.1.5, 3.2.5). Although, it is possible that a similar mafic body intruded earlier than the sampled one and was itself a contaminant of the Swartoup Pluton.

5.3 Genetic relationships

This section is about the possible genetic relationships between the various rock groups; Koenap migmatite, Swartoup granitoid and Polisiehoek Granite-gneiss, using field relationships (Chapter 3) as well as geochemical evidence (Chapter 4).

5.3.1 Assessing protolith composition

Genesis of the Koenap migmatite

Incompatible elements will concentrate within silicic melt, as they are somewhat insoluble when bound within silicates. Meanwhile, the compatible elements will preferentially remain within the restite. As silicic melt moves and segregates from its protolith, we should find discernible enrichment-depletion trends between the resulting restitic melanosome and the segregated leucosome.

Within Koenap Formation migmatites we find such enrichment-depletion trends, such as the positive trends between zirconium and titanium with maficity. Also, the migmatites have P_2O_5 concentrations lower than those of pelites and greywackes, and elevated Ce concentrations. This suggests either the Koenap protolith was (i) originally Ce-enriched and P_2O_5-depleted, or (ii) P_2O_5 was lost at some point in the rocks' geological history, whilst cerium was concentrated (Figure 4.3).

Also, Koenap Formation migmatites plots at similar maficities to the greywacke and pelite compositional fields. This, along with the field structures (e.g., Figure 3.4; stromatic migmatite and

prominent garnet porphyoblast within the leucosome) and thin section evidence (Figure 3.17; garnet resoprtion textures) provide good evidence that the Koenap protolith was metasedimentary, spatially varying from metapelitic to metagreywacke compositions. The migmatite then underwent anatexis during its history, producing melt and peritectic garnet by biotite dehydration melting through a reaction such as ($> 700°C$) Bt + Al_2O_5 ($\pm$ Pl) + Qtz = Grt + Kfs + Liq (e.g., Holdaway and Lee, 1977; Whitehouse and Platt, 2003). The migamatites of the Koenap Formation vary, both in their composition and relative proportions of leucosome to melanosome. This is most likely due to source heterogeneity, as melt does not appear to have been extracted to a high degree (see Chapter 3, this study; and van Huyssteen, 2017).

The Koenap migmatites have low P_2O_5 (Section 4.3.1) and elevated Ce concentrations (Section 4.3.2), consistent with S-type granitoid extraction. Also, as seen in the section on Chemical Variation Diagrams, Section 4.4, the Koenap migmatites show overlap with published both pelitic and greywacke field compositions. This, together with the visible textures suggesting melt extraction (Section 3.1.5), and the positive trends between both zirconium and titanium with maficity (Section 4.4.2) of the migmatite strongly suggests that the migmatite of the Koenap Formation resulted from anatexis of a metasedimentary rock, which also produced S-type granitic material, though probably of limited volume.

Petrogenesis of the Swartoup Pluton

Swartoup group 1 The P_2O_5 versus Rb diagram (Figure 4.3a) shows Swartoup group 1 as having S-type affinity. However, the Ce (Figure 4.3b), Y (Figure 4.3c) and La (Figure 4.3d) diagrams show no clear affinities with either S- or I-type trends, due to overlap of the Rb and SiO_2 contents of Swartoup group 1 and the published pelite and greywacke compositions. Though, in both the (Na_2O + K_2O)/CaO (Figure 5.2a) and FeO^T/MgO (Figure 5.2b) versus Zr + Nb + Ce + Y diagrams, the Swartoup group 1 analyses plot in the A-type field, their relatively low alkali and high CaO contents indicate they cannot be considered A-type granitoids (e.g. Whalen et al., 1987; Eby, 1992). Instead, these diagrams are in better agreement with Swartoup group 1 as having either an S- or I-type affinity, with somewhat elevated Zr + Nb + Ce + Y contents. This may be a result of high apatite or monazite contents, which would be in agreement with their high P_2O_5 contents. If the protolith of the Swartoup group 1 rocks is geochemically closer to Koenap migmatite, then the P_2O_5 and Y diagrams are compatible with S-type trends, and the Ce and La diagrams appear compatible with both S- or I-type trends, for Swartoup group 1. As such, these Swartoup group 1 are probably S-type granitoids, based on high-field strength elements (HFSEs).

This is not in direct agreement with the molar $Al_2O_3/(MgO + FeO^T)$ versus molar $CaO/(MgO + FeO^T)$ diagram (Figure 4.5d), however. This diagram indicates the Swartoup group 1 rocks are likely I-type granitoids, based on major elements, sourced from partial melting of largely metabasaltic to metatonalitic material.

Whalen et al. (1987) proposed multiple diagrams for the discrimination of A-type granitoids from I-, S- and M-type granitoids. Two such diagrams are shown in Figure 5.2, (a) $(Na_2O + K_2O)/CaO$ versus Zr + Nb + Ce + Y and (b) FeO^T/MgO versus Zr + Nb + Ce + Y, where FeO^T is total iron oxide as FeO. Detailed descriptions of these diagrams are shown in Appendix A.2. A-type granitoids are generally characterised in these diagrams by higher $(Na_2O + K_2O)/CaO$ and FeO^T/MgO ratios, as well as somewhat higher Zr + Nb + Ce + Y contents, than the other rock types (see Whalen et al., 1987). However, Whalen et al. (1987) note that highly fractionated I- and S-type granitoids also have high $(Na_2O + K_2O)/CaO$ and FeO^T/MgO ratios.

Figure 5.2c shows a plot of $(Al_2O_3 + CaO)/(FeO^T + Na_2O + K_2O)$ versus $100 \times (MgO + FeO^T + TiO_2)/SiO_2$. This diagram, proposed by Sylvester (1989), distinguishes alkaline from peraluminous and highly fractionated granitoids. This helps confirm classifications of highly fractionated granitoids made based on Figures 5.2a and 5.2b. However, the diagram (Figure 5.2c) does not show agreement with geochemical classifications made by the MALI and ASI diagrams (Figure 4.2b,c) and so is only used with reference to Figures 5.2a and 5.2b as stated previously.

In both the $(Na_2O + K_2O)/CaO$ (Figure 5.2a) and FeO^T/MgO (Figure 5.2b) versus Zr + Nb + Ce + Y diagrams the Swartoup group 1 analyses plot in the A-type field, but their relatively low alkali and high CaO contents indicate they cannot be considered A-type granitoids (Whalen et al., 1987; Eby, 1992). Instead, these diagrams are in better agreement with Swartoup group 1 as having either an S- or I-type affinity, with somewhat elevated Zr + Nb + Ce + Y contents. This may be a result of high apatite or monazite contents, which is consistent with their high P_2O_5 contents.

Swartoup group 1 appears to comprise S-type granitoids, due to their compositional proximity to sedimentary protolith compositions, and its elevated P_2O_5 content, which is characteristic of S-type granitoids.

Swartoup group 2 Though Swartoup group 2 show slight overall increase in P_2O_5 with Rb, an S-type characteristic, their overall low P_2O_5 contents are more commonly an I-type characteristic. Their large variations in Ce contents are also more commonly associated with

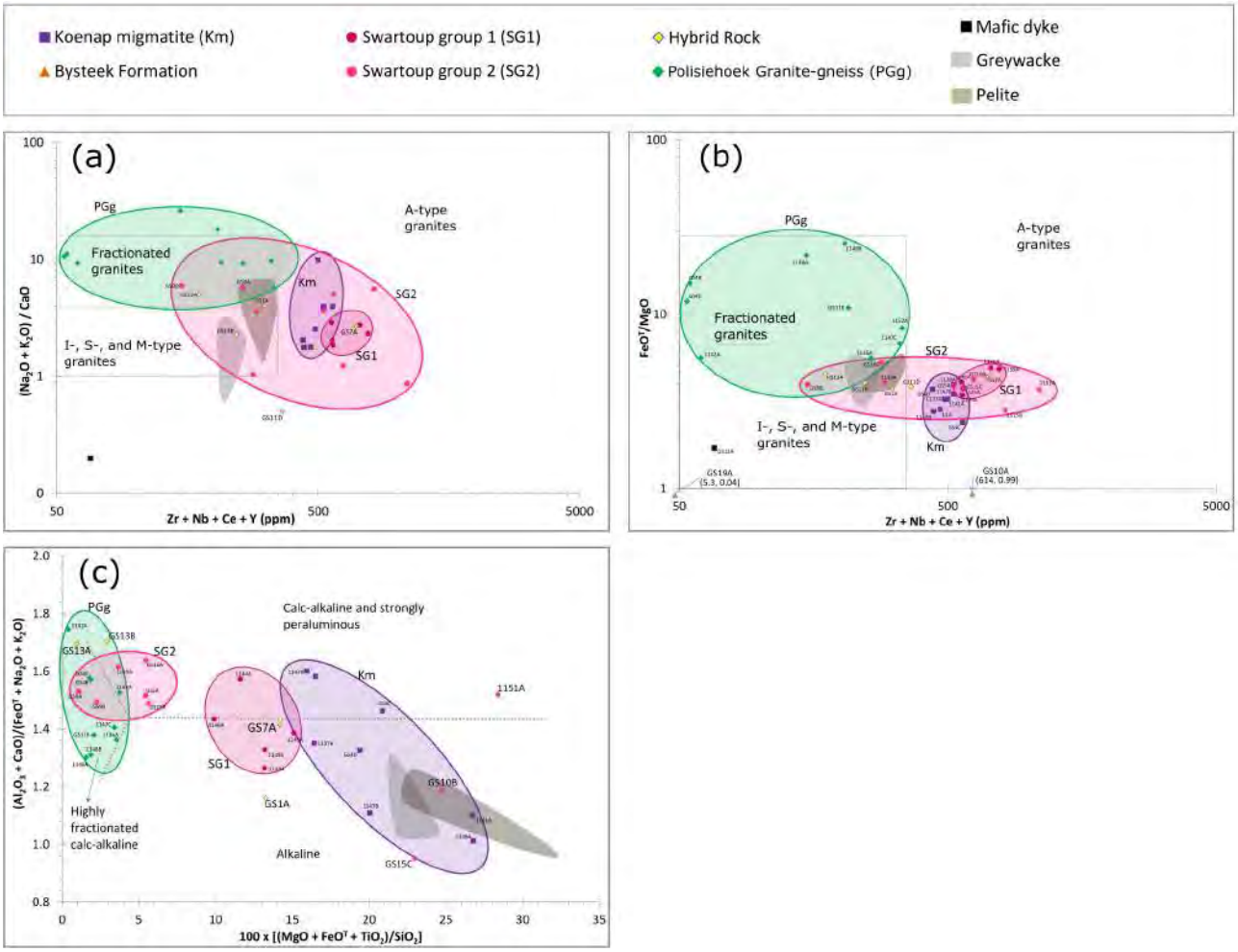

Figure 5.2: *Plots of (a) $(Na_2O + K_2O)/CaO$ and (b) FeO^T/MgO versus $Zr + Nb + Ce + Y$ are used to distinguish A-type granitoids from I-, S- and M-type granitoids, as well as fractionated I-, S- and M-types (e.g., Whalen et al., 1987; Zhang et al., 2019). (c) To confirm distinctions between fractionated and unfractionated granitoids, a plot of $(Al_2O_3 + CaO)/(FeO^T + Na_2O + K_2O)$ versus $100 \times (MgO + FeO^T + TiO_2)/SiO_2$ is also used (Sylvester, 1989). This diagram can also be used to distinguish peraluminous from alkaline rocks (Sylvester, 1989). Koenap migmatite are circled in blue, Swartoup group 1 in red, Swartoup group 2 in magenta and the Polisiehoek Granite-gneisses in green.*

I-type affinities. However, the Y and La diagrams each show two distinct trends. (i) The low-Rb, low-SiO_2 analyses display I-type affinities due to their large Y and La content ranges. (ii) In contrast, the somewhat higher-Rb, higher-SiO_2 analyses, referred to as the granitic Swartoup group 2 rocks, show clear S-type trends, that is, low-Y and decreasing La with SiO_2. Like with Swartoup group 1, the $(Na_2O + K_2O)/CaO$ and FeO^T/MgO versus Zr + Nb + Ce + Y diagrams (Figure 5.2a,b) show Swartoup group 2 to be either I- or S-type granitoids, due to their relatively low $(Na_2O + K_2O)/CaO$ and FeO^T/MgO ratios. The $(Na_2O + K_2O)/CaO$ and FeO^T/MgO diagrams (Figure 5.2a,b) and also the $(Al_2O_3 + CaO)/(FeO^T + Na_2O + K_2O)$ versus $100 \times (MgO + FeO^T + TiO_2)/SiO_2$ diagram (Figure 5.2c) show samples GS9A and GS9B in the fractionated fields. Though they have low P_2O_5 contents, commonly an I-type characteristic, these analyses show relatively low Ce, Y and La at high Rb and SiO_2 contents, typical S-type

characteristics. Therefore, based on these diagrams, Swartoup group 2 may comprise both sedimentary- and igneous-derived granitic rocks, and perhaps also localised, small volumes of highly fractionated S-type granitic material. This is supported by the molar $Al_2O_3/(MgO + FeO^T)$ versus molar $CaO/(MgO + FeO^T)$ diagram (Figure 4.5d). This diagram shows that Swartoup group 2 appear to comprise material derived either from (i) multiple metagreywacke and metatonalitic to metabasaltic compositions, or (ii) from material derived from the partial melting of heterogeneous material comprising greywacke and tonalitic components.

Figure 5.2c shows a plot of $(Al_2O_3 + CaO)/(FeO^T + Na_2O + K_2O)$ versus $100 \times (MgO + FeOT + TiO_2)/SiO_2$. This diagram, proposed by Sylvester (1989), distinguishes alkaline from peraluminous and highly fractionated granitoids. This helps confirm classifications of highly fractionated granitoids made based on Figures 5.2a and 5.2b. The $(Na_2O + K_2O)/CaO$ and FeO^T/MgO diagrams (Figures 5.2a,b) and also the $(Al_2O_3 + CaO)/(FeO^T + Na_2O + K_2O)$ versus $100 \times (MgO + FeO^T + TiO_2)/SiO_2$ diagram (Figure 5.2c) show samples GS9A and GS9B in the Fractionated fields. Though they show low P_2O_5 contents, commonly an I-type characteristic, these analyses show relatively low Ce, Y and La at high Rb and SiO_2 contents (Figure 4.3), typical S-type characteristics. The characteristics of Swartoup group 2 analyses REE-profiles are like those of feldspars, which suggests that the material is the mobilised product of feldspar fractionation and extraction. The REE-profiles of the garnet-bearing granites, samples GS15C and GS16A, are different from each other, despite being petrographically very similar in appearance. Sample GS16A's HREE-profile is consistent with garnet accumulation, but a somewhat scalloped LREE-profile is more reminiscent of plagioclase accumulation. However, garnets have sufficiently low LREE-abundances that the LREE-profile of a polymineralic rock is unlikely to be controlled by garnet.

In contrast, GS15C has high LREE abundances and shows relative HREE depletion, like those shown by typical Swartoup granites, such as samples 1149A and GS5A. Such profiles are often associated with garnet removal. This suggests the garnet of sample GS15C was not the product of entrainment of restitic peritectic garnet associated with the melting event (migmatisation), and so may represent pre-existing metamorphic porphyroblasts, or phenocrysts that grew in the LREE-enriched, HREE-depleted melt. In thin section, garnet shows a resorbed texture and biotite appears to be growing after these crystals (Section 3.2.3).

Swartoup group 2 is likely a highly fractionated S-type granitoid, consistent with its low Ce, Y and La at high Rb and SiO_2 contents. The low P_2O_5 contents the rock probably are a result of the fractionation process.

Petrogenesis of the Polisiehoek Granite-gneiss

The Polisiehoek Granite-gneisses have low P_2O_5 contents, a characteristic common to I-type granitoids. They also show somewhat constant Ce concentrations with Rb, an I-type feature. However, their Ce contents are lower than those of the pelite and greywacke compositions, which is generally more common among S-type granitoids. The Polisiehoek Granite-gneisses also show a strong decrease in La with increase in SiO_2, with SiO_2 contents generally above 75 wt.% SiO_2, another strong S-type characteristic. In addition, the Polisiehoek rocks show two distinct Y trends, one above (I-type) and one below (S-type) the sediment compositions. The diagrams of $(Na_2O + K_2O)/CaO$ and FeO^T/MgO versus Zr + Nb + Ce + Y as well as the $(Al_2O_3 + CaO)/(FeO^T + Na_2O + K_2O)$ versus $100 \times (MgO + FeO^T + TiO_2)/SiO_2$ diagram (Figure 5.2) show that the Polisiehoek Granite-gneisses are highly fractionated granites. This, together with the previous data, suggests that the Polisiehoek Granite-gneisses are highly fractionated granites that may have been derived from a mixture of both sedimentary and igneous sources.

This is somewhat consistent with the titanium and zirconium versus maficity diagrams (Figure 4.6), which show the Polisiehoek Granite-gneiss is consistent with a late stage, more evolved (due to higher incompatible element concentrations) resulting from anatexis.

The molar $Al_2O_3/(MgO + FeO^T)$ versus molar $CaO/(MgO + FeO^T)$ diagram (Figure 4.5d) indicates that the Polisiehoek Granite-gneiss could have resulted from partial melting of metagreywacke source material, as four analyses lie within the metagreywacke partial melt field. However, at least some, possibly localised, additional metapelitic component is also required, as two analyses lie in the metapelite partial melt compositional field. The resulting melt does not seem to have (completely) homogenised, as another two analyses lie within the overlap between those two fields of the diagram. The Polisiehoek Granite-gneiss specimens show LREE depletion, a strong negative europium anomaly and a somewhat flat or slight enrichment in the HREEs (Figure 4.7f). Such profiles are inconsistent with feldspar removal signatures, which suggests the material from which these rocks derive experienced feldspar fractionation. It is then likely feldspar fractionation occurred (possibly in an earlier melting event) prior to the onset of that partial melting event which formed the Polisiehoek Granite-gneiss itself.

This then suggests two possibilities:

- I-type; that is, formation of this granitoid by partial melting of an igneous source rock which had previously experienced feldspar fractionation.
- S-type; whereby the granitoid formed by partial melting of a metasedimentary source rock

from which feldspar had been preferentially removed by 'sedimentary processes'. These can include weathering of feldspar, and extraction of clay minerals prior to the onset of diagenesis. This resulting feldspar-depleted rock then partially melted, forming the Polisiehoek Granite-gneiss.

5.3.2 Did the Swartoup Pluton originate from melting of the the Koenap Formation?

The Koenap migmatites, on average, have more zirconium and titanium than both the greywacke and pelite fields. The maficity diagrams (Figure 4.6) are supposed to arrange data in linear trends originating at the origin (e.g. Clemens et al., 2011), however they are designed for igneous rocks. The Koenap migmatites in Figure 4.6a, appear to form a linear trend directed towards either Swartoup group 1 or between Swartoup groups 1 and 2. In Figure 4.6b they appear to form a linear trend originating above the origin, near the granitic Swartoup group 2 analyses at low Fe + Mg values. These, along with their spatial associations with the Swartoup Pluton (Chapter 3), suggests a genetic relationship between Koenap migmatite and at least some of the Swartoup granitoids.

Immobile zirconium would be expected to be enriched in a rock that has experienced material loss, ignoring metasomatic effects of hydrothermal fluids. Swartoup group 1 rocks contain more Zr than the Koenap migmatites, and the majority of Swartoup group 2 have less than both (Figure 4.6b). The majority of Swartoup group 2 could be regarded as the result of melt segregation and mobilisation after anatexis of the Koenap migmatites. This is supported by the observation that the Koenap migmatites show overlap, at the low-maficity end, with the pelite field. These low-maficity, leucocratic Koenap migmatites could have experienced less material loss than the higher maficity, slightly higher zirconium content, melanocratic migmatites. Such mobilised material appears compatible with the main, granitic Swartoup group 2 cluster (Figure 4.6b).

In contrast, Swartoup group 1 would not be expected to be related to the Koenap migmatites, unless the original protolith was perhaps enriched, at least locally, in zirconium relative to the published sediment compositions used in the diagrams. Alternatively, it is possible that an in-situ differentiation process partitioned the incompatible zirconium into relatively more mafic, granodioritic melt, from a more felsic, granitic melt. This could explain the higher zirconium content (acting as a refractory, restitic mineral) of the Swartoup granodiorites (Swartoup group 1) relative to the typical Swartoup granites (the majority of Swartoup group 2).

Swartoup group 1 rocks have similar titanium contents to the Koenap migmatites (Figure 4.6a). Swartoup group 1 probably resulted from anatexis of a source rock more titanium-rich than the Koenap migmatites. However, as greywackes are generally considered to be more fertile melt sources, and the published greywacke compositions have less titanium than the pelites and Koenap migmatites, this appears unlikely. Rather, it may again be necessary to consider an in-situ differentiation process which preferentially partitions titanium to the more mafic, more biotite–rich granodiorites (Table 3.3). The observation that Swartoup group 1 and the majority of Swartoup group 2 lie along a single, well-defined linear trend in the titanium diagram (Figure 4.6a) strongly suggests they share the same source.

Sample GS15C lies nearer the Koenap migmatites and the published pelite composition fields (Figures 4.6a and 4.6b), at a higher maficity and lower zirconium and titanium contents than the previously discussed Swartoup granitoids. Sample GS16A plots well below the Koenap migmatites, but still at a higher maficity and lower titanium content than the Swartoup granitoid trend. This sample does not appear to differ greatly from the other Swartoup group 2 rocks in terms of zirconium contents, as these rocks show a relatively wide range of Zr values compared to the narrow trend in the Ti versus Fe + Mg diagram (Figure 4.6a). Samples GS15C and GS16A are garnet-bearing granites (Section 3.2.3, Tables 3.3 and 3.4), sampled near Koenap migmatite outcrops. In the maficity diagrams these garnet-bearing granites plot away from the Swartoup granitoid trend, towards either the Koenap migmatites or the published pelite composition field. It is possible that these two samples are sourced from a different protolith to that of the rocks that lie along the Swartoup granitoid trend. However, it is more likely that they share the same or similar source rock, but have been contaminated by some rock that lies off the Swartoup granitoid trend. From field evidence it is likely that such contaminants are xenocrystic garnet, sourced from Koenap migmatite. Peritectic garnet may have been entrained within mobilised Koenap leucosome. Or perhaps Koenap material was assimilated at the pluton walls, forming the garnet-bearing layers seen in the field (Sections 3.1.2, 3.1.3). Assimilation would be less likely, as the Swartoup Pluton was probably not hot enough at the time of emplacement to assimilate surrounding country rock, especially if that rock is a restitic migmatite. Metasomatic processes could also be responsible for material remobilisation, taking place during cooling or late-stage de-watering of the pluton.

5.3.3 The hybrid rock

The hybrid rock specimens appear to follow the Swartoup group 2 trends, showing both I- and S-type affinities. The hybrid rocks have low P_2O_5 (I-type characteristic) which increase with Rb

(an S-type characteristic; see Figure 4.3). They also have a relatively wide range of Ce contents and, though the data set is small, they appear to follow both the high- and low-Y trends shown by Swartoup group 2, indicating both I- and S-type affinities. This is seen also in the (Na_2O + K_2O)/CaO, FeO^T/MgO and (Al_2O_3 + CaO)/(FeO^T + Na_2O + K_2O) diagrams where the hybrid rocks show either overlap with Swartoup group 2 (Figure 5.2a,b) or vary between two distinct trends of Swartoup group 2 analyses (Figure 5.2c). These diagrams also confirm that the hybrid rocks are either I- or S-type granitoids, as opposed to A-type granitoids. In the field (Section 3.1.4) these rocks are spatially associated with outcrop of both Bysteek Formation and Swartoup Pluton. The molar Al_2O_3/(MgO + FeO^T) versus molar CaO/(MgO + FeO^T) diagram (Figure 4.5d) shows the hybrid rock analyses in an extended field of metabasaltic to metatonalitic composition, suggesting an I-type affinity of these rocks. The molar Al_2O_3/(MgO + FeO^T) versus molar CaO/(MgO + FeO^T) diagram is consistent with previous data whereby the hybrid rock analyses follow those of Swartoup group 2.

The hybrid rock specimens (Figure 4.7e) show considerable variation in their REE abundances and profile shapes but remain below the Bysteek calc-silicate in terms of REE abundances, on average. The pyroxene-bearing granodiorites (samples GS11D and GS13B) show similar REE-profiles to the calc-silicate, sample GS10A. This would be expected if the hybrid rocks formed by partial melting of the Bysteek calc-silicate rock caused by intrusion of Swartoup granites, resulting in mixed (hybridized) melts. Sample GS7A also has similar La/Yb ratios, though lower La and Yb concentrations, to samples GS10A, GS11D and GS13B. However, this garnet-rich granodiorite (Section 3.2.4) is slightly more LREE-enriched than sample GS13B, but it has relatively higher HREE concentrations, like those of the Bysteek calc-silicate. Sample GS1A has an REE-profile much like that of sample GS7A, but at lower LREE concentrations that tend to almost the same lutetium contents. It may be that samples GS1A and GS7A inherited their HREEs from garent of the Bysteek calc-silicate rocks. However, as LREEs preferentially partition into plagioclase rather than garnet, this indicates these samples inherited their LREEs from material sourced elsewhere. There is good field evidence for Swartoup granitoid as playing such a role (Sections 3.1.2 and 3.1.4).

Sample GS13A has an REE profile, which differs from the other hybrid rocks, and is mostly at lower REE concentrations. The rock shows LREE depletion, a strong positive europium anomaly and a relatively flat HREE profile. Table 3.5 shows that sample GS13A has the highest plagioclase mode of the hybrid rocks. This rock was sampled adjacent to sample GS13B (Section 3.2.4), which shows a relatively low plagioclase mode. As such, sample GS13A probably inherited the positive Eu-anomaly from, at least localised, plagioclase accumulation. This rock

probably represents an end-member hybrid rock.

CHAPTER 6

Conclusion

6.1 The Koenap Formation

Koenap Formation migmatites show typical crustal ϵ_{Nd} and $^{87}Sr/^{86}Sr$ values (Section 5.2.2). The rocks have low P_2O_5 (Section 4.3.1), elevated Ce concentrations (Section 4.3.2) and positive trends of zirconium and titanium with maficity (Section 4.4.2), consistent with S-type granitoid extraction.

The migmatites of the Koenap Formation resulted from anatexis of heterogeneous metasedimentary (both metapelitic and metagreywacke components) material. However, extraction of an S-type granitic melt was either limited, or the majority of segregated material was extracted to elsewhere, outside the study area.

6.2 The Swartoup Pluton

The Swartoup Pluton comprises mostly granitic and granodioritic material, as classified by the TAS (Middlemost, 1994) and R_1R_2 (De la Roche et al., 1980) diagrams. The rocks of the pluton vary from ferroan to magnesian, alkali-calcic to calc-alkalic, peraluminous granodiorites and granites. Some outcrops of metaluminous granites and orthopyroxene-bearing monzodiorites are also found (see Sections 3.1.3, 4.2).

The rocks show some A-type granitoid trends (Figure 4.4a,b), however they contain too low-alkali contents and too high-CaO contents. Rather, their typically low P_2O_5 (Figure 4.3a) and

elevated Zr + Nb + Ce + Y concentrations typify the body as an S-type granitoid. The Ce and Y trends with Rb (Figure 4.3) also show Swartoup granodiorite (Swartoup group 1 rocks) with typical S-type affinities.

Swartoup group 2 rocks also have ϵ_{Nd} and $^{87}Sr/^{86}Sr$ values that suggest either (i) some mantle component in their source-rocks (Section 5.2.2, Figure 5.1), or (ii) contamination with low-Sm Bysteek marble or (iii) metasomatism/LILE-depletion by fluid loss. However, Swartoup group 2 rocks show both I- and S-type affinities in their P_2O_5 and Y contents (Figures 4.3a,c). However, the low Ce, Y and La at high at high Rb and SiO_2 contents of Swartoup group 2 rocks suggests the S-type granitoids are highly fractionated (see Figures 4.3 and 5.2). The low P_2O_5 contents of Swartoup group 2 are probably a result of the fractionation process.

In conclusion, the Swartoup Pluton comprises S-type granitoids and resulted from partial melting of metasediments, despite the varying geochemistry of its constituent rocks (including granites, granodiorites and orthopyroxene-bearing monzodiorites).

6.2.1 The hybrid rock

These feldspar-rich granodioritic rocks with prominent, euhedral garnet, pyroxene and titanite are commonly found along the contact between the Swartoup Pluton and the surrounding Bysteek Formation calcic metasediments. The hybrid rocks follow many geochemical trends shown by the Swartoup group 2 rocks (Section 5.3.3).

The hybrid rocks show REE-profiles and ϵ_{Nd} values consistent with partial melting of Bysteek calc-silicate rocks (Sectiosn 5.3.3, 5.2.2). The hybrid rocks probably inherited their HREEs from garnet of the Bysteek calc-silicate rocks, and their LREEs are probably sourced from Swartoup material (plagioclase). This is consistent with thin sections which show plagioclase in two distinct habits, (i) one subhedral, and probably crystallised from newly formed melt, (ii) the other anhedral and recrystallised, these are probably xenocrysts originating from Swartoup material (Figure 3.27c, Section 3.2.4).

The granodioritic hybrid rock resulted from contamination of Swartoup melt with Bysteek calcic metasediments, and more-or-less *in situ* crystallisation.

6.3 The Polisiehoek Granite-gneiss

The sheared biotite-K-feldspar-plagioclase-quartz orthogneiss shows strong tectonic foliation (Section 3.2.5) and was emplaced after the Swartoup Pluton had at least partially crystallised

(e.g., Section 3.1.5). The rocks of the Polisiehoek Granite-gneiss show both I- and S-type granitoid characteristics. However, S-type affinites appear dominant, in particular its low P_2O_5 contents and decreasing La with increasing SiO_2 contents. Diagrams of $(Na_2O + K_2O)/CaO$ and FeO^T/MgO versus Zr + Nb + Ce + Y as well as the $(Al_2O_3 + CaO)/(FeO^T + Na_2O + K_2O)$ versus $100 \times (MgO + FeO^T + TiO_2)/SiO_2$ diagram (Figure 5.2) indicate the Polisiehoek Granite-gneisses are highly fractionated S-type granitoids.

The Polisiehoek Granite-gneisses show LREE-depletion and strong negative europium anomalies (Section 4.4.3) that are inconsistent with feldspar removal signatures, suggesting the Polisiehoek source-rocks were depleted in feldspar (Section 5.3.1). Such feldspar depletion is probably due to weathering processes prior to the partial melting event. This is consistent with the S-type characteristics previously shown for the highly Polisiehoek Granite-gneiss.

APPENDIX A

Appendix

A.1 Chemical variation diagram descriptions

The following section contains detailed descriptions of some of the chemical variation diagrams (Figures 4.1–4.9) of Chapter 4. Tables A.1–A.5 show the original major and minor oxide XRF analyses (i.e., Fe is given as Fe_2O_3 and the data have not been normalised to 100 wt% anhydrous).

Table A.1: *Koenap migmatite specimens major and minor oxide XRF analyses.*

Sample	1137A	1138A	1141A	1143A	1143B	1147B	GS4C	GS4D
wt.%								
SiO_2	66.67	64.37	64.15	67.81	68.60	64.35	66.25	65.64
TiO_2	1.09	1.17	1.20	1.04	1.03	1.06	1.24	1.26
Al_2O_3	14.70	14.46	15.12	14.97	14.65	14.54	15.60	14.90
Cr_2O_3	0.01	0.01	0.01	0.01	0.01	*bdl*	0.01	*bdl*
Fe_2O_3	8.38	14.25	13.76	8.35	8.09	10.08	9.88	10.05
MnO	0.10	0.15	0.10	0.14	0.11	0.14	0.10	0.14
MgO	2.32	3.25	3.56	2.64	2.62	2.78	3.70	2.43
CaO	1.86	0.50	0.44	1.70	1.64	0.45	0.54	1.69
Na_2O	2.07	0.43	0.30	1.30	1.21	0.54	0.67	1.67
K_2O	2.65	1.53	1.44	1.72	1.68	3.90	1.47	1.79
P_2O_5	0.07	0.04	0.04	0.07	0.05	0.07	0.03	0.04
LOI	0.08	−0.30	−0.15	0.19	0.33	1.54	0.38	−0.05
Total	100.00	99.86	99.97	99.94	100.02	99.46	99.87	99.56

bdl = below detection limit

Table A.2: *Swartoup granitoid specimens major and minor oxide XRF analyses (continued on page 165).*

Sample	1139A	1140A	1144A	1145A	1146A	1149A	1151A
wt%							
SiO_2	66.38	65.60	64.82	63.32	65.40	75.13	52.96
TiO_2	1.04	1.02	0.95	1.25	0.88	0.37	2.01
Al_2O_3	14.06	14.25	15.22	14.60	15.34	12.31	17.54
Cr_2O_3	0.01	0.01	0.01	0.01	0.01	*bdl*	0.01
Fe_2O_3	7.11	7.05	5.66	7.29	4.99	2.12	11.40
MnO	0.09	0.10	0.08	0.10	0.05	0.03	0.18
MgO	1.32	1.29	1.48	1.75	1.10	0.47	2.77
CaO	2.68	2.50	3.29	3.54	2.82	1.92	6.10
Na_2O	2.49	2.72	2.96	2.70	2.72	2.28	3.44
K_2O	3.71	4.18	3.71	3.82	5.45	4.62	1.86
P_2O_5	0.36	0.36	0.30	0.39	0.25	0.09	0.75
LOI	0.37	0.50	1.11	0.52	0.25	0.31	0.15
Total	99.62	99.58	99.59	99.29	99.26	99.65	99.17

bdl = below detection limit

Table A.3: *Major and minor oxide XRF analyses of Swartoup granitoids, continued from page 165.*

Sample	GS5A	GS9A	GS9B	GS10B	GS15B	GS15C	GS16A
wt%							
SiO_2	72.62	74.48	76.45	57.39	64.98	63.12	83.63
TiO_2	0.61	0.12	0.22	2.22	0.60	0.96	0.26
Al_2O_3	12.71	13.00	11.74	13.87	16.84	14.20	7.01
Cr_2O_3	0.00	0.00	0.00	0.00	0.00	*bdl*	0.01
Fe_2O_3	2.95	0.76	1.32	10.74	2.51	11.91	4.01
MnO	0.03	0.01	0.02	0.12	0.02	0.18	0.14
MgO	0.68	0.00	0.30	2.29	0.80	2.82	0.68
CaO	1.93	1.53	1.26	5.22	1.85	1.05	1.59
Na_2O	2.32	1.71	1.87	2.96	2.81	1.72	1.21
K_2O	4.68	7.10	5.64	3.43	7.49	3.59	0.43
P_2O_5	0.14	0.01	0.03	0.59	0.09	0.06	0.02
LOI	0.49	0.37	0.45	0.22	1.02	0.22	0.23
Total	99.16	99.09	99.30	99.05	99.01	99.84	99.22

bdl = below detection limit

A.1.1 Rock classification schemes

A.1.1.1 TAS diagrams

Figure 4.1a shows the Koenap migmatites cluster reasonably well together. They show a narrow SiO_2O content range from 64 to 69 wt% SiO_2 and lie in the Granodiorite field. These SiO_2O contents are similar to those of Swartoup group 1 but the alkali totals in the migmatites are lower. Samples 1137A, 1143A and GS4D are the most leucocratic Koenap migmatites

Table A.4: *Major and minor oxide XRF analyses of the Bysteek Formation marble and calc-silicate, hybrid rocks and the mafic dyke specimen.*

	Bysteek marble		hybrid rock					Mafic dyke
Sample	GS19A	GS10A	GS1A	GS7A	GS11D	GS13A	GS13B	GS12A
wt.%								
SiO_2	3.94	48.38	71.36	64.25	67.56	75.25	71.33	44.49
TiO_2	0.03	2.13	0.91	0.73	0.70	0.04	0.32	1.15
Al_2O_3	0.01	8.75	11.88	16.23	16.48	13.11	12.93	15.50
Cr_2O_3	0.00	*bdl*	0.01	*bdl*	*bdl*	*bdl*	*bdl*	*bdl*
Fe_2O_3	0.37	4.19	7.50	7.59	1.20	0.61	1.57	15.78
MnO	0.01	0.14	0.09	0.15	0.03	0.01	0.03	0.24
MgO	7.84	3.81	1.81	1.56	0.28	0.12	0.35	8.33
CaO	48.31	27.89	1.10	2.31	8.10	1.62	3.64	11.45
Na_2O	0.00	0.04	1.52	2.68	2.25	2.29	1.91	1.69
K_2O	0.00	0.19	2.91	3.60	1.85	5.85	6.40	0.58
P_2O_5	0.01	0.04	0.05	0.06	0.09	0.02	0.10	0.11
LOI	40.30	4.25	0.18	0.29	1.04	0.45	0.57	0.15
Total	100.82	99.81	99.32	99.45	99.58	99.37	99.15	99.48

bdl = below detection limit

Table A.5: *Polisiehoek Granite-gneiss major and minor oxide XRF analyses.*

Sample	1136A	1142A	1147C	1148A	1148B	1152A	GS4B	GS4E	GS11B
wt%									
SiO_2	75.32	78.69	73.04	76.40	77.40	72.99	77.82	80.54	74.20
TiO_2	0.22	0.04	0.22	0.06	0.12	0.21	0.01	0.02	0.10
Al_2O_3	12.38	12.45	13.78	12.27	11.88	14.09	12.33	10.60	13.12
Cr_2O_3	*bdl*	*bdl*	*bdl*	*bdl*	*bdl*	*bdl*	*bdl*	*bdl*	*bdl*
Fe_2O_3	2.31	0.25	2.19	1.21	1.42	2.50	1.50	1.45	1.45
MnO	0.04	0.01	0.03	0.04	0.04	0.06	0.02	0.02	0.04
MgO	0.37	0.04	0.29	0.05	0.05	0.27	0.09	0.11	0.12
CaO	0.82	0.79	0.87	0.33	0.45	1.37	0.62	0.54	0.94
Na_2O	2.95	4.67	3.18	2.61	2.75	2.80	2.60	2.02	3.09
K_2O	4.66	2.69	5.27	5.98	5.38	5.08	4.29	3.74	5.80
P_2O_5	0.08	0.11	0.09	0.13	0.05	0.06	0.10	0.09	0.06
LOI	0.51	0.19	0.90	0.33	0.09	0.23	0.36	0.31	0.24
Total	99.66	99.93	99.86	99.41	99.63	99.66	99.74	99.44	99.16

bdl = below detection limit

(Section 3.2.1). They lie at somewhat higher total alkali contents (<3 wt% K_2O + Na_2O) than the more melanocratic specimens, samples 1138A, 1141A, 1143B and GS4C. However, sample 1147B is melanocratic and has a relatively high alkali content (around 4 wt% K_2O + Na_2O), which is likely due to its white mica mode (Table 3.1).

The Bysteek calc-silicate (sample GS10A) plots in the Gabbro field, at a much higher silica content (48 wt% SiO_2) compared to the Bysteek marble, which has 3.9 vol% SiO_2 and no detectable K_2O or Na_2O. Their low alkali contents are expected as these specimens are dominated by calcite, clinopyroxene and garnet (Section 3.2.2, Table 3.2).

Figure 4.1a shows the Swartoup group 1 (samples 1139A, 1140A, 1144A, 1145A and 1146A) rocks have similar silica and alkali contents as each other. Most of the Swartoup group 1 specimens plot in the upper portion of the Granodiorite field and range between 6 and 7 wt% K_2O + Na_2O. Sample 1146A has somewhat more alkalis (about 8 wt% K_2O + Na_2O) and plots in the Quartz Monzonite field. The SiO_2 contents of Swartoup group 1 specimens range from 63 to 66 wt% SiO_2, very similar to the Koenap migmatites. In contrast, Swartoup group 2 specimens show SiO_2 contents ranging from 52 to 84 wt% SiO_2. The Swartoup group 2 rocks plot in the Monzodiorite (sample 1151A), Monzonite (sample GS10B), Quartz Monzonite (sample GS15B), Granodiorite (sample GS15C) and Granite fields (samples 1149A, GS5A, GS9A, GS9B). The total alkali contents of Swartoup group 2 rocks show somewhat more variation than those of Swartoup group 1. Most of their K_2O + Na_2O contents range between 5 and 9 wt% K_2O + Na_2O. However, sample GS16A lies away from the rest of the Swartoup granitoids, at a much lower total alkali content of 2 wt% K_2O + Na_2O. This rock plots in the Quartzolite field.

The hybrid rocks plot in the Granodiorite (samples GS1A, GS7A and GS11D) and Granite (samples GS13A and GS13B) fields. They show SiO_2 contents ranging between 64 and 75 wt% SiO_2. The granodioritic hybrid rock specimens have alkalis ranging between 4 and 6 wt% K_2O + Na_2O, similar to Swartoup group 1 specimens and the Koenap migmatites. In contrast, the granitic hybrid rocks have around 8 wt% K_2O + Na_2O, comparable to sample 1146A of Swartoup group 1 and, on average, the granitic Swartoup group 2 rocks.

The Polisiehoek Granite-gneisses plot in the Granite field. Their SiO_2 contents range between 73 and 80 wt% SiO_2, higher than those Swartoup group 1 but comparable to the granitic Swartoup group 2 specimens (samples 1148A, GS5A and GS9A). The total alkali contents of the Polisiehoek Granite-gneisses are, on average, higher than those of the Swartoup group 1 specimens. The main cluster of Polisiehoek Granite-gneiss specimens ranges from 6 to 9 wt% K_2O + Na_2O, with sample GS4E plotting slightly lower around 6 wt% K_2O + Na_2O. These rocks show overlap with the granitic Swartoup group 2 specimens.

The mafic dyke specimen, sample GS12A plots in the Olivine-gabbro field at an SiO_2 content of 44 wt% SiO_2. The rock has a total alkali content under 3 wt% K_2O + Na_2O, which could be expected as the specimen is dominated by orthopyroxene and plagioclase, with around 10 vol% K-feldspar (Section 3.2.6, Table 3.8).

Figure 4.1a shows overlapping SiO_2 compositions of the fields of greywacke (59–68 wt% SiO_2) and pelite (59–67 wt% SiO_2) compositions (Section 2.1, Tables 2.2–2.4). The greywacke (<

2–8 wt% K_2O + Na_2O) and pelite (< 3–5 wt% K_2O + Na_2O) fields also show overlap of their total alkali contents. The Koenap migmatites and Swartoup group 1 specimens show overlap with these pelite and greywacke fields. Koenap migmatites plot either in the lower part of the greywacke field or, where total alkali contents are < 3 wt% K_2O + Na_2O, below it. Samples 1147B and GS4D plot where the pelite and greywacke fields overlap and sample 1137A plots slightly above, at higher alkali and silica contents. Most Swartoup group 1 specimens plot in the upper portion of the pelite field below 7 wt% K_2O + Na_2O. Sample 1146A plots above it, near 8 wt% K_2O + Na_2O. The Polisiehoek Granite-gneisses have total alkali contents which are higher than the greywacke field and similar to the upper pelite field.

A.1.1.2 R_1R_2 diagram

The Koenap migmatites plot mostly in the Granodiorite field (samples 1137A, 1138A, 1141A, 1143A, 1143B GS4C and GS4D). Their R_1 values are above 2700 millications and their R_2 values range between about 400 and 600 millications. Sample 1147B plots within this range but falls outside the Granite field, plotting in the Alkali granite field. This is in good agreement with the TAS diagram (Figure 4.1a, Section 4.1.1), where all Koenap migmatites plot in the Granodiorite field. Also, like the TAS diagram, the R_1R_2 diagram shows the more leucocratic Koenap migmatite specimens, samples 1137A and GS4D, along with the melanocratic sample 1147B, separated from the melanocratic ones.

The Bysteek calc-silicate (sample G10A) and marble (sample GS19A) specimens plot well off the diagram at very high R_2 values (over 3000 millications). The Bysteek marble specimen (sample GS19A) has a low R_1 value because of its low SiO_2 content and plots around R_1 = 250 millications (Table 4.3). Like the TAS diagram (Figure 4.1a), the R_1R_2 diagram does not accommodate the Bysteek marble in any defined field. This can be expected as this diagram is intended for use with igneous plutonic rocks. Likely for this same reason, sample GS10A, the Bysteek calc-silicate, also plots outside the defined fields of the diagram.

Swartoup group 1 rocks all plot in the Granodiorite field, between R_1 values of about 2000 and 2500 millications and R_2 values between about 500 and 650 millications. In contrast, most of the Swartoup group 2 specimens plot below an R_2 value of 500 millications. Samples 1149A, GS5A, GS9A, GS9B and GS15C plot in the Granite field between R_1 values of 2300 and 3100 millications. Sample GS15B plots in the Quartz monzonite field, at a similar R_2 as the previous granite specimens but at an R_1 of about 1500 millications. Sample GS16A lies off the diagram at a very high R_1 value (about 5000 millications), in an extension of the Granite field. This is

due to its high quartz mode and thus, silica content (Sections 3.2.3, 4.1). In contrast to the previous Swartoup specimens, samples 1151A and GS10B plot at higher R_2 values. These two orthopyroxene-bearing rocks (Section 3.2.3, Table 3.3) plot in the Monzodiorite field, between R_2 values of 750 and 1250 millications. Figure 4.1b is in general agreement with the TAS diagram (Section 4.1.1, Figure 4.1a). The R_1R_2 diagram classifies all the Swartoup group 1 specimens as granodiorites, whereas the TAS diagram classifies them all as granodiorites with the exception of sample 1146A (quartz monzonite). Both Figures 4.1a and 4.1b classify samples 1149A, GS5A, GS9A and GS9B as granites. Samples 1151A (monzodiorite) and GS15B (quartz monzonite) are classified the same by them as well. However, the R_1R_2 diagram classifies this specimen as a monzodiorite and by the TAS diagram it is a monzonite. Both samples GS15C and GS16A are classified as granites by the R_1R_2 diagram but the TAS diagram classifies them as a granodiorite and a quartzolite, respectively.

Two hybrid rock specimens, samples GS1A and GS13A, plot in the Granite field, with R_2 values around 500 millications. Sample GS1A has a slightly higher R_1 value (about 3300 millications) than sample GS13A (about 2750 millications). Samples GS7A and GS13B have R_1 values of around 2250 and 2500 millications and plot in the Granodiorite field. They have R_2 values near 500 millications. In contrast to the other hybrid rock specimens, sample GS11D plots at a much higher R_2 value (around 1250 millications). Sample GS11D plots outside of the fields defined by De la Roche et al. (1980) but it does plot within an extended Tonalite field.

Most Polisiehoek Granite-gneiss specimens plot in the Alkali granite field. The only exception is sample 1152A, which plots in the Granite field. They all show values ranging from about 2300 to 3750 millications, and R_2 values between about 250 and 500 millications. The R_1R_2 diagram (Figure 4.1b) is somewhat in agreement with the TAS diagram (Figure 4.1a), as far as sample 1152A being classified as a granite in both diagrams. However, the TAS diagram makes no distinction between granites and alkali granites, unlike the R_1R_2 diagram. The TAS diagram classifies all Polisiehoek Granite-gneiss specimens as granites whereas the R_1R_2 diagram classifies all but sample 1152A as alkali granites.

Sample GS12A, the Mafic dyke specimen, plots in the Pyroxenite field. The rock shows an value of around 2700 millications and an R_2 value slightly lower than 2000 millications. However, like with the Polisiehoek Granite-gneisses, there is no Peridot-gabbro field in the R_1R_2 diagram.

The pelite compositions have typically higher R_1 and lower R_2 contents than the greywacke compositions. The R_1R_2 diagram shows overlap in the R_1 values between the fields of pelite (around 2500 to 3500 millications) and greywacke (about 1100 to 3700 millications) compositions.

The pelite (about 600 to 900 millications) and greywacke (300 to 900 millications) fields also show overlap in their R_2 values. Three of the Koenap migmatites (samples 1137A, 1147B and GS4D) show overlap with the pelite field. The rest plot at higher contents but plot within the R_2 range of the pelites. All the Koenap migmatites plot at lower R_2 values than the greywacke field but are within its R_1 range. The hybrid rocks, samples GS1A and GS13A show overlap with the pelite field, in contrast to samples GS7A and GS13B which show overlap with the greywacke field. Sample GS11D plots at a higher R_2 value than these fields but within both their R_1 range. Three Swartoup group 1 specimens (samples 1144A, 1145A and 1146A) show overlap with the greywacke field. However, all the Swartoup granitoids, except for sample GS16A, plot within the R_1 range of the greywacke field. Samples 1151A and GS10B (Swartoup group 2) plot at higher R_2 values than the greywacke field. The rest of the Swartoup group 1 and 2 specimens plot at lower R_2 values than the greywacke field but are all within the R_2 range of the pelite field. The Polisiehoek Granite-gneisses all plot at lower R_2 values than the pelite and greywacke compositions. However, they plot within the range of the pelites.

A.1.1.3 Fe*, MALI and ASI diagram granitoid classification

Table A.6: *Results of the geochemical classification of Frost et al. (2001), using the Fe*, modified alkali-lime index (MALI) and aluminium saturation index (ASI). This classification scheme lists a number of possible rock names for each geochemical subset. The rock names in brackets are considered less likely, based on specimen petrography.*

Rock unit	Sample	Fe*	MALI	ASI	Rock type
Swartoup group 1	1139A	0.829	3.53	1.120	Two-mica granite
	1140A	0.831	4.42	1.087	Two-mica granite
	1144A	0.775	3.42	1.049	Granodiorite (diorite, monzodiorite)
	1145A	0.789	3.00	1.004	Two-mica granite
	1146A	0.803	5.36	1.009	Two-mica granite
Swartoup group 2	GS5A	0.796	5.10	1.040	Diorite (quartz diorite, tonalite)
	GS9A	1.000	7.27	0.983	Granite
	GS9B	0.798	6.24	1.030	Diorite (quartz diorite, tonalite)
	GS10B	0.808	1.16	0.800	Ferrodiorite (syenite, granite)
	GS15B	0.738	8.43	1.062	[a]
	GS15C	0.792	4.27	1.660	Two-mica granite
	GS16A	0.841	0.05	1.317	Diorite (quartz diorite, tonalite)
	1149A	0.802	5.00	1.014	Diorite (quartz diorite, tonalite)
	1151A	0.787	-0.80	0.982	Ferrodiorite (syenite, granite)
Hybrid rock	GS1A	0.789	3.34	1.565	Diorite (quartz diorite, tonalite)
	GS7A	0.814	3.98	1.305	Two-mica granite
	GS11D	0.794	-4.04	0.811	Diorite (quartz diorite, tonalite)
	GS13A	0.821	6.55	1.007	Diorite (monzodiorite, granodiorite)
	GS13B	0.801	4.70	0.780	Diorite (quartz diorite, tonalite)
Polisiehoek Granite	1142A	0.849	6.58	1.046	Diorite (quartz diorite, tonalite)

[a] Rock not classified by this scheme as it is alkalic and peraluminous.

Table A.7: *Geochemical classification of granitoids using the Fe*, modified alkali-lime index (MALI) and aluminium saturation index (ASI) (after Frost et al., 2001).*

Fe-no. or Fe*:	Magnesian							
MALI:	Calcic		Calc-alkalic		Alkali-calcic		Alkalic	
ASI:	Metaluminous	Peraluminous	Metaluminous	Peraluminous	Metaluminous	Peraluminous	Metaluminous	Peralkaline
Rock types	Diorite, quartz diorite, tonalite		Diorite, monzodiorite, granodiorite		Monzonite, syenite, high-K granite		Monzonite, syenite, granite	Alkali-feldspar syenite, alkali-feldspar granite
Fe-no. or Fe*:	Ferroan							
MALI:	Calcic		Calc-alkalic		Alkali-calcic		Alkalic	
ASI:	Metaluminous	Peraluminous	Metaluminous	Peraluminous	Metaluminous	Peraluminous	Metaluminous	Peralkaline
Rock types	None known	None known	Granite	Two-mica granite	Ferrodiorite, syenite, granite	Two-mica granite	Anorthosite, ferrodiorite, monzonite, granite	Alkali-gabbro, syenite, alkali-granite

A.2 A-type granitoid discrimination

A.2.1 $(Na_2O + K_2O)/CaO$ and FeO^T/MgO versus Zr + Nb + Ce + Y

Whalen et al. (1987) propose multiple diagrams for the discrimination of A-type granitoids from I-, S- and M-type granitoids. Two such diagrams are shown in Figure 5.2, (a) $(Na_2O + K_2O)/CaO$ versus Zr + Nb + Ce + Y and (b) FeO^T/MgO versus Zr + Nb + Ce + Y, where FeO^T is total iron oxide as FeO. A-type granitoids are generally characterised in these diagrams by higher $(Na_2O + K_2O)/CaO$ and FeO^T/MgO ratios, as well as somewhat higher Zr + Nb + Ce + Y contents, than the other rock types (see Whalen et al., 1987). However, Whalen et al. (1987) note that highly fractionated I- and S-type granitoids also show high $(Na_2O + K_2O)/CaO$ and FeO^T/MgO ratios.

The $(Na_2O + K_2O)/CaO$ versus Zr + Nb + Ce + Y diagram, Figure 5.2a, shows Swartoup group 1 with a $(Na_2O + K_2O)/CaO$ ratio of 1.8–2.9. Swartoup group 1 shows overlap of this oxide ratio with both the published pelite (∼0.6–3.2) and greywacke compositions (∼1.4–6.6). However, Swartoup group 1 have higher Zr + Nb + Ce + Y contents (∼560–780 ppm) than the sediment compositions. The pelites have 220–260 ppm Zr + Nb + Ce + Y, while the greywacke compositions have somewhat higher contents, with a range of 250–340 ppm. The Swartoup group 1 analyses plot in the A-type field of Figure 5.2a. However, A-type granitoids are characterised by high $Na_2O + K_2O$ and low CaO contents (e.g. Whalen et al., 1987; Eby, 1992).

The Swartoup group 2 analyses have $(Na_2O + K_2O)/CaO$ ratios of ∼0.9–6.0. Their Zr + Nb + Ce + Y contents range from 150–1100 ppm. Swartoup group 2 vary between all three fields of the $(Na_2O + K_2O)/CaO$ versus Zr + Nb + Ce + Y diagram; the A-type field, the highly fractionated I- and S-type field and the 'normal' I-, S- and M-type field. They also show much overlap with the published sediment compositions.

The hybrid rock analyses have $(Na_2O + K_2O)/CaO$ ratios from 0.5–5.0, and Zr + Nb + Ce + Y contents of 170–700 ppm. These composition ranges are similar to those of Swartoup group 2 and vary between all three fields of the diagram.

The Polisiehoek Granite-gneisses have some of the highest $(Na_2O + K_2O)/CaO$ ratios of the sample set, between 5.8 and 26.0. Their Zr + Nb + Ce + Y contents range from 50–340 ppm. Most of the Polisiehoek Granite-gneisses plot in the field of Fractionated granites. Two samples

show somewhat higher (Na_2O + K_2O)/CaO ratios and plot in the A-type field, though their Zr + Nb + Ce + Y contents are not elevated relative to the rest of the Polisiehoek Granite-gneisses.

The mafic dyke sample has a relatively low (Na_2O + K_2O)/CaO ratio of 0.2. The rock has the lowest Zr + Nb + Ce + Y concentration of the smaple set, around 70 ppm. The analysis does not plot within a defined field in the diagram, which is designed for use with granitic rocks and low (Na_2O + K_2O)/CaO ratios below 1.0 are not catered for.

Like in previous diagrams, the Koenap migmatites are shown for reference in Figure 5.2. They show (Na_2O + K_2O)/CaO ratios of ∼1.8–4.0, with one exception, sample 1147B, at 9.9. These (Na_2O + K_2O)/CaO contents overlap with those of the published sediments and with Swartoup group 1. However, the Koenap migmatites have Zr + Nb + Ce + Y contents of around 440–570 ppm and plot in the A-type field, somewhat between the analyses of Swartoup group 1 (∼560–780 ppm) and the published pelite (220–260 ppm) and greywacke compositions (250–340 ppm).

The Bysteek Formation specimens are not shown on Figure 5.2a, due to their low (Na_2O + K_2O)/CaO ratios. The Bysteek calc-silicate, sample GS10A, has a (Na_2O + K_2O)/CaO ratio less than 0.01 and a Zr + Nb + Ce + Y content of around 610 ppm. The Bysteek marble, sample GS19A, has a (Na_2O + K_2O)/CaO ratio near 0, due to its Na_2O + K_2O and K_2O contents which are both below detection limits. The marble's Zr + Nb + Ce + Y content is around 5 ppm.

The FeO^T/MgO versus Zr + Nb + Ce + Y diagram, Figure 5.2b, shows Swartoup group 1 in the A-type field, like in the (Na_2O + K_2O)/CaO diagram. Swartoup group 1 have FeO^T/MgO ratios between 3.4 and 4.9. Similar to the (Na_2O + K_2O)/CaO diagram, Swartoup group 1 have almost the same range in FeO^T/MgO ratios as the published pelite (∼3.9–5.9) and greywacke compositions (∼3.1–5.8).

Swartoup group 2 have FeO^T/MgO contents of ∼2.8–5.3, showing overlap with the FeO^T/MgO ratios of Swartoup group 1 and the sediment compositions. Three analyses from Swartoup group 2 plot in the I-, S- and M-type field, and five analyses plot in the A-type field due to their higher Zr + Nb + Ce + Y contents. Sample GS9A has an MgO content below the detection limit, and so cannot be shown on Figure 5.2b. The hybrid rocks have FeO^T/MgO ratios of 3.7–4.6. This range is somewhat narrower than that shown by Swartoup group 2 and like them, the hybrid rock analyses plot in both the A-type field and the I-, S- and M-type field.

The Polisiehek Granite-gneisses have FeO^T/MgO ratios between ∼5.6 and 21.8. They mostly

plot in the Fractionated granite field. Three exceptions, samples 1136A, 1142A and 1147C, have slightly lower FeO^T/MgO ratios and plot in the I-, S- and M-type field.

The mafic dyke specimen has a FeO^T/MgO content of 1.7 and plots in the I-, S- and M-type field.

Again, the Koenap migmatites are shown for reference in the FeO^T/MgO versus Zr + Nb + Ce + Y diagram. They have FeO^T/MgO ratios between ∼2.4 and 3.9, slightly lower than those of Swartoup group 1 and the sediment compositions, but with much overlap, like what was seen in the $(Na_2O + K_2O)/CaO$ diagram (Figure 5.2a).

The Bysteek marble has a FeO^T/MgO ratio around 0.04, so is not shown on Figure 5.2b. The Bysteek calc-silicate sample is also not shown on the diagram as the analysis has around 0.99 FeO^T/MgO.

A.2.2 $(Al_2O_3 + CaO)/(FeO^T + Na_2O + K_2O)$ versus $100 \times (MgO + FeO^T + TiO2)/SiO_2$

Figure 5.2c shows a plot of $(Al_2O_3 + CaO)/(FeO^T + Na_2O + K_2O)$ versus $100 \times (MgO + FeO^T + TiO2)/SiO_2$. This diagram, proposed by Sylvester (1989), distinguishes alkaline from peraluminous and highly fractionated granitoids. This helps confirm classifications of highly fractionated granitoids made based on Figures 5.2a and 5.2b.

The $(Al_2O_3 + CaO)/(FeO^T + Na_2O + K_2O)$ versus $100 \times (MgO + FeO^T + TiO2)/SiO_2$ diagram shows Swartoup group 1 with $(Al_2O_3 + CaO)/(FeO^T + Na_2O + K_2O)$ ratios between 1.26 and 1.57, and their $100 \times (MgO + FeO^T + TiO2)/SiO_2$ contents ranging from 9.89 to 15.10. Swartoup group 1 plot mostly in the Alkali field, with only sample 1144A plotting in the calc-alkaline/strongly peraluminous field. This is in agreement with the ASI classification of Frost et al. (2001) (Figure 4.2c), which classified all Swartoup group 1 as peralkaline. Swartoup group 1 have lower $100 \times (MgO + FeO^T + TiO2)/SiO_2$ ratios than the published pelite (22–33) and greywacke compositions (∼21–40), and somewhat higher $(Al_2O_3 + CaO)/(FeO^T + Na_2O + K_2O)$ contents (pelites, ∼0.96–1.25; greywackes, ∼0.60–1.34).

Most of Swartoup group 2 (six analyses) have $(Al_2O_3 + CaO)/(FeO^T + Na_2O + K_2O)$ ratios between 1.48 and 1.64 and $100 \times (MgO + FeO^T + TiO2)/SiO_2$ contents from ∼1–6. Three analyses, samples 1151A, GS10B and GS15C, have higher $100 \times (MgO + FeO^T + TiO2)/SiO_2$ contents of ∼23–28 and somewhat lower $(Al_2O_3 + CaO)/(FeO^T + Na_2O + K_2O)$ ratios of 0.95–1.52, with some overlap. Samples GS10B and GS15C show overlap with the sediments composi-

tions, in the alkaline field, in contrast to sample 1151A which plots in the calc-alkaline/strongly peraluminous field. The lower 100 × (MgO + FeO^T + TiO2)/SiO_2 content group also plots in the calc-alkaline/strongly peraluminous field (four analyses) and two samples (GS9A and GS9B) are in the highly fractionated calc-alkaline field. This classification is not in agreement with the ASI classification of Frost et al. (2001), which classified most Swartoup group 2 analyses as peralkaline, except for sample GS15C as peraluminous (Figure 4.2c).

Most hybrid rock analyses show (Al_2O_3 + CaO)/(FeO^T + Na_2O + K_2O) ratios of ∼1.2–1.7, one exception, sample GS11D, has a ratio of 4.8. They all have 100 × (MgO + FeO^T + TiO2)/SiO_2 contents from ∼1–14, showing overlap with Swartoup groups 1 and 2. Two samples each plot in the Alkaline field, GS1A and GS7A, and the Calc-alkaline/Strongly peraluminous field, GS11D and GS13B. Only sample GS13A plots in the highly fractionated calc-alkaline field. The (Al_2O_3 + CaO)/(FeO^T + Na_2O + K_2O) versus 100 × (MgO + FeO^T + TiO2)/SiO_2 diagram is in poor agreement with the ASI classification of Frost et al. (2001), which classifies the hybrid rocks as peralkaline, except for sample GS1A, which is peraluminous by that scheme.

The Polisiehek Granite-gneiss samples have (Al_2O_3 + CaO)/(FeO^T + Na_2O + K_2O) ratios of 1.30–1.74, and 100 × (MgO + FeO^T + TiO2)/SiO_2 contents of ∼0.4–3.7. They mostly plot in the Highly fractionated calc-alkaline field, only one sample lies closeby in the calc-alkaline/Strongly peraluminous field. This is in good agreement with the (Na_2O + K_2O)/CaO and FeO^T/MgO versus Zr + Nb + Ce + Y diagrams, which classify the Polisiehoek Granite-gneiss as a fractionated I- or S-type granitoid.

The mafic dyke specimen shows ∼1.4 (Al_2O_3 + CaO)/(FeO^T + Na_2O + K_2O) and one of the highest 100 × (MgO + FeO^T + TiO2)/SiO_2 ratios at around 53.

Like in previous diagrams, the Koenap migmatites are shown for reference. They show (Al_2O_3 + CaO)/(FeO^T + Na_2O + K_2O) ratios from ∼1.01–1.60, which overlaps with Swartoup group 1 and the upper portion of the published sediment compositions. The 100 × (MgO + FeO^T + TiO2)/SiO_2 ratios of the Koenap migmatites range from 15.9–26.8, slightly higher than those of Swartoup group 1 and also showing overlap with the sediment compositions, plotting mostly in the Alkaline field with three analyses in the calc-alkaline/strongly peraluminous field. This is in poor agreement with the Frost et al. (2001) ASI classification (Figure 4.2c), which classifies all Koenap migmatites as peraluminous.

The Bysteek Formation marble, sample GS19A, has a (Al_2O_3 + CaO)/(FeO^T + Na_2O + K_2O) ratio of over 145, due to its high calcite and low silicate mineral mode (Section 3.2.2), and the calc-silicate, sample GS10A, also has a relatively high ratio of around 9.2. The 100 × (MgO +

FeO^T + TiO2)/SiO_2 content of the marble is also very high, at 208, and that of the calc-silicate is moderately high at around 20.1.

A.3 Trace element chemical variation diagrams

Pearce et al. (1984) demonstrate the use of trace element discrimination diagrams to distinguish between the intrusive settings of ocean ridge granites (ORG), volcanic arc granites (VAG), within plate granites (WPG) and collision granites (COLG). They found the discrimination to be most effective in Rb-Y-Nb and Rb-Yb-Ta space. Empirically drawn boundaries on projections of Y-Nb, Yb-Ta, Rb-(Y + Nb) and Rb-(Yb + Ta) separate out these four main groups (Pearce et al., 1984).

Förster et al. (1997), however, demonstrate the tectonic interpretations of Pearce et al. (1984) to be problematic. For example, complex or polyphase orogeny can mix source rocks of different tectonic provenance, such as in continental arcs and collisional settings. Compositional trends can also be caused to cross field boundaries by differentiation (Förster et al., 1997). The diagrams themselves (Figure A.1) are shown for discrimination and descriptive purposes, but the tectonic interpretations of Pearce et al. (1984) have not been adhered to. The Koenap and Bysteek Formation specimens are shown in the diagrams of Figure A.1 for comparison.

Niobium versus Yttrium

Figure A.1a shows the Koenap migmatites within the WPG and ORG fields. The Koenap migmatites show higher Y contents ($\sim$ 47–63 ppm) than the published pelite (27–35 ppm) and greywacke (24–33 ppm) composition fields, which show overlap. However, the Nb contents of the Koenap migmatites ($\sim$ 12–17 ppm) are very similar to those of the pelite (11–19 ppm) and greywacke fields (8–12 ppm), which lie within the VAG + syn-COLG field.

The Bysteek marble (sample GS19A) lies in the VAG + syn-COLG field, at the lowest yttrium (2.1 ppm) and one of the lowest niobium contents (1.2 ppm) of the sample set. In contrast, the Bysteek calc-silicate (sample GS10A) lies in the WPG field, having the highest niobium content (81 ppm) of the samples and one of the highest Y contents (91).

Swartoup group 1 define a positive correlation between Y (22–53 ppm) and Nb (12–20 ppm). The analyses span both the VAG + syn-COLG (samples 1144A, 1145A and 1146A) and WPG

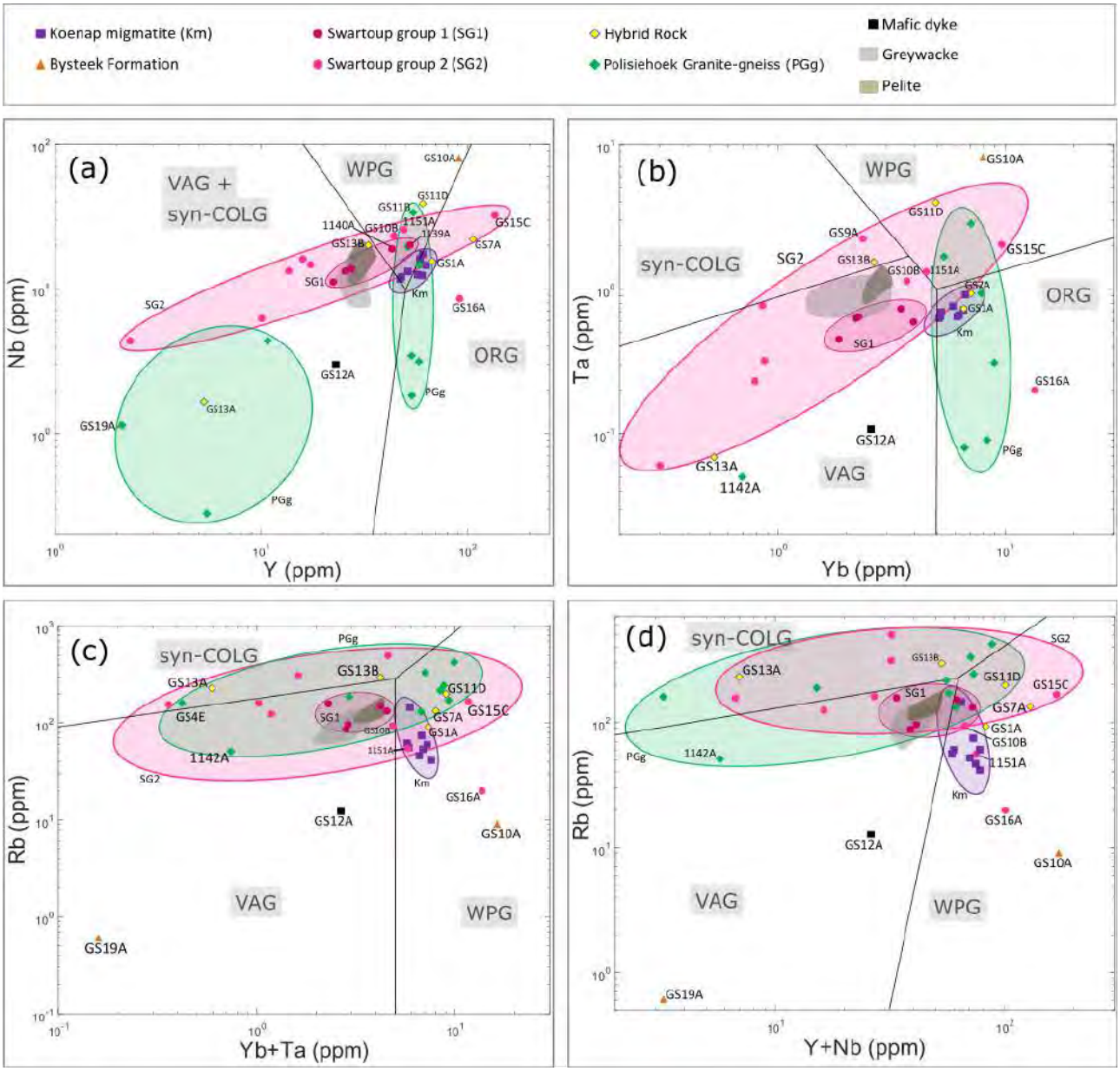

Figure A.1: *Trace element discrimination diagrams, (a) Y-Nb, (b) Yb-Ta, (c) Rb-(Y + Nb) and (d) Rb-(Yb + Ta), (after Pearce et al., 1984).*

fields (samples 1139A and 1140A). Swartoup group 2 have a slightly wider range of Nb contents (4–32 ppm) as Swartoup group 1 and also define positive correlation with Y (2–136 ppm). Swartoup group 2 show overlap with the VAG + syn-COLG (samples 1149A, GS5A, GS9B and GS15B), WPG (samples 1151A and GS10B) and the ORG fields (samples GS15C and GS16A).

Most of the hybrid rock analyses show overlap with the higher Y content Swartoup group 2 samples, with one exception. Sample GS13A has the lowest Y (5.3 ppm) and Nb (1.7 ppm) contents of the hybrid rocks and lies within the VAG + syn-COLG field, below the Swartoup group 2 specimens. The rest of the hybrid rock analyses have niobium contents which vary from 16–40 ppm Nb and their yttrium contents range between 33 and 106 ppm Y. These hybrid rocks lie within the VAG + syn-COLG, WPG and ORG fields, the same as Swartoup group 2.

The Polisiehoek Granite-gneisses can be divided into two distinct groups in the Nb-Y diagram in a similar fashion as done in the Y-Rb diagram (Figure 4.3c). The low Y analyses (three samples) lie in the VAG + syn-COLG field, with between 2 and 11 ppm Y and 0.3–4.3 ppm Nb. One of these analyses coincides with the Bysteek marble analysis in this diagram, Figure A.1a. The higher Y content samples have a narrow range of Y contents between ∼52 and 58 ppm Y, and Nb contents from 1.8–33.8 ppm Nb. These specimens show overlap with the ORG and WPG fields. The mafic dyke specimen, sample GS12A, lies in the VAG + syn-COLG field, with 23 ppm Y and 3 ppm Nb.

Tantalum versus Ytterbium

The tantalum versus ytterbium diagram, Figure A.1b, shows almost the same geometrical relationships between the different lithologies as the Nb versus Y diagram. Koenap migmatite lie within the ORG field, from 0.6–0.9 ppm Ta and 5.1–6.7 ppm Yb. The published pelite (2.4–3.1 ppm Yb, 0.8–1.4 ppm Ta) and greywacke (∼1.4–3.0 ppm Yb, 0.7–0.9 ppm Ta) composition fields show, on average, more Ta and less Yb than Koenap migmatite and they lie within the VAG field.

The Bysteek marbles tantalum content is below detection limits and it has 0.16 ppm Yb. In contrast, the Bysteek calc-silicate specimen lies within the WPG field and has the highest tantalum content of the sample set, 8.3 ppm Ta, and it has almost 8 ppm Yb.

Swartoup group 1 define a positive correlation between Yb and Ta, and lie within the VAG field, at lower Yb contents (1.9–3.9 ppm) than the published greywackes. Swartoup group 1 have similar amounts of Ta as the Koenap migmatites, 0.5–0.7 ppm. Swartoup group 2 analyses have between 0.3 and 13.5 ppm Yb and 0.06–2.2 ppm Ta. Most lie in the VAG field, like Swartoup group 1, and define a positive trend. However, due to Yb and Ta variations, one analysis lies within the syn-COLG field and two are in the WPG field. Sample GS16A is an outlier and plots away from the main Swartoup group 2 trend at lower Yb and Ta contents, within the ORG field.

Most hybrid rocks show between 0.7 and 4.1 ppm Ta with 2.6–7.1 ppm Yb. They show overlap with the higher-Y Swartoup group 2 composition ranges. These specimens vary over the syn-COLG, WPG and ORG fields. One sample, GS13A, has low Ta (0.07 ppm) and Yb (0.5 ppm) contents, like the lowest-Ta Swartoup group 2 analysis and lies within the VAG field.

The Polisiehoek Granite-gneisses show a slightly negative, almost subvertical trend spanning the

ORG and WPG fields. Their analyses have between 5.4–8.9 ppm Yb and range from 2.8 ppm Ta down to 0.08 ppm Ta. However, two samples, GS4B (2.9 ppm Yb) and GS4E (0.4 ppm Yb), have Ta concentrations below detection limits. One outlier, sample 1142A, lies in the VAG field away from this trend and has the lowest detectable tantalum content of the sample set (0.05 ppm Ta) around 0.70 ppm Yb. Note that the same Polisiehoek Granite-gneisses which show S-type granitoid characteristics (Y-Rb diagram, Figure 4.3c), have higher Y contents (Nb-Y diagram) as well as higher Yb contents than the three I-type characteristic, low Y and Yb content specimens. The mafic dyke specimen, sample GS12A, contains 0.25 ppm Yb and 0.11 ppm Ta, so plots within the VAG field.

Rubidium versus Yb + Ta and Y + Nb

Rubidium is shown against Yb + Ta (Figure A.1c) and Y + Nb (Figure A.1d). As these two diagrams show the same geometrical relationships between the various units of the sample set, the diagrams are described together.

Koenap migmatite show Rb contents ranging from about 40 to 150 ppm Rb. Their Yb + Ta contents are between 59 and 78 ppm, Y + Nb between 5.7 and 7.3 ppm. The Koenap migmatite analyses all lie in the WPG fields of Figures A.1c,d. On average, the Koenap migmatites show somewhat more Rb (∼10–165 ppm), at lower Yb + Ta (39–52 ppm) and Y + Nb (3.2–4.2 ppm) contents, than the published pelite composition field. Published greywacke compositions have somewhat lower Rb (∼65–130 ppm), Yb + Ta (∼35–40 ppm) and Y + Nb (2.1–3.7 ppm) contents, on average, than the pelites but also show greater variation. Both the pelite and greywacke fields lie within the VAG fields of the two diagrams.

All five Swartoup group 1 analyses lie in the VAG field of the Rb-Yb + Ta diagram (Figure A.1c), four of which show overlap with the published pelite and greywacke composition fields. The Rb contents of Swartoup group 1 range between 88 and 157 ppm, slightly more, on average, than Koenap migmatite. They also have 34–72 ppm Yb + Ta and 2.3–4.5 ppm Y + Nb. Three Swartoup group 1 samples plot within the VAG field of the Rb-Y + Nb diagram, two of which show overlap with the greywacke compositions, the other two analyses show higher Y + Nb contents and plot within the WPG field (Figure A.1d). The analyses of Swartoup group 2 plot within the syn-COLG, VAG and WPG fields of both the Rb-Yb + Ta and the Rb-Y + Nb diagram. Their Rb contents are mostly between ∼55 and 500 ppm. Their Yb + Ta contents vary from 0.36–13.7 ppm and they have 6.7 to 168 ppm Y + Nb. One outlier, sample GS16A, shows a low Rb content of around 20 ppm.

The hybrid rock specimens appear to vary as Swartoup group 2, like in many previous diagrams. Most have between 4.2–9.0 ppm Yb + Ta and 53–129 ppm Y + Nb, and lie within the syn-COLG and WPG fields. Again, like in previous diagrams, sample GS13A is an outlier due to much lower Yb + Ta (0.6 ppm) and Y + Nb (7 ppm) contents, though it does plot within the syn-COLG fields. All hybrid rock analyses have from 94 to 305 ppm Rb.

The Polisiehoek Granite-gneiss specimens have Rb contents between 51 and 423 ppm, Yb + Ta contents from 0.4–9.9 ppm and 3.2–88.2 ppm Y + Nb. The analyses vary within the syn-COLG, VAG and WPG fields of both the Rb-(Yb + Ta) and the Rb-(Y + Nb) discrimination diagrams.

The mafic dyke analysis shows 12.9 ppm Rb. As a result of this, along with its moderate Yb + Ta (2.7 ppm) and Y + Nb contents (26.1 ppm), the sample lies within the VAG fields of both Figures A.1c and A.1d.

A.4 U/Pb Zircon data

Tables A.8 and A.9 show the U/Pb data provided by Professor Dirk Frei (University of the Western Cape), used to construct the Wetherill Concordia diagrams (Figure 4.9, Section 4.6) of samples J37A (Koenap migmatite) and 980A (Swartoup granitoid).

Table A.8: *U/Pb zircon data for sample J37A, provided by Professor Dirk Frei, University of the Western Cape.*

Sample and analysis	U (ppm)	Pb (ppm)	Th (ppm)	$^{206}Pb/^{204}Pb$	$^{207}Pb/^{235}U$	2σ	$^{206}Pb/^{238}U$	2σ	$^{207}Pb/^{206}Pb$	2σ	$^{207}Pb/^{235}U$ (Ma)	2σ (Ma)	$^{206}Pb/^{238}U$ (Ma)	2σ (Ma)	$^{207}Pb/^{206}Pb$ (Ma)	2σ (Ma)	Conc.
J37A-01	988	208	412	5650	2.369	0.072	0.2109	0.0037	0.0815	0.0020	1233	38	1234	22	1233	49	100
J37A-02	489	103	171	8520	2.352	0.068	0.2107	0.0036	0.59	0.0809	1228	35	1233	21	1220	46	101
J37A-04	2536	292	449	10773	1.217	0.034	0.1153	0.0020	0.61	0.0766	808	23	703	12	1109	44	63
J37A-05	1277	271	550	908017	2.372	0.068	0.2119	0.0036	0.60	0.0812	1234	35	1239	21	1227	45	101
J37A-06	536	114	105	384172	2.417	0.070	0.2137	0.0037	0.59	0.0820	1248	36	1248	21	1246	46	100
J37A-07	440	91	61	6475	2.349	0.069	0.2081	0.0036	0.59	0.0819	1227	36	1218	21	1243	46	98
J37A-09	199	46	106	53640	2.726	0.085	0.2306	0.0040	0.56	0.0858	1336	41	1337	23	1333	50	100
J37A-10	433	158	218	12447	6.201	0.177	0.3647	0.0063	0.60	0.1233	2005	57	2004	34	2005	41	100
J37A-11	466	98	220	81525	2.360	0.070	0.2111	0.0036	0.58	0.0811	1230	36	1235	21	1223	47	101
J37A-12	385	89	41	297985	2.743	0.083	0.2306	0.0040	0.57	0.0863	1340	41	1338	23	1345	48	99
J37A-14	372	86	44	33078	2.706	0.087	0.2304	0.0041	0.55	0.0852	1330	43	1337	24	1319	52	101
J37A-15	382	80	255	8406	2.340	0.070	0.2090	0.0036	0.58	0.0812	1224	37	1223	21	1226	48	100
J37A-16	455	98	77	328674	2.419	0.078	0.2155	0.0038	0.55	0.0814	1248	40	1258	22	1231	53	102
J37A-17	411	87	422	290435	2.385	0.080	0.2106	0.0038	0.53	0.0821	1238	42	1232	22	1249	56	99
J37A-18	188	38	121	1805	2.279	0.121	0.2017	0.0043	0.41	0.0820	1206	64	1185	25	1244	95	95
J37A-19	795	153	293	512826	2.133	0.063	0.1925	0.0033	0.58	0.0804	1160	34	1135	20	1206	48	94
J37A-20	2152	458	229	25271	2.382	0.073	0.2127	0.0037	0.57	0.0813	1237	38	1243	22	1227	50	101
J37A-21	732	169	56	14111	2.736	0.082	0.2310	0.0040	0.58	0.0859	1338	40	1339	23	1336	47	100
J37A-22	1020	236	141	58179	2.701	0.080	0.2310	0.0040	0.58	0.0848	1329	40	1340	23	1311	47	102
J37A-23	706	148	101	10765	2.372	0.079	0.2095	0.0037	0.53	0.0821	1234	41	1226	22	1248	55	98
J37A-24	518	110	232	8801	2.372	0.078	0.2117	0.0038	0.54	0.0813	1234	41	1238	22	1227	55	101
J37A-26	1210	288	460	24656	2.862	0.088	0.2378	0.0041	0.57	0.0873	1372	42	1375	24	1367	49	101
J37A-27	3907	384	881	6935	1.049	0.032	0.0982	0.0017	0.56	0.0775	729	22	604	10	1135	51	53
J37A-28	432	130	280	16033	4.364	0.136	0.3002	0.0052	0.56	0.1054	1706	53	1692	30	1722	47	98

Table A.9: *U/Pb zircon data for sample 980A, provided by Professor Dirk Frei, University of the Western Cape.*

Sample and analysis	U (ppm)	*Pb* (ppm)	*Th* (ppm)	$^{206}Pb/^{204}Pb$	$^{207}Pb/^{235}U$	2σ	$^{206}Pb/^{238}U$	2σ	$^{207}Pb/^{206}Pb$	2σ	$^{207}Pb/^{235}U$ (Ma)	2σ (Ma)	$^{206}Pb/^{238}U$ (Ma)	2σ (Ma)	$^{207}Pb/^{206}Pb$ (Ma)	2σ (Ma)	Conc.
980A-1	425	88	139	17135	2.315	0.090	0.2076	0.0039	0.0809	0.0028	1217	47	1216	23	1219	67	100
980A-2	250	53	195	178081	2.373	0.120	0.2137	0.0045	0.0806	0.0037	1234	62	1248	26	1210	90	103
980A-6	266	42	93	1364	1.809	0.135	0.1587	0.0042	0.0826	0.0058	1049	78	950	25	1261	136	75
980A-7	1966	263	112	591	1.783	0.060	0.1337	0.0024	0.0967	0.0028	1039	35	809	15	1562	54	52
980A-9	671	132	831	6671	2.206	0.104	0.2107	0.0042	0.0817	0.0032	1235	54	1233	24	1239	76	100
980A-11	3708	312	1175	303	1.374	0.047	0.0841	0.0015	0.1185	0.0034	878	30	520	10	1934	52	27
980A-12	2935	280	296	309	1.497	0.051	0.0954	0.0017	0.1138	0.0032	929	31	587	11	1861	51	32
980A-13	5375	281	1841	387	0.742	0.025	0.0523	0.0009	0.1030	0.0030	564	19	329	6	1678	54	20
980A-14	3733	293	941	394	1.128	0.040	0.0785	0.0014	0.1043	0.0032	767	27	487	9	1701	56	29
980A-15	1969	256	874	489	1.826	0.058	0.1301	0.0023	0.1019	0.0027	1055	33	788	14	1658	49	48
980A-16	1078	201	190	3390	2.079	0.079	0.1867	0.0035	0.0808	0.0027	1142	43	1103	20	1216	65	91
980A-17	1556	216	394	617	1.793	0.058	0.1386	0.0025	0.0938	0.0026	1043	34	837	15	1505	52	56
980A-18	3053	339	456	946	1.341	0.045	0.1112	0.0020	0.0875	0.0025	864	29	679	12	1371	55	50
980A-19	1747	401	478	1165	2.723	0.088	0.2295	0.0041	0.0861	0.0023	1335	43	1332	24	1340	52	99
980A-20	988	208	412	5650	2.369	0.072	0.2109	0.0037	0.0815	0.0020	1233	38	1234	22	1233	49	100
980A-21	1141	179	1250	3100	1.773	0.061	0.1569	0.0028	0.0820	0.0024	1035	36	939	17	1244	57	75
980A-22	2907	282	1366	447	1.413	0.045	0.0970	0.0017	0.1056	0.0028	894	29	597	11	1725	49	35
980A-23	7534	390	4065	277	0.817	0.025	0.0518	0.0009	0.1145	0.0028	607	18	325	6	1873	44	17
980A-24	2608	318	598	718	1.570	0.047	0.1218	0.0021	0.0935	0.0023	958	29	741	13	1497	47	49
980A-25	4279	251	1676	341	0.901	0.029	0.0587	0.0010	0.1114	0.0029	652	21	368	7	1822	48	20
980A-26	1105	160	1479	2365	1.622	0.049	0.1452	0.0025	0.0810	0.0020	979	29	874	15	1222	48	72
980A-27	4146	350	401	429	1.221	0.038	0.0844	0.0015	0.1050	0.0027	810	25	522	9	1714	47	30
980A-29	1412	250	626	3810	1.986	0.074	0.1770	0.0033	0.0814	0.0026	1111	42	1051	19	1231	64	85
980A-31	3392	404	318	478	1.627	0.051	0.1192	0.0021	0.0990	0.0026	981	31	726	13	1606	48	45
980A-32	4365	371	1778	373	1.256	0.038	0.0850	0.0015	0.1072	0.0027	826	25	526	9	1753	46	30
980A-33	4134	480	605	455	1.666	0.050	0.1162	0.0020	0.1040	0.0026	996	30	708	12	1697	45	42
980A-34	3840	326	1594	360	1.258	0.039	0.0850	0.0015	0.1074	0.0028	827	26	526	9	1755	47	30
980A-35	260	85	267	25469	5.086	0.160	0.3271	0.0058	0.1128	0.0029	1834	58	1824	32	1845	47	99
980A-36	2445	305	361	348	1.925	0.063	0.1248	0.0022	0.1118	0.0031	1090	36	758	13	1829	50	41
980A-38	384	73	178	3837	2.135	0.093	0.1892	0.0037	0.0819	0.0032	1160	51	1117	22	1242	77	90
980A-39	1219	224	814	5762	2.072	0.064	0.1840	0.0032	0.0817	0.0021	1140	35	1089	19	1237	50	88
980A-40	2041	244	182	630	1.580	0.055	0.1194	0.0022	0.0960	0.0029	962	34	727	13	1547	56	47
980A-41	767	152	98	3483	2.207	0.070	0.1987	0.0035	0.0806	0.0021	1183	38	1168	20	1210	52	97
980A-42	1502	208	179	774	1.744	0.060	0.1385	0.0025	0.0913	0.0027	1025	36	836	15	1453	56	58
980A-43	1971	303	356	622	2.105	0.066	0.1539	0.0027	0.0992	0.0026	1150	36	923	16	1609	48	57
980A-44	976	203	5589	1813	2.391	0.083	0.2079	0.0037	0.0834	0.0025	1240	43	1218	22	1279	58	95
980A-45	787	164	707	7415	2.359	0.076	0.2079	0.0037	0.0823	0.0022	1230	40	1217	21	1253	53	97

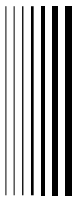

References

Absar, N., Sreenivas, B., 2015. Petrology and geochemistry of greywackes of the $\sim$ 1.6 Ga Middle Aravalli Supergroup, northwest India: evidence for active margin processes. International Geology Review 57(2), 134–158.

Altherr, R., Holl, H., Hegner, E., Langer, C., Kreuzer, H., 2000. High-potassium, calc-alkaline i-type plutonism in the European Variscides: northern Vosges (France) and northern Schwarzwald (Germany). Lithos 50, 51–73.

Ashworth, J. R., Brown, M., 2012. High-temperature metamorphism and crustal anatexis, volume 2. Springer Science & Business Media.

Bial, J., Büttner, S. H., Appel, P., 2016. Timing and conditions of regional metamorphism and crustal shearing in the granulite basement of south Namibia: Implications for the crustal evolution of the Namaqualand metamorphic basement in the Mesoproterozoic. African Journal of Earth Sciences 123, 145–176.

Bial, J., Büttner, S. H., Frei, D., 2015a. Formation and emplacement of two contrasting late-Mesoproterozoic magma types in the central Namaqua Metamorphic Complex (South Africa, Namibia): Evidence from geochemistry and geochronology. Lithos 224–225, 272–294.

Bial, J., Büttner, S. H., Schenk, V., Appel, P., 2015b. The long-term high-temperature history of the central Namaqua Metamorphic Complex: Evidence for a Mesoproterozoic continental back-arc in southern Africa. Precambrian Research 268, 243–278.

Carmichael, R. S., 1989. Practical Handbook of Physical Properties of Rocks and Minerals. Boca Raton: CRC Press.

Chappell, B. W., 1999. Aluminous saturation in I- and S-type granites and the characterization of fractionated hapogranites. Lithos 46, 535–551.

Chappell, B. W., White, A. J. R., 1992. I- and S-type granites in the Lachlan Fold Belt. Earth and Environmental Science Transactions of the Royal Society of Edinburgh 83, 1–26.

Clemens, J. D., 2012. Granitic magmatism, from source to emplacement: a personal view. Applied Earth Science (Trans. Inst. Min. B) 121(3), 107–136.

Clemens, J. D., Stevens, G., 2012. What controls chemical variation in granitic magmas? Lithos 134–135, 317–329.

Clemens, J. D., Stevens, G., Farina, F., 2011. The enigmatic sources of I-type granites: The peritectic connexion. Lithos 126, 174–181.

Collins, W. J., 2002. Hot orogens, tectonic switching, and creation of continental crust. Geology 30(6), 535–538.

Colliston, W. P., Cornell, D. H., Schoch, A. E., Praekelt, H. E., 2015. Geochronological constraints on the Hartbees River Thrust and Augrabies Nappe: New insights into the assembly of the Mesoproterozoic Namaqua-Natal Province of Southern Africa. Precambrian Research 265, 150–165.

Colliston, W. P., Praekelt, H. E., Schoch, A. E., 1989. A broad perspective (Haramoep) of geological relations established by sequence mapping in the Proterozoic Aggeneys Terrane,Bushmanland, South Africa. South African Journal of Geology 92(1), 42–48.

Colliston, W. P., Schoch, A. E., 1996. Proterozoic metavolcanic rocks and associated metasediments along the Orange River in the Pofadder terrane, Namaqua Mobile Belt. South African Journal of Geology 99(3), 309–325.

Colliston, W. P., Schoch, A. E., 2006. The distribition and diagnostic features of deformed plutonic rocks in two terranes of the Namaqua mobile belt along the Orange (Gariep) River, South Africa. South African Journal of Geology 109(3), 369–392.

Condie, K. C., 1993. Chemical composition and evolution of the upper continental crust: Contrasting results from surface samples and shales. Chemical Geology 104, 1–37.

Cornell, D. H., Pettersson, Å., 2007. Ion probe zircon dating of metasediments from the Areachap and Kakamas Terranes, Namaqua-Natal Province and the stratigraphic integrity of the Areachap Group. South African Journal of Geology 110, 575–584.

Cornell, D. H., Pettersson, Å., 2012. Zircon U-Pb incomplete Namaqua-Natal Wilson Cycle. South African Journal of Geology .

Cornell, D. H., Thomas, R. J., Moen, H. F. G., Reid, D. L., Moore, J. M., Gibson, R. L., 2006. The Namaqua-Natal Province. In: Johnson, M. R., Anhaeusser, C. R., Thomas, R. J. (Eds.), Geology of South Africa, chapter 16, pp. 325–379, Geological Society of South Africa, Johannesburg / Council for Geoscience, Pretoria.

Cornell, D. H., van Schijndel, V., Simonsen, S. L., Frei, D., 2015. Geochronology of Mesoproterozoic hybrid intrusions in the Konkiep Terrane, Namibia, from passive to active continental margin in the Namaqua-Natal Wilson Cycle. Precambrian Research 265, 166–188.

Dalziel, I. W. D., Mosher, S., Gahagan, L. M., 2000. Laurentia-Kalahari Collision and the Assembly of Rodinia. Journal of Geology 108, 499–513.

De la Roche, H., Leterrier, J., Grandclaude, P., Marchal, M., 1980. A classification of volcanic and plutonic rocks using R_1R_2 diagrams and major element analyses – its relationships with current nomenclature. Chemical Geology 29, 183–210.

Diener, J. F. A., 2014. Low-P-high-T metamorphism of the Aggeneys terrane, Namaqua Metamorphic Complex, South Africa. South African Journal of Geology 117(1), 31–44.

Eby, G. N., 1992. Chemical subdivision of the A-type granitoids: Petrogenetic and tectonic implications. Geology 20, 641–644.

Ellis, S., Beaumont, C., Jamieson, R., Quinlan, G., 1998. Continental collision including a weak zone - the vise model and its application to the Newfoundland Appalachians. Canadian Journal of Earth Sciences 35(11), 1323–1346.

Fisher, P. M., 2016. Phase relationships and metamorphic evolution of migmatites in the Swartoup Hills. Unpublished BSc (Hons) thesis, Rhodes University, South Africa.

Förster, H.-J., Tischendorf, G., Trumbull, R. B., 1997. An evaluation of the Rb vs. (Y + Nb) discrimination diagram to infer tectonic setting of silicic igneous rocks. Lithos 40, 261–293.

Frei, D., Gerdes, A., 2009. Precise and accurate in situ U-Pb dating of zircon with high sample throughput by automated LA-SF-ICP-MS. Chemical Geology 261, 261–270.

Frost, B. R., Barnes, C. G., Collins, W. J., Arculus, R. J., Ellis, D. J., Frost, C. D., 2001. A Geochemical Classification for Granitic Rocks. Journal of Petrology 42(11), 2033–2048.

Frost, B. R., Frost, C. G., 2008. On charnockites. Gondwana Research 13, 30–44.

Gresse, P. G., Macey, P. H., Smith, H., Hartnady, M. I., Frei, D., 2016. The Pre-Gariep geology east of Rosh Pinah, Karas Region, S. Namibia. Explanation to parts of 1:50 000 Geologial Map Sheets 2716DA, 2716DB, 2716DC, 2716DD, 2717CC, 2816BB and 2817AA. Geological Survey of Namibia, Council for Geoscience South Africa, Ministry of Mines and Energy.

Gromet, L. P., Dymek, R. F., Haskin, L. A., Korotev, R. L., 1984. The "North American shale composite": Its compilation, major and trace element characteristics. Geochimica et Cosmochimica Acta 48(12), 2469–2482.

Harris, C., Le Roux, P., Cochrane, R., Martin, L., Duncan, A. R., Marsh, J. S., Le Roex, A. P., Class, C., 2015. The oxygen isotope composition of Karoo and Etendeka picrites; High δ^{18}O mantle or crustal contamination? Contributions to Mineralogy and Petrology 170, 1–24.

Hartnady, C., Joubert, P., Stowe, C., 1985. Phanerozoic Crustal Evolution in Southwestern Africa. Episodes 8(4), 236–244.

Holdaway, M. J., Lee, S. M., 1977. Fe–Mg cordierite stability in high-grade pelitic rocks based on experimental theoretical and natural observations. Contributions to Mineralogy and Petrology 63(2), 175–198.

Humphreys, H., van Bever Donker, J. M., 1990. Early Namaqua low-pressure metamorphism: deformation and porphyroblast growth in the Zoovoorby staurolite schist, South Africa. Journal of Metamorphic Geology 8, 159–170.

Hyndman, R. D., Currie, C. A., Mazzotti, S. P., 2005. Subduction zone backer, mobile belts, and orogenic heat. GSA Today 15(2), 4–10.

Jacobs, J., Thomas, R. J., Weber, K., 1993. Accretion and indentation tectonics at the southern edge of the Kaapvaal craton during the Kibaran (Grenville) orogeny. Geology 21, 203–206.

King, P. L., White, A. J. R., Chappell, B. W., Allen, C. M., 1997. Characterization and Origin of Aluminous A-type Granites from the Lachlan Fold Belt, Southeastern Australia. Journal of Petrology 38(3), 371–391.

Le Bas, M. J., Le Maitre, R. W., Streckeisen, A., Zanettin, B., 1986. A Chemical Classification of Volcanic Rocks Based on the Total Alkali–Silica Diagram. Journal of Petrology 27(3), 745–750.

Le Maitre, R. W., 1976. The Chemical Variablility of some Common Igneous Rocks. Journal of Petrology 17(6), 589–637.

Ludwig, K. R., 2012. User's manual for Isoplot 3.75: A geochronological toolkit for Microsoft Excel. Berkeley Geochronology Center, Special Publication No. 5.

Macey, P., Minnaar, H., Miller, J., Lambert, C., Kisters, A., Diener, J., Thomas, R., Groenewald, C., Indongo, J., Angombe, M., Smith, H., Shifatoka, G., Le Roux, P., Frei, D., 2015. The Precambrian geology of the Warmbad Region, southern Namibia. An interim explanation to 1:50 000 Geological Map Sheets of the 1:250 000 2818 Warmbad sheet. Geological Survey of Namibia and Council for Geoscience of South Africa.

Mattinson, J. M., 2010. Analysis of the relative decay constants of 235U and 238U by multistep CA-TIMS measurements of closed-system natural zircon samples. Chemical Geology 275, 186–198.

McDonough, W. F., Sun, S.-S., 1995. The composition of the Earth. Chemical Geology 120, 223–253.

Mehnert, K. R., 1968. Migmatites and the Origin of Granitic Rocks. Amsterdam: Elsevier Pub. Co.

Middlemost, E. A. K., 1994. Naming materials in the magma/igneous rock system. Earth-Science Reviews 37, 215–224.

Miller, R. M., Becker, T. (Eds.), 2008. The Geology of Namibia: Archaean to Mesoproterozoic, volume 1. Windhoek: Ministry of Mines and Energy, Geological Survey.

Miller, R. M. G., 2012. Review of Mesoproterozoic magmatism, sedimentation, and terrane amalgamation in southwestern Africa. South African Journal of Geology 115, 417–448.

Moen, H. F. G., 2001. Geological Map 2818 Onseepkans, 1:250 000. Pretoria: Council for Geoscience.

Moen, H. F. G., Toogood, D. J., 2007. Explanation: Sheet 2818. The geology of the Onseepkans area (1:250 000). Council for Geoscience, South Africa.

Moodley, J. A., 2012. Petrogenesis of the Bysteek and Koenap Formation Migmatites, Central Namaqualand. Unpublished MSc thesis, Rhodes University, South Africa, `http://contentpro.seals.ac.za/iii/cpro/DigitalItemViewPage.external?sp=1001574`.

Nasdala, L., Hofmeister, W., Norberg, N., Mattinson, J. M., Corfu, F., Dörr, W., Kamo, S. L., Kennedy, A. K., Kronz, A., Reiners, P., Frei, D., , Kosler, J., Wan, Y., Götze, J., Häger, T., Kröner, A., Valley, J. W., 2008. Zircon M257 - a Homogenous Natural Reference Material for the Ion Microprobe U-Pb Analysis of Zircon. Geostandards and Geoanalytical Research 32, 247–265.

Passchier, C. W., Trouw, R. A. J., 2005. Microtectonics. Springer-Verlag Berlin Heidelberg, 2nd edition.

Peacock, M. A., 1931. Classification of igneous rock series. Journal of Geology 39, 54–67.

Pearce, J. A., Harris, N. B. W., Tindle, A. G., 1984. Trace Element Discrimination Diagrams for the Interpretation of Granitic Rocks. Journal of Petrology 25(4), 956–983.

Pettersson, Å., 2008. Mesoproterozoic crustal evolution in Southern Africa. Unpublished PhD thesis, University of Gothenburg, Sweden, `https://gupea.ub.gu.se/bitstream/2077/17269/1/gupea_2077_17269_1.pdf`.

Pettersson, Å., Cornell, D. H., Moen, H. F. G., Reddy, S., Evans, D., 2007. Ion-probe dating of 1.2 Ga collision and crustal architecture in the Namaqua-Natal Province of southern Africa. Precambrian Research 158, 79–92.

Pettersson, Å., Cornell, D. H., Yuhara, M., Hirahara, Y., 2009. Sm-Nd data for granitoids across the Namaqua-Natal Province, South Africa. In: Reddy, S. M., Mazumder, R., Evans, D. A. D., Collins, A. S. (Eds.), Palaeoproterozoic Supercontinents and Global Evolution, volume 323, pp. 219–230, Geological Society, London, Special Publications.

Pin, C., Briot, D., Bassin, C., Poitrasson, F., 1994. Concominant separation of strontium and samarium–neodymium for isotopic analysis in silicate samples, based on specific extraction chromatography. Analytica Chimica Acta 298, 209–217.

Pin, C., Gannoun, A., Dupont, A., 2014. Rapid, simultaneous separation of Sr, Pb, and Nd by extraction chromatography prior to isotope ratios determination by TIMS and MC-ICP-MS. Journal of Analytical Atomic Spectrometry 29, 1858–1870.

Shaw, D. M., 1956. Geochemistry of pelitic rocks. Part III: Major elements and general geochemistry. Geological Society of America Bulletin 67(7), 919–934.

Stevens, G., Villaros, A., Moyen, J.-F., 2007. Selective peritectic garnet entrainment as the origin of geochemical diversity in S-type granites. Geoligical Society of America 35(1), 9–12.

Stowe, C. W., 1983. The Uppington geotraverse and its implications for craton margin tectonics. In: Botha, B. J. V. (Ed.), Namaqualand Metamorphic Complex, volume 10, pp. 147–171, Special Publication Geological Society of South Africa.

Sylvester, P. J., 1989. Post-collisional alkaline granites. The Journal of Geology 97, 261–280.

Tanaka, T., et al., 2000. JNdi-1: a neodymium isotopic reference in consistency with LaJolla neodymium. Chemical Geology 168, 279–281.

Thomas, R. J., Agenbacht, A. L. D., Cornell, D. H., Moore, J. M., 1994a. The Kibaran of southern Africa: Tectonic evolution and metallogeny. Ore Geology Reviews 9, 131–160.

Thomas, R. J., Cornell, D. H., Moore, J. M., Jacobs, J., 1994b. Crustal evolution of the Namaqua-Natal Metamorphic Province, southern Africa. South African Journal of Geology 97(1), 8–14.

Thomas, R. J., Macey, P. H., Spencer, C., Dahnsay, T., Diener, J. F. A., Lambert, C. W., Frei, D., Nguno, A., 2016. The Sperrgebiet Domain, Aurus Mountains, SW Namibia: A ∼2020-850 Ma window within the Pan-African Gariep Orogen. Precambrian Research 286, 35–58.

van Huyssteen, A., 2017. Field relationships in the high-grade metamorphic Kakamas Terrain of the western Namaqua-Natal belt. Unpublished BSc (Hons) thesis, Rhodes University, South Africa.

Waight, T., 2013. Rb–Sr Geochronology (Igneous Rocks). In: Rink, W. J., Thompson, J. (Eds.), Encyclopedia of Scientific Dating Methods, pp. 1–8, Springer Netherlands, Dordrecht.

Whalen, J. B., Currie, K. L., Chappell, B. W., 1987. A-type granites: geochemical characteristics, discrimination and petrogenesis. Contributions to Mineralogy and Petrology 95, 407–419.

Whitehouse, M. J., Platt, J. P., 2003. Dating high-grade metamorphism–constraints from rare-earth elements in zircon and garnet. Contributions to Mineralogy and Petrology 145(1), 61–74.

Whitney, D. L., Evans, B. W., 2010. Abbreviations for names of rock-forming minerals. American Mineralogist 95(1), 185–187.

Wiedenbeck, M., Allé, P., Corfu, F., Griffin, W. L., Meier, M., Oberli, F., von Quadt, A., Roddick, J. C., Spiegel, W., 1995. Three natural zircon standards for U-Th-Pb, Lu-Hf, trace element and REE analyses. Geostandard Newsletters 19, 1–23.

Wimmenauer, W., Bryhni, I., 2007. Migmatites and related rocks. In D. Fettes and J. Desmons (Ed.), Metamorphic Rocks: A Classification and Glossary of Terms, chapter 6, pp. 43–45. Cambridge University Press, United Kingdom.

Zhang, L.-X., Wang, Q., Zhu, D.-C., Li, S.-M., Zhao, Z.-D., Zhang, L.-L., Chen, Y., Liu, S.-A., Zheng, Y.-C., Wang, R., Liao, Z.-L., 2019. Generation of leucogranites via fractional crystallization: A case from the Late Triassic Luoza batholith in the Lhasa Terrane, southern Tibet. Gondwana Research 66, 63–76.